Pile Foundations in NL

an analysis of the 4D/8D method through numerical modelling

W. Oomen

Technische Universiteit Delft and Royal Haskoning DHV

TU Delft

Royal HaskoningDHV
Enhancing Society Together

Pile Foundations in NL

an analysis of the 4D/8D method through numerical modelling

by

W. Oomen

to obtain the degree of Master of Science
at the Delft University of Technology,
to be defended publicly on Tuesday October 31, 2017 at 14:30 PM.

Student number:	4107527	
Project duration:	February 6, 2017 – October 31, 2017	
Thesis committee:	Prof. dr. ir. K. G. Gavin,	TU Delft, Department of Geo-engineering (chair)
	Dr. ir. M. Korff,	TU Delft, Department of Geo-engineering
	Ir. O. P. M. Mooijman,	Royal Haskoning DHV
	Ir. K. J. Reinders,	TU Delft, Department of Hydraulic engineering

Coverpicture: Photo of the installation of a prefab concrete pile by [Kuipers Funderingstechnieken BV, 2017].
An electronic version of this thesis is available at `http://repository.tudelft.nl/`.

Abbreviations

Abbreviations	Definition
BX	Formation of Boxtel
CPT	Cone penetration test
DR	Formation of Drente
DS	Direct shear
DSS	Direct simple shear
FEM	Finite element method
HP	Hypoplasticity
HS	Hardening soil
ICP	Imperial Collega Pile
KH	Kruithuisweg
KR	Formation of Kreftenheye
KRBXDE	Formation of Kreftenheye and Boxtel with the layer Delwijnen
LCPC	Laboratiore Central des Ponts et Chaussees
LEPP	Linear elastic perfectly plastic
MC	Mohr-Coulomb
MPM	Material Point Method
N.A.P.	Normaal Amsterdams Peil (Main water level)
RHDHV	Royal Haskoning DHV
ST	Formation of Sterksel
STF	Soil testing facility
TC	Triaxial compression
TE	Triaxial extension
TU Delft	Technical University Delft
UWA	University of Western Australia

Symbols

Symbol	Definition	Unit
D	Diameter of the pile tip	m
a	Net area ratio	-
A_b	Area pile tip	m^2
α	Factor taking into account softening behaviour	-
α_b	Factor reducing the maximum pile tip capacity in other methods	-
α_p	Factor reducing the maximum pile tip capacity in Dutch method	-
A_{pile}	Area of a cross section of the pile	m^2
A_s	Area pile shaft	m^2
A_{tip}	Area of the pile tip	m^2
β	Pile tip factor in Dutch method	-
β	Stiffness factor in HP model	-
c	Cohesion	kPa
d	Diameter of the pile shaft	m
D_{50}	Mean grain diameter	m
D_{cone}	Diameter of the tip of the cone	m
d_{cone}	Diameter of the shaft of the cone	m
D_{CPT}	Diameter of CPT cone	m
ΔL	Length over which the pile is installed in granular material	m
D_{eq}	Equivalent pile tip diameter	m
deq	Equivalent pile shaft diameter	m
D_{mould}	Diameter of mould	m
D_{pile}	Diameter of pile tip	m
e	Void ratio	-
E	E-modulus	kPa
e_0	Initial void ratio at zero pressure	-
E_{50}^{ref}	Reference stiffness at 50% of the maximum stress	kPa
e_c	Maximum void ratio	-
e_{c0}	Maximum void ratio at zero pressure	-
e_{cv}	Constant volume void ratio	-
e_d	Minimum void ratio	-
e_{d0}	Minimum void ratio at zero pressure	-
e_i	Maximum void ratio 1.15*emax	-
e_{i0}	Maximum void ratio 1.15*emax at zero pressure	-
e_{ini}	Initial void ratio	-
e_{max}	Maximum void ratio	-
e_{min}	Minimum void ratio	-
E_{pile}	E-modulus pile	kPa
E_{soil}	E-modulus soil	kPa
ϵ	Strain	-
ϵ_1	Major principle strain	-
$\epsilon_{beginningofinstallation}$	Stain at the beginning of installation	-
$\epsilon_{beginningofloadtest}$	Strain at the beginning of the load test	-
$\epsilon_{residualload}$	Strain due to residual load	-
ϵ_v	Volumetric strain	-
ϵ_{yy}	Strain in yy direction	-

F	Force	kN
f_b	density factor	-
f_d	pressure factor	-
f_e	density factor	-
F_r	Load inducing residual load	kN
F_{shaft}	Force along the shaft of the pile	kN
F_{tip}	Force at the pile tip	kN
F_{total}	Total Force	kN
γ'	Unit weight	kN/m^3
h	height of sand cone in angle of repose test	m
h_{mould}	Height of mould	m
h_s	Granular hardness	-
K_0	Pressure coefficient	-
k_c	Pile class factor	-
M_{mould}	Mass of mould	kg
M_{sample}	Mass of sample	kg
n	pressure sensitivity of the grain skeleton	-
ν	poisson's ratio	-
O	Circumference pile	m
O_s	Circumference pile shaft	m
p_a	Atmospheric pressure (100 kPa)	kPa
ϕ'	Angle of internal friction	^{o}
ϕ_c	Angle of repose	^{o}
ϕ'_p	Peak angle of internal friction	^{o}
p_s	Mean skeleton pressure	kPa
ψ	State parameter	^{o}
ψ	Diletancy angle	^{o}
ψ_p	Peak diletancy angle	^{o}
$q_{b,ICP}$	Tip capacity for ICP method	kPa
$q_{b,LCPC}$	Tip capacity for LCPC method	kPa
$q_{b,max}$	Maximum pile tip capacity	kPa
$q_{b,UWA}$	Tip capacity for UWA method	kPa
q_c	Cone resistance from CPT	kPa
$q_{c,avg}$	Average cone resistance used to calculate the maximum tip resistance	kPa
$q_{c,z}$	Cone resistance at specific depth (z)	kPa
$q_{cI,avg}$	Cone resistance in part I	kPa
$q_{cII,avg}$	Cone resistance in part II	kPa
$q_{cIII,avg}$	Cone resistance in part III	kPa
Q_r	Stress inducing the residual load	kPa
q_t	Cone resistance corrected for pore water pressure at the shoulder	kPa
r	R*Deq in logarithmic spiral	m
R	Radius pile	m
r	Ratio between width and length of the pile tip in Dutch method	-
r_0	Radius for $\theta = 0$	m
R_e	Initial relative density	-
ρ_{solids}	Density solids	kg/m^3
s	Pile tip factor	-
σ'_1	Major principle stress	kPa
σ'_3	Minor principle stress	kPa
σ'_{h0}	Effective initial horizontal stress	kPa
$\sigma_{piletip}$	Stress at the pile tip	kPa
σ'_v	Effective vertical stress	kPa
σ_v	Total vertical stress	kPa
σ'_{v0}	Effective initial vertical stress	kPa
$\sigma'_{v0,z}$	Effective initial vertical stress at specific depth (z)	kPa
σ'_{yy}	Effective stress in yy direction	kPa
S_u	Undrained shear strength	kPa
τ_{mob}	Mobilize shear stress	kPa

U_2	Pore water pressure at the shoulder of the cone	kPa
UD-power	rate of stress dependency in other literature also known as m	-
UD-ref	reference pressure in other literature also known as pref	kPa
u_x	Horizontal displacement	m
V_{mould}	Volume of mould	m^3
v_p	Peak diletancy rate	-
V_{solids}	Volume solids	m^3
V_{void}	Volume voids	m^3
w	width of sand cone in angle of repose test	m

Acknowledgement

First, I would like to thank my graduation committee; Prof. dr. ir. K.A. Gavin, Dr. ir. M. Korff, Ir. O.P.M. Mooijman and Ir. K.J. Reinders, for their supervision during the past nine months. The results in this thesis would not have been achieved without their knowledge and commitment.
Furthermore, I would like to say thank you to van 't Hek, Hektech and NVAF, especially P. IJnsen and A. van Heezen, for the execution and contribution of the scaled tests and their practical point of view on pile foundations in the Netherlands.
Last, but not least, I would like to thank my family, Tom and my friends for their unconditional support.

W. Oomen
Delft, October 2017

Preface

This report contains a master thesis research on pile foundations in the Netherlands. It focusses on the pile tip capacity of axially loaded, end bearing, displacement piles. This thesis was done in partial fulfilment of the requirements for the degree of the master track in Geo-Engineering at the faculty of Civil Engineering and Geosciences at the University of Technology in Delft. Besides the TU Delft, Royal Haskoning DHV supervised this research.
The reduction of α_p, which was introduced at the beginning of 2017, is the main motivation for this research. An explanation has to be found on why this reduction was needed. This led to a research on the Dutch method, which is set out in this thesis.

Abstract

The Netherlands is a densely populated country and is located in an area where the shallow subsurface mainly consists of Holocene and Pleistocene soils. To build permanent structures, enough bearing capacity is needed to provide sufficient support for these structures. However, Holocene (soft) soils typically do not provide sufficient support. In the western part of the country, the soft soils from the Holocene overlay the stiffer Pleistocene soils. To still be able to construct at locations where soft soils are found, pile foundations are needed to transfer the loads through the soft soil onto the stiff soil in order to provide for sufficient bearing capacity.
The normative method for determining pile bearing capacity in the Netherlands uses a relatively straightforward semi-empirical approach known as the 4D/8D or the Dutch method. This method was based on the work of [van Mierlo and Koppejan, 1952] who introduce the logarithmic spiral theory. Apart from small modifications and elaborations, the method has been used ever since.

To get to a reasoned solution on how to calculate and design pile foundations the Eurocode [Normcommissie 351 006 'Geotechniek', 2017a] was introduced. One of the (original) aims of the Eurocode was to harmonise rules and regulations regarding, amongst others, pile foundations. To prepare this harmonisation, Belgium, France and the Netherlands took a closer look into their calculation methods. For the Netherlands this research was performed by a committee who presented their findings in CUR 229 - "Axiaal belaste palen" [CUR B&I, 2010].

From CUR 229 it was found the pile tip capacity was overestimated. In other words, the calculated pile tip capacity was higher than the measured pile tip capacity. This overestimation led to a reduction of α_p of 30% starting on the 1^{st} of January 2017. (α_p is the factor which reduces the pile tip resistance for different pile types, see Appendix A.)

A point of interest is the overestimation of the pile tip capacity, which seems to become more prominent when the pile goes deeper into a non-cohesive soil. It was even found, a lower α_p is not required for piles installed less than 8D into the bearing layer.

The reduction of α_p seems to contradict with practice, because no cases of damage are known regarding the bearing capacity of pile foundations. Several explanations for this might be valid. For example, hidden safeties may prevent overall safety issues to arise. In addition, errors may occur in the determination of the pile capacity from pile load tests or in the Dutch method for calculating pile tip capacity. This leads to the two main subjects for this thesis. On the one hand, the hidden mechanism of residual loads is considered and on the other hand, the zone of influence at the pile tip during failure is analysed.

To analyse the above-named subjects, the 4D/8D method was put under scrutiny. First, it was compared to other (international) analytical methods, which determine the bearing capacity directly from CPT data.
Furthermore, the zone of influence around the pile tip is considered in more detail by analysing the analytical approach and comparing this to the results of numerical models. This led to the conclusion that the observed overestimation can partly be explained by the inaccuracy of the assumed zone of influence around the pile tip, especially regarding the extent of this zone above the pile tip (8D). As this extent is too large, the 4D/8D method results in a too low average cone resistance in the 8D zone (for piles installed less than 8D into the bearing soil layer).
In combination with the 'old' α_p, this leads to a reasonably accurate estimation of the pile tip capacity compared to the measured tip capacity. However, the observed extent of the zone of influence above the pile tip, in the FEM models, is in the order of 1 to 1.5D. The average cone resistance in this zone will in most cases be higher than in a zone extending 8D above the pile tip.

The hidden mechanism of residual loads is implemented in a numerical model, with the use of a static load on top of the pile. The residual loads are caused by the installation of the pile and so, they are considered to be installation effects. No analytical or numerical models or procedures were found in literature to quantify the residual load. Residual loads were implemented using a procedure defined in this thesis, taking into account the maximum pile tip capacity as indicator for the order of magnitude for the residual load.

This is done, because a drawback of FEM models is; they are not able to calculate large strains, which occur during installation of a pile. Therefore the installations effects (like residual loads) have to be implemented indirectly. The horizontal compression due to installation is modelled as an installation effect according to the procedure of [Broere and van Tol, 2006]. Both installation effects are validated using data from CUR 229 and they are subjected to a sensitivity analysis.

Furthermore, the softening or peak behaviour of soils might have a significant influence on the zone of influence around the pile and on the residual loads, as for both cases, the soil is loaded up to failure. Most regular constitutive models do not take into account this behaviour. Due to the fact the Hypo Plasticity (HP) model takes into account this peak behaviour, it was used to perform the FEM analysis.

During the final stages of this thesis, scaled pile load tests were performed. The results of these tests were analysed to find the presence and order of magnitude of the residual load in a pile. However, as the test results were incomplete, only first assumptions were made that indicated the presence of residual loads. No substantiated conclusion could be drawn regarding the magnitude.

Due to the observed importance of residual loads in this thesis, the residual loads should be measured during load tests more extensively using Osterberg cells or fibre optics.

The installation effects are modelled in the Hypo Plasticity model with reasonable confidence, but future research is needed on models that can model the installation process (for example the Material Point Method). Furthermore, the small strain parameters of the HP model should be taken into account.

This thesis questions the 4D/8D method and shows some of its inaccuracies. However, more extensive research should be done considering the extent of the zone of influence and the limiting value defined by in the Dutch method.
Also, the interaction between the shaft and the pile tip resistance has to be evaluated, as this thesis indicates they interfere with each other if the Dutch method is considered.

Besides the zone of influence and the residual loads, the failure criterion stated by NEN 9997-1 is questioned. Failure of a pile happens when the pile tip has moved 10%D [Normcommissie 351 006 'Geotechniek', 2017a], but the FEM models show more displacements at failure, where failure is defined by the moment the models cannot stabilise anymore and therefore fail to calculate for a certain load step.

Contents

1 Introduction

The normative method used for determining pile bearing capacity in the Netherlands is the relatively straightforward semi-empirical formula based on the work of [van Mierlo and Koppejan, 1952] who introduce the logarithmic spiral theory. This method is known as the 4D/8D or the Dutch method and is a direct CPT-based method, in which the CPT (cone penetration test) is seen as a scaled-down test pile. Direct correlations with the cone resistance are used to calculate the bearing capacity of piles.
As mentioned above, the 4D/8D method is based on the logarithmic spiral theory which was introduced in 1952 by [van Mierlo and Koppejan, 1952]. Apart from modifications based on new insights, the basic approach has been used ever since.

To get to a reasoned solution on how to calculate and design pile foundations the Eurocode [Normcommissie 351 006 'Geotechniek', 2017a] was introduced. One of the (original) aims of the Eurocode was to harmonise rules and regulations regarding, amongst others, pile foundations. To prepare this harmonisation, Belgium, France and the Netherlands took a closer look at their calculation methods for pile foundations. For the Netherlands this research was performed by a committee who presented their findings in CUR 229 - "Axiaal belaste palen" [CUR B&I, 2010].

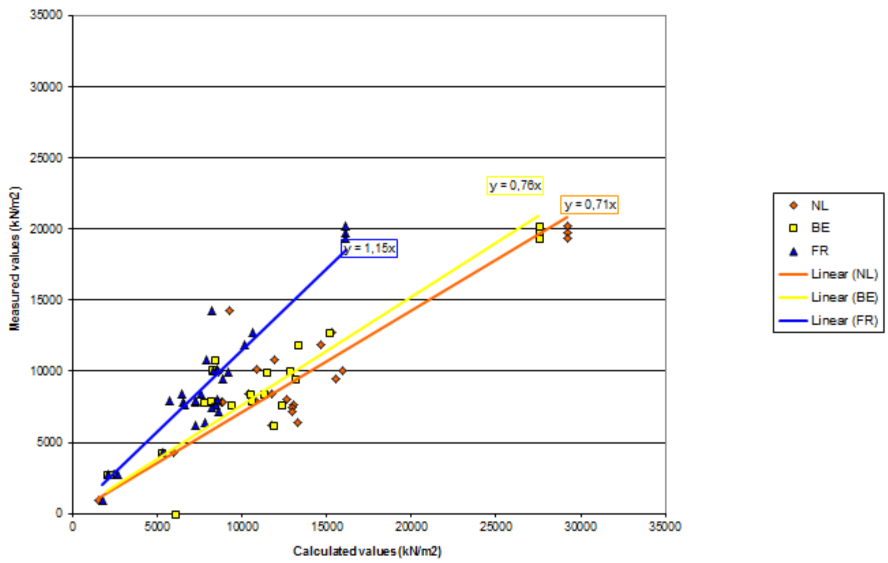

Figure 1.1: Calculated versus tested pile tip capacity [CUR B&I, 2010]

One of the main findings of CUR 229 is the fact that the Dutch method has overestimated the pile tip capacity for years (Figure 1.1). In other words, the calculated pile tip capacity was higher than the measured pile tip capacity during load tests. Therefore, the reduction of α_p (α_p is the factor which reduces the pile tip resistance, during calculation, for different pile types, see Appendix A)of 30% was introduced, starting on the 1^{st} of January 2017. Another point of interest which was found during the research of CUR 229 is the overestimation of the pile tip capacity seems to become more dominant when the pile penetrates deeper into a (non-cohesive) bearing soil.

So far, no cases of damage are known regarding the bearing capacity of pile foundations. Several explanations for this might be valid. For example, hidden safeties may prevent overall safety issues to arise. Also, errors may occur in the determination of the total pile capacity from pile load tests or in the Dutch calculation method for the total pile capacity.

Besides the (semi-)empirical and analytical approaches, more and more geotechnical analyses are elaborated using finite element methods (FEM). Soil behaviour around the pile tip is difficult to measure and/or visualise directly. FEM, using constitutive models, which are available for this particular geotechnical problem, can have added value in understanding the geotechnical mechanisms that occur around the pile tip. However, commonly used constitutive models cannot describe soil behaviour when large strains occur. For driven and jacked piles this is a problem. During installation, large strains will occur, and the soil will deform drastically. Therefore, it is important to either find a way to model the installation effects of pile driving without generating large strains or to make sure the robust analytical or empirical method approaches reality with a sufficient degree of confidence.
This thesis aims to get a better understanding of the nature of α_p in conjunction with the Dutch method for determining the maximum pile tip capacity.

From all the above, a central question arises for this thesis:

"Can the reduction of α_p be explained through the fundamental aspects of geotechnical engineering focussing on the soil behaviour at the pile tip?"

1.1. Research Question

To be able to find a solution to the above-stated question, single, axially loaded, end bearing piles are considered. A fundamental approach is needed, in order to understand the mechanisms occurring during installation and loading of the pile. If the fundamentals are clear, conclusions can be drawn. Several sub-questions are listed below to help to get to the final conclusions.

- Which mechanism or feature can explain the increase in overestimation of the pile tip capacity with increasing penetration depth of the bearing soil layers?
- Can residual loads be the cause of the deviation between the calculated and measured pile tip capacity?
- CUR 229 results show a difference in α_p for piles deep (>8D) in the sand layer compared to piles less deep (<8D) into the sand layer. Can this be explained from shortcomings in de 4D/8D method?
- Is the shape of the zone of influence around the pile tip as described by Koppejan's logarithmic spiral correct for all soil types?
- Is the extent of the zone of influence as assumed when adopting the 4D/8D method valid (for all soil types)?
- Do the limiting values, used in conjunction with the 4D/8D method, have a physical meaning or do they result in hidden safety?

1.2. Research Plan

To be able to answer the above-stated research question this report is split up into three phases:

1. Literature
2. Analysis (analytic and numerical)

3. Validation (numerical)

From these three phases, recommendations are formulated, and conclusions are drawn. The different sections all contribute to getting to a usable, well substantiated, possibly changed approach to calculating the pile tip capacity. In the following subsections, the focus of the phases as mentioned earlier will be discussed in more detail.

1.2.1. Literature

In this section, several CPT based methods for calculations of the bearing capacity of piles are discussed. The different methods are compared to the Dutch method quantitatively. In this comparison, the primary focus will be why the approaches are chosen, if they are substantiated by theory or by test results and if the approach is consistent for different soil profiles and different pile types.
In addition, geological and geotechnical background information regarding the Dutch approach is provided. Furthermore, the fundamental aspects of soil mechanics for pile foundations are discussed.

1.2.2. Analysis

In the analysis section, the Dutch (4D/8D) approach is considered at a detailed level. All facets of the calculation of the pile tip capacity from CPTs are covered separatly. Fundamental aspects of pile driving and loading are also considered. The possible influence on the pile tip capacity is assessed for each of these aspects. The aspects discussed will be:

- the zone of influence, from failure zones;
- the influence of the angle of internal friction;
- the influence of the vertical stresses in the soil;
- the influence of a nearby cohesive soil layer;
- the behaviour of the soil during installation of the pile;
- the behaviour of the soil during loading of the pile.

The analysis section also discusses the residual loads, what they are, and their possible influence on the pile bearing capacity.

1.2.3. Validation

The FEM model PLAXIS is used to conduct the above-explained analyses. Different models are evaluated to decide which one to use to do the investigation and validation. Along with this, the data from CUR 229 is used to validate the results.

1.3. Objectives

The aim of this master thesis is to improve the understanding on the pile tip capacity of axially loaded, end bearing piles. The research focusses on driven piles, used in commonly encountered Dutch granular soils. When a consistent approach is generated for these conditions, the next step can be to validate it for other soil types and soils with a different geological history. The main objective of this thesis is to understand pile tip capacity from a soil mechanical point of view. To achieve this, the following steps are undertaken:

- A complete review of Dutch 4D/8D method.
- Evaluate different (non-Dutch) CPT-based methods and compare with the 4D/8D method. Assess possible advantages and disadvantages.
- Investigate soil behaviour around the pile tip in a FEM model. Validate the model based on CUR229 data.
- Assessment of the Dutch approach based on FEM results.
- Provide conclusions and recommendations.

1.4. Boundaries and Limitations

To be able to answer the main research question and all the sub-questions for this master thesis some limitations are set to create a framework which is researchable and useful. These limitations are set out to be as follows:

- Only single piles will be considered.
- Axially loaded compression piles are considered.
- The piles considered are driven into a non-cohesive soil, i.e. the driven piles are end-bearing piles.
- Only Dutch soils are considered.
- Overconsolidated soils are not considered, i.e. the soils considered have an OCR=1.
- The safety philosophy is not taking into account, i.e. material factors, partial factors, correlation factors are not taken into account.
- Pile factors β and s are set to 1.0, i.e. round or square piles with continuous cross sections are considered.
- The shaft resistance is only considered if required. The present, normative shaft friction model is considered valid and is not investigated within the scope of this thesis.

2

CPT Based Methods

In the pile foundations practice most formulas used to calculate the bearing capacity of piles are based on Cone Penetration Test (CPT). Based on these test results, empirical relationships are used to determine the pile bearing capacity. This thesis focusses on the Dutch method which is a direct CPT based method to calculate the bearing capacity of a foundation pile. A direct CPT method is based on the fact closed-end or prefab pile is very similar in shape to a CPT cone. Therefore a simple correlation is found between the cone resistance and the bearing capacity of the pile.This bearing capacity (R_c in Equation (2.1)) is divided into two parts; the capacity from (positive) shaft friction (R_s in Equation (2.3)) and the end bearing or pile tip capacity (R_b in Equation (2.2)). The equations are set out below:

$$R_c = R_b + R_s \tag{2.1}$$

$$R_b = q_b * A_b \tag{2.2}$$

$$R_s = O_s * \int q_s \, dz \tag{2.3}$$

R_c	:	Total bearing capacity (kN)
R_b	:	Pile tip capacity (kN)
R_s	:	Shaft capacity (kN)
q_b	:	Pile tip capacity (MPa)
A_b	:	Area of pile tip (m^2)
q_s	:	Shaft friction (MPa)
O_s	:	Circumference pile shaft (m)

As mentioned before this thesis only investigates the contribution of the pile tip capacity. Therefore no further notice will be given to equation (2.3).

2.1. Methods

In the following sections, several different CPT based methods are studied, but not all known CPT based methods will be discussed. Only the methods comparable to the Dutch approach will be considered in more detail i.e. only direct CPT methods will be evaluated. A list of the, to be discussed, CPT based methods is given below:

- **4D/8D or Dutch method** [Normcommissie 351 006 'Geotechniek', 2017a]
- **LCPC or French method** [Lunne et al., 1997]
- **University of West Australia method** [Lehane et al., 2005]
- **Imperial College Pile method** [Tomlinson, 2001]

Besides the above-mentioned methods, several other methods are used around the world to calculate pile bearing capacity (for example Norlund's method, Van Der Beer or Belgian method, Schmertmann and Nottingham method, etc.). However, as they are not direct CPT methods, like the Dutch method, they will not be discussed.

2.1.1. Koppejan's logarithmic spiral

Before going deeper into the different methods, one needs to know the details on logarithmic spirals. Logarithmic spirals form the basis of the failure surface around the pile tip and were introduced by [van Mierlo and Koppejan, 1952] and [Meyerhof, 1951] and form the basis of both the Dutch and the French method.
The origin of logarithmic failure surface is evaluated, by starting to consider the logarithmic spiral as defined by [van Mierlo and Koppejan, 1952]. The formula of the logarithmic spiral is as follows:

$$r = r_0 * e^{\theta \tan\phi'} \tag{2.4}$$

$$r_o = \frac{1}{2}\sin\left(\frac{\pi}{4} - \frac{\phi'}{2}\right) \tag{2.5}$$

θ	: Angle between r and r_0	$(^o)$
r	: Radius $*D_{eq}$	(m)
r_0	: Radius for $theta = 0$	(m)
ϕ'	: Angle of internal friction	$(^o)$

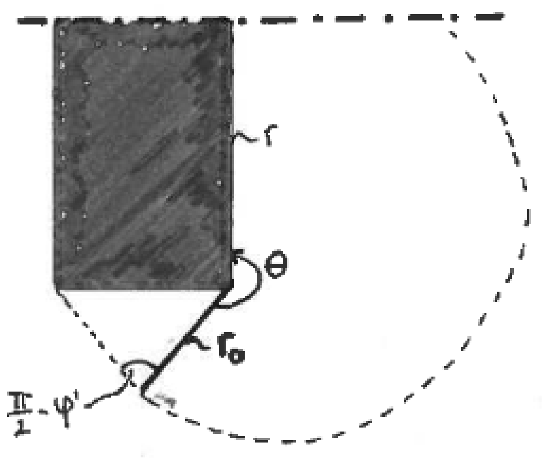

Figure 2.1: Detail of the logarithmic spiral at the pile tip

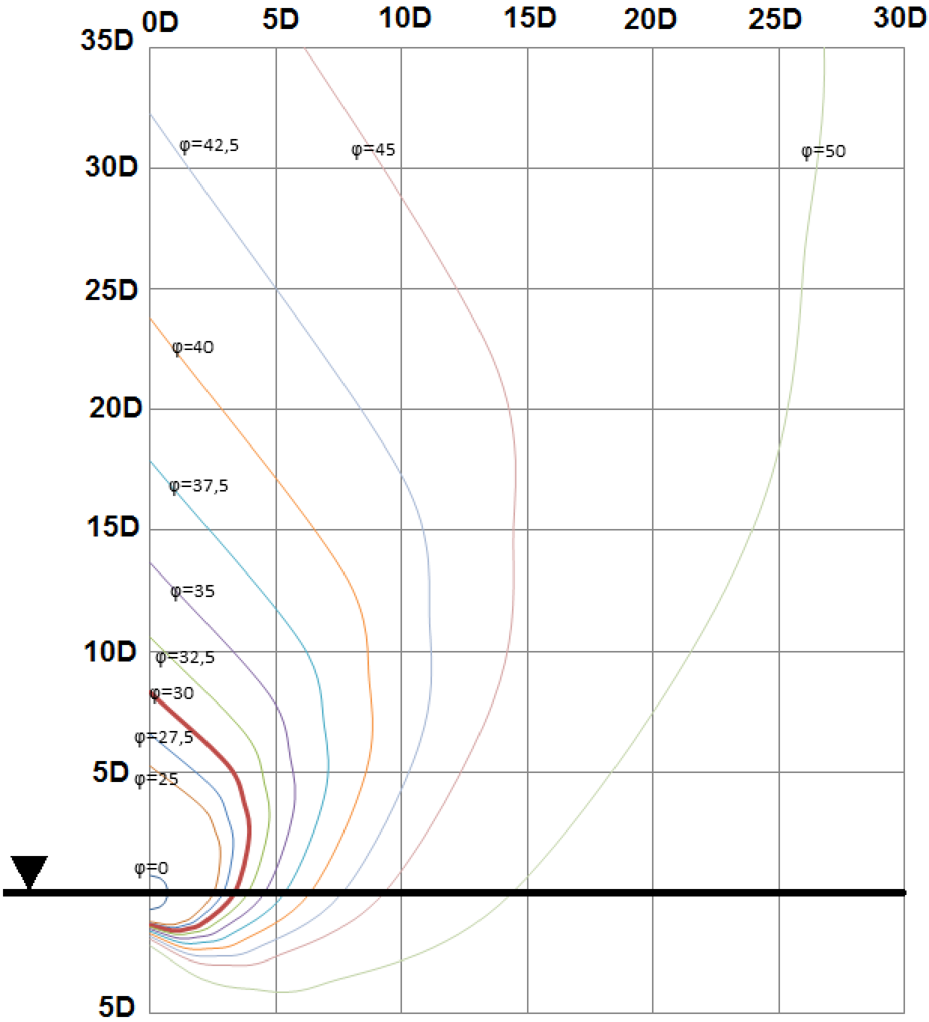

Figure 2.2: Koppejan's failure surface for a range of $0.1^o \leq \phi' \leq 50^o$

More details on the failure surface around the pile tip as described by the logarithmic spiral theory can be found in Chapter 4.

2.1.2. 4D/8D method or Dutch method

Since the logarithmic spirals are clear, the focus of this chapter will go back to the different CPT based methods, starting with the 4D/8D method. The 4D/8D method or Dutch method is the focus of this master thesis. It is an empirically based method. The method to calculate the pile tip resistance or end-bearing resistance is as follows:

$$q_{b,max,NL} = \frac{1}{2} * \alpha_p * \beta * s * \left(\frac{q_{c,I,avg} + q_{c,II,avg}}{2} + q_{c,III,avg} \right) \tag{2.6}$$

[Normcommissie 351 006 'Geotechniek', 2017a]
An example on how to calculate $q_{c,I/II/III}$ can be found in Appendix B

The zone of 4D below the pile tip is to encounter weaker layers right below the pile tip. If such weaker layers occur, the pile may punch through these layers. Taking into account a larger zone of 4D below the pile tip prevents this from happening. The 8D zone above the pile is based on one single pile test [van Mierlo and Koppejan, 1952]. No literature was found to substantiate this zone further.
Finally, it is important to note that the logarithmic spiral theory by [van Mierlo and Koppejan, 1952] is used as a basis for the 4D/8D method. However, it does not define the procedure described in Equation (2.6). The primary focus of Koppejan and van Mierlo was to validate a direct CPT approach and not to design a guideline on how to calculate the bearing capacity of a pile.

$q_{b,NL}$	: Maximum pile tip capacity $\leq 15 MPa$	MPa
β	: Factor taking into account the pile tip shape (=1 for this thesis)	–
s	: Factor taking into account the shape of the cross-section of the pile tip (=1 for this thesis)	–
$q_{c,I,avg}$	: The average cone resistance in section I, this section is located from pile tip level down to at least 0.7*Deq and at most 4*Deq. The end of this section is located in such a way qb.max has its lowest value for this section.	MPa
$q_{c,II,avg}$	: The average cone resistance in section II, this section is the same as section I. However the q_c taken into account cannot be higher than the q_c in deeper layers of this section.	MPa
$q_{c,III,avg}$	: The average cone resistance in section III, this section starts at the pile tip and runs up 8*Deq from there. Again q_c-values taken into account cannot be higher than the q_c-values in deeper layers of sections I, II and III.	MPa
α_p	: Pile class factor (see Appendix [Normcommissie 351 006 'Geotechniek', 2017a])	–

2.1.3. LCPC method by Bustamante and Gianeselli

The Laboratoire Central des Ponts et Chaussees (LCPC) method takes into account an influence zone of 1.5D above and below the pile tip level. The dimensions of this zone were established by using 197 load tests [Bustamante and Gianeselli, 1982]. Like the Dutch method, this method is an empirically based method. The main difference is that the Dutch method uses the indication of Koppejan's logarithmic spirals while the LCPC method uses Meyerhof's logarithmic spirals. Figure 2.3 shows Meyerhof's logarithmic spiral is smaller than Koppejan's logarithmic spiral. This results in a smaller zone of influence, respectively 1.5D/1.5D and 4D/8D.

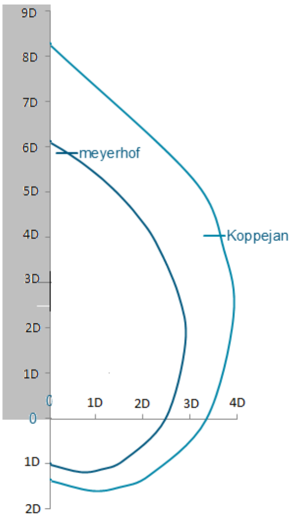

Figure 2.3: Logarithmic spiral of Meyerhof versus Koppejan

In the 1.5D/1.5D zone an average is taken and multiplied by a, so called, penetrometer bearing capacity factor [Bustamante and Gianeselli, 1982]. This factor (k_c) takes into account the installation method and the soil type.

$$q_{b,LCPC} = k_c * q_{c,avg} \tag{2.7}$$

[Bustamante and Gianeselli, 1982]
$q_{c,avg}$ is the average like shown in Figure 2.4. Extremely high and extremely low values are not included when determining the average cone resistance over the 1.5D/1.5D trajectory. They are limited by applying a factor 0.7 or 1.3 to the average q_c, respectively for the low and high peaks of the CPT. Next, a new average for q_c is calculated, and this value is used in Equation (2.7)

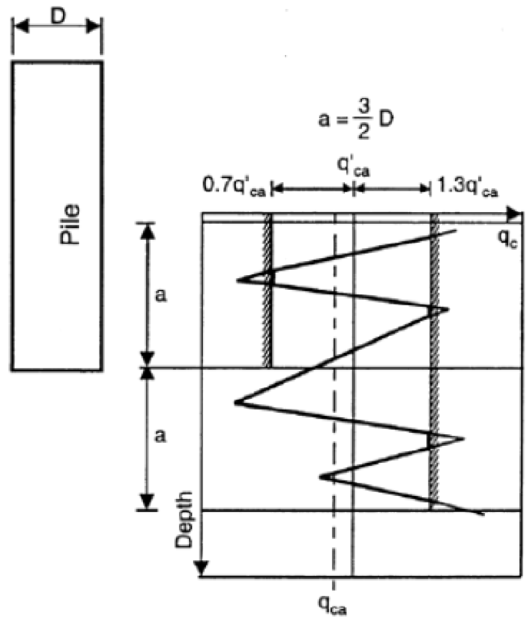

Figure 2.4: Determining $q_{c,avg}$ [Bustamante and Gianeselli, 1982]

Nature of Soil	q_c (MPa)	Factor Group I	k_c Group II
Soft clay and mud	<1	0.4	0.5
Moderately compact clay	1 to 5	0.35	0.45
Silt and loose sand	<5	0.4	0.5
Compact to stiff clay and compact silt	>5	0.45	0.55
Soft chalk	<5	0.2	0.3
Moderately compact sand and gravel	**5 to 12**	**0.4**	**0.5**
Weathered to fragmented chalk	>5	0.2	0.4
Compact to very compact sand and gravel	**>12**	**0.3**	**0.4**

Group I: plain bored piles; mud bored piles; micro piles (grouted under low pressure); cased bored piles; hollow auger bored piles; piers; barrettes
Group II: cast screwed piles; driven precast piles; prestressed tubular piles; driven cast piles; jacked metal piles; micropiles (small diameter piles grouted under high pressure with diameter <250 mm); driven grouted piles (low pressure grouting); driven metal piles; driven rammed piles; jacked concrete piles; high pressure grouted piles of large diameter

Figure 2.5: k_c-values, In bolt are the values comparable to the Dutch soil conditions and as driven piles are considered the values of Group II have to be taken into account [Bustamante and Gianeselli, 1982]

k_c takes into account similar aspects of the pile foundation practice as α_p. However as the approach for determining $q_{c,avg}$ is different, the values for k_c differ from the α_p values. The k_c-values can be found in Figure 2.5.

2.1.4. ICP method by Jardine

The Imperial College Pile (ICP) method for coarse-grained soils is also based on the cone penetration test.

$$q_{b,ICP} = q_{c,avg} * \left(1 - 0.5 * log\frac{D}{D_{CPT}}\right) \tag{2.8}$$

[Tomlinson, 2001]
$q_{c,avg}$ is the average cone resistance taken over 1.5D above and below the pile tip level. This is similar to the LCPC method. The difference between the ICP and LCPC methods is; the ICP method uses a different factor to reduce the cone resistance. It is not influenced by the way of installation, but by the ratio D/D_{CPT} in which $D_{CPT} = 0.036m$ [Lehane et al., 2005]. The reason why the ICP method does not take into account the installation effects is that the method in Equation (2.8) is only valid for driven piles. To be exact, steel closed-end piles driven in sand to deep penetration are considered [Tomlinson, 2001].

Which, in a way, takes into account the same aspects as the k_c value in the LCPC method, but in a slightly different manner.
Figure 2.6 sets out the difference between the ICP and the LCPC method.

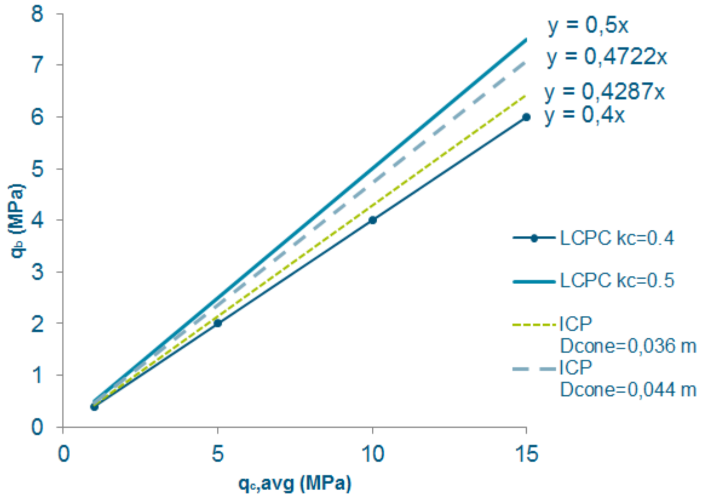

Figure 2.6: q_b,q_c-diagram for LCPC and ICP method, for $D_{pile} = 500mm$

2.1.5. UWA method by Lehane

The University of Western Australia developed a method, which is mainly based on the Dutch approach. According to the findings of the researchers of the UWA, the Dutch approach is more consistent than the LCPC approach [Lehane et al., 2016]. Several methods were designed by UWA, but in this thesis, only the closed-end pile method is considered. The cone resistance is measured while the cone is pushed to 'infinity'. On the other hand, for the closed-end pile, only a vertical displacement of the pile tip of 10%D is allowed in the UWA method, which is the same for the Dutch method [Normcommissie 351 006 'Geotechniek', 2017a]. This restriction makes it impossible to mobilise the total q_c-value [Lehane et al., 2016]. Therefore, some reduction is needed. This results in the following equation:

$$q_{b,UWA} = 0.6 * q_{c,avg} \tag{2.9}$$

[Lehane et al., 2016]

In this case $q_{c,avg}$ is the average cone resistance determined through the Dutch 4D/8D method which was explained in a previous paragraph. The 0.6 is a factor similar to α_p, but it is smaller. This minor difference between the Dutch and the UWA method is set out in Figure 2.7.

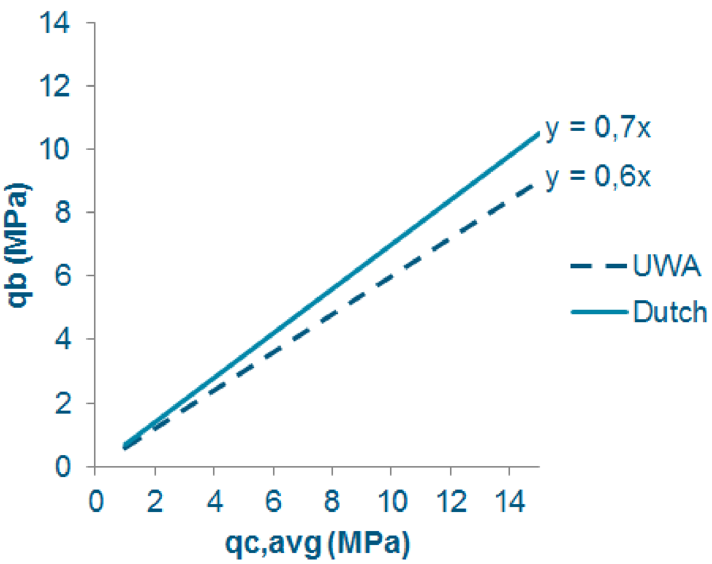

Figure 2.7: q_b,q_c-diagram for Dutch and UWA method

2.2. Preliminary Comparison

It is important to notice the 1.5D/1.5D and the 4D/8D method are very different in the way they determine the average cone resistance. Due to this difference, it is hard to compare the two methods without using data. However, in Figure 1.1 from CUR 229, the difference between the LCPC (French) and the Dutch method is set out, for a comparison between the calculated tip capacity and the pile tip capacity measured during load tests.

Here it can be seen the LCPC method is more conservative than the Dutch method. On the other hand, one has to bear in mind the consistency of both methods. The LCPC method might work in most of the cases, but if lower q_c values are found below 1.5D below the pile tip level, the LCPC method will not account for the punch-through possibility of the pile. The Dutch method does take into account lower q_c values below the pile tip up to a depth of 4D below the pile tip. The effects and extent of the zone above the pile tip are more complex and will be further discussed in Chapters 4 and 5.

To get a better understanding of the different methods, Table 2.1 sets out $q_{b,max}$-values for the different methods for three different CPTs, the CPTs can be found in Appendix C.

Assumptions to calculate $q_{b,max}$ for the four different methods mentioned in this section are:

D_{eq}	:0.4 m
Dutch	:α_p=0.7
LCPC	:k_c=0.4
ICP	:D_{CPT}=0.036 m
UWA	:α_b=0.6
pile tip level CPT1	: N.A.P. -15 m
pile tip level CPT2	: N.A.P. -15 m
pile tip level CPT3	: N.A.P. -18 m

	CPT 1	CPT 2	CPT 3
Dutch	10.5	3.0	5.5
LCPC	14.2	6.4	4.8
ICP	16.9	7.6	5.7
UWA	9.0	2.6	4.7

Table 2.1: Comparison of $q_{b,max}$ (MPa) for given CPT

As the zone of influence around the pile tip is one of the subjects considered in this thesis, Table 2.2 displays the average q_c-values in the trajectory above and below the pile tip for the different methods for the three different CPTs used in Table 2.1.

	CPT 1		**CPT 2**		**CPT 3**	
	above pile tip	below pile tip	above pile tip	below pile tip	above pile tip	below pile tip
4D/8D	12	27	2	6.5	3.75	12
1.5D/1.5D	37	33	17.25	14.75	11.5	12.5

Table 2.2: Average q_c-values (MPa) for the the 4D/8D and 1.5D/1.5D method above and below the pile tip for given CPT

Table 2.2 shows that the French method for averaging q_c-values results in a higher $q_{c,avg}$ than the Dutch method, especially in the zone above the pile tip.

3

Geological and Geotechnical Background Information

This thesis focusses on the Dutch method to determine the pile tip capacity, in typical Dutch soil types, using CPT data. Hence, background information on the Dutch soils and the way CPTs are made is needed. As the 4D/8D method is applied for all Dutch soils, the main soils will be discussed below.

3.1. Geological History

When considering pile foundation in the Netherlands two eras play a major role; the Holocene, and the Pleistocene. The Holocene soils can be found in the western part of the Netherlands. Due to the sea water level changes of the past 10,000 years the Holocene soils are cohesive, soft soils, mainly consisting of marine clays interlaid with peat [Berendsen, 2008]. Below the Holocene layers, stiffer soils and over-consolidated clays from the Pleistocene can be found.

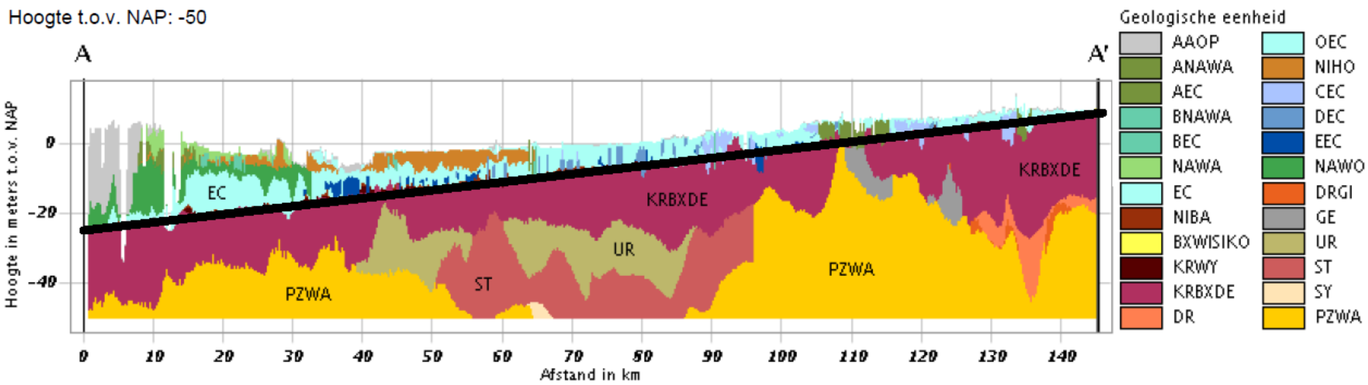

Figure 3.1: Soil profile from west to east of the Netherlands [TNO, 2016]

Figure 3.2: Overview location cross-section in 3.1

Figure 3.1 is a cross-section, from west to east, of the Netherlands. It shows the soil profile with its different geological units. Everything shown above the black diagonal line in Figure 3.1 is from the Holocene. Below the diagonal, the Pleistocene starts. As can be seen from Figure 3.1 and 3.2 the start of the Pleistocene varies from west to east. (This is also shown in Figure 3.3.)

As the soft Holocene layers are not able to provide enough bearing capacity, pile foundations are used. These pile foundations find their bearing capacity in the deeper Pleistocene sand layers.
Depending on the type of construction, pile lengths vary between 10 to 20 m for middle weight type of constructions. For high-rise buildings, pile lengths can go up to 50 to 60 m. These larger lengths can also be necessary if the Pleistocene sand layers are disturbed due to erosion processes (contributed by committee members).

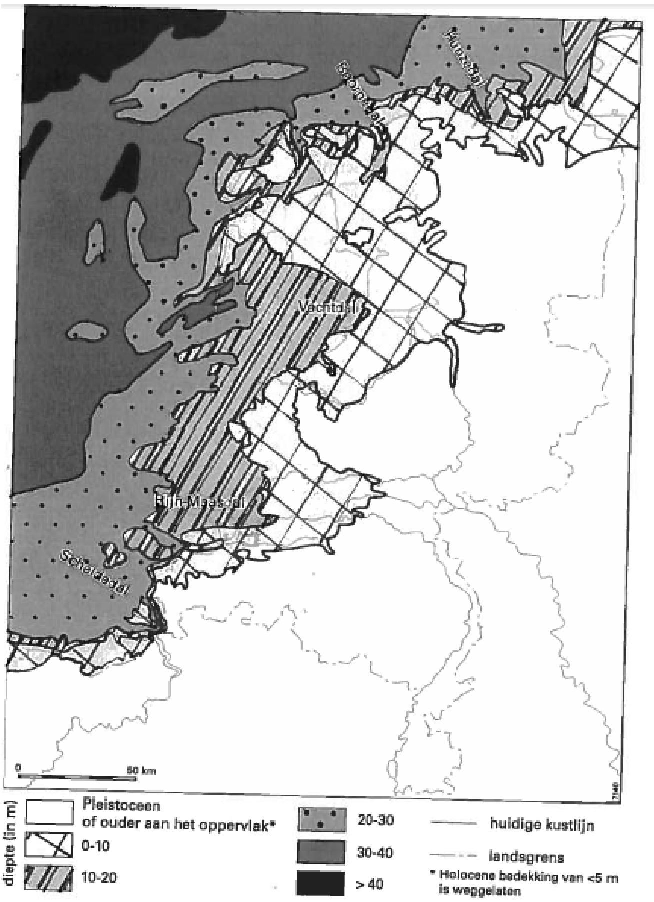

Figure 3.3: Top of Pleistocene from ground surface level [Berendsen, 2008]

Considering foundations, the Netherlands can roughly be split into four areas. These four areas are:

- The western provinces (Noord-Holland, Zuid-Holland, Zeeland)
- The northern provinces (Groningen, Friesland)
- A band reaching from Haarlem towards Nijmegen
- The rest (Noord-Brabant, Limburg and parts of Gelderland, Drenthe and Overijssel)

These four areas are explained in more detail using Figures 3.4 - 3.7.

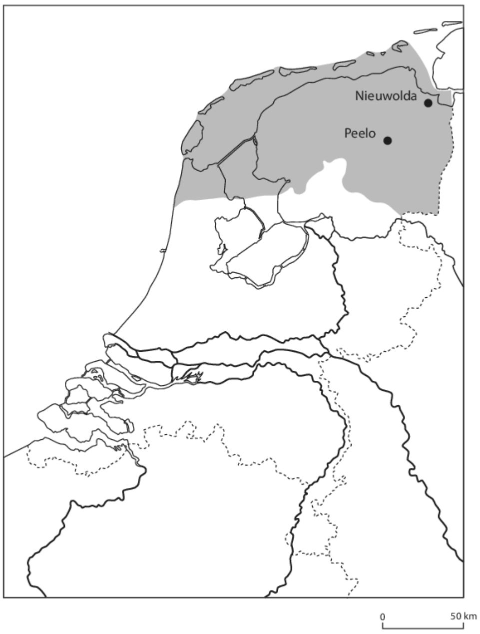

Figure 3.4: Over-consolidated clays [TNO, 2013]

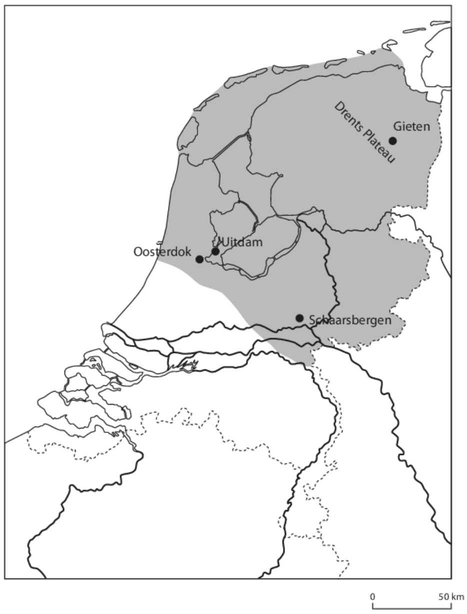

Figure 3.5: Over-consolidated sands in so called ice-pushed ridges [TNO, 2013]

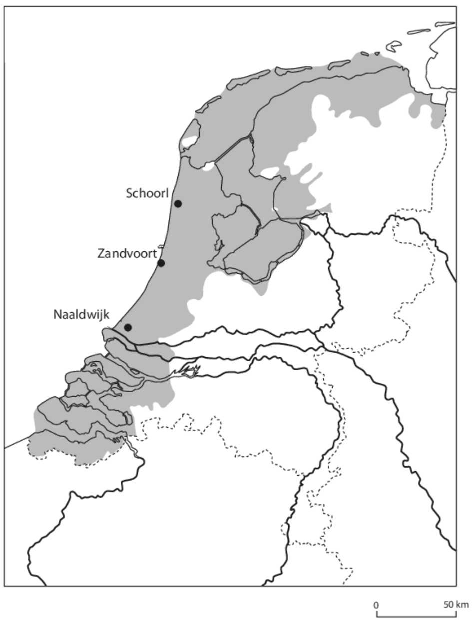

Figure 3.6: Holocene soils [TNO, 2013]

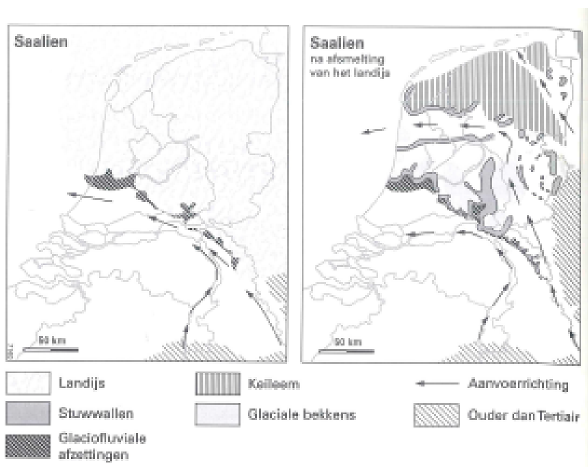

Figure 3.7: Ice-pushed ridges [Berendsen, 2008]

1. The grey area in Figure 3.4 shows the over-consolidated clays in the North. In most areas, dense sand layers are also present. The extension of these deposits is often irregular due to glacial processes.

2. The south border of the grey area in Figure 3.5 shows the part of the Netherlands where ice-pushed deposits can be encountered (at the margins of glacial basins). In these glacial margins, the soil mass is often deformed. Highly variable soil conditions are often encountered, for example in Almere [Spikker, 2010], the Utrechtse Heuvelrug, the Veluwe and Nijmegen.

3. The grey area in Figure 3.6 shows the area in the Netherlands where the Pleistocene soils are overlaid by intra-tidal and river (soft marine) deposits from the Holocene. These soft marine deposits mainly consist of the Formation of Naaldwijk. This is the area where deep pile foundations are used. [Berendsen, 2008]

4. The parts of the Netherlands which were not indicated in one of the Figures (3.4, 3.5 and 3.6) are build up by Pleistocene or even older (Tertiary) soils which are not over-consolidated by glacial processes (e.g. the southern provinces Noord-Brabant and Limburg). The primary formation found in these areas is the Formation of Boxtel [Berendsen, 2008]. For this part of the Netherlands, shallow foundations will generally be of sufficient support.

3.2. History of the CPT

Two main types of CPT are known, one using a mechanical cone penetrometer (see Figure 3.8) and one using an electrical cone penetrometer. Nowadays, the electrical cone penetrometer (see Figure 3.9) is mainly used. However, back in the days (1950-1960), when most CPT based methods for determining the bearing capacity of piles were developed, CPTs were done using a mechanical cone penetrometer.

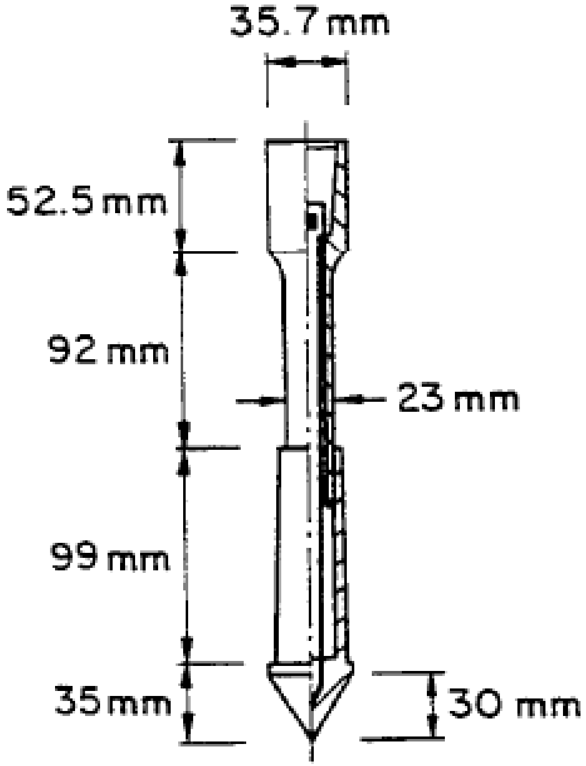

Figure 3.8: Mechanical cone penetrometer [Kulhawy and Mayne, 1990]

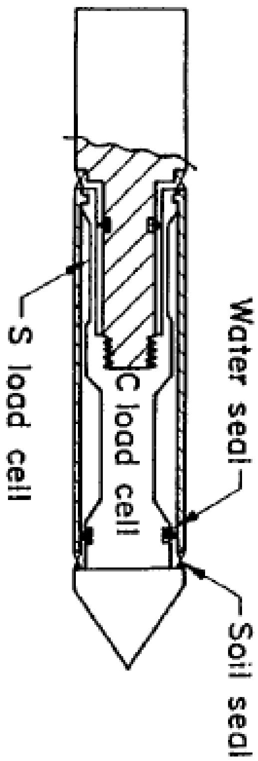

Figure 3.9: Electrical cone penetrometer in which the surface area of the cone is $10cm^2$ or $15cm^2$ [Kulhawy and Mayne, 1990]

The difference between the two types of cones is the way of determining the sleeve friction. The electrical cone uses sensors on the sleeve to directly determine the sleeve friction at a penetration speed of $2cm/s$

[Normcommissie 351 006 ’Geotechniek’, 2017a]. On the other hand, the mechanical cone determines the total resistance and the cone tip resistance. Next, they are subtracted from each other to determine the sleeve friction. In this case, the cone tip resistance is determined by pushing in the cone tip a little more every few centimetres. The sleeve stays behind for a few seconds before following the cone tip. Due to the movement of the mechanical cone, it can suffer from friction losses [Kulhawy and Mayne, 1990].

As the electrical CPT uses direct information, it is more accurate than the mechanical CPT. This might also be one of the reasons the Dutch method for determining the pile tip capacity gives an overestimated value for the pile tip capacity. As mentioned above, the Dutch method was developed using mechanical CPT data. These data (q_c and f_s) are often less accurate for a mechanical CPT, especially in the lower bound of the spectrum (soft soils). Overall, this lack of precision equals out to the same average cone resistance for both electrical and mechanical CPT as both high and low peaks are better detected by an electrical CPT. However, when the end bearing soil layer is a homogeneous sand layer, the values from an electrical CPT can be much higher than those of a mechanical CPT [Kulhawy and Mayne, 1990].

In the present days, mechanical CPTs are sometimes still used in stiffer soils like gravels, but this will not be considered in this thesis.

4

Fundamental Aspects of Pile Foundations

One of the main objectives of this thesis is to improve the understanding of the Dutch method for pile foundations, primarily focussing on the calculation of the pile tip capacity, through analysis of the geotechnical processes which occur around the pile tip. The following fundamental geotechnical concepts and aspects for driven piles will be addressed in this chapter:

- Stress states
- Compaction
- Dilation
- Influences of the failure surfaces
- Residual Loads

After analysing the mechanisms mentioned above, relevant aspects will be incorporated into the numerical models (if technically feasible).

4.1. Stress states

The stress state changes during the different phases of pile installation and pile loading. To improve the understanding of the different stress states, the different phases of pile driving are explained as follows:

Phase 0: the initial phase. This is the phases in which the soil is assumed to be in its initial (virgin) state, in which the following relationships are applicable:

$$\sigma'_{v0} = \gamma' * d \tag{4.1}$$

$$\sigma'_{h0} = K_0 * \sigma'_{v0} \tag{4.2}$$

$$K_0 = 1 - sin\phi' \tag{4.3}$$

σ'_{v0}	: Initial vertical effective stress	(kN/m^2)
γ'	: Effective unit weight of the soil	(kN/m^3)
d	: Depth	(m)
σ'_{h0}	: Initial horizontal effective stress	(kN/m^2)
K_0	: Earth pressure coefficient	$(-)$
ϕ'	: Angle of internal friction	$(^o)$

Phase 0 can be found in Figure 4.1.

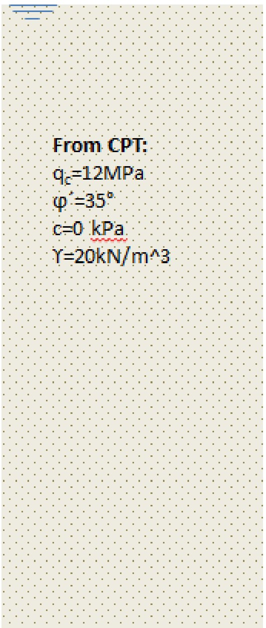

Figure 4.1: Phase 0: Initial phase

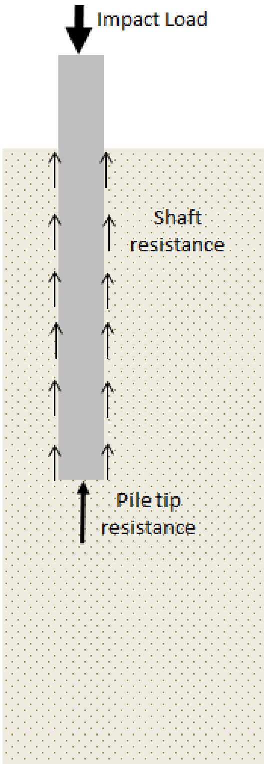

Figure 4.2: Phase 1.a: Installation phase

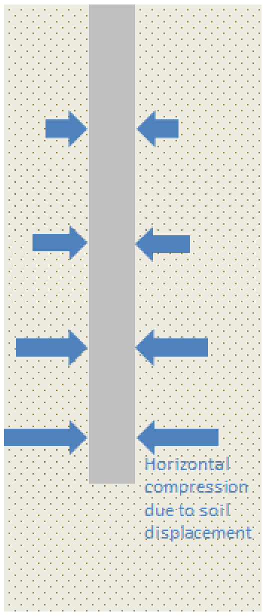

Figure 4.3: Phase 1.b: Horizontal compression phase

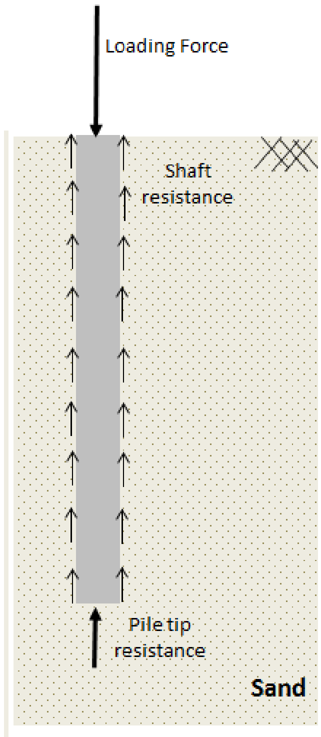

Figure 4.4: Phase 2: Loading phase

Phase 1.a: the installation phase. During pile driving, a repetitive impact load acts on top of the pile (also called pile head). The impact load is a dynamic load and leads to reaction forces in the soil as shown in Figure 4.2. When a homogeneous granular soil is considered, the shaft resistance is formed over the total length of the pile in the soil, while in a cohesive soil the shaft resistance is almost negligible during driving. For non-cohesive soils, excess pore pressures around the pile tip may not fully dissipate in between two hammer blows, due to the dynamic character of the loading. Due to the soil displacement caused by the volume of the pile, the soil is compressed horizontally, this effect is explained in phase 1.b.

Phase 1.b: this phase occurs simultaneously to the installation phase. Due to the soil displacement caused by the installation of the pile, the soil is compressed horizontally. However, as the horizontal compression is relatively essential considering installation effects. Hence, it is mentioned in a separate phase.

Phase 2: the loading phase (static load). A load is applied onto the pile head, which leads to reaction forces in the soil. If residual loads are ignored, the pile reacts as shown in Figure 4.4.

In Figures 4.5 and 4.6, the forces in the soil around the pile tip are illustrated in more detail, using principal stress crosses. Both figures show the formation of radial stresses (stresses directed towards the pile tip) developing around the pile tip during loading. Furthermore, these figures clearly indicate a rotation of the principal stresses around the pile tip when it is loaded up to failure.

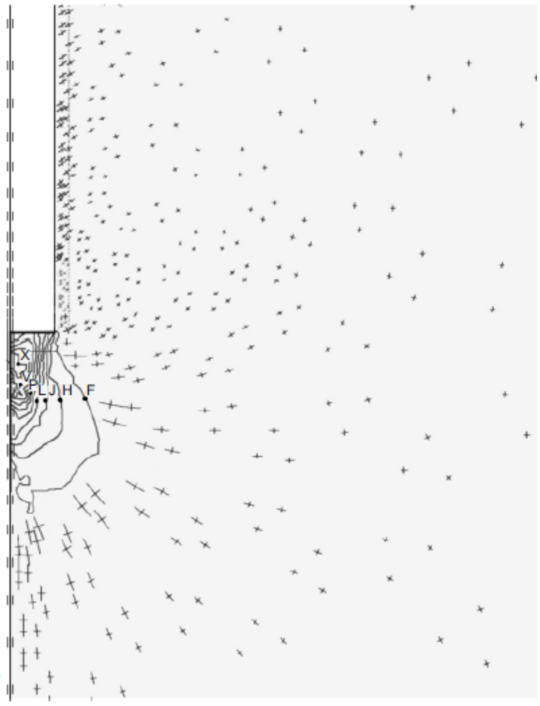

Figure 4.5: Principal stress crosses for phase 1 and 2: Installation and Horizontal compression phase [Broere and van Tol, 2006]

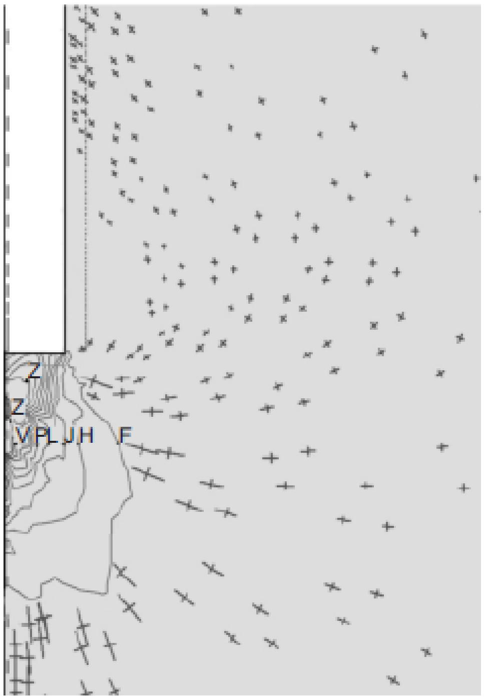

Figure 4.6: Principal stress crosses for phase 3: Loading phase at failure [Broere and van Tol, 2006]

4.1.1. Detail at pile tip

Direct CPT methods are based on the assumption the soil behaviour at failure for a large-scale pile is similar to the soil behaviour around the CPT cone while performing a CPT. With this assumption, the CPT cone can be seen as a small-scale pile test. Many authors, for example,[Arshad et al., 2014], [Silva and Bolton, 2004], have described the soil behaviour around the tip of a CPT cone in more detail. Their interpretation of the soil behaviour around the tip of the cone is used to describe the soil behaviour at the pile tip. Therefore, their results will be discussed in this subsection.

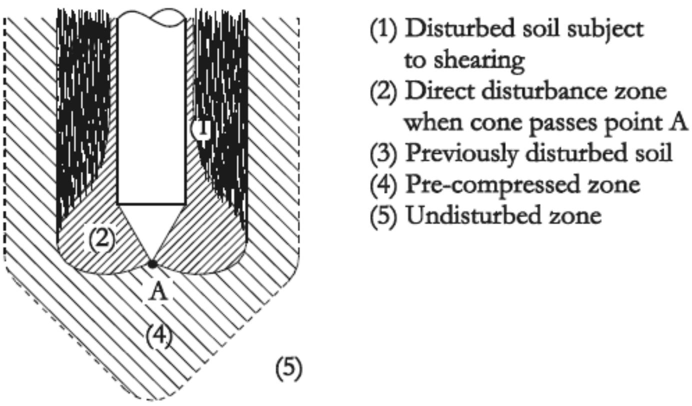

Figure 4.7: Characteristic disturbance zones near pile tip of a cone, i.e. at failure [Silva and Bolton, 2004]

Figure 4.7 shows the different zones of disturbance around the pile tip [Silva and Bolton, 2004].
[Arshad et al., 2014] split up these zones in an axial compression zone, a transition zone and a cavity expansion zone, he used the digital image correlation (DIC) technique to assess these three zones as can be seen in Figure 4.8 and Figure 4.9. Directly below the cone, axial compression dominates. In the cavity expansion zone, almost perpendicular to the cone tip, radial stresses dominate. In between these two zones, the transition zone is found, containing an approximately equal amount of vertical and radial stresses.

Figure 4.9 illustrates the displacements of the soil around the cone tip. The displacements show a changing pattern in which vertical displacements dominate right below the tip in zone 1 to horizontal in zone 4.

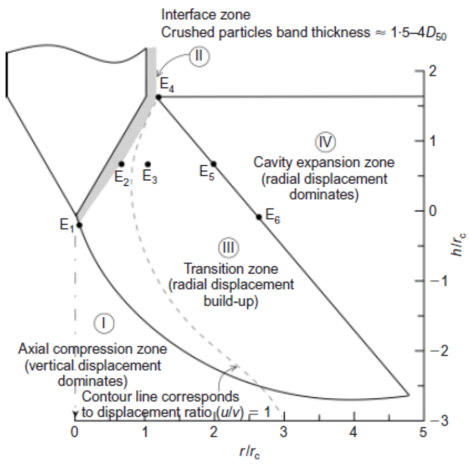

Figure 4.8: Characteristic zones near pile tip of a cone, i.e. at failure [Arshad et al., 2014]

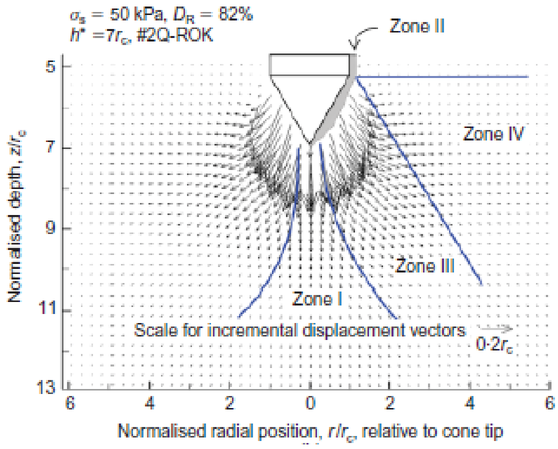

Figure 4.9: Characteristic zones near pile tip of a cone, i.e. at failure [Arshad et al., 2014]

4.1.2. Laboratory testing and in-situ conditions

Figure 4.6 indicates the presence of a sliding plain or failure surface around the pile tip. The shape of this failure surface closely resembles the logarithmic spiral which is expected to form, by for example [van Mierlo and Koppejan, 1952] and [Meyerhof, 1951] like presented in Chapter, 2 at the pile tip during failure.

The stress states along this failure surface vary and can be related to geotechnical laboratory tests, namely, triaxial compression (TC), triaxial extension (TE), direct shear (DS) or direct simple shear (DSS). For sands, direct shear is used [Kulhawy and Mayne, 1990]. Figure 4.10 shows where the same condition, as used in the different lab tests can be found along the failure surface. As shown in Figure 4.7, but also by, e.g. Koppejan [van Mierlo and Koppejan, 1952] and Meyerhof [Meyerhof, 1951] the failure surface extends above the pile tip. This is shown in Figure 4.11.

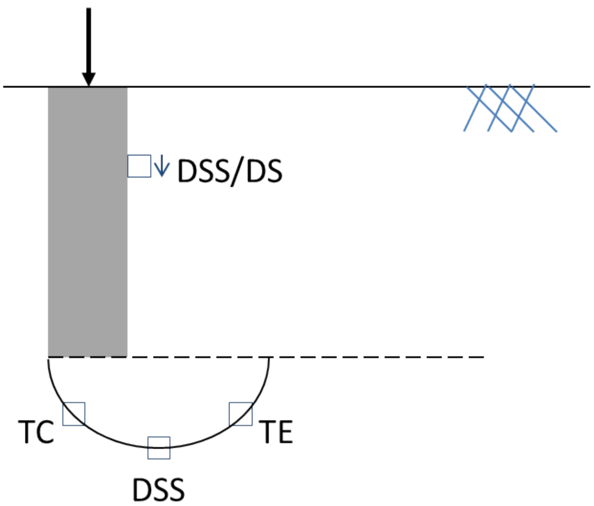

Figure 4.10: Laboratory test conditions along failure surface [Kulhawy and Mayne, 1990]

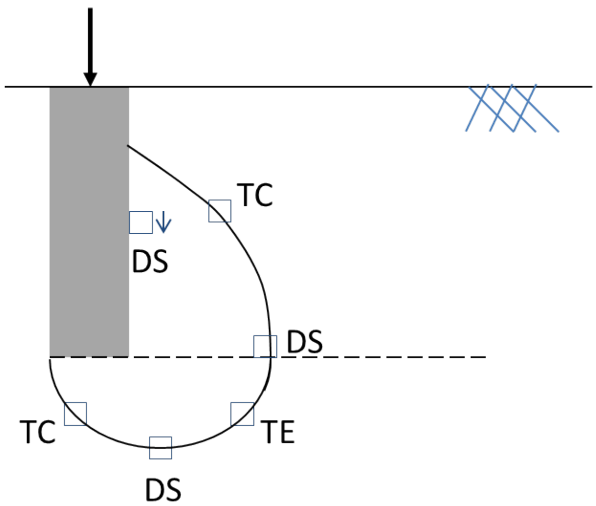

Figure 4.11: Laboratory test conditions along failure surface (when pile is loaded) extended above pile tip level

Figure 4.11 indicates a zone within in the failure surface where both shaft friction and pile tip capacity are taken into account.

According to [Normcommissie 351 006 'Geotechniek', 2017a] half of the bearing capacity at the pile tip is mobilised below the pile tip ($q_{c,IandII}$) and the other half in de range of 8D above the pile tip ($q_{c,III}$). However, this would mean the soil is accounted for twice in the zone 8D above the pile tip as it contributes to the pile tip capacity and to the shaft friction, which is not possible. Probably one of the two mechanisms dominates, making it impossible for the other mechanisms to mobilise fully.

In CUR 229 [CUR B&I, 2010] the measured shaft friction seems to agree with the calculated shaft resistance. This would mean the pile tip resistance is not fully mobilised in a section of 8D above the pile tip. Both the analyses and the geotechnical aspects introduced in the numerical model can be found in Chapter 5.

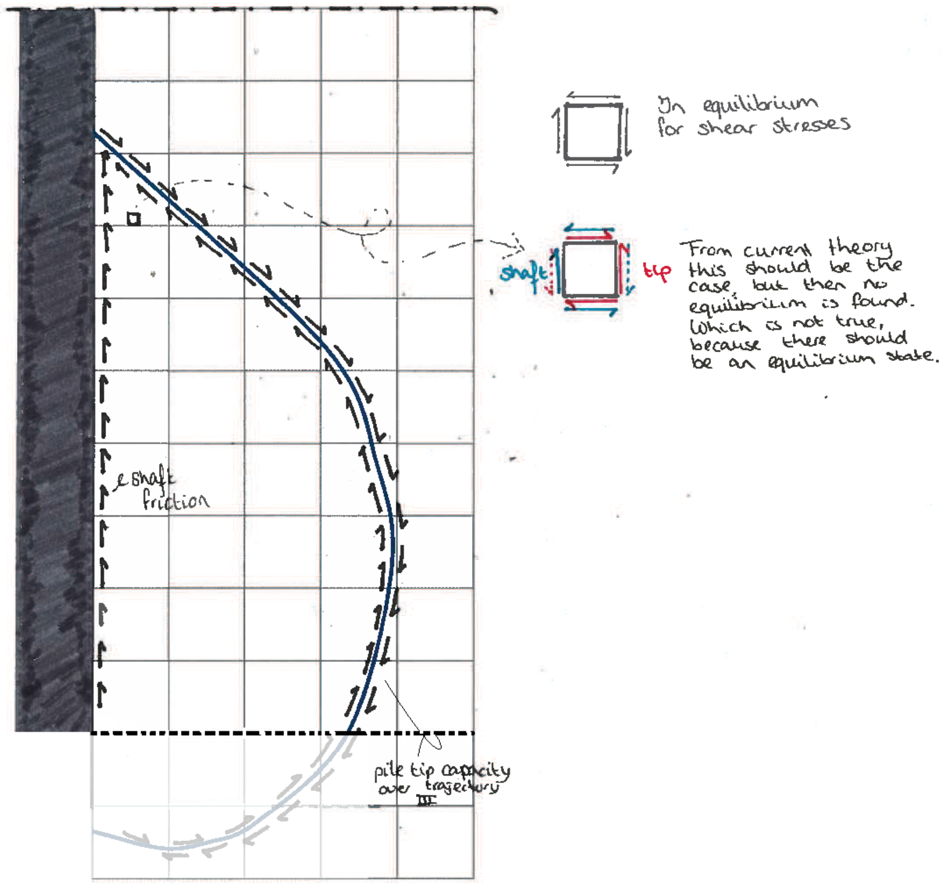

Figure 4.12: Shear stresses working within the zone limited by the logarithmic spiral

4.2. Compaction

The horizontal compression of the soil due to the driving process has briefly been discussed in Section 4.1, in this section, it will be elaborated a bit more. This compression is generated because the volume of the pile displaces the soil during installation. This soil displacement can also be seen as compaction.

In principle, α_p is said to be a pile class factor, see Section 2.1.2. However, when taking a close look, it seems to be a factor taking into account the installation effect. The factor reduces if less compaction occurs due to the installation process. For example, according to the 'old' code, for driven piles (a lot of compaction) $\alpha_p = 1$. On the other hand for bored, cast-in-place piles (less compaction) $\alpha_p = 0.8$. The values according to the new code (including the reduction of α_p of 30%) can be found in Appendix A.

The 'old' α_p factor for driven piles is 1. I.e. the installation of driven piles gives a similar soil response as pushing a CPT cone into the soil, especially considering the amount of compaction. However, this compaction is introduced with the installation process. As the installation process cannot be modelled in PLAXIS this might cause a lack of accuracy. To implemented the compaction of the soil several methods can be considered for example procedure designed by [Broere and van Tol, 2006]. This will be discussed in more detail in Chapter 5.

4.3. Dilation

Dilation is the movement of the soil grains from a dense state to a loser state during shearing illustrated in Figure 4.13.

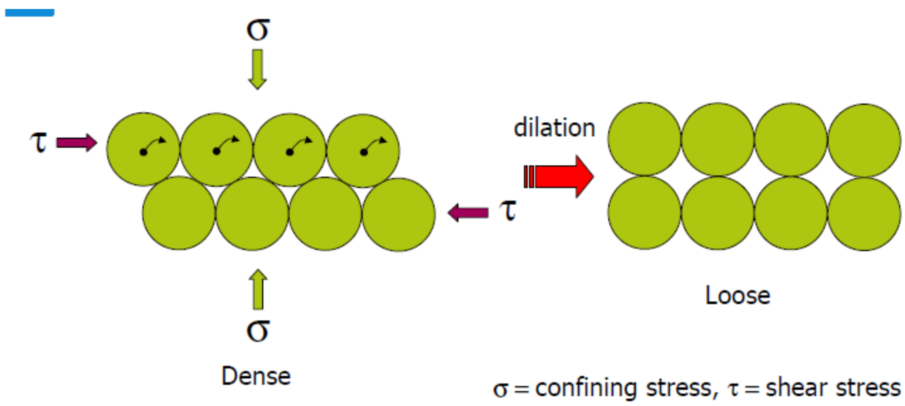

Figure 4.13: Dilative behaviour under drained shearing conditions [Hicks, 2015]

Dilative behaviour is influence by both relative density and stress state. It is often mistaken that dilation only depends on relative density [Bolton, 1986] i.e. if the soil is in a dense state it dilates and if it is in a loose state it compacts. This is not true. Figure 4.14 shows a situation in which a dense soil will not dilate due to relatively high confining pressures. In this case, the soil particles will not be able to roll over the other soil particles and dilation will not occur.

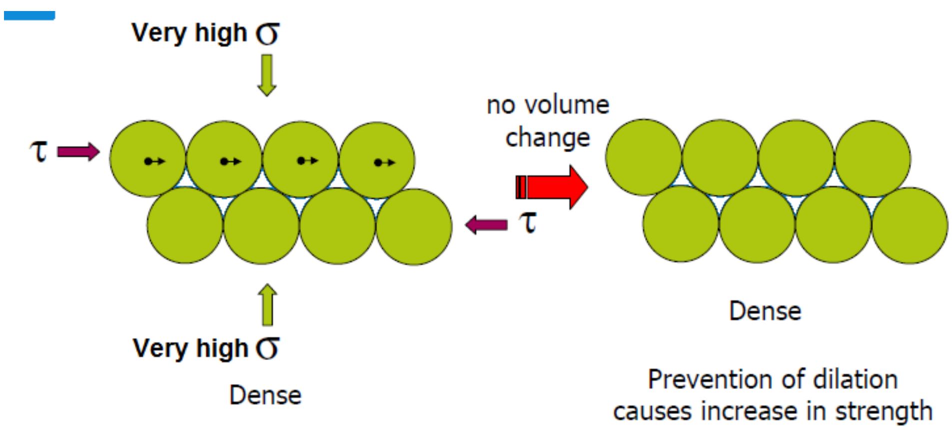

Figure 4.14: 'Dilative' behaviour under high pressures, adapted from [Hicks, 2015]

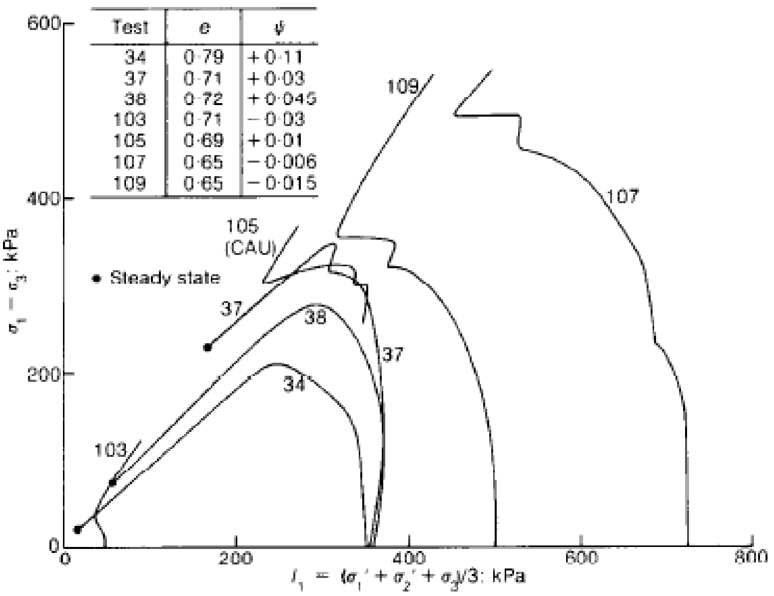

Figure 4.15: Undrained stress path for same sand at different void ratios [Been and Jefferies, 1985]

Figure 4.15 shows the stress paths for the same sand at different void ratios. Void ratio and relative density are proportionally correlated. The void ratios for tests 37 and 103 are the equal, but test 103 shows dilative (peak) behaviour while test 37 does not. That is why the state parameter (ψ) is introduced. ψ takes into account both the relative density (or void ratio) and the stress conditions. ψ is defined as follows:

$$\psi = e - e_{cv} \tag{4.4}$$

$$R_e = \frac{e_{max} - e}{e_{max} - e_{min}} \tag{4.5}$$

$$R_e = 0.34 * ln\left(\frac{q_c}{61 * (\sigma'_{v0,z})^{0.71}}\right) \tag{4.6}$$

Combining equation (4.4) by [Been and Jefferies, 1985], (4.5) by [Verruijt, 2012] and (4.6) by [Lunne et al., 1997] results in:

$$\psi = -0.34 * \frac{e_{max} - e_{min}}{e_{max} - e_{cv}} * ln\left(\frac{q_c}{61 * (\sigma'_{v0,z})^{0.71}}\right) \tag{4.7}$$

Now, ψ can be calculated using CPT data and disturbed soil samples. There is no need to prepare undisturbed soil samples as e_{cv} is independent of relative density and stress state. This also means e_{cv} can be determined in a triaxial test or shear box test at any confining pressure.
ψ is a measure to determine if the non-cohesive soil will act dilative or compressive. Several authors, [Hicks, 2015] and [Been and Jefferies, 1985] give ranges for this. These ranges are set out in Table 4.1.

-0.20	≤	ψ	≤	-0.10	major dilative behaviour
-0.10	≤	ψ	≤	-0.05	dilative behaviour
-0.05	≤	ψ	≤	0	minor dilative behaviour
0	≤	ψ	≤		compressive behaviour

Table 4.1: Ranges for ψ according to [Hicks, 2015]

The above is explained, as dilatancy causes peak (or softening) behaviour of the soil. When driving the pile, or loading it up to failure, it is assumed dilatancy will occur as the shear forces are relatively high during these processes, if possible this should be taken into account in the FEM models, see Chapter 5.

4.4. Failure surfaces

As already briefly pointed out in Chapter 2 and Section 4.1 the failure surface close to the pile tip has a logarithmic shape. Several different authors, Meyerhof [Meyerhof, 1951], Koppejan [van Mierlo and Koppejan, 1952], Prandtl [Prandtl, 1921] and Terzaghi [Terzaghi, 1943], describe a logarithmic shaped failure surface around the pile tip in a homogeneous soil.

Out of all these authors, Prandtl [Prandtl, 1921] was the first to consider this logarithmic shaped failure surface for shallow foundations. Prandtl's approach is a generally accepted approach to calculate the bearing capacity of shallow foundations. Terzaghi adapted Prandtl's theory for slender foundations like shown in Figure 4.17. Both Terzaghi and Prandtl based their theory on a homogeneous soil layer, such a soil layer is almost never found.

Prandtl was the first to consider the logarithmic shape of failure. However, he based his theory on shallow foundations. Many authors, [Lehane et al., 2005], [Bustamante and Gianeselli, 1982], [Lunne et al., 1997] and [van Mierlo and Koppejan, 1952] recognised, the full logarithmic spiral (Figure 4.18) is a better approach to reality for a slender foundation. The details of the logarithmic spiral adapted by Koppejan can be found in Chapter 2.

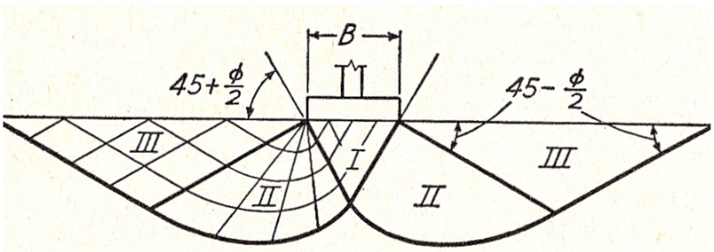

Figure 4.16: Failure surface underneath a shallow foundation according to Prandtl [Prandtl, 1921]

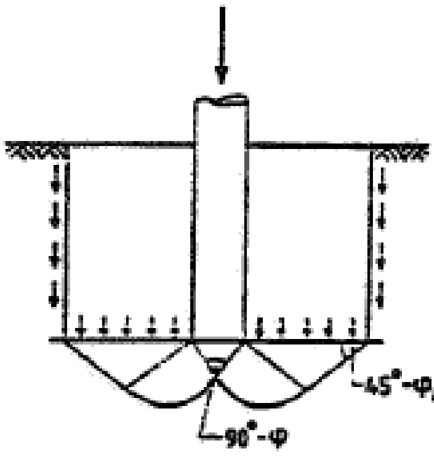

Figure 4.17: Prandtl's failure surface adjusted by Terzaghi [Terzaghi, 1943]

The main factor of influence for the logarithmic spiral is the angle of internal friction (ϕ'). However, ϕ' is stress dependent and therefore the depth of the pile tip and stress conditions around the pile tip play an important role in the size of the failure surface as well. Several ways to determine ϕ' (based on CPT data) are set out in Appendix F.

To summarise, the shape and extent of the failure surface are influenced by the following aspects:

- ϕ' (at the given stress state)
- Vertical effective stress as function of depth
- Interface between different soil types
- 2-layered profile

The aspects as mentioned above are discussed in slightly more detail in the coming subsections.

4.4.1. Influence of the Angle of Internal Friction

If the logarithmic spiral is set out for different ϕ' like explained in Chapter 2, the boundaries for the 4D/8D method can be found. Figure 4.18 and Figure 4.19 show the logarithmic spirals for ϕ' varying between the theoretical minimum 0^o and 50^o. The minimum is 0^o for cohesive soils and the maximum is set to 50^o which can be the case for gravels. The smallest vertical distance below the pile tip is found at $\phi' = 0^o$ and equals $0.7D_{eq}$ (D_{eq} is the equivalent pile diameter). The largest vertical distance below the pile tip is found at $\phi' = 50^o$ and is equal to $4D_{eq}$. For this reason, the trajectory over which $q_{c,I}$ and $q_{c,II}$ are calculated is set to a range between $0.7D_{eq}$ and $4D_{eq}$, see Subsection 2.1.2. It seems fair to consider the trajectory which gives the lowest $q_{c,I}$ value, because a decreasing friction angle results in a decrease in strength of the soil, and therefore a lower bearing capacity. With a decreasing friction angle, the vertical distance over which the failure surface extends declines as well, so fewer shear stresses will be mobilised.

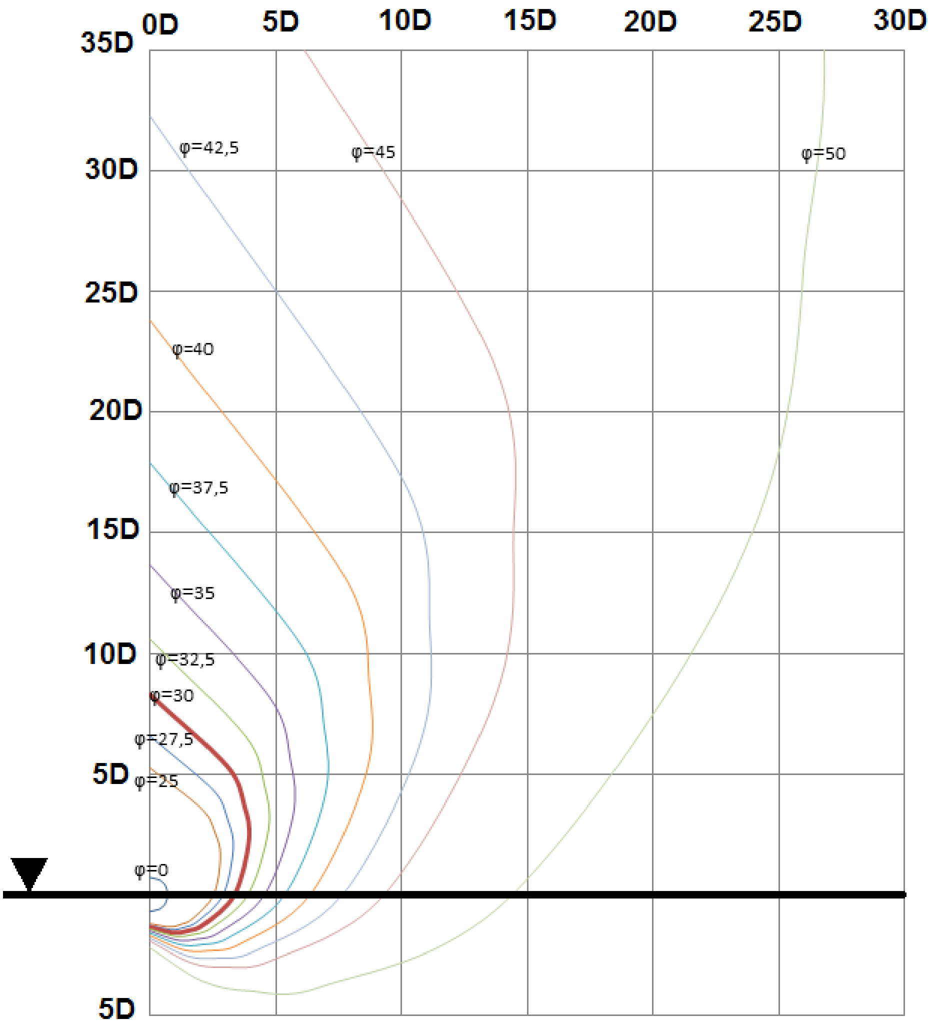

Figure 4.18: Koppejan's failure surface for a range of $0^o \leq \phi' \leq 50^o$

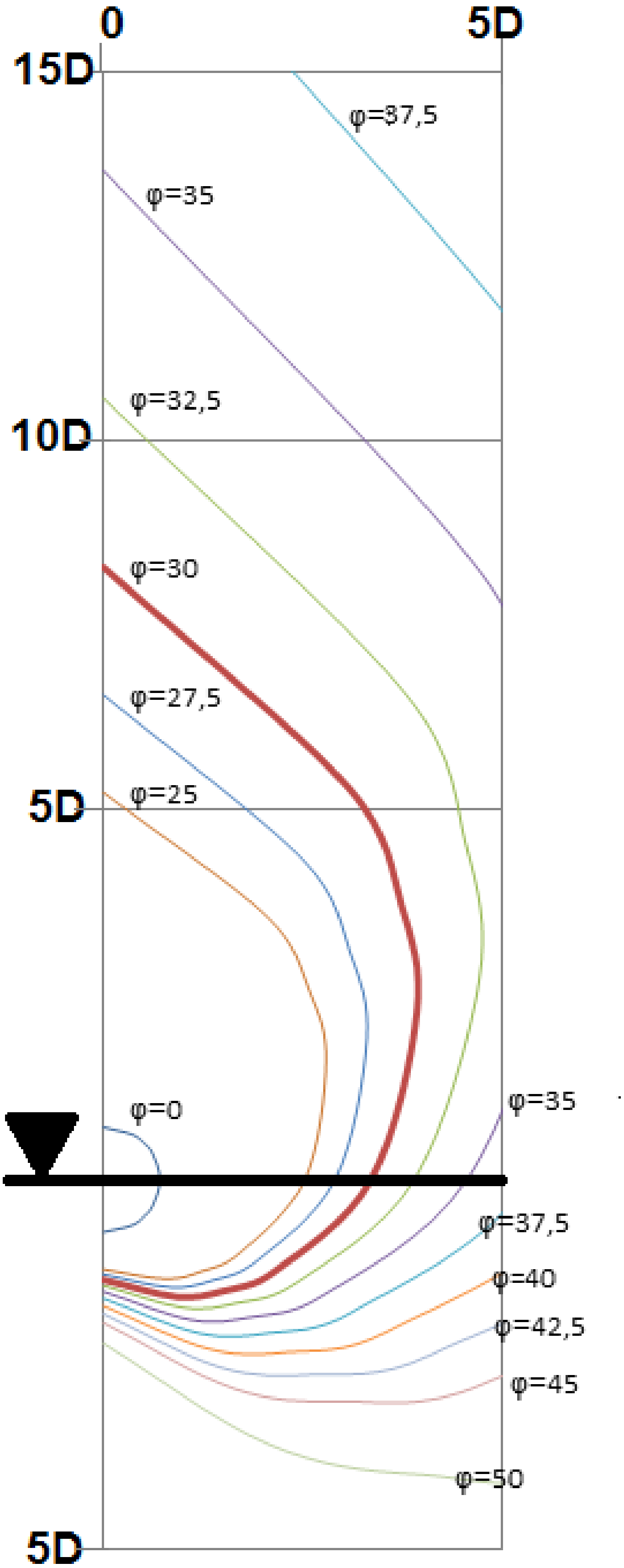

Figure 4.19: Detail Koppejan's failure surface for a range of $0^o \leq \phi' \leq 50^o$

The 4D range is chosen in a well-substantiated manner. However, from Figure 4.18 the 8D range is not as substantiated as the 4D range. For $\phi' = 30^o$ the upper bound of the failure surface is approximately 8D. It is noticed that $\phi' = 30^o$ lies within the range of values for granular soils in the Netherlands according to table 2.b [Normcommissie 351 006 'Geotechniek', 2017a]. However one has to bear in mind the values, which are given in this table (which can be found in Appendix A), are low characteristic values. These values are intended for both calculation of the ultimate limit state and the serviceability limit state and do not represent a mean value, but a low characteristic value. Furthermore, it is noticed that the extent of the failure surface should be calculated using the constant volume friction angle, as the strains around the pile tip will be significant during loading up to failure [Engin, 2013] (Figure 4.20).

Figure 4.20 also shows a curve with dilative behaviour. From the curves in this figure, it can be seen the pressure is an important factor when considering dilative or softening behaviour. This was already concluded when explaining the state parameter in Section 4.3. Although the state parameter is not used to conduct calculation in this thesis, it is important to note that the state parameter influences the softening behaviour and takes into account both the stress states and the relative density. Using the state parameter in future research might give a better insight into the softening behaviour.

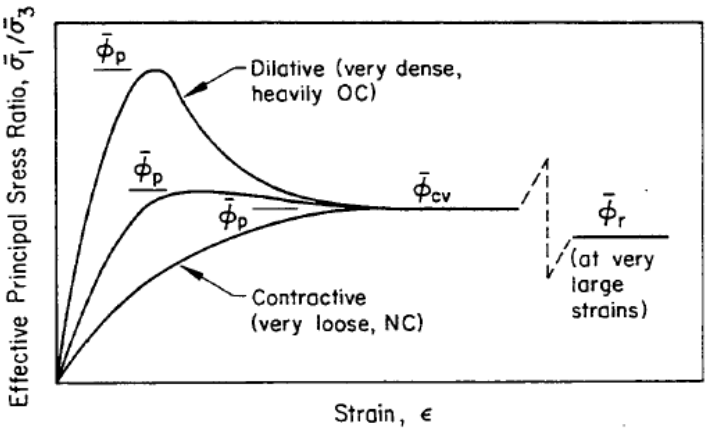

Figure 4.20: Several stages of ϕ on the σ,ϵ-curve [Kulhawy and Mayne, 1990]

4.4.2. Influence of Depth

As ϕ' is stress dependent, the depth of the pile tip level will influence the size of the failure surface. Figure 4.21 (not to scale) shows an approximation of the two failure surfaces at different depths.

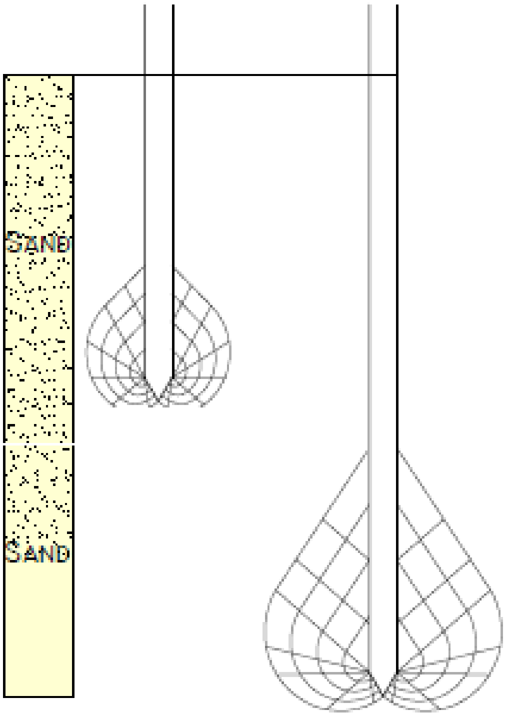

Figure 4.21: Influence of depth adapted from [van der Linden, 2016]

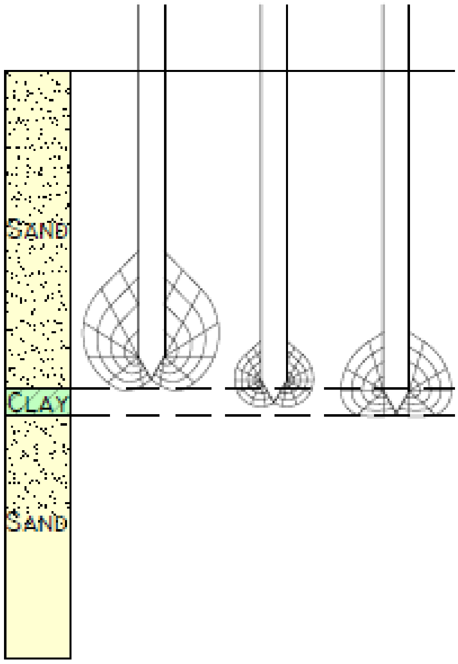

Figure 4.22: Influence of an interface adapted from [van der Linden, 2016]

4.4.3. Influence of the interface between two soil types

The interface between two different soil types is a weak part of a soil profile, through which failure surfaces can propagate more easily. This is indicated in Figure 4.22, as the failure surface does not go through the interface but along the interface as the pile tip approaches it.

4.4.4. Influence of 2-layered soil

If a cohesive soil layer overlies the non-cohesive end-bearing soil layer, the friction angle between the two layers will most likely be different (lower for cohesive soils). As can be seen in Figure 4.18 and Figure 4.23, the logarithmic spiral becomes almost circular for cohesive soils. The change between the failure surface at the boundary of a cohesive and a non-cohesive soil is displayed in Figure 4.23.

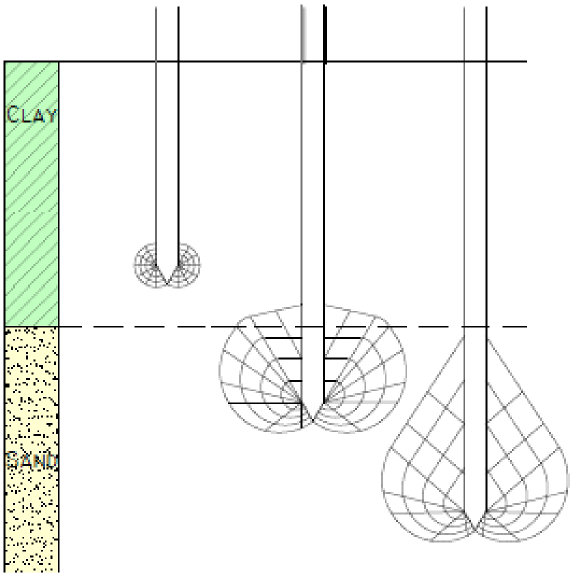

Figure 4.23: Influence of a 2-layered soil adapted from [van der Linden, 2016]

Figures 4.21 to 4.23 are based on the analytical approach of [van Mierlo and Koppejan, 1952] and are expected to suffice for all different stress states, soil properties and strains which are expected to occur around the pile tip. The actual soil behaviour is more complicated, and difficult to expose directly through field or laboratory tests. Present-day numerical methods using advanced constitutive models can give a better insight in the complex soil behaviour. Chapter 5 gives an in-depth analysis using FEM models to analyse the previously mentioned influences.

4.5. Residual Loads

The residual load is an often ignored load that is generated in the pile due to the pile driving process. Regarding this residual load, [Fellenius, 2015] states the following:

"Residual load (also called residual force or locked-in force) in a pile is the axial force present in a pile at the outset of a static loading test."

For driven piles, it is usually assumed the stress state in the axial direction of the pile after installation is zero. However, when residual loads are taken into account, this is not the case. In other words, residual loads influence the pile tip capacity and the shaft resistance. This influence and the way residual loads are generated is explained in Figures 4.24 to 4.30 and their guiding text.

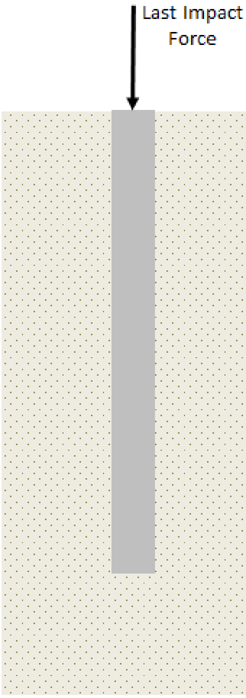

Figure 4.24: Step 1: Last Impact

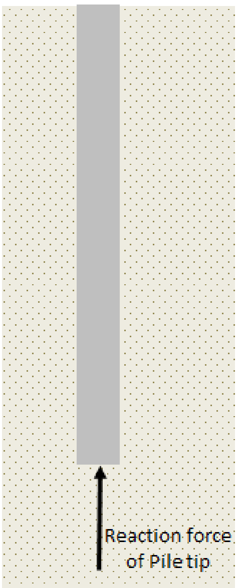

Figure 4.25: Step 2: Reaction pile tip

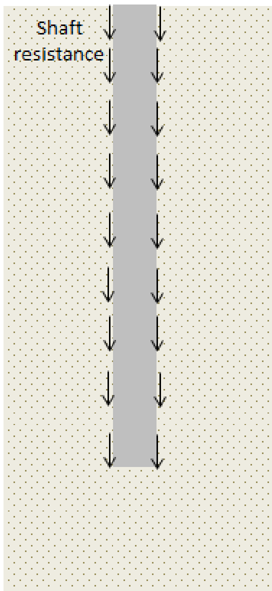

Figure 4.26: Step 3: Reaction pile shaft

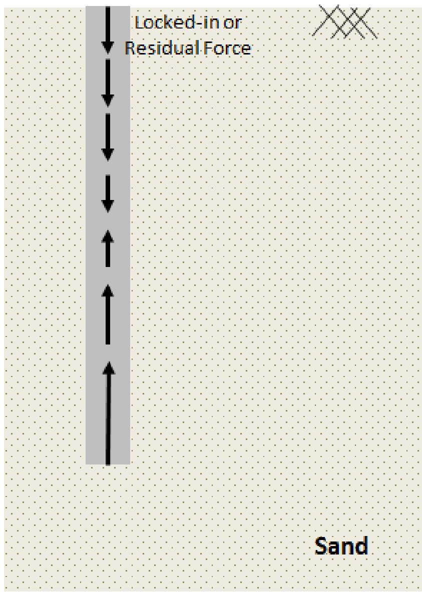

Figure 4.27: Step 4: Residual Load in the pile

Step 1: The development of residual loads starts with the last impact of the driving process. This is shown in Figure 4.24.

Step 2: Due to the last-impact-load (see Step 1), the soil produces a reaction force at the pile tip as shown in Figure 4.24.

Step 3: The reaction force at the tip and the energy stored in the elastic shortening cause the pile to rebound. A new equilibrium is reached as a counteracting force is formed. This counteracting force is formed along the shaft and is directed downwards, in a similar fashion as a pile subjected to a tensile loading. This is shown in Figure 4.26.

Step 4: As a result of Step 2 and 3, the so-called residual load is trapped within the pile (Figure 4.27).

Step 5: In Step 5, the pile is subjected to a static load as illustrated in Figure 4.28.

Step 6: Due to the loading of the pile, the pile tip and shaft will develop reaction forces as shown in Figure 4.29.

Total: Combining all the above steps results in a loading scheme, which is presented in Figure 4.30. Adding the residual load (Step 4) to the shaft friction and pile tip capacity (Step 6) results in Figure 4.31.

According to[Fellenius, 2015], the residual load is a force locked inside the pile i.e. an axial force in the pile as shown in Figure 4.27. However, as contributed by the supervising committee of this thesis, Figure 4.31 is more representative of the distribution of the residual load and the reaction force of the soil due to the loading and driving of the pile.

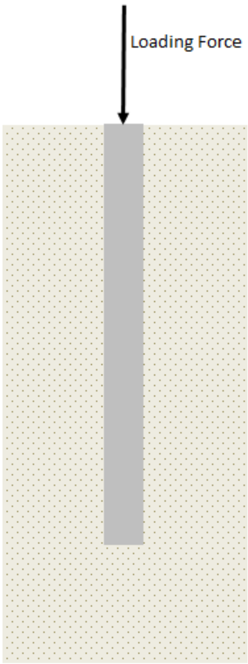

Figure 4.28: Step 5:
Static Loading

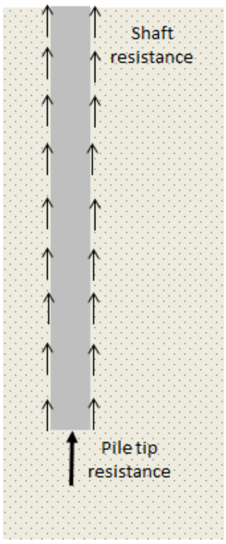

Figure 4.29: Step 6:
Reaction Forces

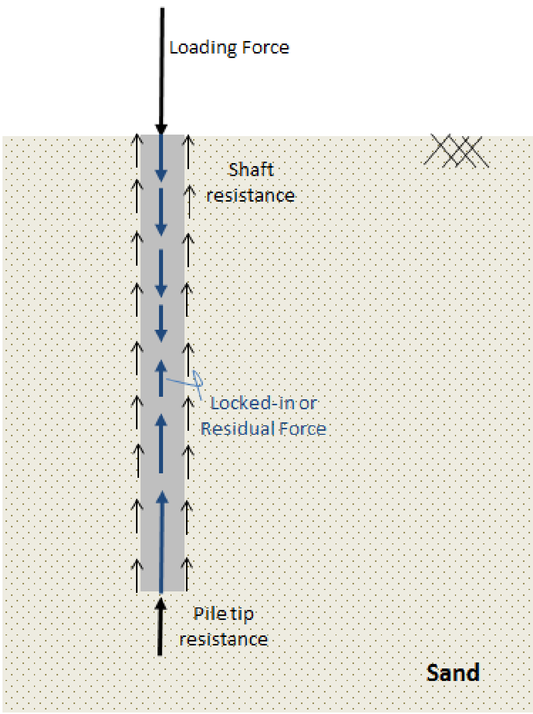

Figure 4.30: Total of force acting on the pile during loading (displaying residual load)

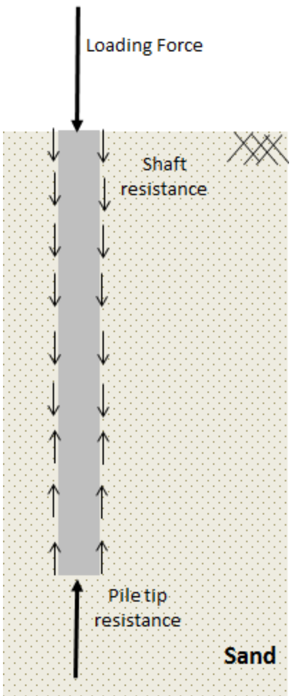

Figure 4.31: Total of force acting on the pile during loading

To summarise the above steps, the residual load at the pile tip is direct upwards, which is similar to the soil response at the pile tip during loading. Therefore, the total tip resistance should be seen as the residual load plus the pile tip resistance during loading.
In contrast to this, the shaft resistance due to the residual loads mechanism is directed downwards, i.e. negative shaft friction, while loading a pile, positive shaft friction is generated (directed upward). This results in

a total shaft resistance with a magnitude of the measured shaft resistance minus the shaft resistance due to residual loads.
This can also be expressed in Equations (4.8) and (4.9).

$$q_{b,total} = q_{b,measured} + q_{b,residual} \tag{4.8}$$
$$q_{s,total} = q_{s,measured} - q_{s,residual} \tag{4.9}$$

The above-explained steps consider a stiff response of the soil. Figures 4.32 and 4.33 show the difference in the distribution of the residual loads in a pile for a stiff (stiff soils) and flexible (soft soils) soil response. For the flexible response, shown in Figure 4.32, it can be seen no force at the pile tip is developed. This is due to the fact the rebound response (explained in Step 3) of cohesive soils is smaller than for non-cohesive soils.

Figure 4.33 shows the residual load, the measured load in a pile and the (so-called) true load distribution in a pile installed in a stiff soil. In this case, a significant residual load does develop at the pile tip. Figure 4.33 also illustrates that the (so-called) true force distribution in the pile is the sum of the residual load and the measured load. If the pile test is analysed assuming a stressless state in the pile at the beginning of loading, residual loads are neglected and the (so-called) true load distribution cannot be determined.

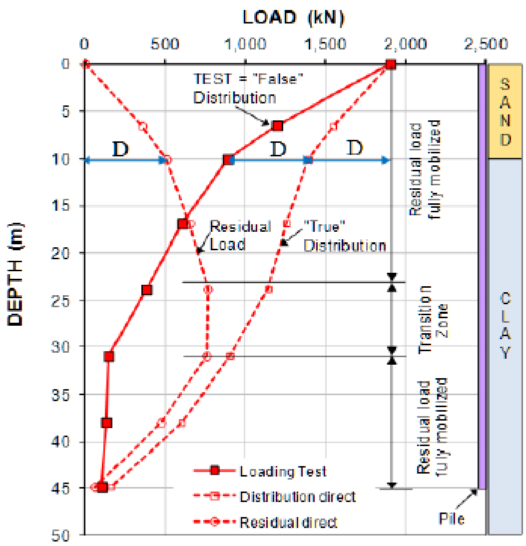

Figure 4.32: Load distribution in pile in clay [Fellenius, 2015]

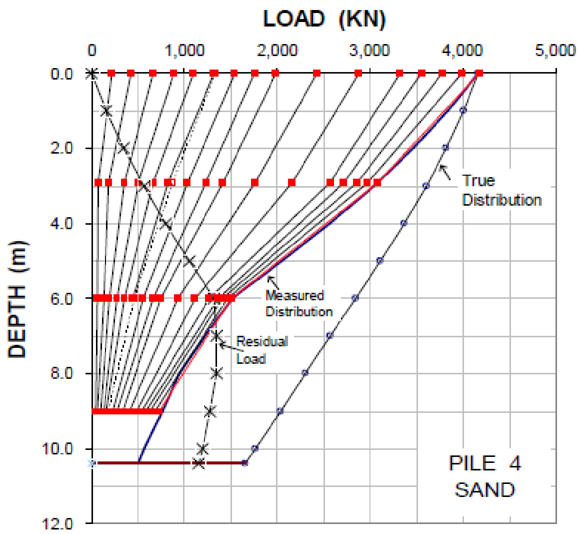

Figure 4.33: Load distribution in pile in sand [Fellenius, 2015]

From Figures 4.32 and 4.33 it was evaluated, the total (or 'true') resistance of the pile is a sum of the residual loads and the measured resistance. Figure 4.34 illustrates the shaft, toe and total resistance including and excluding the residual load, respectively depicted in the red and green curves, in more detail. Considering the toe resistance, Figure 4.34 shows that the toe resistance at 10%D (in this case 60 mm) movement of the pile tip (failure according to NEN 9997-1 [Normcommissie 351 006 'Geotechniek', 2017a]) is larger when residual loads are taken into account. The opposite is true for the shaft resistance. At 10%D movement of the pile tip, the shaft resistance, for the case including residual loads, is smaller than the measured shaft resistance. In other words, if residual loads are not taken into account the toe resistance is underestimated, and the shaft resistance is overestimated.

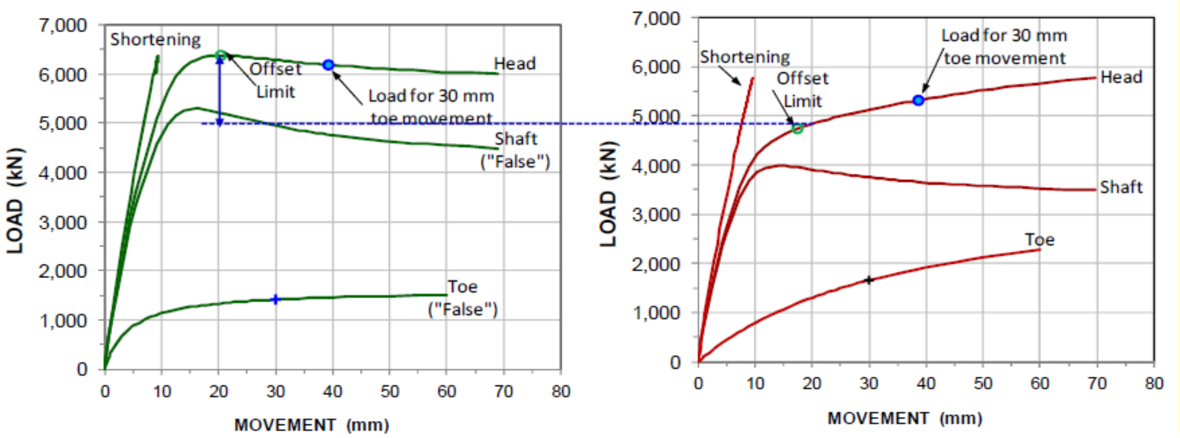

Figure 4.34: Load,movement-curve: green) excluding residual load, red) including residual load [Fellenius, 2015]

Additionally, it is important to conclude that the total bearing capacity at 10%D movement of the pile tip is almost the same for the red and the green curve (respectively including the residual loads and excluding the residual loads).However, if residual loads are taken into account the total load,displacement-curve moves up to failure more gradually than the total load,displacement-curve for the case in which residual loads are not considered. In other words, if residual loads are not taken into account, the final bearing capacity is reached at less pile tip displacement (movement), as the stiffness of the soil response suddenly drops, instead of gradually for the case in which residual loads are considered.

Although the total bearing capacity is similar for both cases (including and excluding residual loads), the sudden drop in stiffness for the case of no residual loads is an indicator of why residual loads should be considered in more detail, especially when it is assumed the 10%D failure criterium is true.

The correct monitoring of the stresses directly after installation and right before the load test can be complicated. However, it is not impossible, for example, O-cells or optic fibre sensors can be used to measure the load at the pile tip or the strain in the pile tip respectively. These techniques are expensive and time consuming and therefore, almost no data can be found regarding the residual load.

Although almost no literature was found on calculating or simulating residual loads, it can be concluded from the above that residual loads do contribute to the pile-soil behaviour significanlty and therefore, they should be taken into account. This thesis tries to implement residuals loads into numerical models using the following conceptual idea of residual loads at the pile tip and how they can be applied in this thesis:

1. The residual load can be seen as the still present load in the soil underneath the pile tip when performing an unloading-reloading cycle. In Figure 4.35, this is the difference in pile toe resistance between point II and O. In this figure, path O-X is the 'virgin' loading during the last impact of the driving process, (see Figure 4.24).

2. Directly after the last hammer blow, unloading starts. This is displayed by stress path X-II (see Figure 4.25).

3. When reloading starts, (actual loading of the pile, Step 5) the stress path has its origin in II and extends towards Y, passing X. While passing through X the steepness of the curve changes. This is caused by the fact that reloading response is usually stiffer than the virgin loading response.

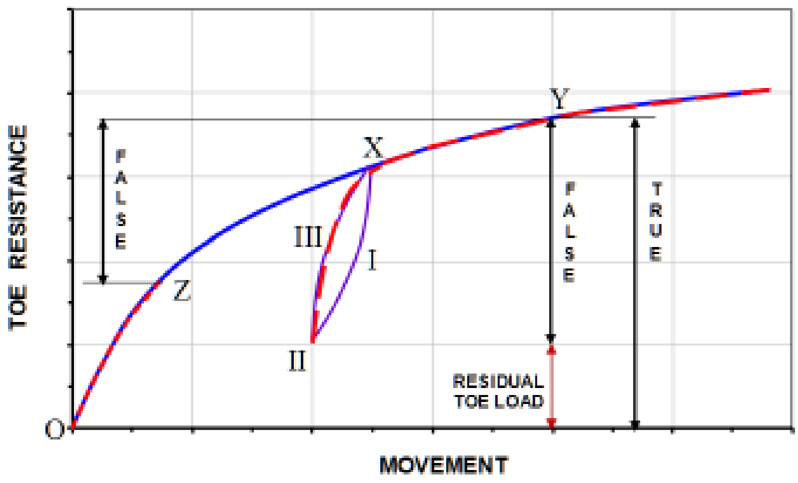

Figure 4.35: Unloading/Reloading curve and residual loads for pile tip[Fellenius, 2015]

With the above-mentioned conceptual idea, numerical models like PLAXIS should be able to integrate and calculate the residual load. This is elaborated in Chapter 5.

4.6. Synthesis

In the beginning of this chapter, it was already mentioned, several fundamental geotechnical aspects of the pile foundation practice are discussed and the relevant aspects will be taken into account in the FEM analysis of this thesis. To conclude from the above-discussed aspects, the following will be considered in the FEM modelling:

- Horizontal compression using a method designed by [Broere and van Tol, 2006].
- Dilatancy or peak behaviour through the Hypoplastic model.
- Residual loads through the conceptual idea developed in this thesis.
- (Stress states, automatically done by the FEM model).
- Influence of depth, interface between two soil layers and a 2-layered soil on the failure surface around the pile tip.
- The interaction between the shaft friction and the pile tip capacity, considering the following:

5 Numerical Modelling

For the readability of this thesis, failure is defined as the load step for which PLAXIS cannot stabilise anymore and stops calculating. If failure is defined otherwise, for example as a movement of the pile tip of 10%D, it is mentioned in the specific context.

From previous chapters, it became clear that the 4D/8D might not be as accurate as assumed. Therefore, this chapter analyses the following aspects through numerical models:

- Residual loads
- Installation depth
- Zone of influence around the pile tip
- Limiting values

5.1. Constitutive Model Selection

This thesis aims to improve the understanding of the geotechnical processes that occur around the pile tip during loading. It focusses on the Dutch method and so, the soils commonly encountered in the Netherlands are considered. To be able to get a better understanding of the complex soil behaviour, numerical models are used. Different constitutive models can be used to model the behaviour of the different soils.

When choosing a constitutive model, one has to bear in mind the granular soil is most important considering pile foundations in this thesis. In the first place, the constitutive model should be able to give an accurate representation of the soil-pile interaction in the non-cohesive soil. Secondly, it should be able to model all installation effects correctly.

To obtain useful results, the constitutive model used for the non-cohesive layer must be highly accurate. The constitutive model used for the cohesive layer is less important. Hence the soft soil layer is modelled using Mohr-Coulomb constitutive model (see Appendix G.1 for a more extensive explanation). This simple model gives a proper first estimation of the soil behaviour. As the non-cohesive soil does not contribute much to the soil-pile interaction, this model is adequate.

For the granular soil layer, the following two constitutive models are considered:

- Hardening Soil model (HS)
- Hypo plasticity model (HP)

These constitutive models are not able to model large strain behaviour, like the installation process. Therefore, the installation effects should be implemented with good care to create a representative model.

The HS model has relatively straightforward parameters and takes into account unloading/reloading response reasonably well. The HS model is often used in the engineering practice, and so good correlations between CPT and the HS parameters are available.
The main drawback of the HS model is that softening or peak behaviour cannot be modelled and the soil reacts stiffer than in reality [Brinkgreve, 2017].

In Chapter 4 it is argued, peak behaviour will play an essential role in modelling the installation effects and the loading of the pile. Therefore, it should be taken into account in the FEM models used in this thesis. As this is not done in the HS model, the HP model is taken into consideration, as it does take into account the peak behaviour of granular soils. On the downside, the HP model does not take into account an accurate unloading/reloading response if the small strain HP parameters are not taken into account.

It is difficult to determine the HP parameters, and it is even more challenging to determine the small strain HP parameters. The small strain parameters require advanced laboratory testing (cyclic triaxial, cyclic shear and biaxial tests) and could not be determined for the purpose of this thesis. As the HP model is not used frequently in engineering practice, only a few reference datasets are found. However, these datasets are for soils which have a completely different geological history from the Dutch soils, so they cannot be used in this thesis.
Although the HP model lacks accuracy regarding the unloading/reloading response, it is selected for this thesis, because including the softening behaviour is considered to be more important. More detailed information on both the HS and the HP model can be found in Appendix G.1.

5.2. Boundaries and Limitations of the Model

All numerical models require correctly set limitations and boundaries. Additionally, the model should be constructed in such a way the calculation time is limited. In this thesis, a single pile is considered.

5.2.1. Model Dimensions

As single piles give a symmetrical response, the pile is modelled in an axis-symmetrical model, which also captures the 3D behaviour of the soil-pile response. This means, only half of the pile is modelled. The pile radius is 0.1775 m (half of 0.355 m which is equivalent to the piles used for validation), and the penetration depth of pile varies per model. These models will be explained further on in this section.

5.2.2. Geometry of the Model

Furthermore, the boundaries are set in such a way that they do not (significantly) influence the outcome. This is accomplished by setting the boundaries at an appropriate distance from the pile shaft and tip. The lower boundary is fixed in displacement both vertically and horizontally, whereas the side boundaries are only fixed in a horizontal way. The top boundary is not fixed.

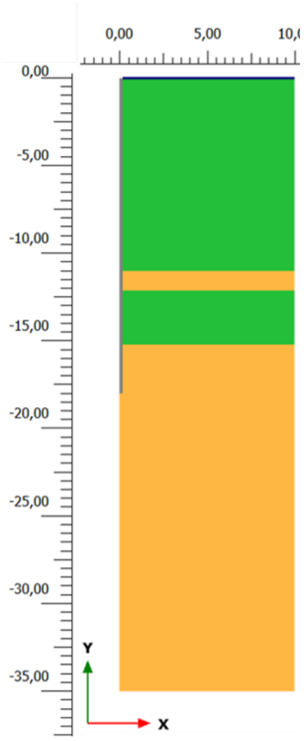

Figure 5.1: Geometry for the piles of the load test performed at the Kruithuisweg, Delft (model 1) (scale in m)

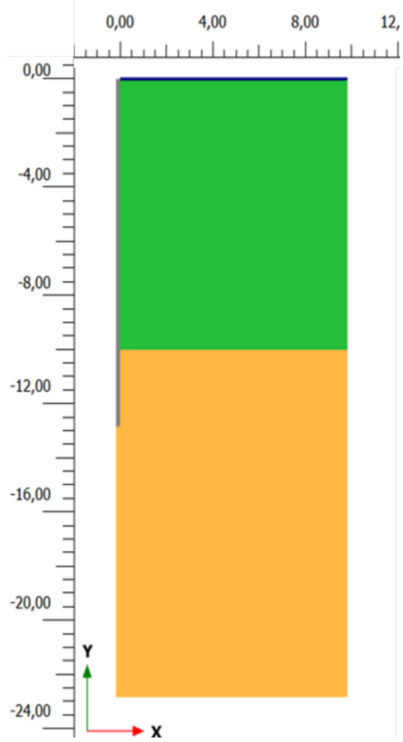

Figure 5.2: Geometry for the piles of the 2-layered soil profile (model 2) (scale in m)

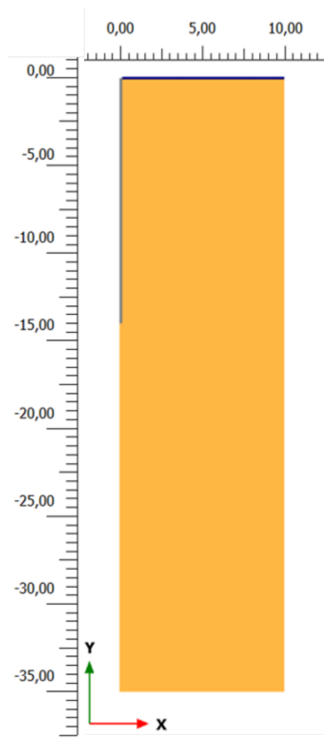

Figure 5.3: Geometry for the piles of the non-cohesive soil column (model 3) (scale in m)

Figures 5.1-5.3 show the three main soil profiles used for the different analysis carried out in this thesis. The first model, shown in Figure 5.1, is based on the CPTs which belong to the data from the CUR 229 dataset [CUR B&I, 2010]. This model is used to validate the installation effects (horizontal pre-stressing and residual load).

The second model focusses on the influence of a clay layer closely spaced above the pile tip, Figure 5.2. The bottom of the clay layer is set at -10 m (the reference level of the model is 0 m). The pile tip level is varied from 0D to 16D below the bottom of the clay layer.

The third model is used to analyse the influence of depth and the influence of the increase in cone resistance and possible limiting values. In NEN 9997-1 [Normcommissie 351 006 'Geotechniek', 2017a], the limiting value for the base resistance is set to 15 MPa. To evaluate this limit, a model consisting of only one sand layer is used, shown in Figure 5.3.
All geometries can be found in Appendix G.3

5.2.3. Modelling of the Installation

This thesis considers two methods to model the installation of the pile. On the one hand, the advanced, but time-consuming Push-and-Replace method [Engin, 2013], and on the other hand the relatively simple horizontal pre-stressing method [Broere and van Tol, 2006]. The Push-and-Replace method coincides with the inducing of residual loads, as the residual loads are generated automatically using the Push-and-Replace method. As the influence of residual loads is a main subject in this thesis, it is preferable to model them separately to get a better understanding of their influence.

This thesis analyses the importance of residual loads consequently, they are implemented in the FEM model. Besides the residual loads, the horizontal compression due to the installation should be considered as well.

To conclude, the Push-and-Replace method is an advanced technique to model installation effects in PLAXIS. On the downside, it is a complex and time-consuming method with a lack of inside in the separate mechanism occurring during pile driving. Therefore, it is chosen to implement the installation effects using a combination of implementing the horizontal compression using a wished-in-place technique and the residual loads (which is explained in phase 3).

5.3. Material Properties

As explained before, two soil types (clay and sand) are used in the FEM model for the analyses in this thesis. As defined in Section 5.1, the clay is modelled using the Mohr-Coulomb constitutive model, and the sand is modelled using the Hypo Plasticity constitutive model. In Table 5.1 the main soil parameters are summarised.

Mohr-Coulomb (clay)	E (kPa)	ν (-)	S_u (kPa)					
Hypoplasticity (sand)	$\phi_c (^o)$	h_s (GPa)	n (-)	e_{d0} (-)	e_{c0} (-)	e_{i0} (-)	α (-)	β (-)

Table 5.1: Input parameters different models

The clay parameters are set relatively weak (especially S_u). This is to ensure that the clay does not contribute to the pile tip resistance. In the current Dutch method [Normcommissie 351 006 'Geotechniek', 2017a] it is considered that clay does not contribute to the shaft friction either. The parameters used to model clay can be found in Table 5.2.

E (kPa)	ν (-)	S_u (kPa)
5000	0.3	5

Table 5.2: Mohr-Coulomb parameters clay [Plaxis, 2016]

The HP parameters for sand were determined using several different laboratory tests. Before being able to test the sand, a representative sample had to be found. As only samples of the formation of Sterksel and Drente were available, their properties had to be compared to the properties of the formation of Kreftenheye and Boxtel, as the latter two formations are mainly present at pile tip levels in the western part of the Netherlands. Comparing the properties was done qualitatively in Appendix D. From this comparison, it was concluded that the sand of the formation of Drente was most representative. Hence, the sand from the Drente formation was used to conduct the laboratory tests.

The tests performed to determine the different HP parameters are:

- Angle of Repose [JGS, 1996].
- Void ratio test [JGS, 1996].
- Oedometer test [Herle and Gudehus, 1999].
- Direct Shear test.

The tests for the angle of repose and the void ratio were done three times, see Appendix G.2 for detailed results.

The oedometer tests were performed at three different initial relative densities. From this h_s and n could be determined as explained in Appendix G.2.

The direct shear tests were performed at two different relative densities. For each relative density, three different vertical pressures were tested. These vertical pressure range from 100 to 300 kPa, which are representative values for vertical pressures for piles installed ± 10 to 30 m into a granular soil.

Finally, the results of the laboratory tests were compared with the results from the soil testing facility in PLAXIS (STF). The exact procedure of determining the HP parameters and the comparison with the STF can be found in Appendix G.2. An example of the comparison between the test data and the STF results for a direct shear test is displayed in Figure 5.4.

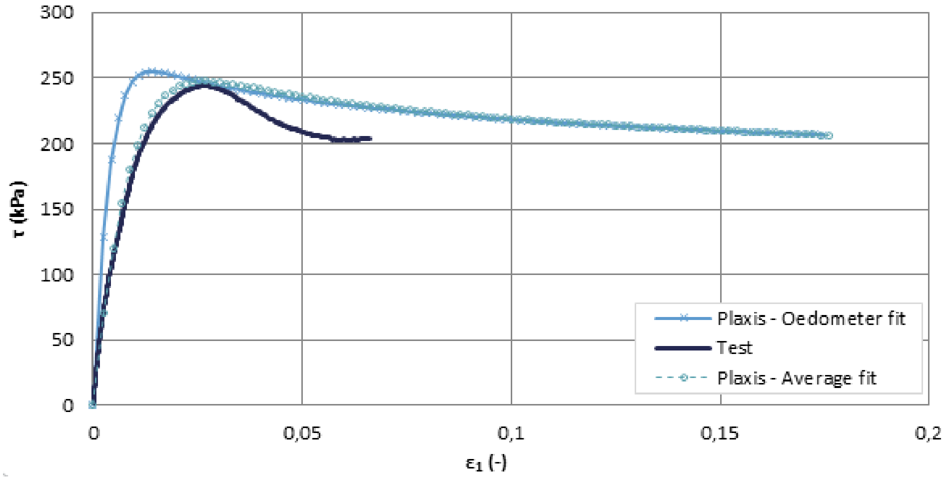

Figure 5.4: τ,ϵ_1-diagram - Drente (R.D. = 80%, $\sigma'_{yy} = 300kPa$)

Figure G.47 depicts three lines, the thick solid line representing the test results from a direct shear test, the dotted line which is the best fit on average for different relative densities and vertical pressures (see Appendix G.2), and the line with crosses which is the fit when using the h_s and n parameters derived from fitting the oedometer results. A more detailed explanation can be found in Appendix G.2
The results of these tests and comparison are presented in Table 5.3.

	$\phi_c(^o)$	h_s (GPa)	n	e_{d0}	e_{c0}	e_{i0}	α	β
Drente (B320-13)	31.06	13	0.27	0.513	0.744	0.857	0.1510	1

Table 5.3: Hypoplasticity parameters Drente Formation

While implementing the above determined HP soil parameters in model 1 (the model based on CPT data), it was noticed the stiffness response of the soil, in the model, was lower than determined through empirical Equation 5.1 which correlates CPT data to stiffness [Brinkgreve et al., 2015]. The empirical correlation in Equation (5.1) is used on a large scale for example when working with the HS model in PLAXIS. Therefore it is assumpted to be validated and more correct than the procedure to determine the stiffness parameters of HP model.

$$E_{50}^{ref} = 60000R_e/100 \tag{5.1}$$

From this comparison, it became clear the stiffness parameters n and h_s had to be adjusted. E_{50} was determined from CPT data and in the STF. In the ideal situation, the value for E_{50} is the same for both ways of determination. To get to equal values, n and h_s are adjusted to the values which can be found in Table 5.4. The complete procedure on how this is done is explained in Appendix G.2. In the end, it became clear only n needed to be adjusted.

	$\phi_c(^o)$	h_s (GPa)	n	e_{d0}	e_{c0}	e_{i0}	α	β
Drente (B320-13)	31.06	13	0.32	0.513	0.744	0.857	0.1510	1

Table 5.4: Hypoplasticity parameters Drente Formation, adjusted n

Besides the general HP and MC parameters, the interface between the soil and pile is regulated by a specific parameter set for the different constitutive models. For clay the interface factor R_{inter} was set to 0.1 (the smallest, numerically stable value possible) as the shaft friction in clay is not accounted for. The interface parameters for sand are a little more complex. They are set out in Table 5.5.

E (kPa)	$\phi(^o)$	$\psi(^o)$	c (kPa)	UD-power (-)	UD-ref (kPa)
50000	31.06	0	1	0.5	100

Table 5.5: Interface parameters sand in HP model [Brinkgreve, 2017]

The shaft of the pile is expected to be so smooth no dilatancy will occur [Tan et al., 2014] ($\psi = 0$). In addition, the strength of the soil will reach a constant volume state as it fails. As it is expected, failure will occur along the pile shaft during loading ($\phi = \phi_{cv}$). Last, a stress-dependent stiffness is considered, to take into account the that if stresses increase the stiffness decreases [Brinkgreve, 2017].
Apart from the two soil types used, the pile is modelled as a concrete pile. The stiffness of the pile is adapted from the PLAXIS manual [Plaxis, 2016] and is set to 30 GPa. The pile is modelled as linear elastic, non-porous material.

5.4. Phasing Characteristics

The numerical model is split up into different phases, mirroring the actual installation process for driven piles. Chapter 4 described these phases conceptually. The phases for the FEM procedure are described in the following sections.

0. Initial Phase In the initial phase, the K_0 procedure is used to generate the initial effective stresses (σ'_{v0} and σ'_{h0}) as well as the initial pore pressures. The following formulas (5.2) - (5.4) are used to calculate the effective stresses.

$$\sigma'_{v0} = d * \gamma' \tag{5.2}$$
$$\sigma'_{h0} = K_0 * \sigma'_{v0} \tag{5.3}$$
$$K_0 = 1 - sin\phi \tag{5.4}$$

1. Horizontal Pre-stressing Due to the installation method, in this case, driven, the soil is subjected to large displacements. As this cannot be modelled in PLAXIS, installation effects should be taken into account.
In this thesis, 2 different methods of implementing these installation effects are considered, namely the Push-and-Replace technique [J.Dijkstra, 2009] and [Engin, 2013] and the horizontal pre-stressing technique [Broere and van Tol, 2006], like discussed in Subsection 5.2.3.

The horizontal pre-stressing is modelled using a horizontal line displacement. This horizontal line displacement simulates the horizontal compression of the soil due to the installation of a soil displacement pile [Broere and van Tol, 2006].

2. Activating Pile In the initial phase (0), a volume element was created at the eventual location of the pile. Initially, this volume element was filled with soil material (during the initial phase) and emptied during the horizontal pre-stressing phase. In this phase, the volume element is changed to the concrete pile material. Due to the high stiffness of the concrete pile (compared with the soil stiffness), the pile will not deform significantly, as the soil starts to exert pressure on the pile (and the horizontal pre-stress is not affected). The validation of this procedure is described in Section 5.5.

3. Inducing the Residual Load As explained in Chapter 4, the residual load is a load in and around driven and jacked piles. A reaction force at the pile tip and along the shaft maintains equilibrium. The last blows of the driving hammer mainly induce the residual load. Modelling this soil-pile interaction for the dynamic load of the driving process requires an extensive analysis, which was not feasible within the scope of this thesis. Therefore, the residual load is induced by modelling a uniformly distributed static load on top of the pile. The order of magnitude of this load is determined through a sensitivity analysis and validation. During this phase, the interface strength along the shaft is set to 0.1. In other words, the residual load only influences the soil right below the pile tip at this stage. The validation of this procedure is described in Section 5.5.

4. Unloading In the unloading phase the static load, inducing the residual load is switched off, and the shaft friction is switched on again. A new equilibrium is reached between the pile tip resistance (directed upwards) and the shaft friction (directed downwards). As for the previous phases (0-4), the displacements are reset to zero after this phase, as we are only interested in the displacements during the actual loading phases.

5. Start Load Test The actual loading starts by placing a load of 200 kN on the pile head. The load is modelled as a uniformly distributed load on the pile head. The area of the pile is $\approx 0.1 m^2$, so the distributed load is $2000 kN/m^2$. Additional 200 kN loads are added each load step until the numerical model cannot stabilise anymore. This means, the pile tip displacement sometimes exceeds the failure criterium stated by NEN 9997-1. Pile failure is defined as the it is defined as the moment where the pile tip has moved more than 10%D of the pile [Normcommissie 351 006 'Geotechniek', 2017a].

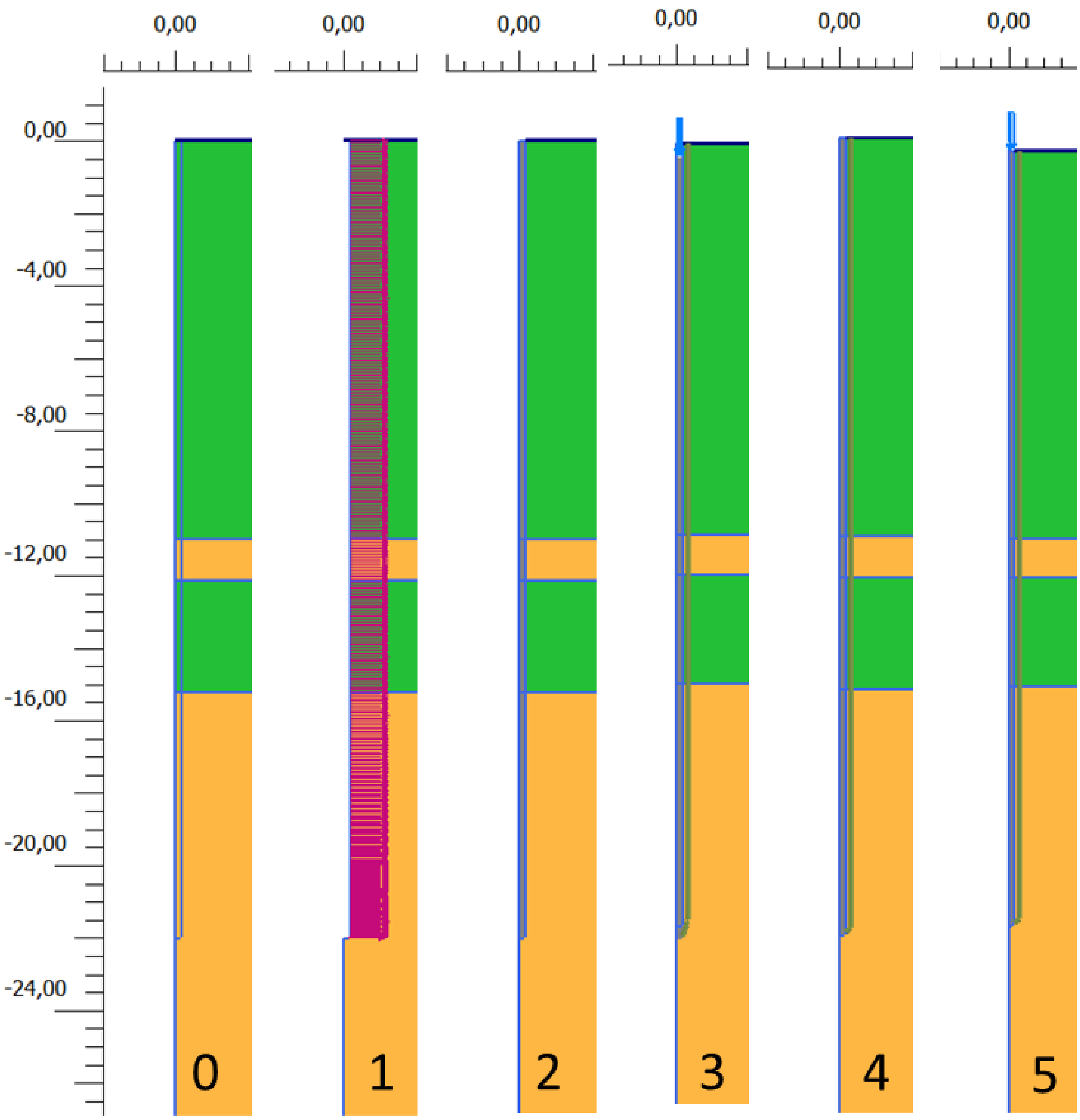

Figure 5.5: Geometry of the model during the different phases. Phase 0. Initial conditions, Phase 1. Horizontal pre-stressing, Phase 2. Activating Piles, Phase 3. Inducing Residual Load, Phase 4. Unloading, Phase 5. Load Test

5.5. Model 1: Installation effects

In Section 5.4 the different phases of the modelling procedure are explained. Phases 1 to 4 account for the installation effects that occur during installation of a driven pile. The numerical approach chosen for this thesis does not allow for complete, quantitative modelling of the installation effects. Hence, these effects are introduced indirectly. Besides the installation effects, the void ratio is an important variable, because the HP model is void ratio dependent. A change in the void ratio can influences the results significantly. From the CPTs available for the three studied cases, the void ratios are determined right at the pile tip level applying the following equations (5.5) and (5.6):

$$R_e = \frac{e_{max} - e}{e_{max} - e_{min}} \tag{5.5}$$

$$R_e = 0.34 * ln\left(\frac{q_c}{61 * (\sigma'_{v0,z})^{0.71}}\right) \tag{5.6}$$

In which R_e is the relative density (-) and e_{min} and e_{max} are the minimum and maximum void ratio (-).
As well as the void ratio, the stiffness parameter n is an important variable, mainly because it is complicated to determine. As mentioned in Section 5.3, the n parameter is determined in three different ways, namely:

- Through the formula of [Herle and Gudehus, 1999]
- Fitting the oedometer results to the STF results
- Checking the stiffness (E_{50}^{ref} from CPT data) in the STF [Brinkgreve, 2017]

The different methods resulted in different n values. Hence, the sensitivity of n was considered and a sensitivity analysis was conducted. This sensitivity analysis can be found in Appendix G.4.

Three piles are modelled in PLAXIS, to check if the assumptions made for the residual load and the horizontal pre-stressing are correct. The three piles were chosen after assessing the datasets of CUR 229. In this assessment the soil profile, the geological history, the installation depth, and the availability of sufficient CPT were considered. An overview of this assessment can be found in Appendix D. The pile tests at Kruithuisweg, Delft were selected for further analysis. Five piles were tested at this location, but only three pile test results (KH II, KH III and KH IV) were considered to be sufficiently reliable. KH I was rejected as the pile tip seems to be installed on top of a clay layer. Pile KH V was installed at the largest depth (in a sand layer) of all five piles, but its capacity is lower than all the other piles tested except for KH I. Due to this discrepancy, pile KH V was also discarded.

5.5.1. Horizontal Pre-stressing

The horizontal pre-stressing mainly influences the strength of the soil along the shaft. According to [Broere and van Tol, 2006], the horizontal pre-stressing should be in the order of magnitude of $7.5R_{pile}$. However, they determined this specific amount of horizontal pre-stressing in combination with a vertical pre-stressing, as the soil below the pile is also compressed due to the driving or jacking process. This thesis takes into account this vertical pre-stressing in terms of residual loads. This is done using a different procedure.

In addition, they used the HS constitutive model instead of the HP model. They are able to do so, because they use line displacements to introduce the pre-stressing. This is a more stable approach, but less accurate as displacements of up to 1 m could be implemented in the model. Hence, for this thesis it is chosen to work with the HP model in combination with residual loads, which are not able to be modelled using the HS model as the peak (of stresses) is exceeded. It was concluded by [Broere and van Tol, 2006] the PLAXIS results for the shaft friction were too high, using $7.5R_{pile}$, compared to the centrifuge test, they used to validate their research. This thesis uses the magnitude of the horizontal displacement described by [Broere and van Tol, 2006] as an indication for the models used in this thesis.

Given the above-stated differences between the approach by [Broere and van Tol, 2006] and the approach used in this thesis, a sensitivity analysis is performed on the order of magnitude of the horizontal pre-stressing. The results of this sensitivity analysis are displayed in Figure 5.6. Based on this analysis, the horizontal line displacement is set to $u_x = 0.005m$ which is 3%R.

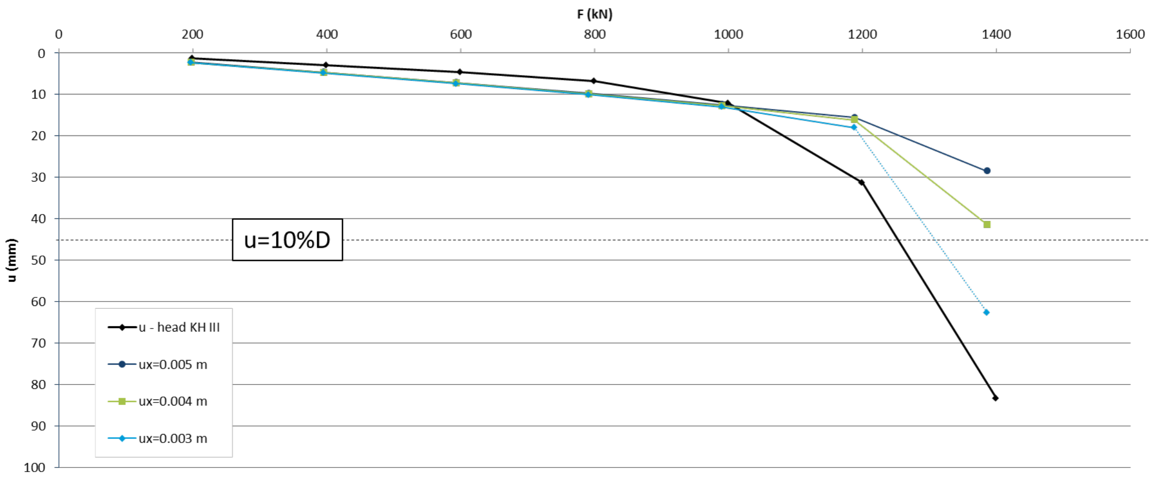

Figure 5.6: F, u_y-diagram varying horizontal line displacement (u_x) for KH III

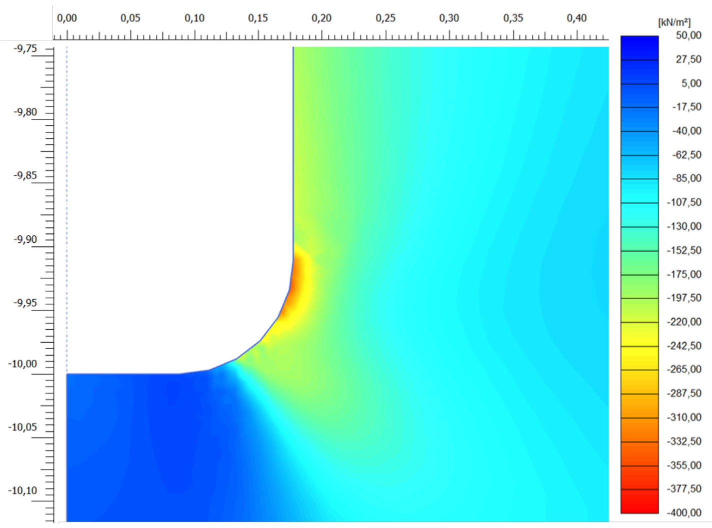

Figure 5.7: Influence of the horizontal pre-stressing on the surrounding soil in terms of σ'_{yy}

Figure 5.7 indicates the horizontal line displacement mainly influences the soil right of the pile and not below the pile tip.

5.5.2. Inducing Residual Load

The residual load at the pile tip is induced using a static load on top of the pile (shaft friction is set to 0). This static load represents the driving process in which an impulse load exhibits on the head of the pile, causing elastic shortening and penetration of the pile. No reliable analytical or numerical methods are available to quantify the residual load.

To determine the size of the static load, one should bear in mind that the soil fails as the pile penetrates the soill. Thus, it is considered the static load on top of the pile should be in the order of magnitude of the failure load (during a load test).

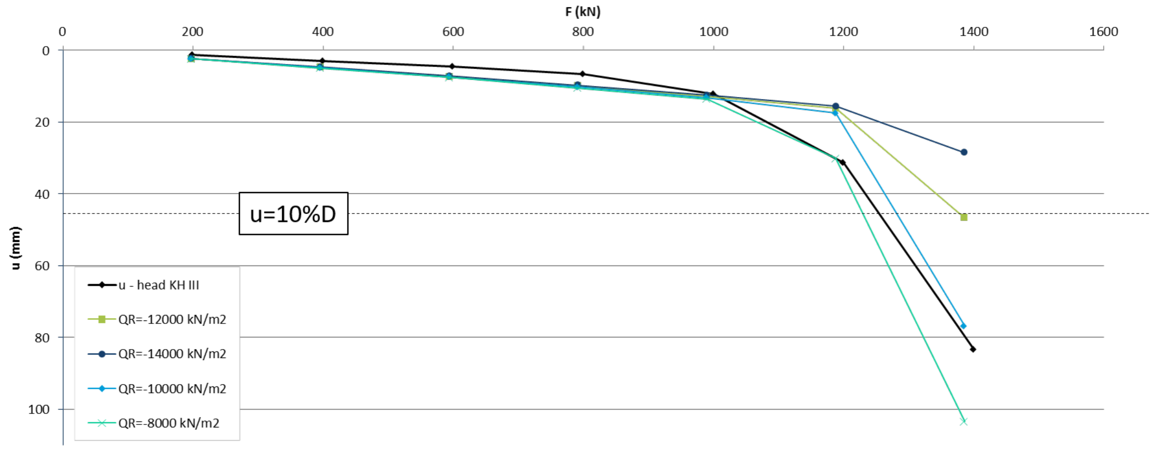

Figure 5.8: F, u_y-diagram varying the static load inducing the residual load for KH III

Given the uncertainties regarding the order of magnitude of the residual load, sensitivity analyses are conducted and presented in Figure 5.8 and Appendix G.4. Based on these results, the static load which induces the residual load is set to 80 – 90% of the failure load.

5.5.3. Combination of Installation Effects and n

In the end, the best combination of the different discussed parameters (u_x, Static load inducing the residual load (Q_r), initial void ratio and stiffness parameter n) resulted in Figure 5.9. In addition to varying only one of the parameters, combinations of the variations are conducted in the sensitivity analysis as well. This is done, because it is assumed the different parameters also influence each other [Anaraki, 2008], but within the scope of this thesis, no extensive analysis was performed regarding this influence.

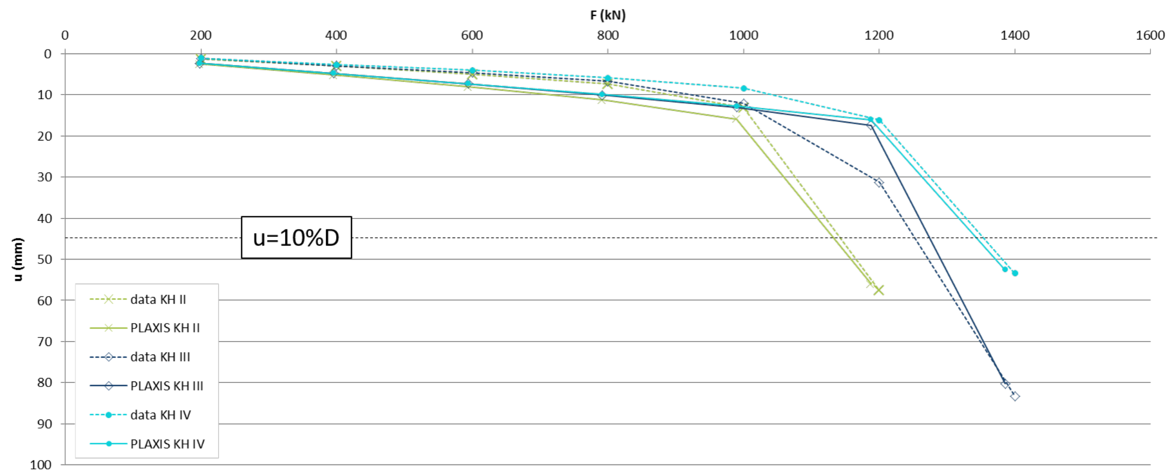

Figure 5.9: F, u_y-diagram best fitting combination of parameters for KH II, KH III and KH IV

Table 5.6 sets out the best combinations of parameters for the three different field test used for the validation.

	pile tip level (N.A.P. m)	Residual Load $Q_r (kN/m^2)$	Horizontal pre-stressing u_x (m)	Initial void ratio e (-)	Stiffness parameter n (-)
KH II	-18	-10000	0.05	0.56	0.32
KH III	-20	-10000	0.05	0.59	0.33
KH IV	-22	-10000	0.05	0.63	0.30

Table 5.6: Parameter combination for best fit in PLAXIS

From Figure 5.9, it can be seen the data response is still slightly stiffer, in the beginning of the load test. When moving towards the end of loading (F=1200 – 1400kN), the field test data and the PLAXIS response start to match quite well. A likely reason for the initially less stiff behaviour is the fact unloading/reloading could not be taken into account entirely. It is assumed the beginning of loading should react stiffer, as reloading is considered (Chapter 4). Although the residual load (virgin load) is induced in this model the lack of accuracy in the unloading/reloading behaviour due to the missing out of the small strain parameters results in a less stiff response.

Furthermore, the pile tip capacity was back-calculated for the PLAXIS model and compared to the measured pile tip capacity. The back-calculation was done by checking the mobilised shear strength along the pile shaft as shown in Figure 5.11. Next, this shear strength was back calculated to a force using the equation (5.7). Finally, equation (5.8) is used to calculate the pile tip capacity.
The results of the comparison between the pile tip capacity in PLAXIS and the measured pile tip capacity can be found in Table 5.7 and are in the same order of magnitude.

$$F_{shaft} = \tau_{mob} * \Delta L * O \tag{5.7}$$

$$F_{tip} = F_{total} - F_{shaft} \tag{5.8}$$

F_{shaft}	: Force generated due to shaft friction	(kN)
F_{tip}	: Force at the pile tip	(kN)
τ_{mob}	: Mobilised shear stress	(kN/m^2)
ΔL	: Length of the pile over which shaft friction is generated (non-cohesive soil)	(m)
O	: Circumference of the pile	(m)
F_{total}	: Total force on top of the pile	(kN)

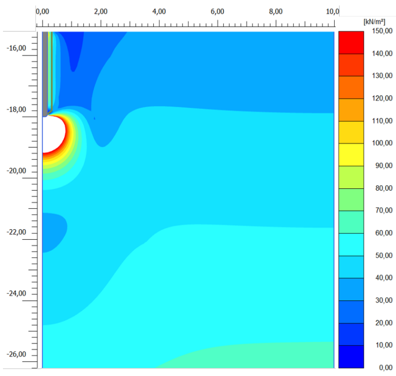

Figure 5.10: Mobilized shear strength along the shaft for KH II

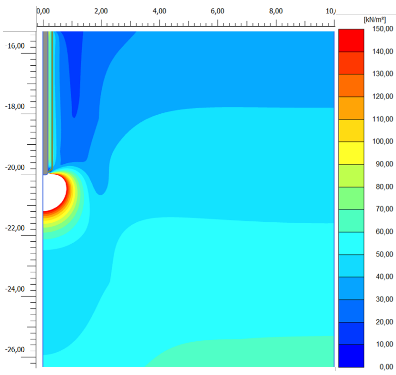

Figure 5.11: Mobilized shear strength along the shaft for KH III

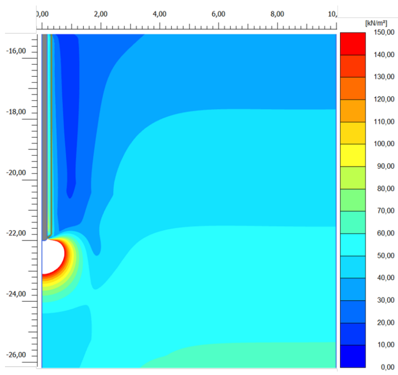

Figure 5.12: Mobilized shear strength along the shaft for KH IV

	KH II	KH III	KH IV
Pile tip capacity - data (kN)	850	820	755
Pile tip capacity - PLAXIS (kN)	888	972	945
Difference (%)	4	19	25

Table 5.7: Difference PLAXIS and measured pile tip resistance for KH II, KH III, KH IV

From Table 5.7, it can be concluded that the pile tip capacity in PLAXIS increases non-linearly with increasing installation depth. This is due to the residual loads mechanism. This mechanism plays a more significant role for piles installed deeper into a non-cohesive soil layer. This will be further evaluated and explained in Section 5.6.

5.6. Model 2: Influence of a Cohesive Soil Layer (close above the pile tip)

Analysing the influence of a cohesive soil layer located closely above the pile tip follows a procedure in which the installation depth is varied, starting at 0D from the bottom of the cohesive soil layer to 16D from the bottom of the cohesive soil layer. This approach is specifically chosen to be able to compare the results to the data from CUR 229 [CUR B&I, 2010].

To refresh one's memory; the reduction of α_p was necessary for piles deeper than approximately 8D into the non-cohesive soil layer, see Table 5.8. α_p reduces to around 0.62 for piles deeper than ±8D into the non-cohesive soil layer. If the pile is installed less than approximately 8D into the non-cohesive soil layer, $\alpha_p \approx 0.99$.

In order to find an explanation for this, the stresses and displacements around the pile tip are assessed for piles installed at different distances from the bottom of a soft soil layer. In addition to this, load,settlement-curves of the piles might give better insight on the influence of a cohesive soil layer to the capacity of the pile (regarding the tip and shaft resistance).

Pile	**Lenght in non-cohesive soil layer (m)**	**D (m)**	**xD (m)**	$F_{tip,calc}$ **(kN)**	$F_{tip,test}$ **(kN)**	α_p **(-)**
CIAD heiproef	0.60	0.4	1.5	1745	1630	0.93
Lim II B1	1.01	0.35	2.9	1796	1448	0.81
Haringvliet paal 10 sond s03	1.40	0.4	3.5	955	700	0.73
Lim II B2	1.37	0.35	3.9	1837	1564	0.85
Lim 1 cpt 5 concrete pile (p8)	1.25	0.29	4.3	728	836	1.15
Kruithuisweg -18 elec cpt	1.63	0.355	4.6	885	850	0.96
Lim I CPT 5 tub pile (p4)	1.30	0.272	4.8	540	830	1.54
Kruithuisweg -12 elec cpt	1.90	0.355	5.4	240	245	1.02
ESOPT II heiproef	1.70	0.25	6.8	744	675	0.91
Stress Wave conference Delft pile 1	1.89	0.25	7.6	98	60	0.61
Kruithuisweg -20 elec cpt	3.63	0.355	10.2	1159	820	0.71
Kallo III EI (pile a tube)	6.80	0.6	11.3	4241	2677	0.63
Kallo III EII (pile b tube)	6.80	0.6	11.3	4241	2849	0.67
Stress Wave conference Delft pile 5	3.06	0.25	12.2	792	500	0.63
Stress Wave conference Delft pile 4	3.11	0.25	12.4	812	450	0.55
Prepal TNO Delft betonpaal 1	3.70	0.29	12.8	1117	740	0.66
Prepal TNO Delft betonpaal 2	4.00	0.29	13.8	987	517	0.52
Stress Wave conference Delft pile 3	3.53	0.25	14.1	810	470	0.58
Kruithuisweg -22 elec cpt	5.63	0.355	15.9	1264	755	0.60
Kruithuisweg -24 elec cpt	7.63	0.355	21.5	1071	670	0.63

Table 5.8: CUR data [CUR B&I, 2010]

In Figure 8.1 the load,settlement-curves are given for the 9 piles installed in the above-described procedure. For every installation depth, the pile load test is modelled with and without residual load. The results show that the application of residual loads has no significant impact on strength or stiffness for the piles installed within the 8D range below the bottom of the cohesive soil layer. The influence of the induced residual load becomes apparent for pile tip levels in the range of 8D-16D below the bottom of the cohesive soil layer. For these cases, the stiffness significantly increases during the final load stages.

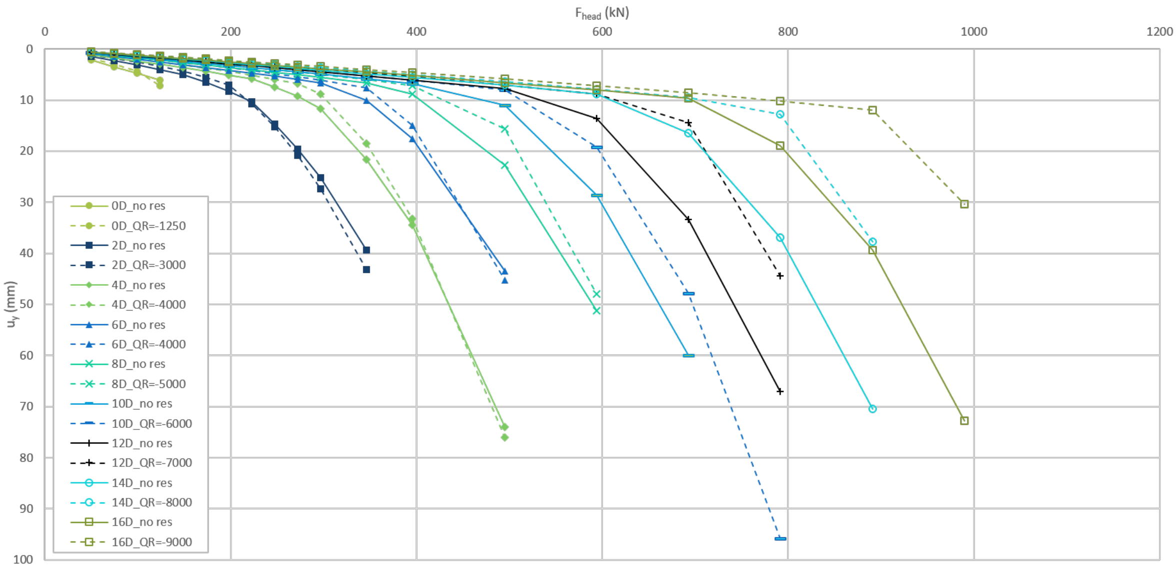

Figure 5.13: F, u_y-diagram for different installation depths. The different installation depths result in different residual loads (which are in the order of magnitude of 80-90% of the failure load if no residual loads are taken into account in PLAXIS

To check if PLAXIS does not overestimate the residual loads found at the pile tip at the end of the unloading phase (induced as described in Section 5.4), the residual loads form PLAXIS are compared to the maximum tensile capacity of the pile according to NEN 9997-1 [Normcommissie 351 006 'Geotechniek', 2017a].The residual load at the pile tip cannot exceed the tensile capacity of the pile, because if it does, the pile will be forced out of the soil. Table 5.9 shows the residual load at the pile tip does not exceed the maximum tensile capacity.

Peneteration length in sand (m)	$F_{tensile}$ according to NEN 9997-1 [Normcommissie 351 006 'Geotechniek', 2017a] (kN)	$F_{residual}$ at pile tip from PLAXIS (kN)
0D	0	-1
2D	60	15
4D	127	54
6D	202	74
8D	284	99
10D	373	144
12D	468	158
14D	571	247
16D	680	297

Table 5.9: Calculated tensile capacity compared to the residual load at the pile tip in PLAXIS

5.7. Model:3 Influence of Depth

Model 3 is used to analyse the influence of depth on the failure surface, the extent of the failure zone and limiting values.

5.7.1. Influence of Depth

To analyse the influence of depth to the soil behaviour at the pile tip a third model type is introduced. A homogeneous, non-cohesive soil mass is created in which the installation depth of the pile is varied to analyse the influence of depth.
To be able to evaluate the failure surface at the tip of the pile, regarding for example, the mobilised shear stresses or strains, the displacements of the pile tip have to be similar at the moment of failure for all piles

(even though they are installed at different depths). If this is not the case, various mobilisation levels will occur which makes it impossible to compare the stresses and strains around the pile tip for different installation depths. In this thesis, a load inducing procedure is followed to test the pile. In other words, the model is load controlled and not displacement controlled.

Therefore, the model was altered to a displacement controlled model. Instead of loading the pile on top, a line displacement was forced upon the pile tip. Using a line displacement, the model becomes more stable compared to using a line load.Due to this, a relatively large displacement of the pile tip can be present (up to 1m). This is not realistic.

Remarkably, no failure mechanisms were observed at the pile tip for a displacement of the pile tip of 10%D (failure criteria for the pile according to NEN 9997-1 [Normcommissie 351 006 'Geotechniek', 2017a]) nor for larger displacements. For these reasons, it was not possible to investigate the influence of depth on the failure mechanism.

5.7.2. Extent and shape of the zone of influence

Although the model was not useful for the investigation of the influence of depth on the failure mechanism, it allowed for examination of the mobilised shear stresses an principal stresses that occur around the pile tip.The results on this are described in the following section.

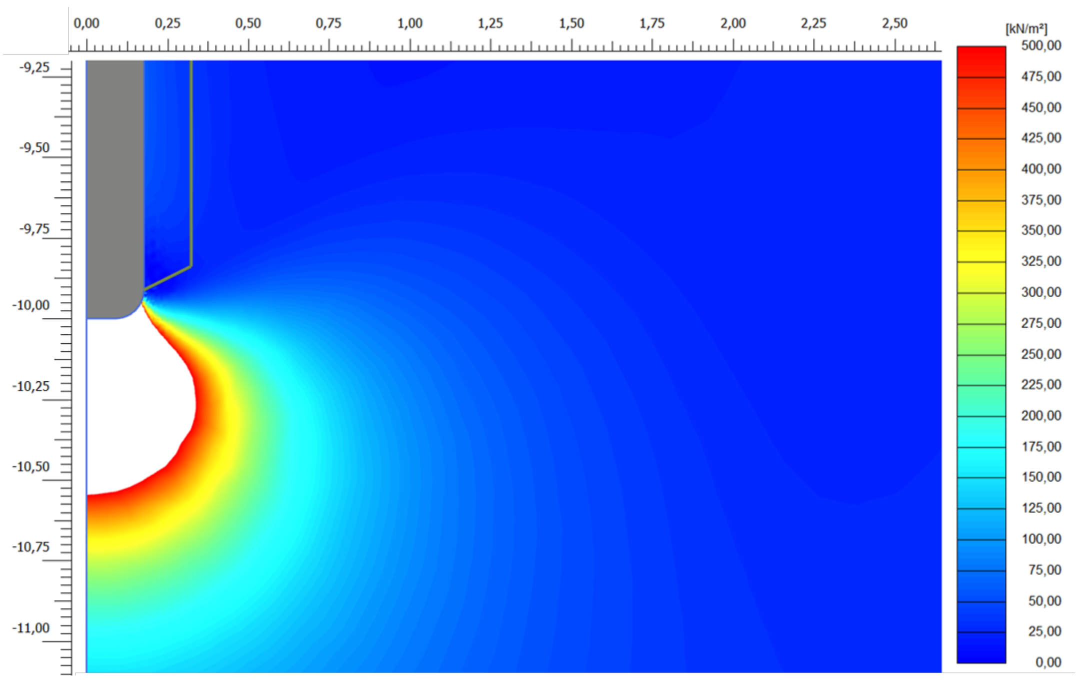

Figure 5.14: Mobilized shear stresses around the pile tip

The first observation, which can be made from Figure 5.14 is that no clear signs of a shear band formation are present. It is noted that for Figure 5.14, the scale does not cover the full range of mobilised shear stresses. The white zone underneath the pile tip contains mobilised shear stresses which are not depicted on the scale, this was done in order to show the development of the shear stresses around the pile tip more clearly.

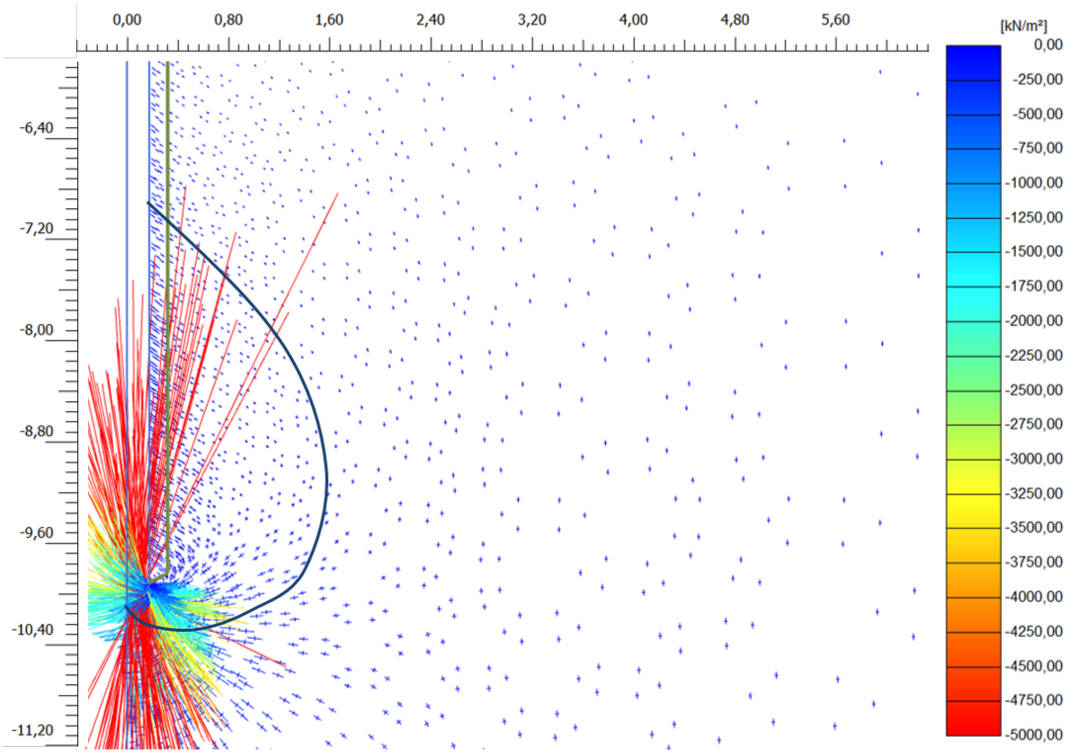

Figure 5.15: Principal cross stresses around the pile during failure including an indication of the logarithmic spiral

At first sight, the principal cross stresses in Figure 5.15, seem to show a similar trend as the logarithmic failure surface on which the 4D/8D method is based. Zooming in on Figure 5.15, (Figure 5.16) a difference is noted between the logarithmic spiral and the PLAXIS results. Figure 5.17 introduces a concept of 7 zones. These 7 zones are defined using the work of [Arshad et al., 2014] as a starting point.

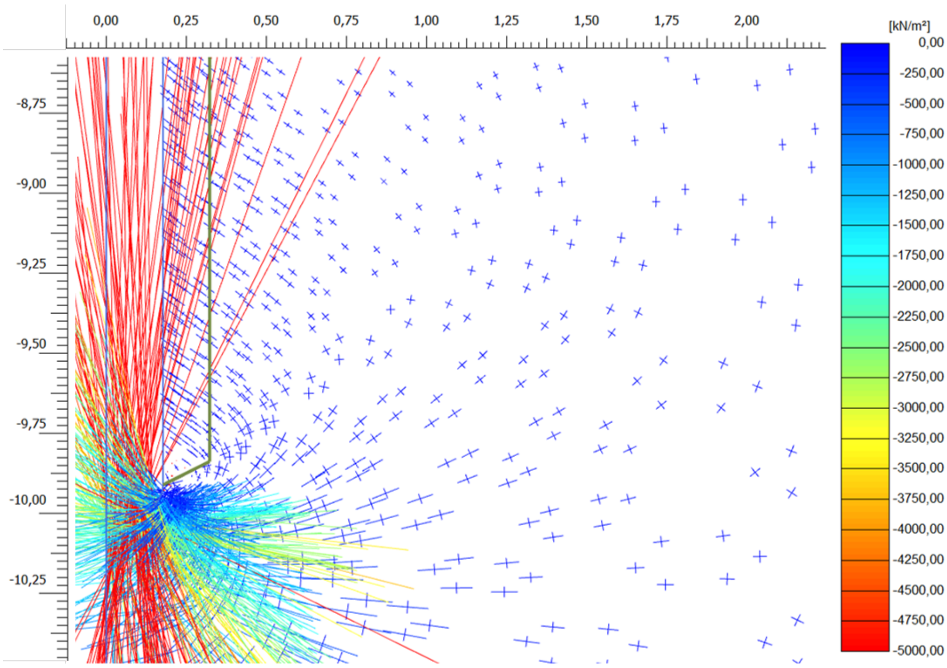

Figure 5.16: Close-up at the pile tip of Figure 5.15

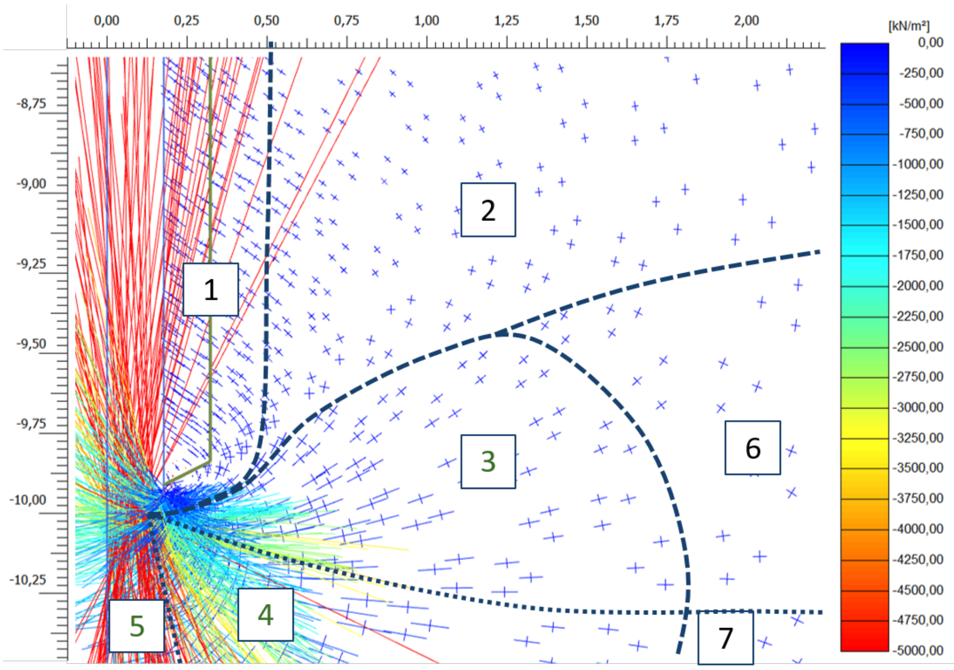

Figure 5.17: Principal cross stresses divided into zones: 1. Shaft friction; 2. Transition zone between 1 and 3; 3. Horizontal stress dominates [Arshad et al., 2014]; 4. Transition zone between 3 and 5 [Arshad et al., 2014]; 5. Vertical stress dominates [Arshad et al., 2014]; 6 and 7. outer area, transition zone towards no influence zone

As explained by [Arshad et al., 2014] zone 3 is dominated by horizontal stresses, vertical stresses dominate in zone 5 and zone 4 is a transition zone between zones 3 and 5. Zone 1 can be denoted to shaft friction, and zone 2 is again a transition zone, but now between zone 1 and 3. Finally, zone 6 and 7 can be seen as outer zones of respectively zones 3 and 4. In these outer zones, the influence of the pile to the soil is still present, but to a much lesser extent than for the other zones. The outer zones can also be seen as a transition zone to the surrounding, unaffected soil.
From these zones, it can be seen the influence of the pile tip does not extend to a distance of 8D above the pile tip.

Although the results of Table 5.10 are derived from model 2, they find a more rightful place in this part of the analysis. From Table 5.10, it can be seen that the extent of the zone of influence above the pile tip is smaller than 8D. This result coincides with the result of the mobilized shear stresses and the principal stresses around the pile tip. Only a zone of approximately 1D above the pile tip is influence by the pile tip failure mechanism. In Figure 5.18, the displacements during failure are shown. From this figure the extent of the zone of influence can be found, the dashed line indicates this. The straight line indicates the pile tip level.

Distance pile tip from bottom clay layer	Pile tip level at N.A.P (m)	Extent top at N.A.P. (m)	Length of extention zone for displacements at failure (m)	Length of extention zone for displacements at failure (in D)
0D	-10	?	-	-
2D	-10.71	-10.44	0.27	0.76
4D	-11.42	-11.1	0.32	0.90
6D	-12.13	-11.84	0.29	0.82
8D	-12.84	-12.52	0.32	0.90
10D	-13.55	-13.24	0.31	0.87
12D	-14.26	-14.00	0.26	0.73
14D	-14.97	-14.90	0.07	0.20
16D	-15.68	-15.44	0.24	0.68

Table 5.10: Zone of influence, considering displacements, above the pile tip for different installation depths below a clay layer at failure (failure is defined as the load step for which PLAXIS cannot stabilise anymore and stops calculating

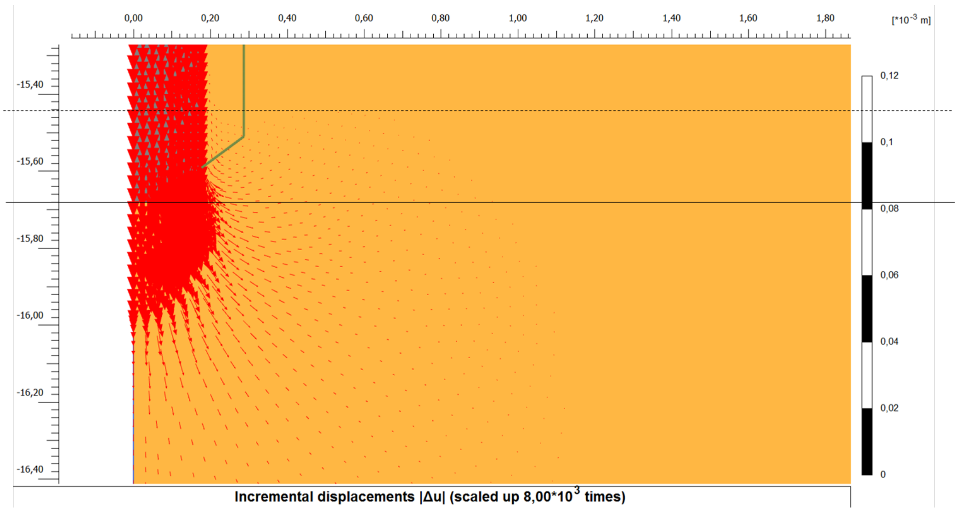

Figure 5.18: Displacement around the pile tip during failure

5.7.3. Limiting Values

According to NEN 9997-1 [Normcommissie 351 006 'Geotechniek', 2017a] the maximum value for pile tip capacity ($q_{b,max}$) is limited to a maximum of 15 MPa. The precise background for this limiting value could not be traced back to a literature source. Furthermore, the French method does not use a limiting value in the way the Dutch method does, see Chapter 2. In addition to this, several experts (A. van Seters, R. Spruit, K. Gavin) in the field of pile foundations cannot explain this limiting value.

To check if such a limiting value is approached, model 3 is used. For a pile with an installation depth of 10 m, the q_c-value of the sand is varied from 10 MPa to 35 MPa.
To be able to introduce the variation in q_c-values, the initial void ratios are changed, this is stated in Table 5.11. The correlation used to back-calculate the different soil parameters from the cone resistance are as explained in the previous sections of this chapter, according to [Brinkgreve et al., 2015].

q_c (Mpa)	R_e (%)	e (-)	E_{50}^{ref} (kPa)	$\phi' (^o)$
10	62,21305	0,600288	37327,83	35,77663
15	75,99887	0,568443	45599,32	37,49986
20	85,78006	0,545848	51468,03	38,72251
25	93,36694	0,528322	56020,16	39,67087
30	99,56587	0,514003	59739,52	40,44573
35	104,80700	0,501896	62884,20	41,10087

Table 5.11: Initial void ratio correlated to cone resistance

As can be seen in Table 5.11, the void ratios for 30 and 35 MPa are higher than e_{min} (e_{min}=0.513). This is unrealistic; hence, PLAXIS is not able to calculate with these initial void ratios for this specific type of sand.

For the four remaining q_c-values, the model is run like explained in Section 5.5. The load,displacement-curves at the pile head are presented in Figure 5.19. Figure 5.20 shows the models with the higher q_c-values (15, 20 and 25 MPa) have not mobilised the full tip capacity at a load of 800 kN on top of the pile as the pile only displaced a $\pm 10mm$. When this load is increased to 1000 kN, only the model with $q_c = 25MPa$ has not fully mobilised at the pile tip. Althoug the case of $q_c = 15MPa$ and $q_c = 20MPa$ fail (PLAXIS stops calculating) at in the same load step, the results show the vertical displacement of the pile is less for the case of $q_c = 20MPa$.

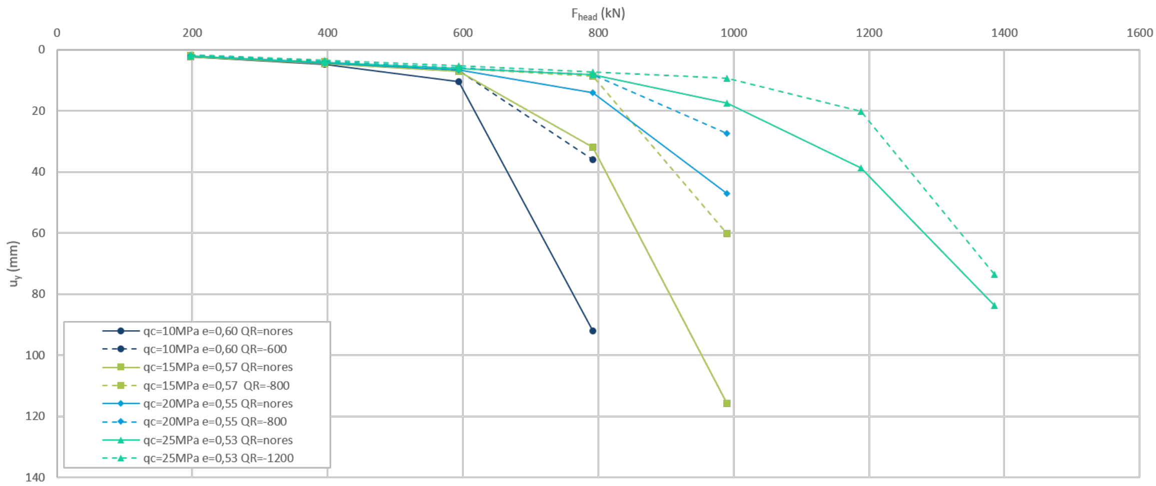

Figure 5.19: F, u_y-diagram for different q_c-values

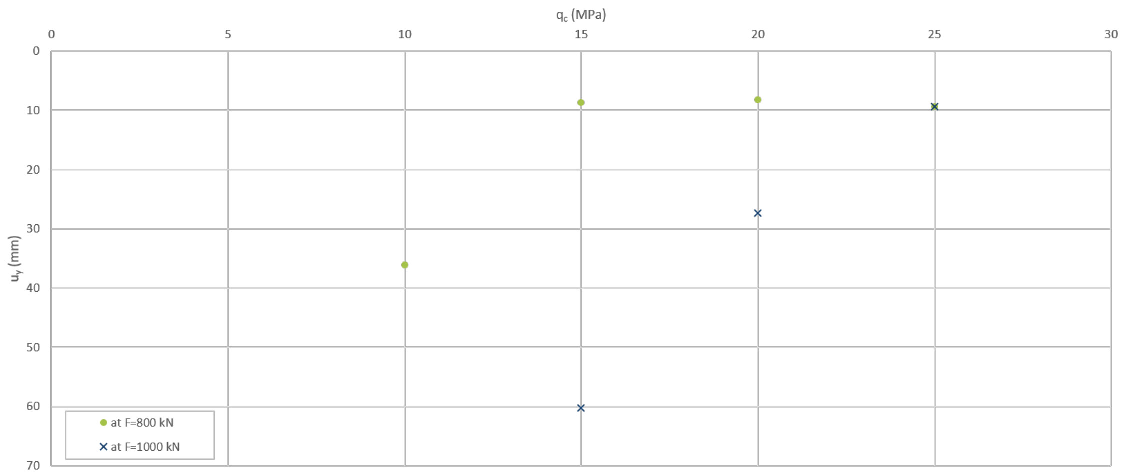

Figure 5.20: u_y, q_c-diagram

Considering the above, a closer look is taken at Figure 5.21. In this figure it can be seen, an almost linear relation can be found between q_c and q_b, so no limiting value is approach. It is noted that apparent non-linearities of the PLAXIS results are cased by the load step discretization used for this model.

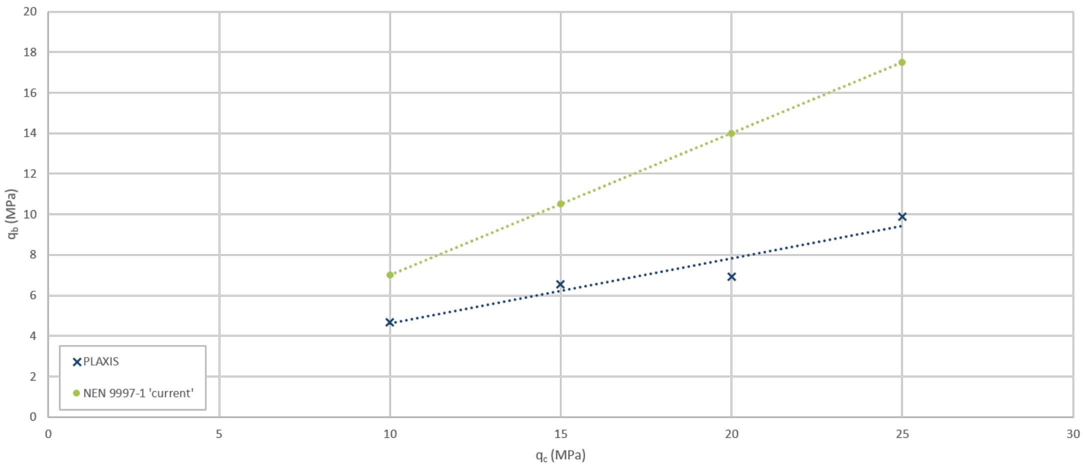

Figure 5.21: q_b, q_c-diagram

6 Scaled Tests

While this thesis took place, scaled pile load tests have been performed in a test pit in Zuid-Oost Beemster. These tests were initiated by van 't Hek, BAM and VolkerWessels. Although the tests were not executed for the purpose of this thesis, first estimation and results are evaluated with the aim to detect the presence and if possible the order of magnitude of the residual load at the pile tip of a driven pile. Based on such an evaluation the procedure used in the numerical model regarding the residual load can be backed-up.

As explained in more detail in Appendix H four scaled closed-end driven piles are tested using optic fibres. The test pit was first excavated and next back-filled with sand of known grain-size distribution. The back filling is done layer by layer to make sure the soil profile is as homogeneous as possible. The optic fibres in the pile, measure the strain along the pile shaft and very close to the pile tip. The exact location of the optic fibres is displayed in Figure 6.1.

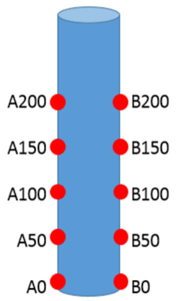

Figure 6.1: Location of the sensors along the pile shaft

The strains measured by the optic fibres are micro strains. This means a factor 10^6 smaller than strains. From the micro strains, the load in a pile can be calculated using equations (6.1).

$$F = Residual.load.in.pile = \epsilon * E * A_{pile} \tag{6.1}$$

Specification of the pile:

Outer diameter	0,15	m
Inner diameter	0,131	m
Wall thickness	0,0095	m
Cross-sectional area (A_{pile})	0,0041932	m^2
Tip area(A_{tip})	0,0176715	m^2
E-modulus steel (E)	2,10E+08	kPa
Pipe length	3	m
Pile length	3,0095	m
Pile weigth	7850	kg/m^3

To be able to translate this load, in a pile, to a stress in the soil at the pile tip Equation (6.2) is used.

$$\sigma_{piletip} = Residual.load.in.soil = \frac{F}{A_{tip}} \tag{6.2}$$

Besides Equation (6.1), the 0-Load or 0-Force moment has to be chosen. This moment is selected to be at the beginning of the installation. In this stage, the pile is standing up straight. This way the self-weight of the pile is distributed over the pile similarly as for the pile after installation and during loading. As explained in Chapter 4, the residual load is the load in and around the pile right before testing/loading the pile. Therefore, just before the beginning of loading is the moment the residual load should be measured. Of course, the strains present at the 0-Force moment have to be subtracted from the strains just before loading. The above can be summarised in equation (6.3).

$$\epsilon_{residualload} = \epsilon_{beginningofloadtest} - \epsilon_{beginningofinstallation} \tag{6.3}$$

The results of the measurements will be discussed in the coming sections. However, before presenting the results, some expectations are set out. First, the residual load in a pile is expected to be highest at the bottom and lowest at the top. This is due to the fact the residual load can be seen as a spring response from the soil at the pile tip. So a load, or actually stress, is acting on the pile tip in an upward direction. At the shaft, the soil wants to resist this spring response, so it starts to mobilise shaft frictions, orientated downwards. The higher one moves up in a pile the lower the force in the pile is, as it is mobilised by the shaft friction (more shaft means more shaft friction). The previous is also explained in Chapter 4. Furthermore, the load in a pile should be a compression load, due to the above-explained mechanism.

6.1. Results

From the four piles considered, one lacked measurement data in the first 20 minutes of the load test, and another pile missed the first 5 minutes of the strain measurements for the load test. This severely limits the usability of these tests, because the missing data is needed to be able to fulfil the analyses of finding the presence of a residual load as pointed out in Equation (6.3).
The results for the two other piles are presented in Figures 6.2 and 6.3.

Both Figure 6.2 and Figure 6.3 show results, which contradict the expectations. As the residual load in a pile is induced from the bottom, it is expected, the load at a pile tip is largest and that this load decrease when moving up in the pile. This reduction is expected as the shaft friction takes over part of the load. Furthermore, both piles show contradicting results comparing side A and B of one pile. Hence, it is impossible to draw conclusions from this data.

It is suspected, the cross-sectional area of the piles might not be constant. A small change in the area will result in significant changes in the back-calculated load in a pile. Therefore, the wall thickness of the piles has to be checked after the piles are pulled out of the soil. The checking should take place close to the location of the optic fibres.

Another inconsistency might occur at the bottom plate, which is welded on. Due to the welding, the E-modulus of the steel can changes (due to temperature effects) resulting in small changes in the load in the pile.
To conclude, it is essential to check the EA-modulus and re-calculate the residual loads in a pile.

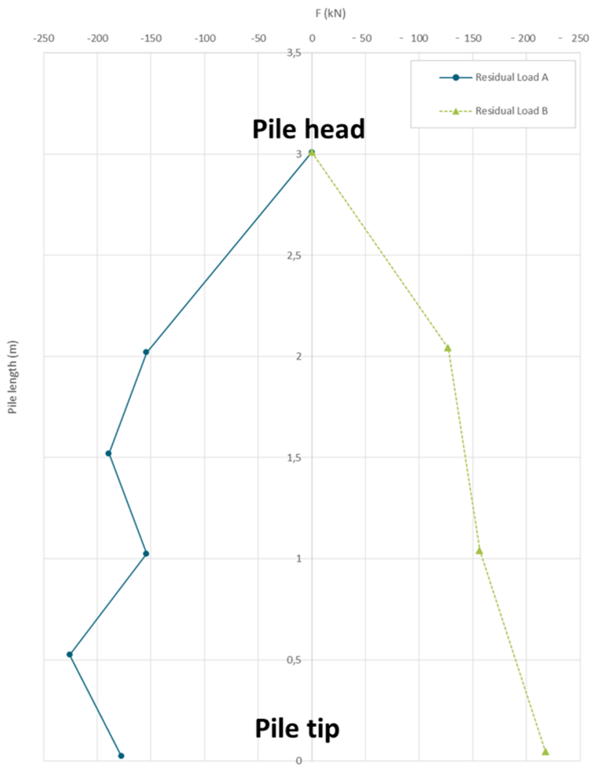

Figure 6.2: Residual load in the pile (pile 1) for side A and B

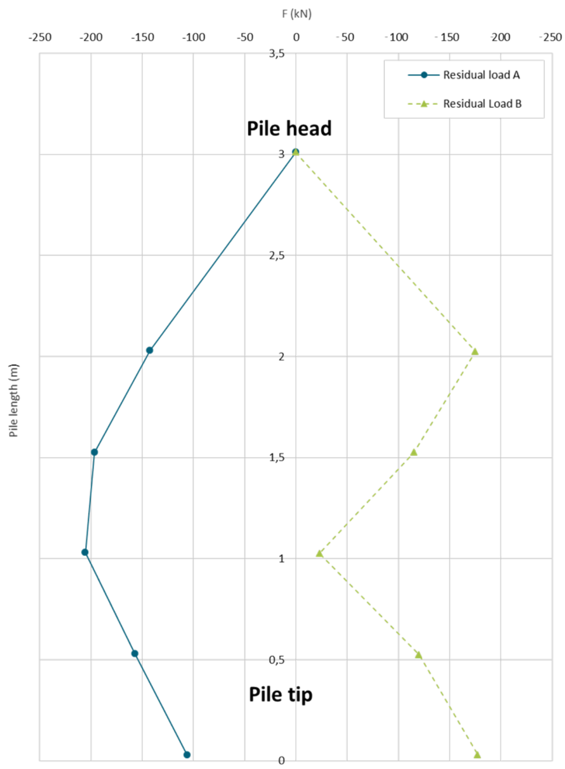

Figure 6.3: Residual load in the pile (pile 8) for side A and B

Finally, it is noted the order of magnitude of the residual load is similar to the maximum load, Figure 6.4. Point X in this figure might be the point where the load test stopped, as the pile did not stabilise anymore. However, it could also indicate a change in stiffness response as the soil gets out of the reloading phase onto a new virgin loading phase (path YX). Future load test should extend the loading procedure to check if this is true. Load test should continue even though the pile is not able to fully stabilise anymore.

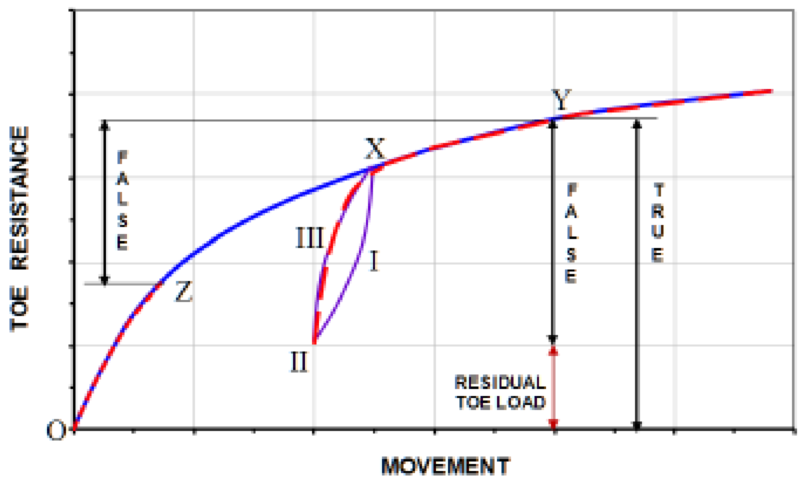

Figure 6.4: Unloading/Reloading curve and residual loads for pile tip[Fellenius, 2015]

6.2. Conclusion

Due to all uncertainties, it is concluded the data is insufficient to reach quantitative findings regarding the residual loads without further in-depth analysis of all factors influencing the field data. However, both data sets (assumed to be of sufficient quality) do show the presence of the residual load. More tests have to be performed, to analyse the contribution of residual loads to a larger extent.

7

Discussion and Remarks

To accurately judge the results presented in this thesis, several points of discussion and remarks have to be taken into account. These points of discussion and remarks mainly consider the implementation of the FEM models, the parameter determination and the scaled tests.

7.1. Points of Discussion

Various decisions made during the model research phase of this thesis could not be validated entirely and are open for discussions. The main points of discussion relate to the numerical modelling phase and are listed as follows:

1. Use of the Hypo Plasticity constitutive model for the FEM analysis of the pile behaviour.
2. Implementation of the residual loads in the FEM model.
3. Implementation of the horizontal pre-stressing in the FEM model.

The above items will be discussed in the coming subsections.

7.1.1. Use of the Hypo Plasticity constitutive model for the FEM analysis

The Hypo Plasticity model is a highly non-linear constitutive model. Due to this non-linearity, it is important to take into account a high level of accuracy, which can be done through the numerical control parameters. When a pile is loaded in tension a lot of stress concentrations occur along the shaft. These stress concentration occur as the model is not able to distribute the load correctly, this results in false stress distributions. Although the pile is loaded in compression for this thesis, the above-explained phenomenon occurs at a minor extent.

7.1.2. Implementation of the residual loads in the FEM model

Since taking into account the residual loads in a FEM model has not been done before, this thesis tried to find a way to implement the residual load as an installation effect into the FEM models. The residual load can be seen as an installation effect, as the driving process induces it. However, the complete installation process cannot be modelled (easily) in PLAXIS, as large strains occur. Therefore, it was chosen to implement the residual loads as an installation effect indirectly.

Obviously, the actual driving process is a complex, dynamic event dominated by large deformations and temporary excess pore pressures. In this thesis, a more simple approach is considered and only the tensile capacity of the shaft is presumed to influence the residual load at the pile tip. The results of the FEM models in this thesis are validated using field test results. This validation showed the FEM models described the measured data well. Of course, additional research is required to find a substantiated approach to introducing the residual load in FEM models.

7.1.3. Implementing the Horizontal Pre-stressing in the FEM model

The horizontal compression was implemented using a known procedure which uses a horizontal line displacement [Broere and van Tol, 2006]. The amount of horizontal displacement is 7.5% R according to [Broere and van Tol, 2006]. For the pile considered in this thesis, this results in a lateral displacement of approximately 0.013 m.

From the sensitivity analysis (Appendix G.4), it was found a lateral displacement of 0.005 m sufficed to match the load,displacement-curves of the field data used to validate the FEM model. Obviously, there are many differences between the model tests performed by [Broere and van Tol, 2006] and the back-analysis of the full-scale pile load tests in PLAXIS. Besides, the difference in scale of the tests, introducing the residual load may cause deviation. The exact reasons for the difference are not discussed in this thesis.

7.2. Other Remarks and Limitations

Besides the points of discussion, remarks and limitation arose during this thesis as limited time and lack of availability of equipment or knowledge. The effect of these remarks and limitation and their possible impact will be discussed in the following subsection:

1. General
2. Parameter determination
3. Numerical modelling
4. Scaled tests

7.2.1. General

The following general limitations were identified:

- Although the results of this thesis indicate the interaction between the shaft resistance and the pile tip capacity, the impact of shaft friction on the pile tip capacity was not investigated.

7.2.2. Parameter determination

To determine the HP parameters, laboratory tests were performed for this thesis, regarding these test limitations and remarks are listed as follows:

- The measurement accuracy of the instruments available at the TU Delft is sometimes lacking.
- The α parameter for the HP model should be derived from triaxial tests [Herle and Gudehus, 1999] and [Anaraki, 2008], but no triaxial test set-ups were available within the time frame of this thesis. Hence, direct shear tests are performed to determine the α parameter.
- The stiffness parameters h_s and especially n proved to be very sensitive to the approach used to determine them. Different approaches were followed, leading to a relatively confident determination of h_s. As this was not the case for the n parameter, a sensitivity analysis was done to conclude on the n parameter.

7.2.3. Numerical Modelling

Besides the points of discussion in the previous section, also some limitations and remarks identified regarding the numerical modelling.

- The HP model used in this thesis allows for the use of the small strain parameters. However, these parameters can only be determined using biaxial tests, cyclic shear tests and cyclic triaxial tests, these tests are not available for this thesis. Preliminary results in the STF, using estimated small strain parameters indicated that the use of small strain parameters could increase the accuracy regarding the unloading/reloading behaviour response of the soil using the HP model. However, the results also showed the high sensitivity of the small strain parameters and their influence on the complete HP parameter set. Therefore, small strain parameters were not implemented in the FEM models for this thesis.
- PLAXIS and the HP model cannot take into account large strains, which is a clear limitation considering the installation process.

7.2.4. Scaled tests

The planning of the scaled tests did not allow for a comprehensive analysis of the results within the timespan of this thesis. The results of the scaled tests are influenced by many variables, while measurements were in some cases incomplete. To be able to draw confident conclusions regarding the scale tests, an in-depth analysis of the results is required. This could not be done within the scope of this thesis, but some first observations, which seemed to be reliable and useful for this thesis were taken into account.

8

Conclusions and Recommendations

8.1. Conclusion

The goal of this thesis was to find an answer to the question:

Can the reduction of α_p be explained through the fundamental aspects of geotechnical engineering for the soil behaviour at the pile tip?

To be able to answer this question, sub-questions were stated. The answers to the sub-questions are as follows:

1. **Which mechanism or feature can explain the increase in overestimation of the pile tip capacity with increasing penetration depth (in granular soils)?**

   Both the literature, and the numerical modelling suggest this effect may be caused by either the extent and presence of the zone of influence above the pile tip or the fact that residual loads are not taken into account for jacked and driven piles.
   To assess the influence of the above-named phenomenon on the increase in overestimation of the pile tip capacity with increasing penetration depth into a granular soil, the possible influence of the 8D zone is further discussed in Question 3. Question 2 explains the influence of residual loads in more detail.

2. **Can residual loads be the cause of the deviation between the calculated and measured pile tip capacity?**

   From the beginning of this thesis, it was clear residual loads can have influence on the bearing capacity of the pile. In the standard pile load tests described by [Normcommissie 351 006 'Geotechniek', 2017b], residual loads are not taken into account.The residual load at the pile tip should be added to the pile tip capacity measured during load tests to get to the total pile tip capacity.
   The residual load is positively correlated to the negative shaft friction as denoted in Chapter 4. In other words, an increase in negative shaft friction results in a higher residual load at the pile tip. Hence, it is assumed the residual load increases with increasing penetration depth of a pile into the granular soil layer.

   Although it seems relatively clear that the residual loads do influence the pile tip capacity, currently no reliable prediction methods exist to quantify the residual load at the pile tip. To be able to investigate the possible effects of residual loads on the geotechnical mechanisms around the pile tip, the residual load is induced by implementing a static load (on the pile head), in FEM models for this thesis. The results from the previously mentioned procedure are validated using data from CUR 229.

   Although the procedure of inducing the residual load in FEM models, like done in this thesis, is not substantiated by literature or tests, implementing residuals loads this way gave promising results depicted in Figure 8.1. From Figure 8.1 it can be concluded, residual loads start playing a role for piles installed deeper than 8D into the granular soil.

This boundary, for piles installed 8D into a non-cohesive soil, can also be indicated from the results found by CUR 229 [CUR B&I, 2010]. For CUR 229, the boundary indicates the necessity of the reduction of α_p or not. In the end, CUR 229 decided to reduce α_p for all penetration depths, to prevent confusion.

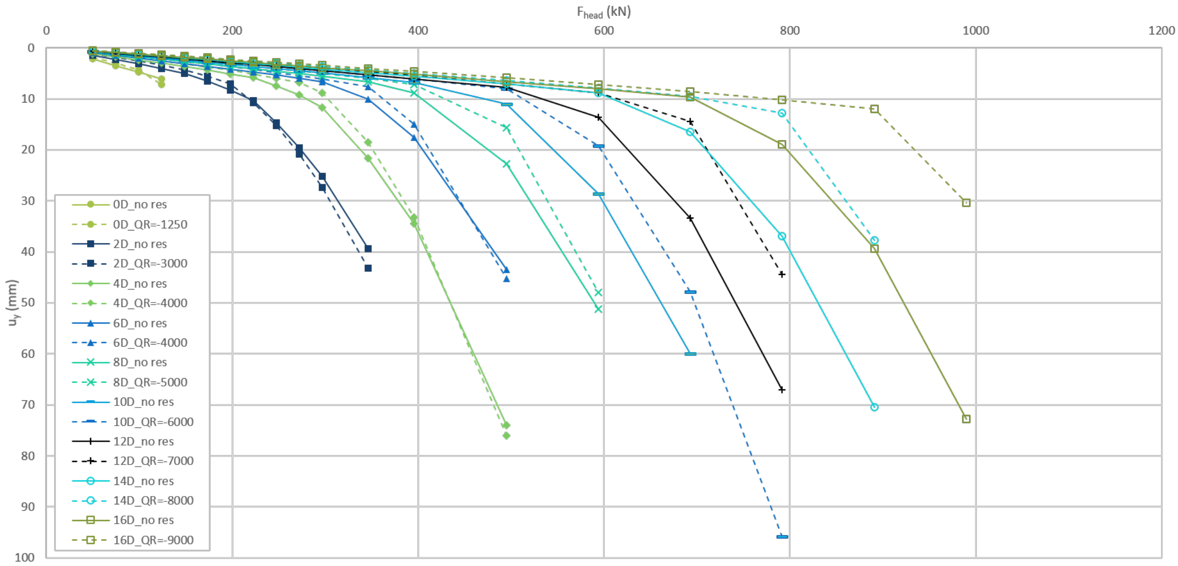

Figure 8.1: F, u_y-diagram for different installation depths. The different installation depths result in different residual loads (which are in the order of magnitude of 80-90% of the failure load if no residual loads are taken into account in PLAXIS

In Chapter 6, the preliminary results of four scaled piles were analysed. Two of the four piles lack data, so they are disregarded for this thesis, while the other two tests show some unexpected results.
Although the order of magnitude of the residual loads cannot be determined, the two piles showed a significant load in the pile (close to the pile tip) just before starting the load test. Therefore, these preliminary results indicate the presence of a residual load. However, in-depth analyses are needed to draw hard conclusions on this.

3. **CUR 229 results show a difference in α_p for piles deep (>8D) in the sand layer compared to piles less deep (<8D) into the sand layer. Can this be explained from shortcomings in de 4D/8D method?**

   Answering this question requires an integral analysis, using several results obtained in this thesis. First off, Chapter 2 already showed the zone of influence below the pile tip, which is 4D (actually a zone of 0.7D to 4D) is substantiated quite well. From the analysis of the logarithmic spiral, as set out in Chapter 2, the zone of influence below the pile tip extends from 0.7D for $\phi = 0^o$ up to 4D for $\phi = 50^o$.
   On the other hand, the zone of influence above the pile tip of 8D varies considerably from 0.7D (for $\phi = 0^o$) to >35D (for $\phi \approx 45^o$).

   From the previous, the misinterpretation of the zone of influence above the pile tip is another cause of the observed deviation of CUR 229 [CUR B&I, 2010]. To find out if these expectations are correct, the shape and the extent of the zone of influence are discussed in a more in-depth (numerical) analysis in Question 4 and 5.

4. **Is the shape of the zone of influence, around the pile tip, described by Koppejan's logarithmic spiral theory correct for all soil types?**

   The logarithmic spiral theory introduced by Koppejan, finds its origin at the Prandtl wedge theory for shallow foundations. According to Koppejan, the maximum bearing capacity of a pile tip is governed by an onion-shaped failure surface. It was already noted by [van Mierlo and Koppejan, 1952], the extent and shape of the failure surface do not apply for all soil types. This observation is confirmed in the FEM analysis. The FEM analysis suggests a more circular zone of influence like shown in Figure 8.2. Furthermore, no shear band formation is found in the FEM analysis. Although no failure surface is present, a zone of influence in the soil is encountered around the pile tip.

As the failure surface (described by Koppejan's logarithmic spiral) was not encountered for in the FEM analysis, the zone right underneath the pile tip was investigated in more detail for the failure load step. A total of 7 distinct zones were identified as shown in Figure 8.3 zone 1 and 3.

Although the result (Figure 8.3) were not validated in this thesis, the results do coincide with the analysis of the fundamental aspects in Chapter 4, which suggests the shaft friction and the mobilisation of the shear forces in the zone of influence at the pile tip cannot act simultaneously. This is also seen in Figure 8.3.

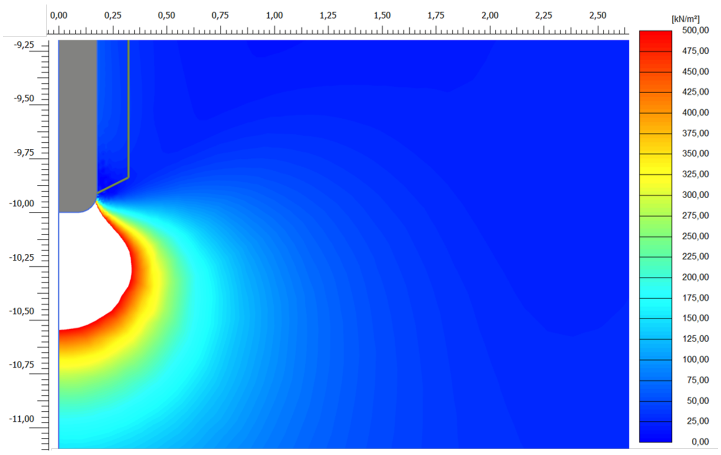

Figure 8.2: Mobilized shear stresses around the pile tip

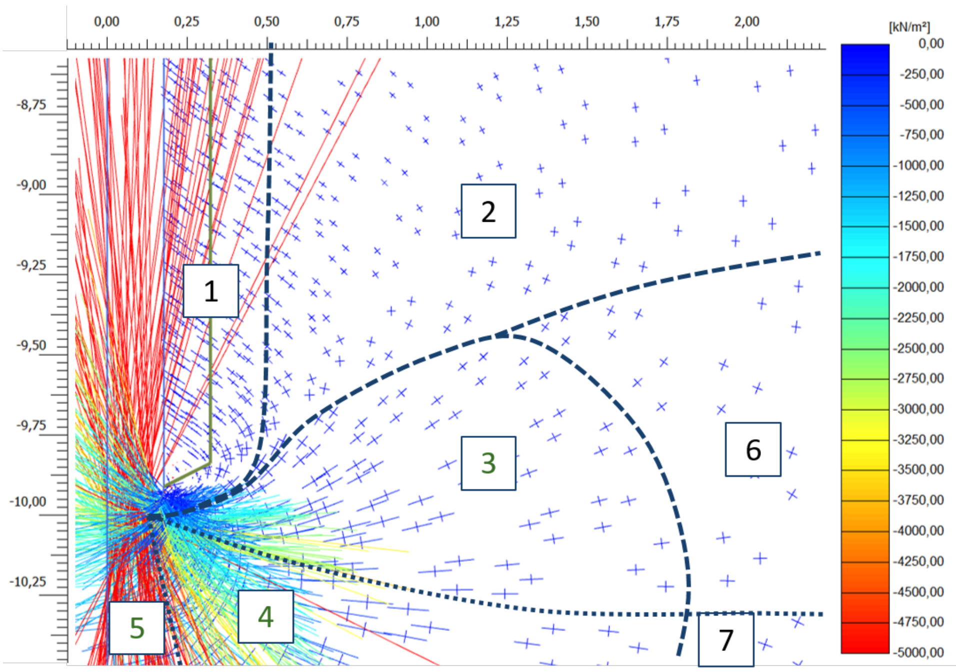

Figure 8.3: Principal cross stresses divided into zones: 1. Shaft friction; 2. Transition zone between 1 and 3; 3. Horizontal stress dominates; 4. Transition zone between 3 and 5; 5. Vertical stress dominates; 6 and 7. outer area, transition zone towards no influence zone

5. **Is the extent of the zone of influence as assumed, when adopting the 4D/8D method valid for all soil types?**

With the logarithmic spiral theory adapted by [van Mierlo and Koppejan, 1952], only ϕ' influences the extent of the failure surface around the pile tip. If ϕ' tends to zero degrees (theoretical minimum for cohesive soils in case of undrained behaviour), the failure surface becomes circular instead of onion-shaped. Due to the circular shape, the extent of the failure surface decreases significantly, especially in the zone above the pile tip.

When a pile is installed at a depth <8D from the bottom of a cohesive soil layer, this cohesive soil layer is taken into account in calculation of $q_{c,III}$, which is not correct. The net effect is a reduction of $q_{b,max}$. This effect was also noted, in more general terms by Koppejan as a flaw in theory. The correction of this effect will improve the accuracy of the pile tip capacity calculations (for piles installed less than 8D into the bearing layer). If a revised method is developed to calculate the average cone resistance (valid for all penetration depths), α_p must be reconsidered.

Although the FEM results do no show a clear failure surface, it does show a zone of influence. The extent of this zone of influence above the pile tip is smaller than 8D. Strain distributions around the pile tip are further investigated for nine different installation depths. The FEM results show that the strains in the soil extend, at most, to approximately 1D above the pile tip. Therefore, it can be concluded the zone of 8D above the pile tip (according to the Dutch method) is too large. The zone of 1D is more in line with the French method which suggests a zone of 1.5D above the pile tip. However, it is essential to notice the FEM results describe a zone of influence, which is different from the failure surface used in the 4D/8D method.

6. **Do the limiting values, normatively prescribed in conjunction with the 4D/8D method, have a physical meaning?**

   Void ratio and cone resistance are correlated through the equation of Lunne [Lunne et al., 1997]. As the HP model is void ratio dependent, the influence of a change in void ratio and therefore cone resistance on the end bearing capacity can be analysed. q_c-values varying from 10 MPa to 35 MPa were considered. Increasing the cone resistance, i.e. decreasing the void ratio did not result in limiting values.

8.1.1. Synthesis

In this thesis, the following aspects of the Dutch method for calculating the pile tip capacity for closed-end, driven, axially loaded, end-bearing piles were examined:

- The effects of residual loads.
- The shape of the failure surface around pile tip for different soil profiles.
- The extent of the zone of influence around the pile tip for different soil profiles.
- The need of limiting values for the cone resistance (as normatively prescribed).

This thesis revealed new insights with respect to above-summoned aspects and identified shortcoming and incorrectness of the Dutch method.
In the present engineering practice, residual loads are not taken into account when performing and analysing load tests. Therefore, the pile tip capacity measured during a load test is smaller than it actually is.

Furthermore, this thesis confirms the drawback noted by Koppejan regarding the logarithmic spiral and its description of the failure surface for a layered soil. FEM results, obtained in this thesis, suggest no failure surface is found at failure as defined in the Dutch code (at 10% D displacement of the pile tip). Even for larger displacements of the pile tip, a failure surface could not be detected.

In addition to the above, the FEM results only show a zone of influence of 1D above the pile tip instead of 8D as suggested in the Dutch method. This is more in line with the French method, as this method suggests a zone of influence of 1.5D above the pile tip.
The observed overestimation of the calculated pile tip capacity with increasing penetration depth can be traced back to the too large extent (8D) for the zone above the pile tip by the Dutch method. Piles driven to a

penetration depth of less than 8D into a granular soil layer encounter a reduction of the bearing capacity due to the soft soil layer that is taken into account. Combined with a too high α_p-value the overall calculated pile tip capacity matches the measured pile tip capacity. This inherent flaw in the 4D/8D method also implies a single α_p, valid for all penetration depths cannot be defined for this method. If the method for determining the average cone resistance is revised, α_p will need reconsideration.

No theoretical basis was found for the limiting values for the cone resistance that are normatively described in the Dutch method. This may introduce a hidden margin of safety. However, installation effects are only considered with simplifications. The effects of pile installation resulting into limiting values should be further investigated.

Finally, from all the above, an answer will be presented on the question:

Can the reduction of α_p be explained through the fundamental aspects of geotechnical engineering for the soil behaviour at the pile tip?

With confidence, it can be stated, part of the reduction of α_p can be explained through the fundamental aspects of geotechnical engineering for the soil behaviour at the pile tip. On the one hand, the analysis of the residual load at the pile tip indicates an underestimation of the measured pile tip capacity if residual loads are not taken into account. If this underestimation is not present, α_p would probably be higher.

On the other hand, the zone of influence around the pile tip, especially considering the zone of 8D above the pile tip, is expected to be too large. If a too large zone is taken into account the unrealistic low values for $q_{c,III,avg}$ will be found in most cases for pile installed less than 8D below a cohesive soil layer. This is a possible trigger for the reduction of α_p for a fundamental soil behaviour point of view.

Both causes explain part of the reduction of α_p, but this thesis does not quantify what part. Therefore, recommendations are given in the following section.

8.2. Recommendations

As this thesis mainly focussed on the numerical modelling of the residual load and the failure zones developing at the pile tip, some limitations, and therefore recommendations can be found. The recommendations are split into four categories:

1. Recommendations regarding the residual loads
2. Recommendations regarding FEM modelling
3. Recommendations regarding the 4D/8D method and the reduction of α_p

8.2.1. Recommendations Regarding the Residual Loads

- It has been shown in this thesis, the residual loads play an important role for the pile tip capacity. Residual loads can be monitored during pile load tests using for example, Osterbeg cells in the pile tip or optic fibres sensors in the pile. More experience is required regarding the test procedure for residual loads. Pile handling and environmental circumstances can have a significant impact on the results and should be understood and controlled with a high level of detail. Further research into predicting the magnitude of residual loads and implementing this method in the direct CPT methods is recommended and will significantly improve the accuracy of these methods.

8.2.2. Recommendations Regarding FEM modelling

- In the FEM analysis performed in this thesis, the advance Hypo Plasticity constitutive model was used. This model takes into account softening behaviour of the soil, which might occur during driving and at failure. However, the driving process of the pile is modelled using installation effects, and not the process itself as PLAXIS cannot model large strains. Future numerical modelling research into the topic of this thesis should ideally be performed using a theoretical framework that does allow large strains in order to model the installation effects. In addition to this, softening behaviour should be taken into account at all times.

- To increase the accuracy of the HP model with regards to the unloading/reloading behaviour, the small strain parameters should be determined and implemented in the model to check if the soil response is stiffer in the beginning of loading. As the other HP parameters are influenced by the small strain parameters, they should be checked again using the STF to see if changes are needed here.
- The way of inducing the residual load and the order of magnitude of both the horizontal pre-stressing and the residual load should be checked, using more than three pile load tests to validate the results.
- Using the HP model introduces uncertainties that are mainly caused by the input parameters. To be able to minimise the uncertainties more accurate (and more advanced) laboratory tests are required.

8.2.3. Recommendations regarding the 4D/8D method and the reduction of α_p

- In this thesis, it is concluded that the failure surface described by the logarithmic spiral does not occur. Reconsideration of the 4D/8D method is required (in conjunction with α_p).
- The zone of influence found around the pile tip in the FEM results shows an extent of around 1D above the pile tip. To conclude on the extent described by the 4D/8D method it should be investigated if the zone of influence can be compared to the failure surface.
- Limiting values for the cone resistance as prescribed normatively in the Dutch method do not appear in the FEM results. Therefore these limiting values may cause hidden safety in the calculations of the pile tip capacity, but further research is needed on the influence the installation method has on these limiting values to conclude on this.

During the elaboration of this thesis, several other possible causes for the deviation between the calculated and measured pile tip capacity were found. These mechanisms could not be investigated within the scope of this thesis. However, the following remarks can be made:

- Results indicate that the shaft friction cannot be generated in the zone of influence of the pile tip. This interaction needs further investigation.
- The FEM results, in terms of the load,displacement-curves, suggest failure later on in the loading process than defined by the Dutch method. Therefore, further research is needed considering the failure criterium defined by the Dutch method or the definition of failure.

References

Anaraki, K. (2008). Hypoplasticity investigated: Parameter Determination and Numerical Simulation. Technical report, Technische Universiteit Delft.

Arshad, M., Tehrani, F., Prezzi, M., and Salgado, R. (2014). Experimental study of ocne penetration in silica sand using digital image correlation. *Géotechnique 64*.

Baldi, G., Bellotti, R., Ghionna, V., Jamiolkowski, M., and Pasqualini, E. (1986). Interpretation of CPTs and CPTUs; Second part: Drained Penetration of Sands. *Proceedings, 4th International Geotechnical Seminar, Singapore*.

Been, K. and Jefferies, M. (1985). A state parameter for sands. *Géotechnique 35*.

Berendsen, H. (2008). *De vorming van het land*. van Gorcum.

Bolton, M. (1986). The strength and dilatancy of sands. *Géotechnique 36*.

Brinkgreve, R. (2017). Contributed by PLAXIS expert.

Brinkgreve, R., Engin, E., and Engin, H. (2015). Validation of empirical formulas to derive model parameters for sands. -.

Broere, W. and van Tol, A. (2006). Modelling the bearing capacity of displacement piles in sand. *Proceedings of the Institution of Civil Engineers, Geotechnical Enigneering 159*.

Bustamante, M. and Gianeselli, L. (1982). Pile bearing capacity prediction by means of static penetrometer CPT. *Proceedings of the Second European Symposium on Penetration Testing, Amsterdam*.

Cho, G., Dodds, J., and Santamarina, J. (2006). Particle shape effects on packing density, stiffness and strength: natural and crushed sands. *Journal of geotechnical and geoenvironmental engineering*.

CUR B&I (2010). CUR rapport 229 axiaal draagvermogen van palen. Technical report, SBR CURnet.

Engin, H. (2013). Modelling Pile Installation effects, A Numerical Approach. Technical report, Technische Universiteit Delft.

Fellenius, B. (2015). Static tests on instrumented piles affected by residual load. *Journal of the Deep Foundation Institute*.

Gudehus, G. (1996). A Comprehensive Constitutive Equation for Granular Materials. *Soils and Foundations*.

Herle, I. and Gudehus, G. (1999). Determination of parameters of a hypoplastic constitutive model from properties of grain assemblies. *Mechanics of cohesive-frictional materials*.

Hicks, M. (2015). Risk and Variability Sandfills.

Jamiolkowski, M., Ladd, C., and adn R. Lancellolta, J. G. (1985). New developments in field and laboratory testing of soils. *Proceedings, 11th International Conference on Soil Mechanics and Foundation Engineering, San Francisco*.

J.Dijkstra (2009). On the Modelling of Pile Installation. Technical report, Technische Universiteit Delft.

JGS (1996). *Japanese Geotechnical Society, Soil Testing Standards*. -.

Kuipers Funderingstechnieken BV (2017). Prefab pile.

Kulhawy, F. and Mayne, P. (1990). Manual on Estimating Soil Properties for Foundation Design. Technical report, Geotechnical Engineering Group Hollister Hall.

Lehane, B., Schneider, J., and Xu, X. (2005). *A Review of Design Methods for Offshore Driven Piles in Siliceous Sand*. University of Western Australia.

Lehane, B., Schneider, J., and Xu, X. (2016). The UWA-05 method for prediciton of axial capacity of driven piles in sand. -.

Lunne, T. and Christoffersen, H. (1983). Interpretation of cone pentrometer data for offshore sands. *Proceedings of Offshore Technology conference, Texas*.

Lunne, T., Robertson, P., and Powell, J. (1997). *Cone Penetration Testing in Geotechnical Practice*. Blackie Academic and Professional.

Mayne, P. (2014). Interpretation of geotechnical parameters from seismic piezocone tests. *Proceedings, 3rd International Symposium on Cone Penetration Testing*.

Meyerhof, G. (1951). The ultimate bearing capacity of foundations. *Geotechnique*.

Normcommissie 351 006 'Geotechniek' (2017a). NEN9997-1. Technical report, Nederlands Normalisatie-instituut.

Normcommissie 351 006 'Geotechniek' (2017b). NPR 7201. Technical report, Nederlands Normalisatie-instituut.

Plaxis (2016). *Material Models Manual*. PLAXIS.

Prandtl, L. (1921). Uber Die Eindringungsfestigkeit (Harte) Plastischer Baustoffe Und Die Festigkeit Von Schneiden. *Z. Angew. Math. Mech.*

Robertson, P. and Cabal, K. (2010). *Guide to Cone Penetration Testing for Geotechnical Engineering*. Gregg Drilling & Testing, Inc.

Robertson, P., Campanella, R., and Wightman, A. (1983). SPT-CPT Correlations. *ASCE Journal of Geotechnical Engineering 109*.

Silva, M. and Bolton, M. (2004). Centrifuge penetration tests in saturated layered sands. *Proceedings ISC-2 on Geotechnical and Geophysical Site Characterization*.

Spikker, M. (2010). Funderen in Almere. Technical report, Technische Universiteit Delft.

Tan, S., J.Sun, and Ng, K. (2014). Numerical simulation of strain softening behavior at pile-soil interface. *Numerical Methods in Geotechnical Engineering*.

Terzaghi, K. (1943). *Theoretical soil mechanics*. Wiley.

TNO (2013). Lithostratigrafische Nomenclator van de Ondiepe Ondergrond.

TNO (2016). GeoTOP versie 1.3.

Tomlinson, M. (2001). *Foundation Design and Construction*. Pearson Eduction limited.

van der Linden, T. (2016). Influence of Multiple Thisn Soft Layers on the Cone Resistance in Intermediate Soils. Technical report, Technische Universiteit Delft.

van Mierlo, W. and Koppejan, A. (1952). Lengte en draagvermogen van heipalen. *Bouw*.

van Tol, A. (1993). Funderingstechnieken ontwerpaspecten. Technical report, Technische Universiteit Delft.

Verruijt, A. (2012). *Grondmechanica*. Nederlands Normalisatie-instituut.

A
NEN 9997-1

A.1. Table 2.b

1. In table 2.b from NEN 9997-1 [Normcommissie 351 006 ’Geotechniek’, 2017a] the characteristic values for different soil parameters are given. As these are the characteristic values one has to bear in mind the real soil parameter values are higher.

Tabel 2.b — Karakteristieke waarden van grondeigenschappen

Grondsoort			Karakteristieke waarde [a] van grondeigenschap											
Hoofd-naam	Bijmengsel	Consis-tentie [b]	γ [c]	γ_{sat}	q_c [d g]	C'_p [g]	C'_s	$C_c/(1+e_0)$ [g]	C_α [f]	$C_{sw}/(1+e_0)$ [g]	E_{100} [g h]	φ' [g]	c'	c_u
			kN/m³	kN/m³	MPa			[-]	[-]	[-]	MPa	Graden	kPa	kPa
Grind	Zwak siltig	Los	17	19	15	500	∞	0,004 6	0	0,001 5	45	32,5	0	
		Matig	18	20	25	1 000	∞	0,002 3	0	0,000 8	75	35,0	0	N.v.t.
		Vast	19 20	21 22	30	1 200 1 400	∞	0,001 9 0,001 6	0	0,000 6 0,000 5	90 105	37,5 40,0	0	
	Sterk siltig	Los	18	20	10	400	∞	0,005 8	0	0,001 9	30	30,0	0	
		Matig	19	21	15	600	∞	0,003 8	0	0,001 3	45	32,5	0	N.v.t.
		Vast	20 21	22 22,5	25	1 000 1 500	∞	0,002 3 0,001 5	0	0,000 8 0,000 5	75 110	35,0 40,0	0	
Zand	Schoon	Los	17	19	5	200	∞	0,011 5	0	0,003 8	15	30,0	0	
		Matig	18	20	15	600	∞	0,003 8	0	0,001 3	45	32,5	0	N.v.t.
		Vast	19 20	21 22	25	1 000 1 500	∞	0,002 3 0,001 5	0	0,000 8 0,000 5	75 110	35,0 40,0	0	
	Zwak siltig, kleiig		18 19	20 21	12	450 650	∞	0,005 1 0,003 5	0	0,001 7 0,001 2	35 50	27,0 32,5	0	N.v.t.
	Sterk siltig, kleiig		18 19	20 21	8	200 400	∞	0,011 5 0,005 8	0	0,003 8 0,001 9	15 30	25,0 30,0	0	N.v.t.
Leem [e]	Zwak zandig	Slap	19	19	1	25	650	0,092 0	0,003 7	0,030 7	2	27,5 30,0	0	50
		Matig	20	20	2	45	1 300	0,051 1	0,002 0	0,017 0	3	27,5 32,5	1	100
		Vast	21 22	21 22	3	70 100	1 900 2 500	0,032 9 0,023 0	0,001 3 0,000 9	0,011 0 0,007 7	5 7	27,5 35,0	2,5 3,8	200 300
	Sterk zandig		19 20	19 20	2	45 70	1 300 2 000	0,051 1 0,032 9	0,002 0 0,001 3	0,017 0 0,011 0	3 5	27,5 35,0	0 1	50 100
Klei	Schoon	Slap	14	14	0,5	7	80	0,328 6	0,013 1	0,109 5	1	17,5	0	25
		Matig	17	17	1,0	15	160	0,153 3	0,006 1	0,051 1	2	17,5	5	50
		Vast	19 20	19 20	2,0	25 30	320 500	0,092 0 0,076 7	0,003 7 0,003 1	0,030 7 0,025 6	4 10	17,5 25,0	13 15	100 200
	Zwak zandig	Slap	15	15	0,7	10	110	0,230 0	0,009 2	0,076 7	1,5	22,5	0	40
		Matig	18	18	1,5	20	240	0,115 0	0,004 6	0,038 3	3	22,5	5	80
		Vast	20 21	20 21	2,5	30 50	400 600	0,076 7 0,046 0	0,003 1 0,001 8	0,025 6 0,015 3	5 10	22,5 27,5	13 15	120 170
	Sterk zandig	-	18 20	18 20	1,0	25 140	320 1 680	0,092 0 0,016 4	0,003 7 0,000 7	0,030 7 0,005 5	2 5	27,5 32,5	0 1	0 10
	Organisch	Slap	13	13	0,2	7,5	30	0,306 7	0,015 3	0,102 2	0,5	15,0	0 1	10
		Matig	15 16	15 16	0,5	10 15	40 60	0,230 0 0,153 3	0,011 5 0,007 7	0,076 7 0,051 1	1,0 2,0	15,0	0 1	25 30
Veen	Niet voorbelast	Slap	10 12	10 12	0,1	5 7,5	20 30	0,460 0 0,306 7	0,023 0 0,015 3	0,153 3 0,102 2	0,2 0,5	15,0	1 2,5	10 20
	Matig voorbelast	Matig	12 13	12 13	0,2	7,5 10	30 40	0,306 7 0,230 0	0,015 3 0,011 5	0,102 2 0,076 7	0,5 1,0	15,0	2,5 5	20 30
Variatiecoëfficiënt v			0,05		–	0,25					0,10		0,20	

[a] De tabel geeft van de desbetreffende grondsoort de lage, respectievelijk de hoge karakteristieke waarde van gemiddelden. Binnen een gebied, vastgesteld door de rij van het bijmengsel en de kolom van de parameter (een cel), geldt:

— als een verhoging van de waarde van een van de grondeigenschappen tot een ongunstiger situatie leidt dan de toepassing van de in de tabel gepresenteerde lagere karakteristieke waarde, moet de rechterwaarde op dezelfde regel zijn gebruikt. Is er rechts geen waarde vermeld, dan moet de waarde er recht onder zijn toegepast;

OPMERKING Dit is bijvoorbeeld het geval bij negatieve kleef op een paal waar een hogere waarde van φ', c' en c_u ook een hogere waarde van de negatieve kleef oplevert.

— voor $C_c/(1+e_0)$, C_α en $C_{sw}/(1+e_0)$ zijn in de tabel de hoge karakteristieke gemiddelde waarden vermeld.

[b]	Los:	0	$< R_n <$	0,33
	Matig:	0,33	$\leq R_n \leq$	0,67
	Vast:	0,67	$< R_n <$	1,00

[c] De γ-waarden zijn van toepassing bij een natuurlijk vochtgehalte.

[d] De hier gegeven q_c-waarden (conusweerstand) behoren beschouwd te worden als ingang in de tabel en mogen niet in de berekeningen worden gebruikt.

[e] De waarden hebben betrekking op verzadigd leem.

[f] De C_α-waarden zijn geldig voor een spanningverhogingstraject van ten hoogste 100 %.

[g] Voor grind, zand en in beperkte mate ook voor leem en sterk zandige klei zijn q_c, E_{100}, φ' en de samendrukkingsparameters C'_p, $C_c/(1+e_0)$ en $C_{sw}/(1+e_0)$ genormeerd voor een effectieve verticale grondspanning σ'_v van 100 kPa. Om voor de in het terrein gemeten waarden van q_c een juiste ingang in de tabel te krijgen moeten deze waarden zijn geconverteerd naar het niveau van de effectieve verticale grondspanning σ'_v van 100 kPa. In dat kader moet de formule $q_{c;tabel} = q_{c;terrein} \times C_{qc}$ worden gebruikt, waarbij C_{qc} moet zijn ontleend aan $C_{qc} = (100/\sigma'_v)^{0,67}$. Voor de hoek van inwendige wrijving φ' en de cohesie c' geldt dat deze afhankelijk zijn van de consistentie van de grond. Dit betekent dat deze conversie ook nodig is voor φ' en c'. Als $q_{c;tabel}$ groter wordt dan de in de tabel gegeven waarde geldt de onderste regel voor de desbetreffende grondsoort.

[h] De elasticiteitsmodulus bij belastingsherhalingen mag zijn aangenomen als zijnde driemaal de aangegeven waarde.

VOORBEELD In schoon zand op een diepte van 5 m onder water is gemeten: $q_{c;terrein}$ = 9 MPa en σ'_v = 50 kPa. Uit de formule voor C_{qc} volgt dan $C_{qc} = 2^{0,67} \approx 1,6$. Volgens de formule voor $q_{c;tabel}$ geldt dan in dit voorbeeld $q_{c;tabel} = 9 \times 1,6 = 14,4$ MPa. Dit betekent dat E = 45 MPa, φ' = 32,5 graden, C'_p = 600, $C_c/(1+e_0)$= 0,003 8 en $C_{sw}/(1+e_0)$ = 0,001 3.

A.2. α_p conform new rules

Paaltype			Paalklassefactor [a]			Last-zakkingslijn figuren 7.n en 7.o
Type	Nadere specificatie	Wijze van installeren	α_p	α_s	α_t	
Beton-paal	Geprefabriceerd; met constante dwarsafmeting	Geheid	0,7	0,010	0,007	1
	In de grond gevormd met een gladde mantelbuis op een voetplaat, waarbij het beton direct tegen de grond drukt	Geheid; de mantelbuis wordt terugheiend in combinatie met statisch trekken uit de grond verwijderd; de voetplaat blijft in de grond achter	0,7	0,014	0,012[c]	1
	In de grond gevormd met een gladde mantelbuis op een voetplaat, waarbij het beton direct tegen de grond drukt	Geheid; de mantelbuis wordt trillend in combinatie met statisch trekken uit de grond verwijderd; de voetplaat blijft in de grond achter	0,7	0,012	0,010[c]	1
	In de grond gevormd met een gladde mantelbuis op een schroefpunt, waarbij het beton direct tegen de grond drukt	Geschroefd; bij het trekken van de mantelbuis blijft de schroefpunt in de grond achter	0,63	0,009	0,009	1
	In de grond gevormd met behulp van een avegaar	Geschroefd	0,56	0,006	0,0045	2
	In de grond gevormd met behulp van een steunvloeistof	Gegraven of geboord	0,35	0,006	0,0045	3
Stalen paal	Constante dwarsafmeting; buis met gesloten punt [b]	Geheid	0,70	0,010	0,007	1
	Constante dwarsafmeting; profiel	Geheid	0,70	0,006	0,004	1
	Constante dwarsafmeting; open buis	Geheid	0,70	0,006	0,004	1
	In de grond gevormde groutschil rond profiel met voetplaat	Geheid; met groutinjectie	0,70	0,014	0,012	1

Paaltype			Paalklassefactor [a]			Last-zakkingslijn figuren 7.n en 7.o
Type	Nadere specificatie	Wijze van installeren	α_p	α_s	α_t	
	Constante dwarsafmeting boven de schroefpunt	Geschroefd	0,56	0,006	0,0045	1
	In de grond gevormde groutschil rond buis met schroefpunt (schachtmiddellijn 300 mm of groter)	Geschroefd zonder de paal tijdens het aanbrengen op en neer te halen; menging van de grond met grout	0,63	0,009	0,009	1
	Constante dwarsafmeting	Gepulst	0,35	0,005	-	3
Micro-paal [d e]	In de grond gevormd met dubbele boorbuis, waarbij het grout direct tegen de grond drukt	Spoelboren met groutinjectie, niet afgeperst	0,35	0,008 [f]	0,008 [f]	2
		Spoelboren met groutinjectie, wel afgeperst	0,35	0,011 [g]	0,011 [g]	1
	In de grond gevormd met enkele boorbuis, waarbij het grout direct tegen de grond drukt	Spoelboren buitenom met groutinjectie, niet afgeperst	0,35	0,008 [f]	0,008 [f]	2
		Spoelboren buitenom met groutinjectie, wel afgeperst	0,35	0,011 [g]	0,011 [g]	1
	In de grond gevormd met ankerbuizen en boorkop, waarbij het grout direct tegen de grond drukt	Zelfborend met groutinjectie	0,35 [h]	0,008 [f]	0,008 [f]	2
	In de grond gevormd met ankerbuizen en schroefbladen, waarbij het grout direct tegen de grond drukt	Geschroefd; menging van de grond met grout	0,35 [h]	0,008 [f]	0,008 [f]	2
	In de grond gevormd met stalen hulpbuis, waarbij het grout direct tegen de grond drukt	Ingetrild met groutinjectie	0,35	0,006	0,006	2
Houten paal	Constante dwarsafmeting	Geheid	0,7	0,010	0,007	1
	Taps toelopend	Geheid	0,7	0,012	0,007	1

[a]
- Uit proefbelastingen kunnen hogere waarden voor α_p, α_s of α_t volgen dan de in deze tabel gegeven waarden.
- Wanneer (projectgebonden) proefbelastingen volgens 7.6.2.2 respectievelijk 7.6.2.3 zijn uitgevoerd, dan zijn de resultaten van de proefbelastingen alleen geldig voor die specifieke geotechnische constructie.
- Wanneer voldaan is aan 7.5 en de proeven volgens 7.5.2.2(3)P(f) op ten minste 2 terreinen zijn uitgevoerd en waarbij het rapport van de paalbelastingsproef (de beschrijving van het paalsysteem en van het installatieproces) volgens 7.5.4 samen met het rapport van toezicht op de uitvoering volgens 7.9 voor iedereen toegankelijk zijn, dan zijn deze paalfactoren α_p, α_s of α_t voor het specifieke beproefde paalsysteem van de betreffende leverancier van toepassing.
- Totdat de toepasselijke aanwijzing in de bouwregelgeving heeft plaatsgevonden, mogen de in deze tabel gegeven waarden voor α_p zijn vermenigvuldigd met 1,43 (=1/0,7).

[b] De voetplaat van de buispaal met gesloten voet mag niet meer dan 10 mm uitsteken buiten de buis.

[c] Bij trekpalen van dit type paal mag de voetplaat niet meer dan 25 mm uitsteken buiten de mantelbuis.

B

4D/8D Calculation of $q_{c,I,II,III}$

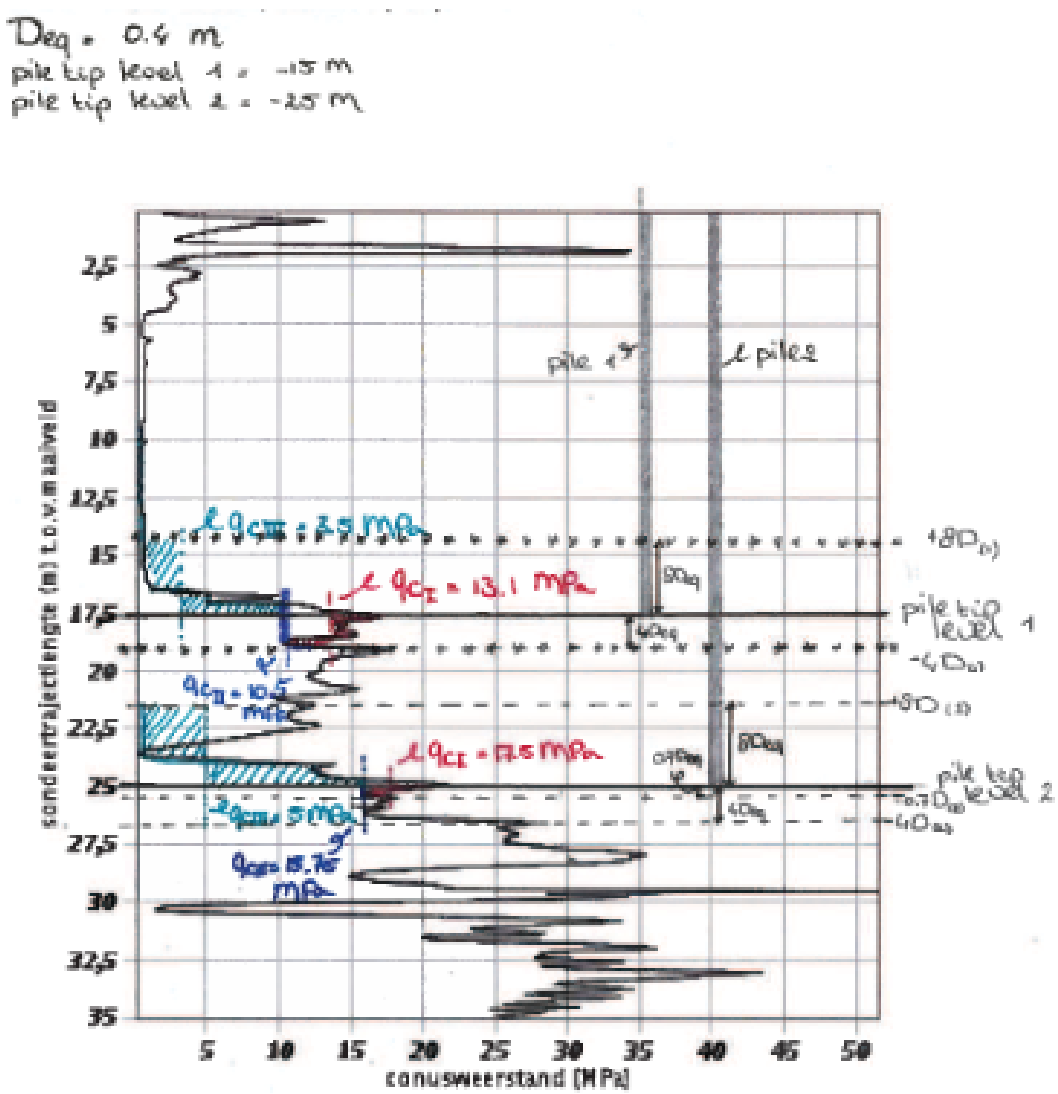

Figure B.1: Example on how to calculate $q_{c,I,II,III}$

C
Comparison CPT-based methods

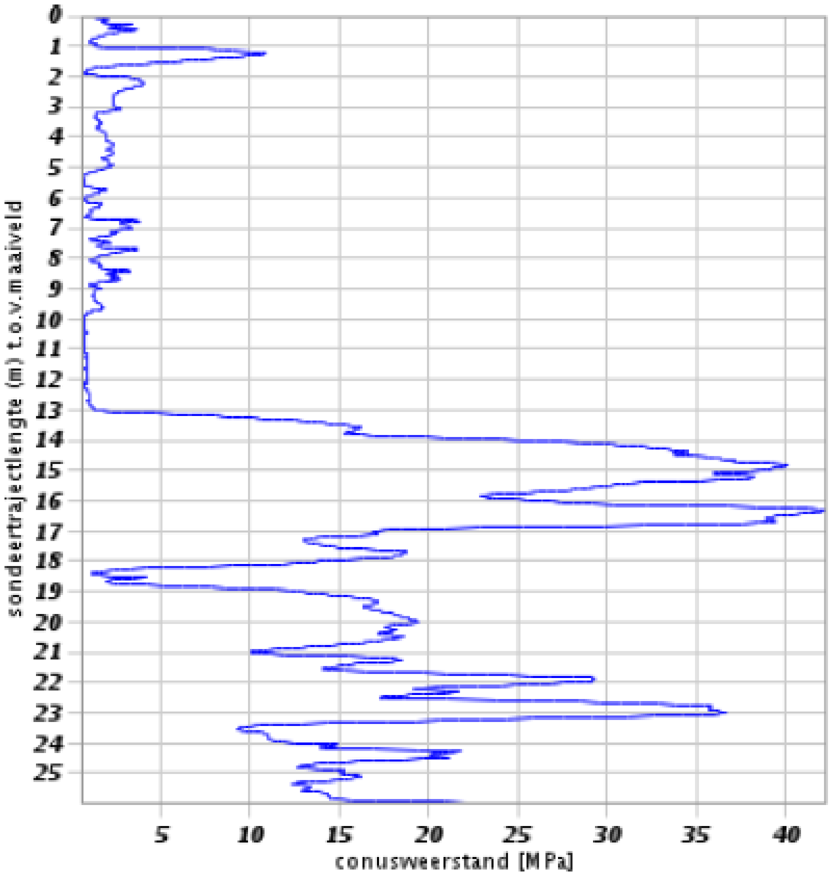

Figure C.1: CPT1

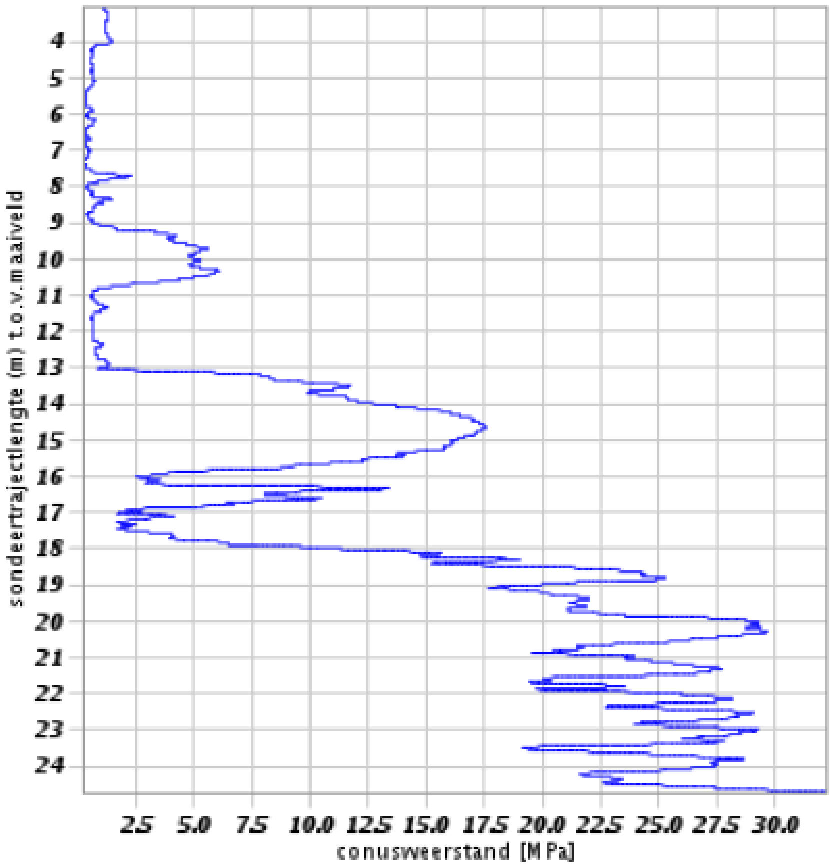

Figure C.2: CPT2

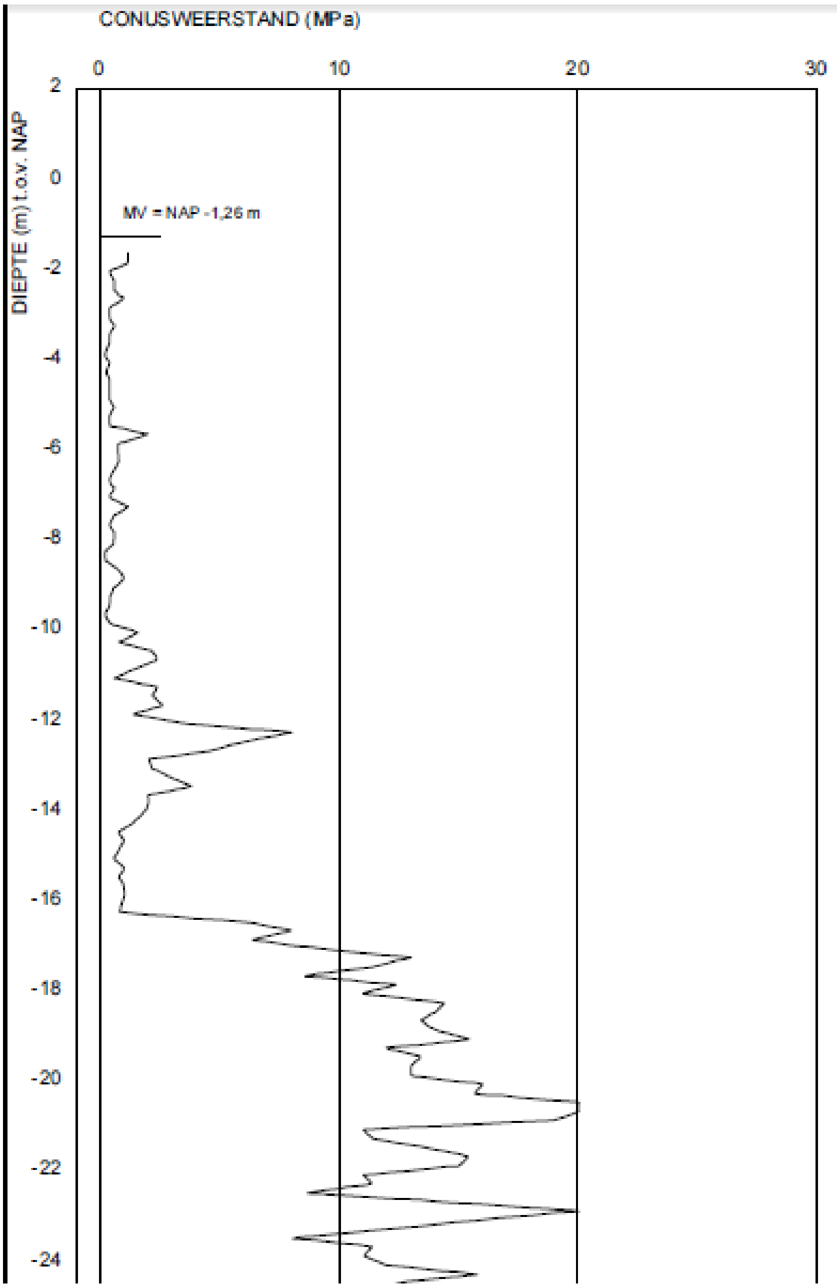

Figure C.3: CPT3

D

Data Assesment

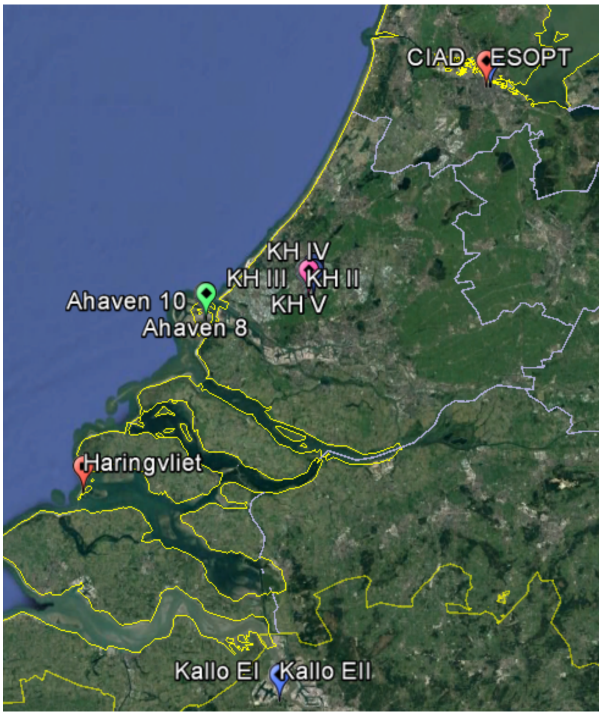

Figure D.1: Location of tests

Figure D.2: Location of tests Limelette

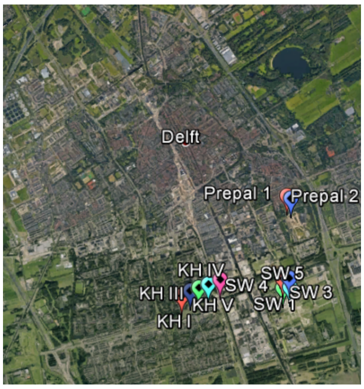

Figure D.3: Location of tests Delft

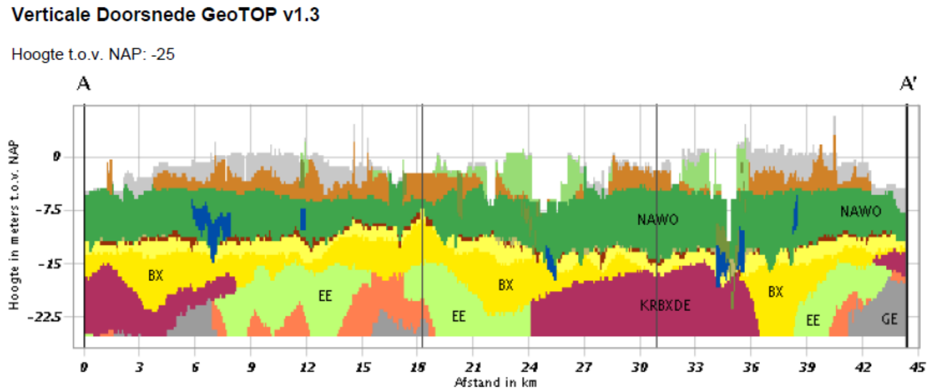

Figure D.5: Map Amsterdam

Figure D.4: Geological cross-section Amsterdam [TNO, 2016]

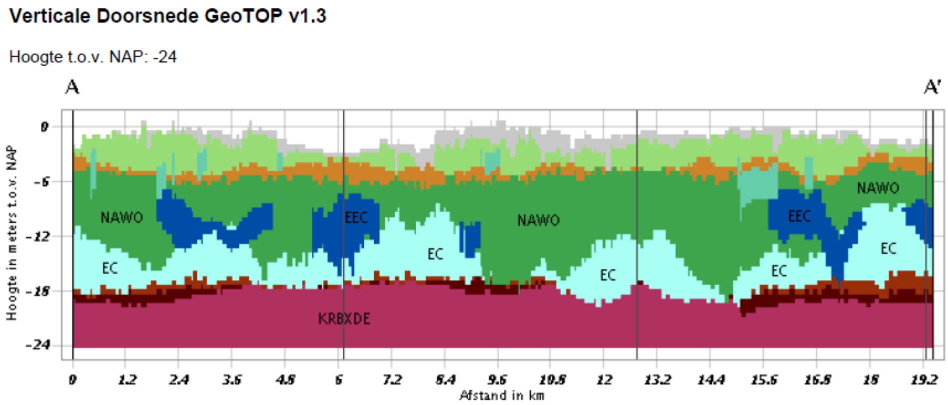

Figure D.7: Map Delft

Figure D.6: Geological cross-section Delft [TNO, 2016]

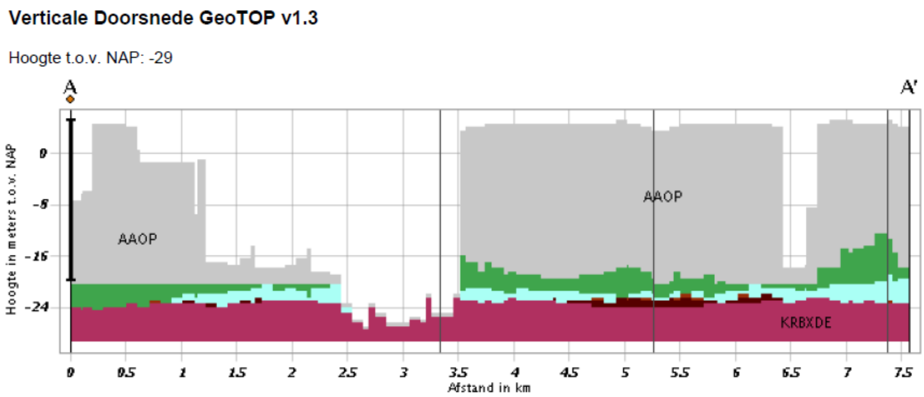

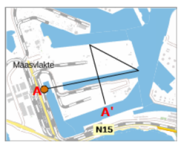

Figure D.9: Map Amazonehaven

Figure D.8: Geological cross-section Amazonehaven [TNO, 2016]

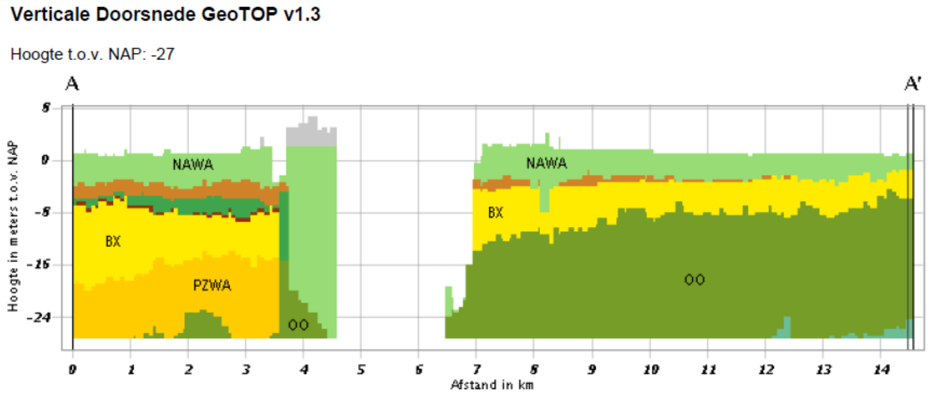

Figure D.11: Map Kallo

Figure D.10: Geological cross-section Kallo [TNO, 2016]

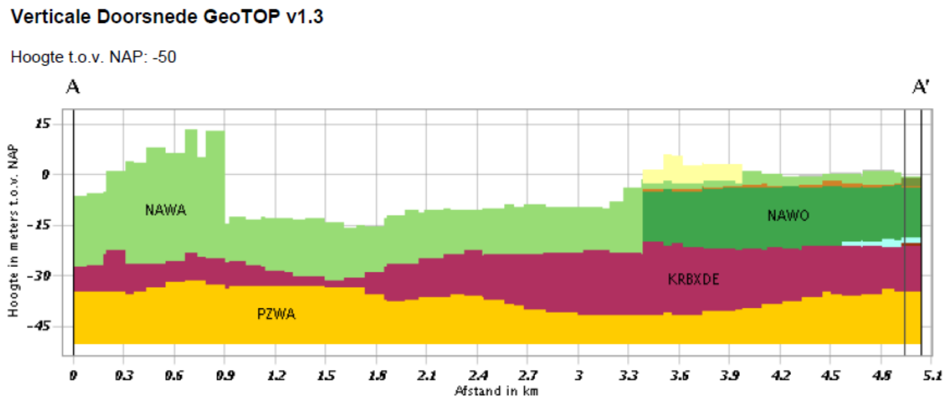

Figure D.13: Map Haringvliet

Figure D.12: Geological cross-section Haringvliet [TNO, 2016]

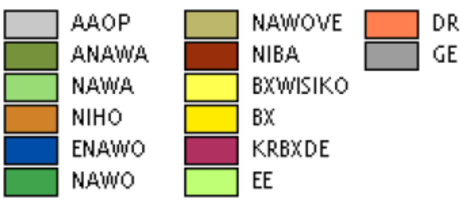

Figure D.14: Geological units

From figures D.4, D.6, D.8, D.10 and D.12, table D.1 was created to compare the test locations based on the geological unit.

Name	Location	Pile tip level	Formation from bore-hole	q_c (Mpa)	Formation from CPT	Age
Ahaven 10	Maasvlakte	-25	KRBXDE	43	KR	?
Ahaven 6	Maasvlakte	-25	KRBXDE	43	KR	?
Ahaven 8	Maasvlakte	-25	KRBXDE	43	KR	?
CIAD	Amsterdam	-21,8	?	18	KR	?
ESOPT II	Amsterdam	-13	BX	16	BX	Holocene/ Pleistocene
Haringvliet	Zeeland	-11,2	KRBXDE	20	KR	?
Kallo EI	Antwerpen	-10	BX	17	?	Holocene/ Pleistocene
Kallo EII	Antwerpen	-10	BX	16	?	Holocene/ Pleistocene
KH I	Delft	-12	KRBXDE	12	KR	?
KH II	Delft	-18	KRBXDE	12	KR	?
KH III	Delft	-20	KRBXDE	12	KR	?
KH IV	Delft	-22	KRBXDE	12	KR	?
KH V	Delft	-24	KRBXDE	12	KR	?
Prepal 1	Delft	-19,5	KRBXDE	15	KR	?
Prepal 2	Delft	-19,5	KRBXDE	14	KR	?
SW 1	Delft	-12	KRBXDE	6	BX	?
SW 3	Delft	-19,25	KRBXDE	15	KR	?
SW 4	Delft	-19,1	KRBXDE	15	KR	?
SW 5	Delft	-19,1	KRBXDE	15	KR	?
Lim 1 cpt 5 concrete pile (p8)	Brussel	-9,5	?		?	?
Lim I CPT 5 tub pile (p4)	Brussel	-9,5	?		?	?
Lim II B1	Brussel	-9,5	?		?	?
Lim II B2	Brussel	-9,5	?		?	?

Table D.1: Data assessment

In table D.1 KRBXDE stands for the formation of Boxtel, Kreftenheye and the layer of Delwijnen i.e. in this area it is not known which deposit belongs to this layer. This makes it hard to eliminate certain test based on the geological unit. For Limelette the geological unit is expected to be completely different as the geographical location is very off. Therefore, it will be neglected during the analysis. For the CIAD test, the variation in the geological unit at the pile tip level of the test is large in Amsterdam. However as it could be the Boxtel, the Kreftenheye or the Eem Formation, it will not be neglected during the analysis, but it will be handled carefully.

	van Boxtel	van Kreftenheye
Abbreviation	BX	KR
Grain size	Medium (105-300um)	Coarse (210-2000um)
Age	Holocene/ Middle and Late Pleistocene	Late Pleistocene
Deposit	Unknown	Fluvial
Confusions	Over the middle line of the Netherlands it can be hard to distinguish between BX and KR.	The river dune deposit is fine grained, so it is more similar to the Boxtel formation. This deposit is called the layer of Delwijnen and although it belongs to the KR formation considering age, it was assigned to the Boxtel formation as the grain distribution is more similar.

Table D.2: van Boxtel versus van Kreftenheye [TNO, 2013]

Furthermore one has to notice the relatively large amount of test done in Delft. This might influence the accuracy of the different analysis. Therefore it is important to always bear this in mind and look at the data with a critical geotechnical point of view.

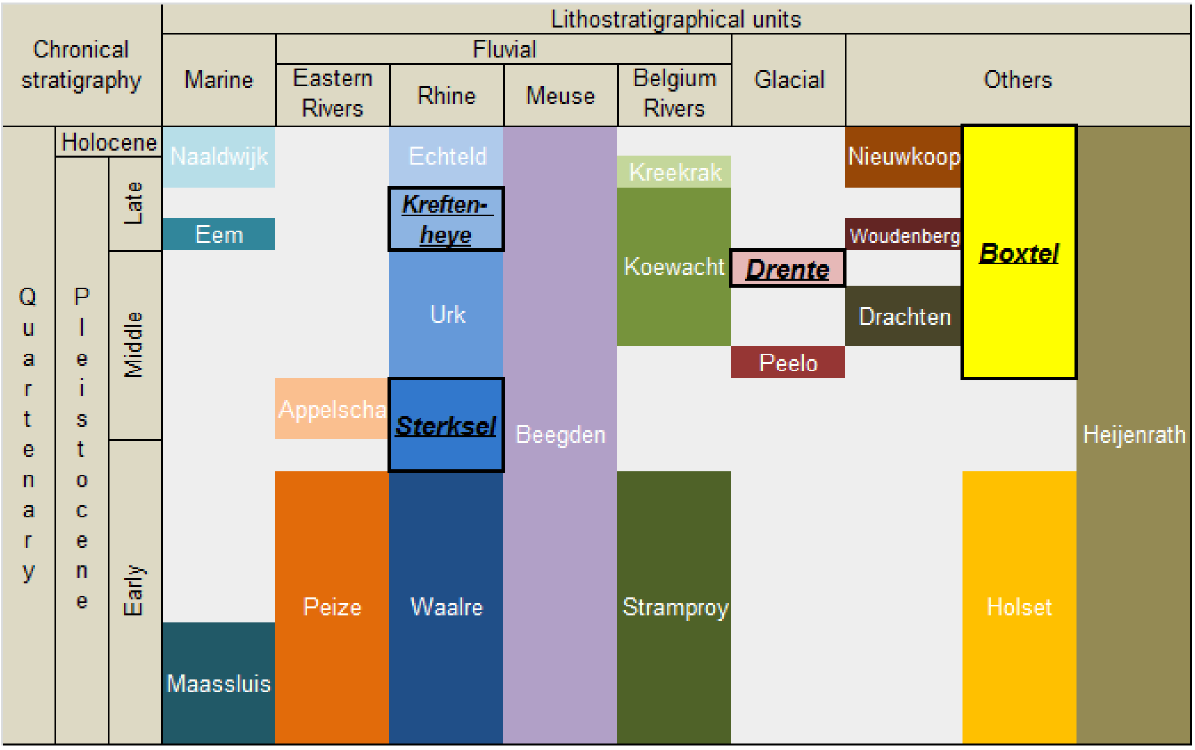

Figure D.15: Overview of the Geological units adapted from [TNO, 2013]

	van Drente	**van Kreftenheye**
Abbreviation	DR	KR
Grain size	Coarse (210-2000um)	Coarse (210-2000um)
Age	Middle Pleistocene	Late Pleistocene
Deposit	Glaciofluvial	Fluvial
Confusions	The layer of Schaarsbergen can be confused with KR.	In the middle and west part of the Netherlands, it is hard to distinguish KR from the Glaciofluvial deposits (DR).

Table D.3: van Drente versus van Kreftenheye [TNO, 2013]

	van Drente	**van Sterksel**
Abbreviation	DR	ST
Grain size	Coarse (210-2000um)	Coarse (210-2000um)
Age	Middle Pleistocene	Early and Middle Pleistocene
Deposit	Glaciofluvial	Fluvial
Confusions	The layer of Schaarsbergen can be confused with KR.	In some parts of the country, BX might be confused with ST. This only happens if sedimentation of BX took place.

Table D.4: van Drente versus van Sterksel [TNO, 2013]

E

CPTs and correlations for Pile Load Test at Kruithuisweg, Delft

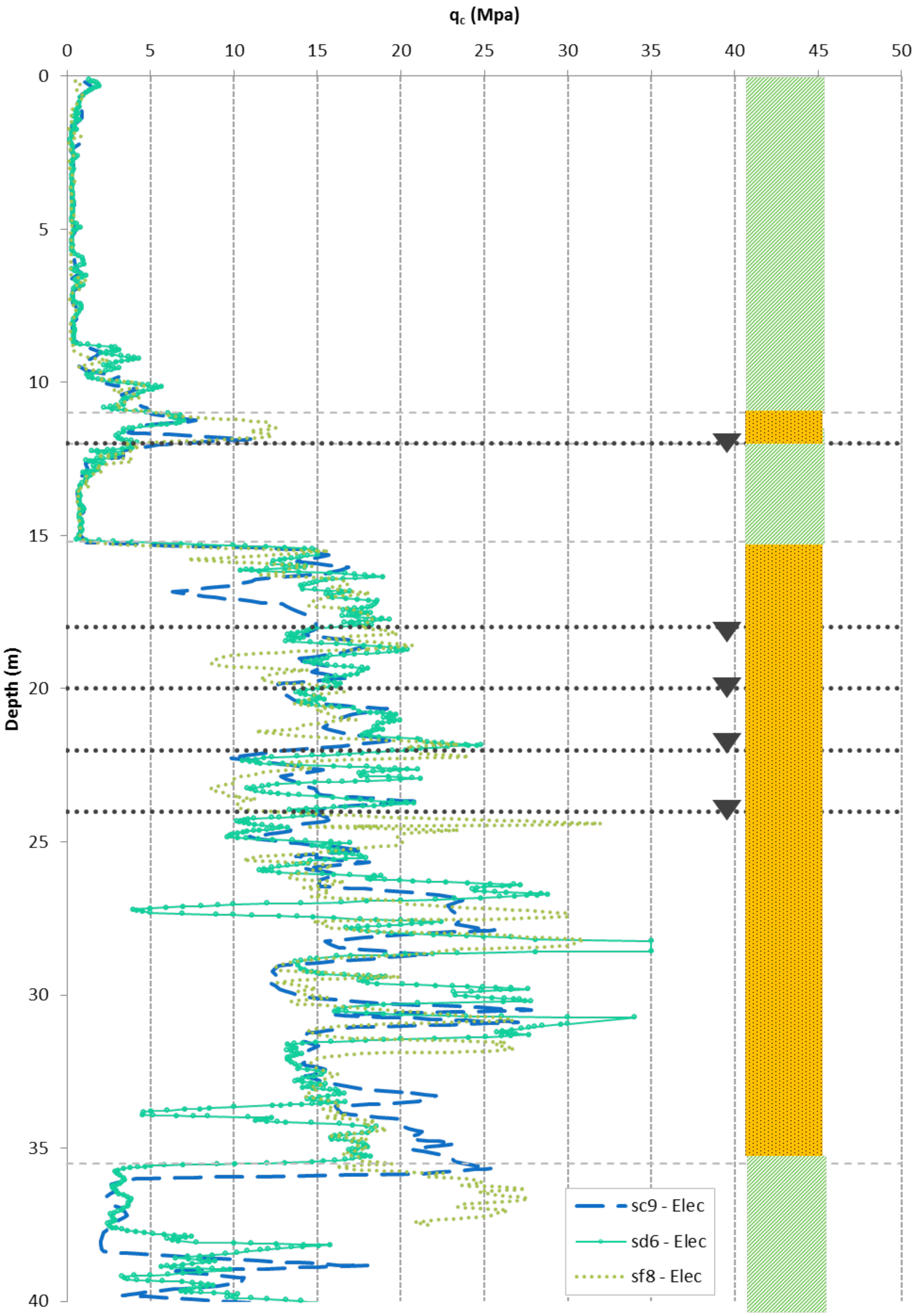

Figure E.1: CPT

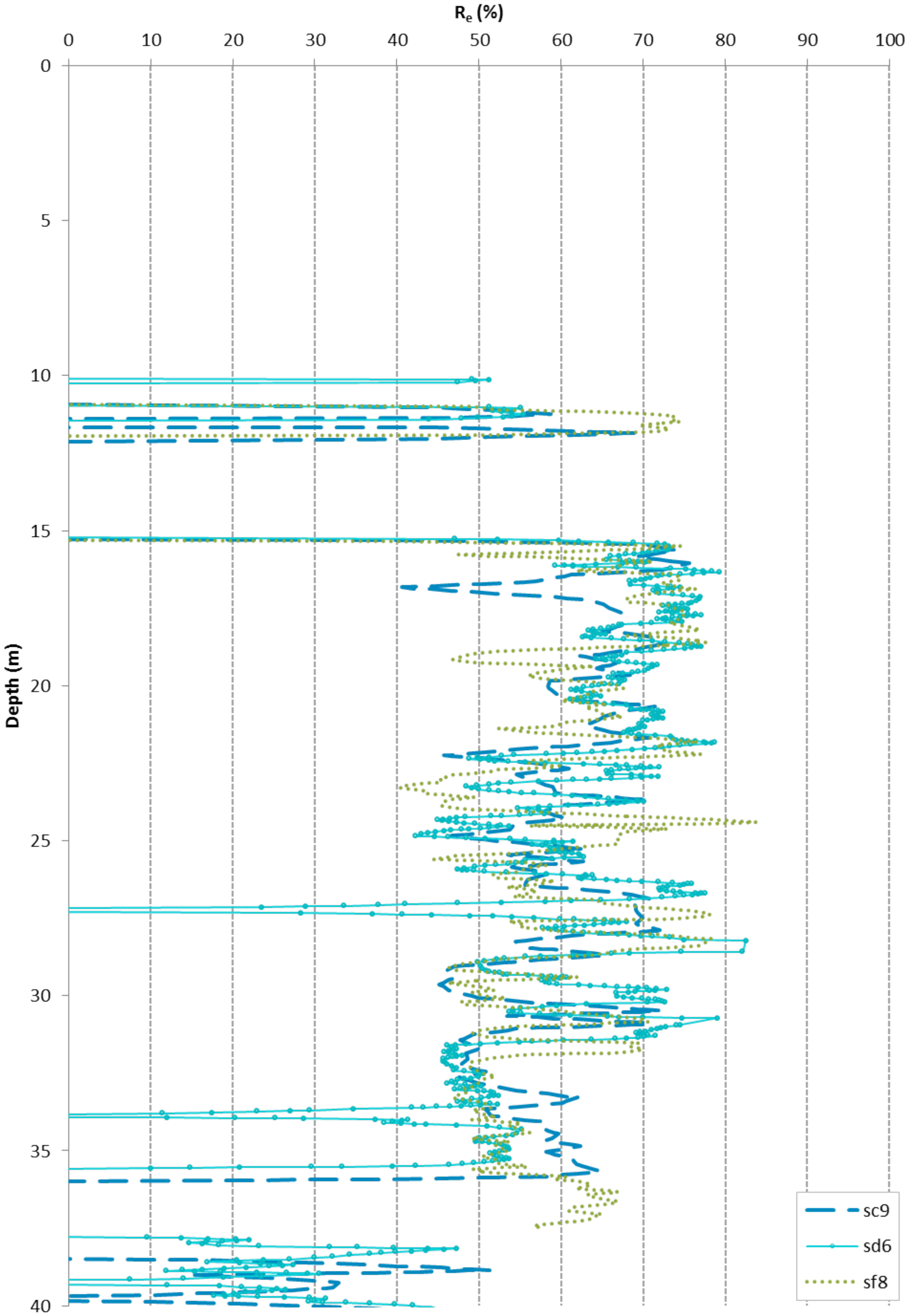

Figure E.2: Relative density [Lunne et al., 1997]

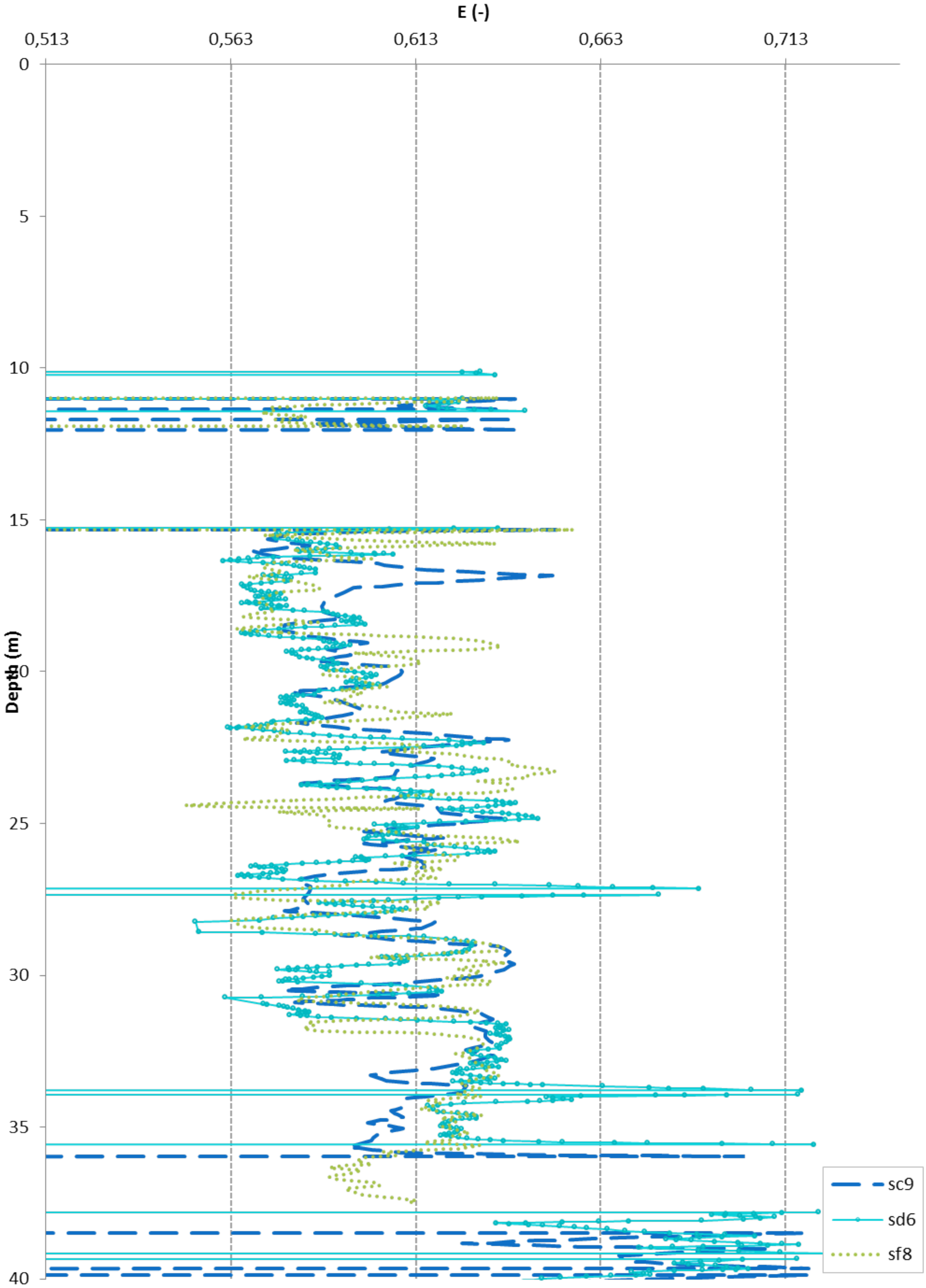

Figure E.3: void ratio

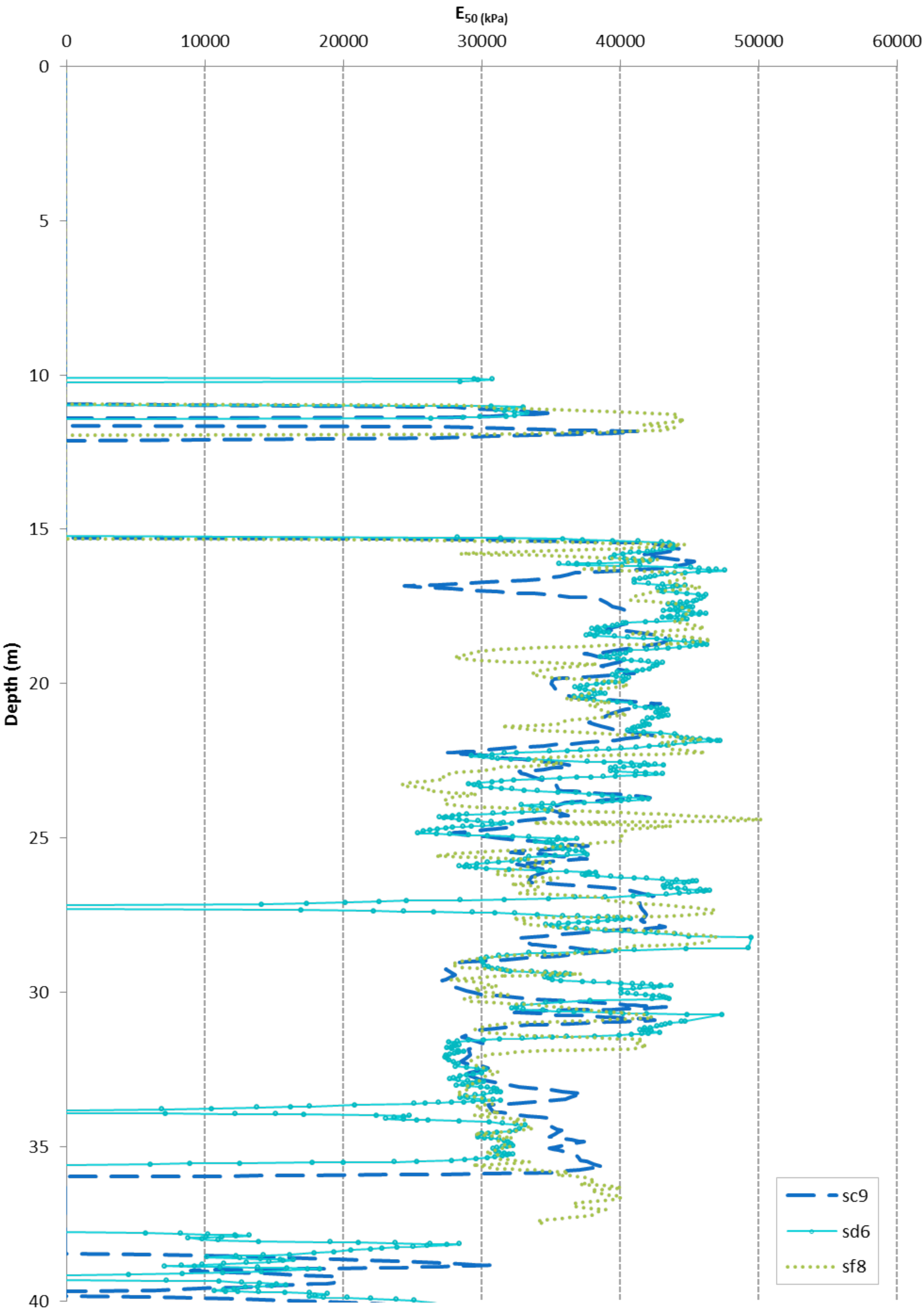

Figure E.4: E_{50}^{ref} [Brinkgreve et al., 2015]

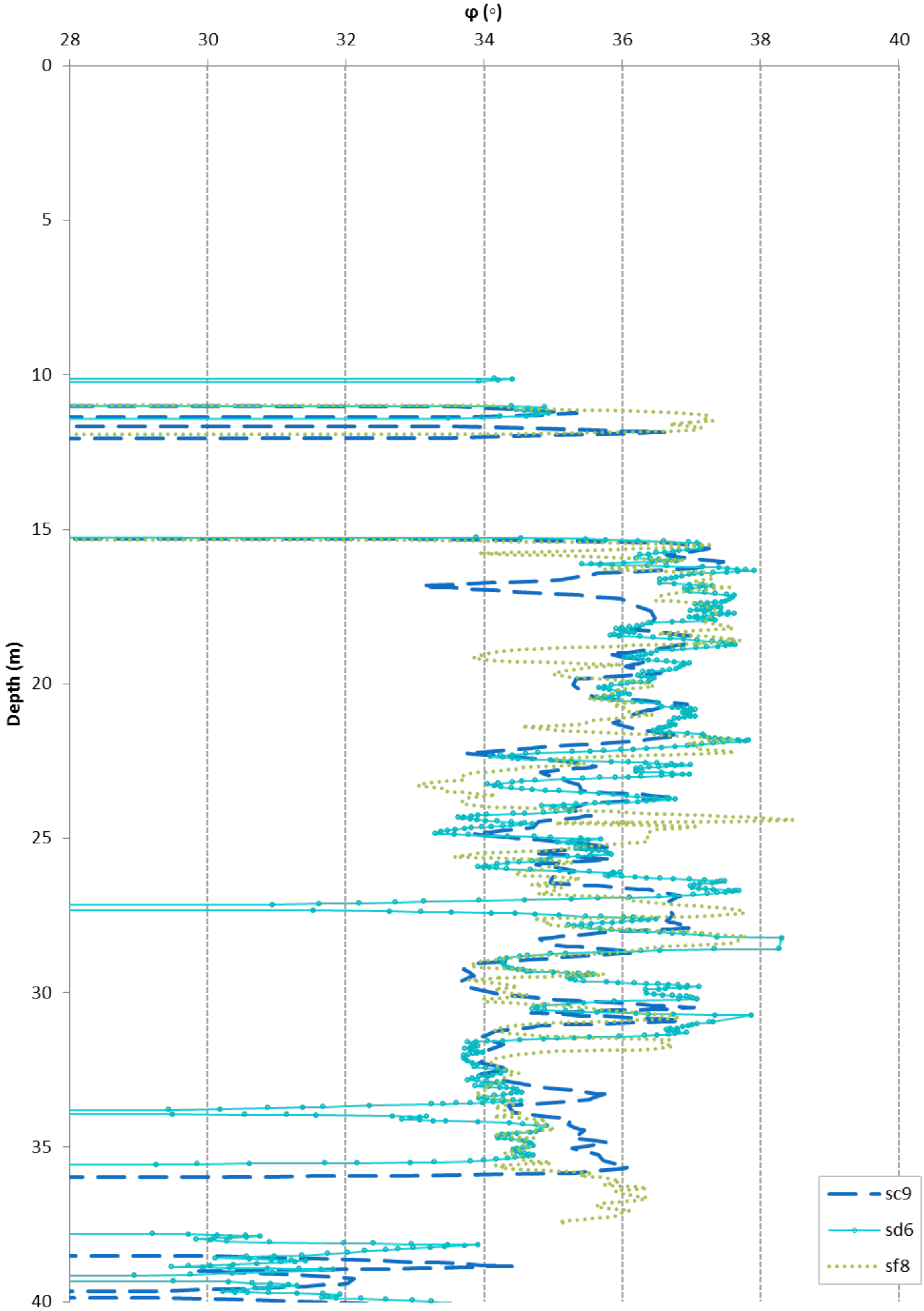

Figure E.5: ϕ' [Brinkgreve et al., 2015]

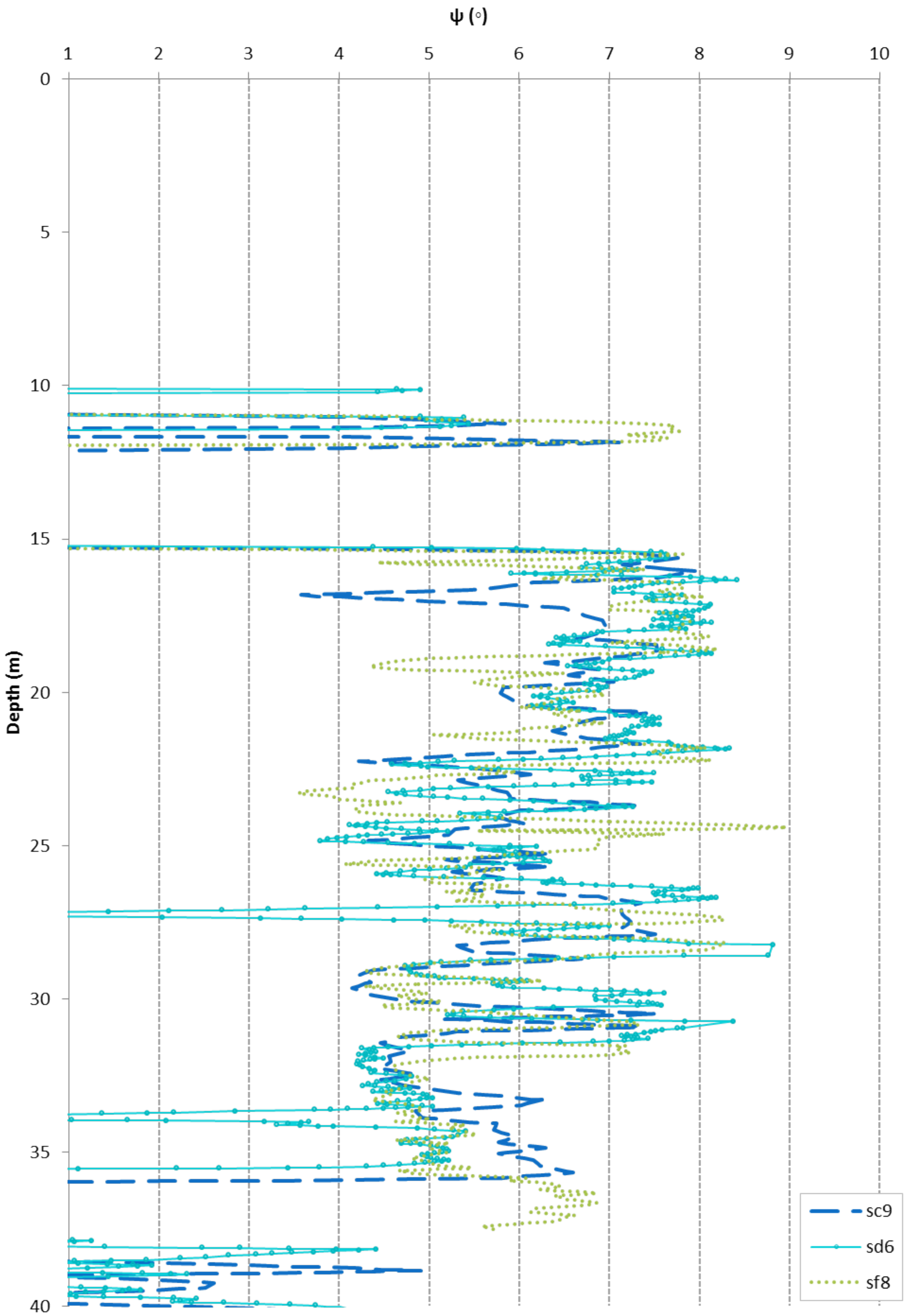

Figure E.6: psi' [Brinkgreve et al., 2015]

F
Determination of ϕ'

The influence of a small change in ϕ' is quite significant. Therefore choosing the most suitable method for determine ϕ' is important. From CPT data ϕ' can be determined directly and indirectly. Directly means, CPT data are correlated through a formula to ϕ'. Indirect, in this case, means, ϕ' is calculated through R_e. The following methods will be set out and discussed.

- Direct:
  1. Robertson and Campanella
  2. Kulhawy and Mayne
  3. Uzielli
  4. NEN 9997-1
- Indirect - R_e:
  1. Lunne
  2. Baldi
  3. Jamiolkowski

F.1. Vertical Effective Stresses

Before going deeper into the different methods, all methods normalize the cone resistance for the vertical stresses. To be able to determine the vertical stresses the unit weight of soil has to be known. This can be derived from CPTs with the help of Robertson's classification chart, shown in Figure F.1.

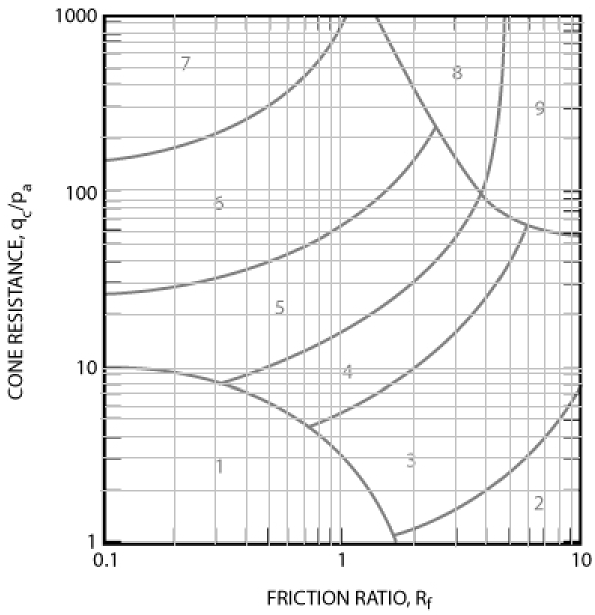

Figure F.1: Robertson's classification chart [Robertson and Cabal, 2010]

Zone	Soil behaviour type	Approximate unit weight (kN/m^3)
1	Sensitive fine grained	17.5
2	Organic clay	12.5
3	Clay - Silty clay to clay	18
4	Silt mixture - Silty clay to clayey silt	18
5	Sand mixture - Silty sand to sandy silt	18.5
6	Sand - Clean sand to silty sand	19
7	Gravelly sand to dense sand	20
8	Very stiff sand to clayey sand (OC or cemented)	19
9	Very stiff fine grained (OC or cemented)	20.5

Table F.1: Preliminary approximate estimate of soil unit weight based on Robertson classification chart [Lunne et al., 1997]

Soil behaviour type	Approximate unit weight (kN/m^3) according to [Lunne et al., 1997]	Approximate unit weight (kN/m^3) according to [Normcommissie 351 006 'Geotechniek', 2017a]	Difference
Sensitive fine grained	17.5	-	-
Organic clay	12.5	13	0.5
Clay - Silty clay to clay	18	18	0
Silt mixture - Silty clay to clayey silt	18	18	0
Sand mixture - Silty sand to sandy silt	18.5	20	1.5
Sand - Clean sand to silty sand	19	20	1
Gravelly sand to dense sand	20	21	1
Very stiff sand to clayey sand (OC or cemented)	19	-	-
Very stiff fine grained (OC or cemented)	20.5	-	-

Table F.2: [Lunne et al., 1997] versus [Normcommissie 351 006 'Geotechniek', 2017a]

Lunne correlated the soil behaviour type from Robertson's classification chart to an approximate unit weight, see table F.1.
The soil behaviour types can also be correlated back to unit weight using table 2.b [Normcommissie 351 006 'Geotechniek', 2017a]. Table F.2 sets out the difference in soil unit weight between Lunne and NEN. As the difference is minor and the Dutch situation is considered calculations will be done using the approximate unit weight according to table 2.b from NEN 9997-1.

F.2. Direct Methods

F.2.1. Robertson and Campanella

Robertson and Campanella were the first to come up with a formula to determine ϕ' from a CPT. This formula is only valid for quartzitic sands. It happens to be the Dutch non-cohesive soils are quartzitic sands [Robertson et al., 1983].

$$\tan\phi'_p = \frac{1}{2.68}\left(\log\frac{q_c}{\sigma'_{v0}} + 0.29\right) \tag{F.1}$$

[Robertson et al., 1983]

F.2.2. Kulhawy and Mayne

Next Kulhawy and Mayne come up with a similar looking formula as Robertson and Campanella. The main difference is, they used the normalized cone resistance q_t. Especially in cohesive soils using q_t is a better approach. The given formula, again is only valid for quartz to siliceous sands. It happens to be the Dutch sandy soils are quartz silica sands. This means the formula from Kulhawy and Mayne should be valid in the Netherlands.

$$\phi'_p = 17.6 + 11\log q_{t1} \tag{F.2}$$

$$q_{t1} = \frac{q_t - \sigma_{v0}}{\sqrt{\sigma'_{v0} * p_a}} \tag{F.3}$$

$$q_t = q_c + U_2 * (1-a) \tag{F.4}$$

$$a = \frac{d^2}{D^2} \tag{F.5}$$

$$p_a = 100kPa \tag{F.6}$$

[Kulhawy and Mayne, 1990]

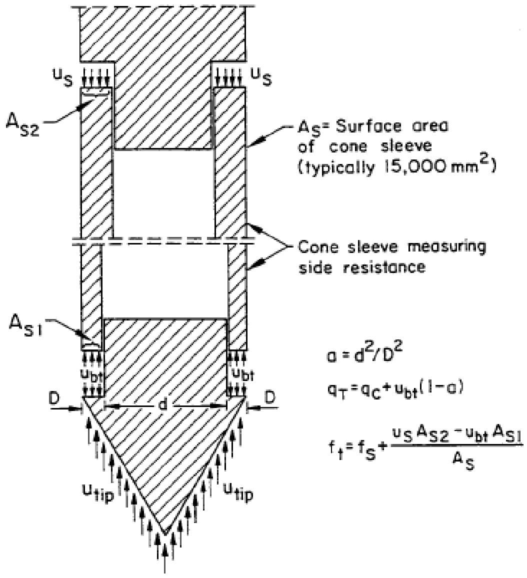

Figure F.2: How to determine q_t [Kulhawy and Mayne, 1990]

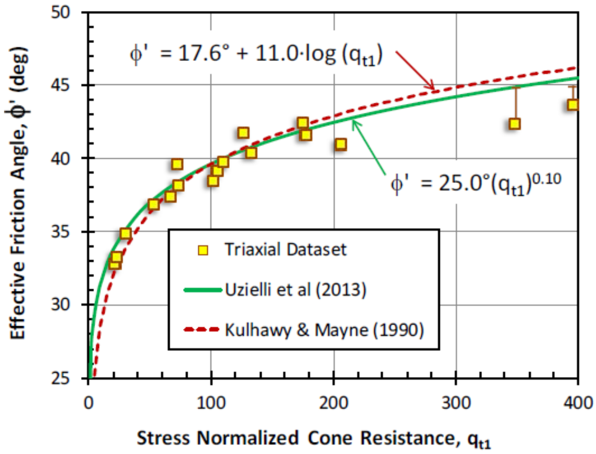

Figure F.3: ϕ', q_t-diagram according to Kulhawy and Mayne [Mayne, 2014]

In Figure F.2 u_{bt} is referred to as U_2 from now on. In general $q_t = q_c$ for sandy soils [Robertson and Cabal, 2010].

F.2.3. Uzielli

$$\phi' = 25 q_{t1}^{0.1} \tag{F.7}$$

[Mayne, 2014]

Uzielli set out a formula with a slide difference from the two previous named formulas for calculating ϕ' from CPT data. Figure F.3 shows the validation of equations (F.2) and (F.7), using data derived from CPTs and lab tests. Earlier it was mentioned lab testing for non-cohesive soils does not give reliable results. However, for the tests used in Figure F.3 the soil was frozen before extracting it from the ground. This way the samples could be moved without disturbing the soil properties.

F.2.4. Caquot, Koppejan and de Beer

$$\frac{q_c}{\sigma'_v} = 10^{3.04*\tan\phi'} \tag{F.8}$$

$$\frac{q_c}{\sigma'_v} = 1.3e^{\left(\frac{5\pi}{2}-\phi'\right)\tan\phi'} * \frac{1+\sin\phi'}{1-\sin\phi'} \tag{F.9}$$

$$\frac{q_c}{\sigma'_v} = 1.3e^{2\pi\tan\phi'} * \tan^2\left(45+\frac{\phi'}{2}\right) \tag{F.10}$$

Equation (F.8), (F.9) and (F.10) respectively were designed by Caquot, Koppejan and the Beer [van Tol, 1993]. These equations look different from equations (F.1), (F.2) and (F.7), but are quite similar.

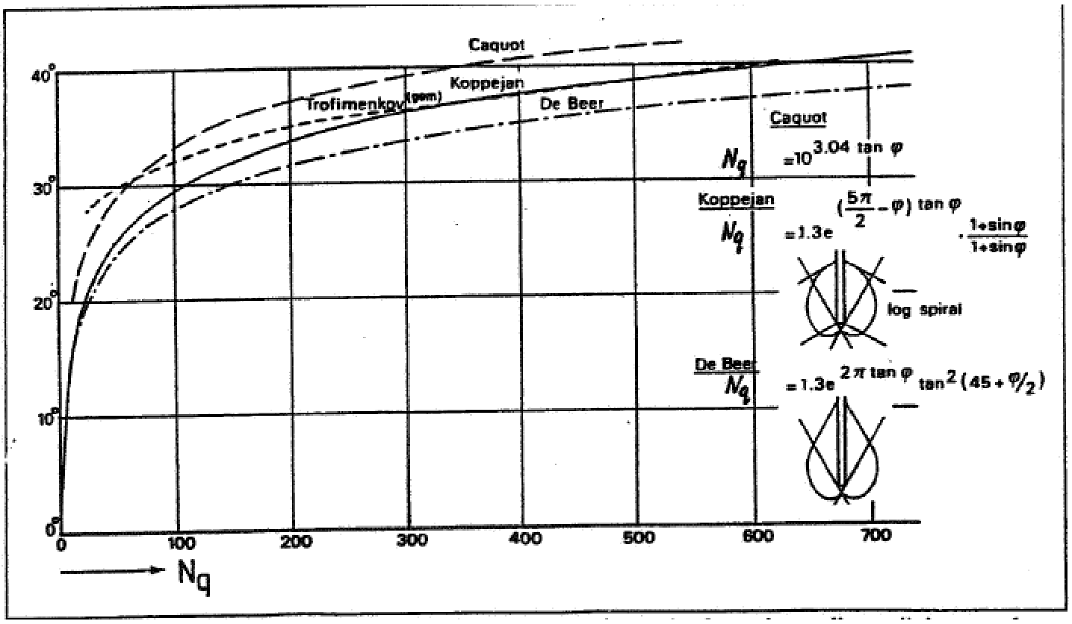

Figure F.4: Correlation between q_c and ϕ', $N_q = \frac{q_c}{\sigma'_v}$ [van Tol, 1993]

F.2.5. NEN table 2.b

Last the values from table 2.b in NEN 9997-1 are considered. As already mentioned several times the values given for ϕ' in this table are low characteristic values and therefore not usable for the scope of this thesis. However, as it is known it is not usable for the analysis of the influence of ϕ' on the failure surface around the pile tip, it can be used as a comparison to other methods determining ϕ', like the methods explained above. Therefore the values from the NEN are included in Figure F.7.

F.3. Indirect Methods (through R_e)

$$R_e = \frac{e_{max} - e}{e_{max} - e_{min}} \tag{F.11}$$

From (F.11) [Verruijt, 2012], it can be noticed the relative density has a value between 0 and 1. If the value is 1, the soil is in its densest state for values lower than 0.5 the soil is likely to compact even under small/short vibrations [Verruijt, 2012]. In other words, the state of the soil for $R_e < 0.5$ is very loose.

F.3.1. Lunne

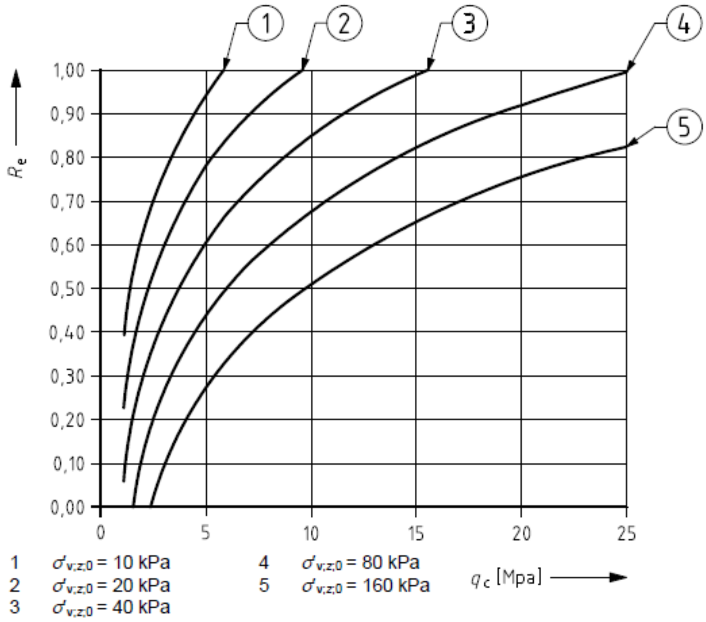

Figure F.5: R_e, q_c-diagram for different σ'_{vo} [Normcommissie 351 006 'Geotechniek', 2017a]

The formulas designed to calculate R_e from CPTs are well known and validated for Dutch non-cohesive soils. For example Figure F.5 comes from NEN 9997-1. The formula behind this figure is:

$$R_e = 0.34 * \ln\left(\frac{q_{c,z}}{61 * (\sigma'_{v0,z})^{0.71}}\right) \tag{F.12}$$

and was designed by [Lunne and Christoffersen, 1983].

F.3.2. Baldi and Jamiolkowski

Not only Lunne designed a formula to calculate the R_e from CPT data, equation (F.13) [Baldi et al., 1986] and equation (F.14) [Jamiolkowski et al., 1985] were respectively designed by Baldi and Jamiolkowski.

$$R_e = \frac{1}{2.61} * \ln\left(\frac{q_{c,z}}{181 * (\sigma'_{v0,z})^{0.55}}\right) \tag{F.13}$$

$$R_e = -0.98 + 0.66 * log\left(\frac{q_c * \frac{1}{9.81}}{\sqrt{\sigma'_{v0,z} * \frac{1}{9.81}}}\right) \tag{F.14}$$

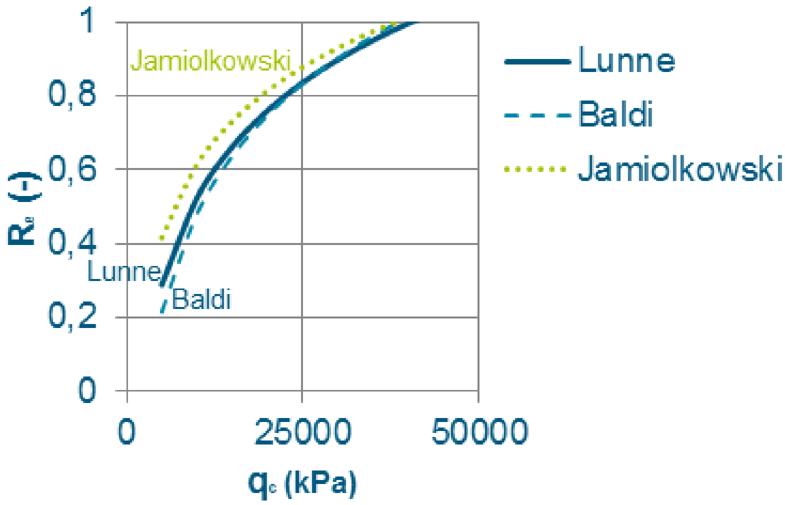

Figure F.6: [Lunne and Christoffersen, 1983] versus [Baldi et al., 1986] versus [Jamiolkowski et al., 1985] at $\sigma'_{v0} = 150kPa$

All three equations named in this section are set out in Figure F.6. The top boundary in the graph is set to $R_e = 1$, because, as mentioned before R_e cannot be larger than 1. The minimum value for q_c is chosen to be 5 MPa as sands are considered.
Only a small difference is noticeable between the three different formulas. Therefore equation (F.12) by Lunne is used as it is also used in NEN 9997-1.

Next a correlation between ϕ' and R_e has to be found. This was done by [Brinkgreve et al., 2015] expressing the following formula:

$$\phi' = 28 + 12.5R_e \tag{F.15}$$

Filling out this formula for the maximum and minimum values of R_e respectively gives ϕ's of 40.5^o and 28^o. Earlier in this thesis a range for ϕ' of 25^o and 50^o was given. However, this also included gravels, which is not the case for equation (F.15).
Combining equation (F.12) and (F.15) results in the following formula:

$$\phi' = 28 + 4.25 * \ln\left(\frac{q_{c,z}}{61 * (\sigma'_{v0,z})^{0.71}}\right) \tag{F.16}$$

F.4. Conclusion on determining ϕ'

From Figure F.7 it can be seen the 'direct' methods for determining ϕ' are very close together. On the other hand Caquot's method and determining ϕ' through R_e give lower results for ϕ'. These results are more of the order of the NEN. In Subsection F.2.5 it was mentioned these values are too low and therefore Caquot's method and the method using R_e can be eliminated as an option to calculate ϕ'. (The methods of Koppejan and de Beer were not plotted in Figure F.7 as their results for ϕ' are even lower than for Caquot's method, as seen in Figure F.4)

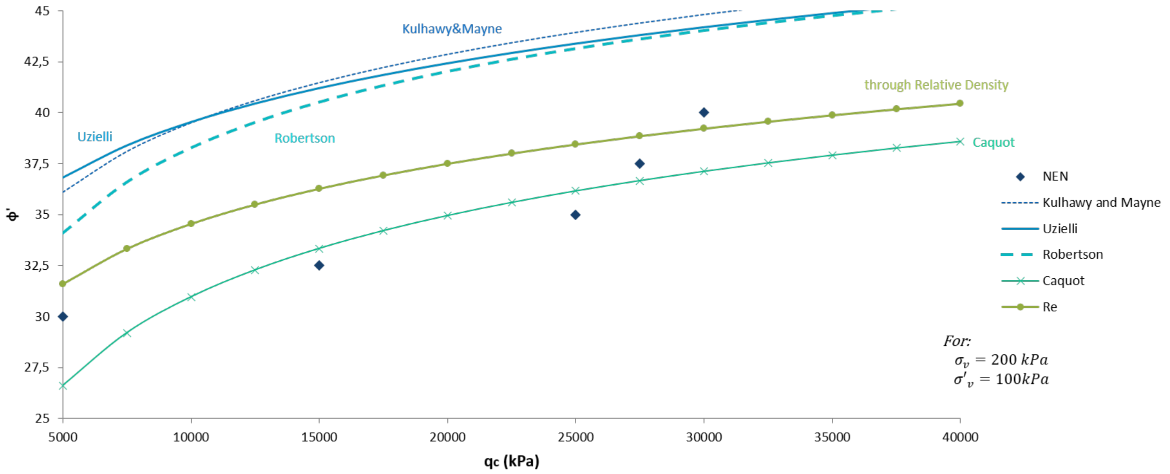

Figure F.7: Different methods for determining ϕ'

The difference between Uzielli, Kulhawy and Mayne and Robertson and Campanella is very small. Especially in the range of $10MPa \leq q_c \leq 20MPa$. Dutch soils are very likely to be within this range, especially at pile tip level. From Figure F.3 it can be seen Uzielli's formula was a slightly better match with the lab data than Kulhawy and Mayne's formula and therefore equation (F.7) will be used further on.

G

Plaxis

G.1. Models

G.1.1. Mohr-Coulomb Model

To get a first estimation on the outcome of the problem, Mohr-Coulomb or MC model can be used. MC is a linear elastic perfectly plastic (LEPP) model. Coulomb's formula is as follows:

$$\tau_f \quad = \quad c' + \sigma'_n \tan\phi' \tag{G.1}$$

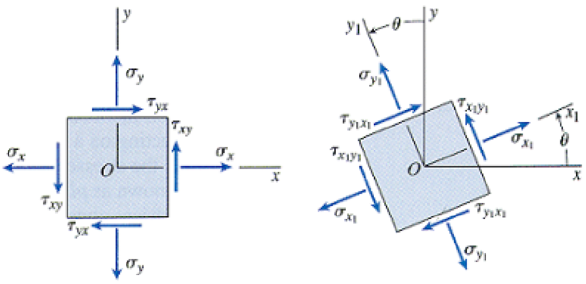

Figure G.1: Stresses on a rotated plane

By using the theory of stresses, like shown in figure G.1 on equation (G.1) the equation can be written like:

$$\left(\frac{\sigma'_1 - \sigma'_3}{2}\right) - \left(\frac{\sigma'_1 + \sigma'_3}{2}\right)\sin\phi' - \cos\phi' = 0 \tag{G.2}$$

Equation (G.2) is better known as the Mohr-Coulomb formula.

Pro	**Con**
First estimation	Less applicable for clays as pore pressures need time to dissipate and time is not a model parameter
Easy	Only usable for drained behaviour
	No strain- or stress- or stress path-dependent stiffness behaviour

Table G.1: [Plaxis, 2016]

G.1.2. Hardening Soil Small Strain Model

A more complex model than the MC model is the Harding Soil Small Strain (HSsmall) model. It is a hyperbolic model based on hardening plasticity. This hardening plasticity can be divided into two parts, shear hardening and cap hardening. In this shear hardening mainly denotes for the generation of plastic deviatoric strains in deviatoric loading. The HSsmall model does use the MC failure line like shown in Figure **??**. This figure also shows dilatancy occurs when above the constant volume or critical state line for the angle of internal friction. This line also represents a dilatancy angle of zero ($\psi_m = 0$). The part where $\psi_m < 0$ is not taken into account by shear hardening as compaction is already accounted for by cap hardening.

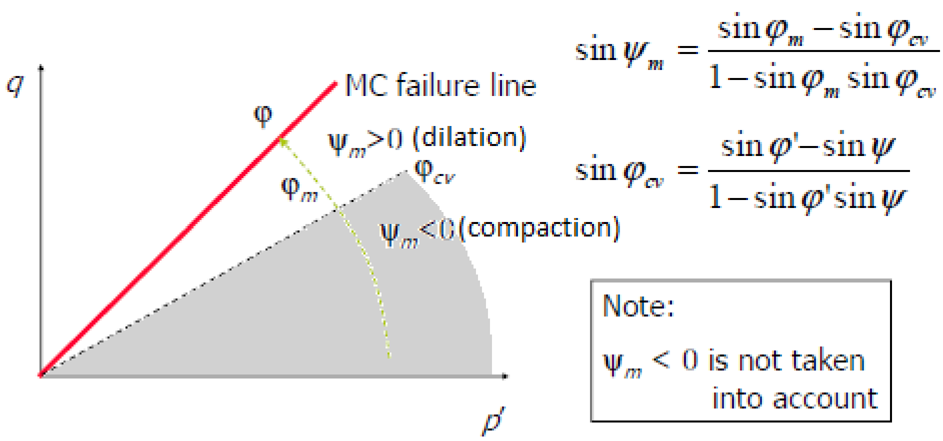

Figure G.2: Shear hardening

Cap hardening mainly denotes for the generation of plastic volumetric strains in primary compression i.e. compression of the soil. The small strain part of the model accounts for the strain-dependency of the stiffness of the soils i.e. at small strains soils react very stiff.

Pro	Con
Stress-dependent stiffness	No softening
Stain-dependent stiffness	No time dependency
Partly non-linear approach	
Memory of pre-consolidation	

Table G.2: [Plaxis, 2016]

G.1.3. Hypo Plastic Model

The last model to be considered is the hypoplastic model. It is the most complex model, regarding the models considered for this thesis. It does not only account for plasticity, but also nonlinearity is taken into account. Therefore this model gives an accurate description of the behaviour of non-cohesive soils. The model is defined as follows:

$$\dot{T}_s = f_e f_b (L(\hat{T}_s, D) + f_d N(\hat{T}_s) \| D \|) \tag{G.3}$$

The details of this equation are not considered here, but can be found in [Gudehus, 1996]. For this model to be an accurate representation of non-cohesive soil behaviour, the complex soil parameters used in this model should be determined properly. Factors f_e and f_b are density dependent and factor f_d is pressure dependent, [Gudehus, 1996].

$$f_e = \left(\frac{e_c}{e}\right)^{\beta} \tag{G.4}$$

$$f_d = \left(\frac{e-e_d}{e_c-e_d}\right)^{\alpha} \tag{G.5}$$

$$f_b = \frac{h_s}{n}\left(\frac{1+e_i}{e_i}\right)\left(\frac{e_{i0}}{e_{c0}}\right)^{\beta}\left(\frac{\text{-}trT_s}{h_s}\right)^{1-n}\left(3+a^2-\sqrt{3}a*\left(\frac{e_{i0}-e_{d0}}{e_{c0}-e_{d0}}\right)^{\alpha}\right)^{-1} \tag{G.6}$$

[Gudehus, 1996]

in which:

$$a = \frac{\sqrt{3}(3-sin\phi'_c}{2\sqrt{2}sin\phi'_c} \tag{G.7}$$

$$\alpha = \frac{ln\left(\frac{6((2+K_p)^2+a^2K_p(K_p-1-tan\psi_p))}{a(2+K_P)(5K_p-2)\sqrt{4+2(1+tan\psi_p)}}\right)}{ln\left(\frac{e-e_d}{e_c-e_d}\right)} \tag{G.8}$$

$$K_p = \frac{1+sin\phi'_p}{1-sin\phi'_p} \tag{G.9}$$

[Anaraki, 2008]

From equation (G.5), (G.6) and (G.4) the soil parameters needed for this model are derived. The soil parameters are:

- e_{c0} (maximum void ratio)
- e_{d0} (minimum void ratio)
- e_i (maximum void ratio $1.15*e_{max}$ [Gudehus, 1996] and [Anaraki, 2008])
- h_s (granular hardness)
- n (pressure sensitivity of the grain skeleton)
- a derived using ϕ'_c (critical friction angle)
- α derived using ϕ'_p and ψ_p (peak dilatancy angle)
- β is 1 for non-cohesive soils [Anaraki, 2008]

Pro	**Con**
Stress-dependent stiffness	Lot of complex parameters
Stain-dependent stiffness	Sensitive to changes of parameters
Non-linear approach	
Softening taken into account	
Cyclic loading	

Table G.3: [Plaxis, 2016]

G.2. Parameter Determination

The Hypoplastic (HP) model in PLAXIS uses complex and sensitive parameters. Therefore, it is important to determine the input parameters for the HP model with the use of laboratory tests. No proper empirical correlations, with for example CPTs, exist for this model. The input parameters for the HP model are:

- e_{c0} (maximum void ratio)
- e_{d0} (minimum void ratio)
- e_i (ultimate maximum void ratio, $1.15 * e_{max}$ [Gudehus, 1996] and [Anaraki, 2008])
- h_s (granular hardness)
- n (pressure sensitivity of the grain skeleton)
- ϕ'_c (constant volume friction angle)
- α (derived using ϕ'_p, υ_p (peak friction and dilatancy rate) and ϕ'_c)
- β (1 for natural, non-cohesive soils [Anaraki, 2008])

To be able to determine these parameters, several element tests have to be performed. Based on these tests the input parameters are determined. The following tests will be carried out:

- Angle of repose test [JGS, 1996]
- Void ratios test [JGS, 1996]
- Oedometer test
- Direct Shear test

The different tests and their results will be discussed in the coming sections. Primarily to this, the soil samples will be discussed. Two different non-cohesive soils are used from the same borehole; one from the formation of Drente (B320-13) and one from the formation of Sterksel (B320-16). Both are Pleistocene soils. They can be characterized as coarse, well-graded sands, respectively glaciofluvial and fluvial. The grain distributions of both soils can be found in Figure G.3. It can be denoted sample B320-16, in contrast to B320-13, contains a small gravel fraction.

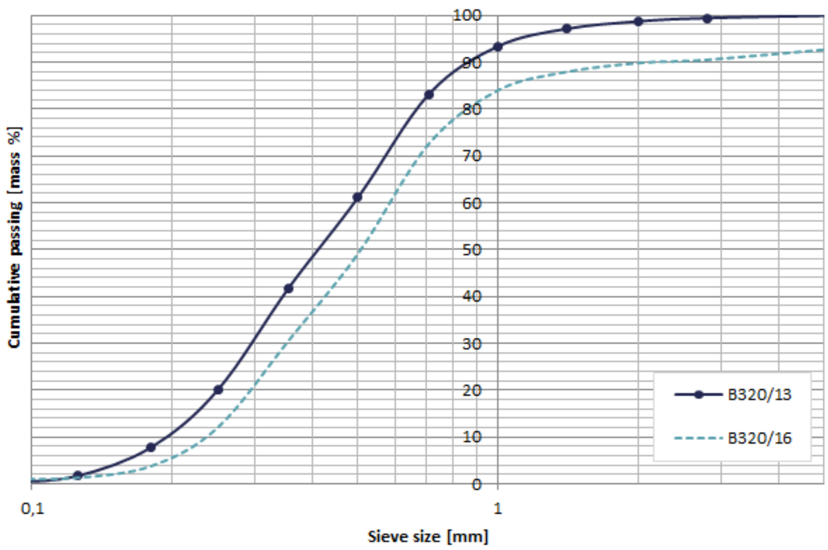

Figure G.3: Sieve curvatures for Drente and Sterksel formation soil samples

Figure G.4: Microscopic photo B320-13

Figure G.5: Microscopic photo B320-13 detail

Figure G.6: Microscopic photo B320-16

Figure G.7: Microscopic photo B320-16 detail

Microscopic photographs show both samples are relatively angular, please refer to Figures G.5 and G.7. Using Figure G.8, the angularity and sphericity can be approximated. Both soils can be categorized in the red circle in Figure G.8. The angularity influences the HP parameters significantly more than the sphericity. This influence according to [Gudehus, 1996] is set out in Table G.4. For an increasing angularity:

ϕ_c	Increases
h_s	Independent
n	Decreases
e_{d0}	Increases
e_{c0}	Increases
e_{i0}	Increases
α	Increases

Table G.4: Influence of angularity

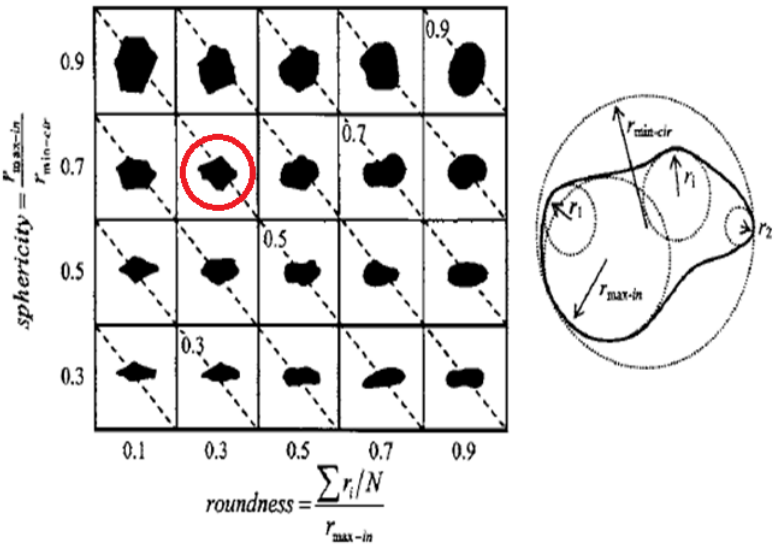

Figure G.8: Angularity and Sphericity [Cho et al., 2006]

G.2.1. Angle of Repose

The constant volume angle (ϕ'_c) can directly be determined from the angle of repose test as describe in the next subsection.

Test procedure

ϕ'_c or in this case, the angle of repose can be determined using a 12 mm funnel, [JGS, 1996]. By very slowly and gradually lifting the funnel opening away from a surface, a conically shaped, in its loosest state mass of sand is obtained. By measuring the angle of the slope of this mass $\phi'_c$is determined (see Figure G.9). The measuring technique is shown in Figure G.10.

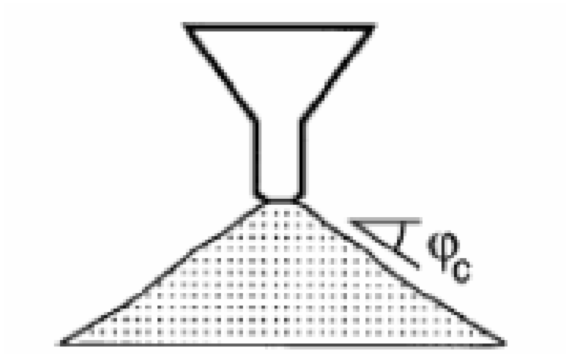

Figure G.9: Angle of repose according to [JGS, 1996]

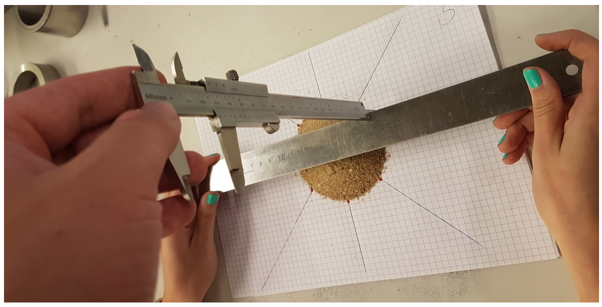

Figure G.10: Measuring the height to calculate the angle of repose

By measuring the height (h) and the width (w) of the conically shaped sand mass ϕ'_c can be determined using the following equation:

$$\phi'_c = tan^{-1}\left(\frac{h}{0.5 * w}\right) \tag{G.10}$$

Five tests are performed per soil sample. For each test, the width is determined in four different directions. Subsequently, these results are averaged. This procedure is chosen to average out the inconsistency due to arbitrary grain orientation.

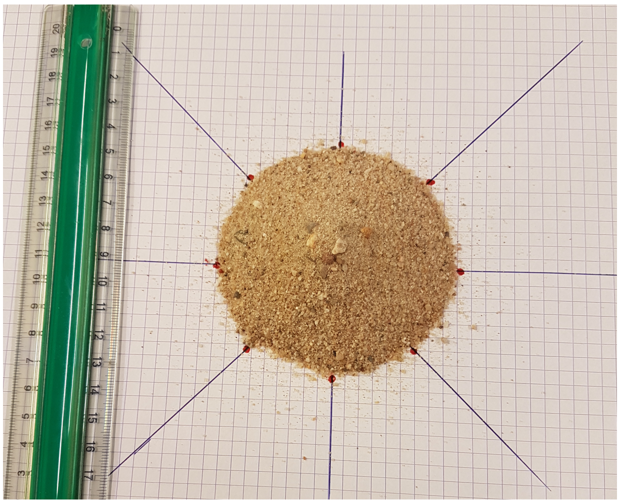

Figure G.11: Test angle of repose: top view

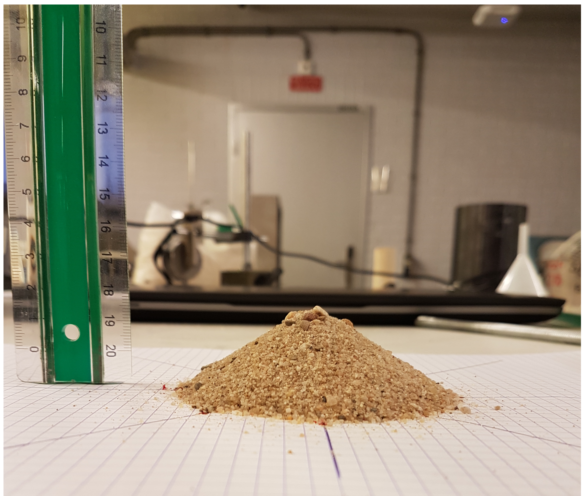

Figure G.12: Test angle of repose: side view

Test Results

# Test	**1**	**2**	**3**	**4**	**5**
w (mm)	83.10	87.60	79.00	84.20	82.90
	82.90	86.30	78.65	82.20	85.20
	81.00	90.20	81.50	81.70	84.90
	80.75	87.50	80.20	82.25	83.40
Average (mm)	81.938	87.900	79.838	82.588	84.100
h_{mass} (mm)	24.65	27.20	23.90	24.20	25.50

Table G.5: measurements for ϕ_c Drente

# Test	**1**	**2**	**3**	**4**	**5**
w (mm)	80.45	83.00	85.55	84.05	85.30
	82.50	84.00	84.85	83.35	85.90
	80.05	85.10	83.50	83.90	85.25
	80.00	85.10	82.80	83.50	84.75
Average (mm)	80.750	84.300	84.175	83.700	85.300
h_{mass} (mm)	25.35	27.80	27.20	27.70	26.50

Table G.6: measurements for ϕ_c Sterksel

Parameter Results

# Test	**1**	**2**	**3**	**4**	**5**	*Average*
$\phi_c (^o)$	31.03	31.75	30.91	30.37	31.23	**31.06**

Table G.7: ϕ_c Drente

# Test	**1**	**2**	**3**	**4**	**5**	*Average*
$\phi_c (^o)$	32.12	33.41	32.87	33.50	31.85	**32.75**

Table G.8: ϕ_c Sterksel

G.2.2. Void ratio determination

The different void ratios are determined in accordance with the Japanese standard [JGS, 1996]. The different void ratios which have to be determined are: $e_{c0} = e_{max}, e_{d0} = e_{min}$ and $e_{i0} = 1.15 * e_{max}$.

Test Procedure

The maximum void ratio was determined by slowly pouring the sand into the mould using a funnel. During this process, it is important to keep the opening of the funnel as close to the sand surface as possible. This way, the compaction of the sand will be limited or even non-existent. The sample made to determine the minimum void ratio was prepared in five layers. Each layer was compacted using a 60g stick to tap the mould. After preparing both samples the void ratios could be calculated using the weight of the samples and the following equations:

$$e = \frac{V_{voids}}{V_{solids}} \tag{G.11}$$

$$V_{solids} = \frac{M_{sample}}{\rho_{solids}} \tag{G.12}$$

$$V_{voids} = V_{sample} - V_{solids} \tag{G.13}$$

$$\rho_{solids} = 2.65 g/cm^3 \tag{G.14}$$

mould	
$M_{mould}(g)$	930.53
$D_{mould}(cm)$	5.981
$h_{mould}(cm)$	4.01
$V_{mould}(cm^3)$	112.7

Figure G.13: Measurements mould

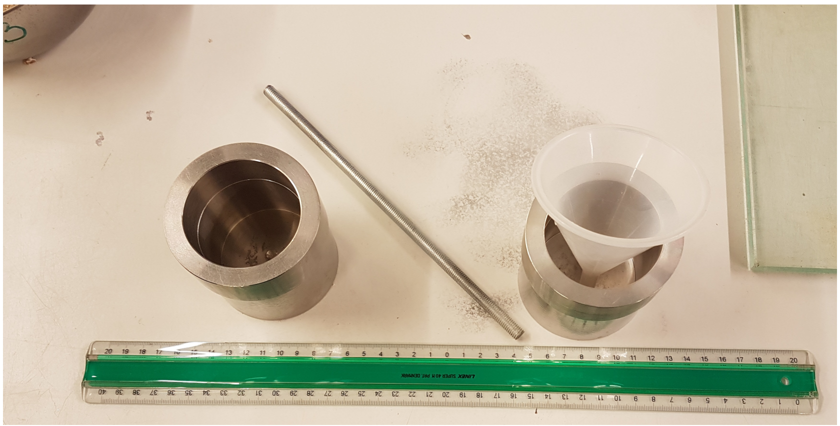

Figure G.14: Equipment to determine the void ratio

Test Results

# Test	**1**	**2**	**3**	**4**	**5**	**6**
$M_{sample,loose}(g)$	1102.66	1101.50	1101.48	1101.40	1101.38	1101.03
$M_{sample,dense}$ (g)	1125.93	1127.93	1128.36	1128.21	1130.40	1126.11

Table G.9: Mass samples Drente to determine the void ratios

# Test	**1**	**2**	**3**	**4**	**5**	**6**
$M_{sample,loose}(g)$	1103.62	1102.60	1103.56	1101.47	1101.15	1101.57
$M_{sample,dense}$ (g)	1126.15	1129.40	1128.73	1128.87	1128.46	1130.91

Table G.10: Mass samples Sterksel to determine the void ratios

Parameter results

Using the test results and equations (G.11) to (G.13) the void ratios in Figures G.15 and G.16 are found.

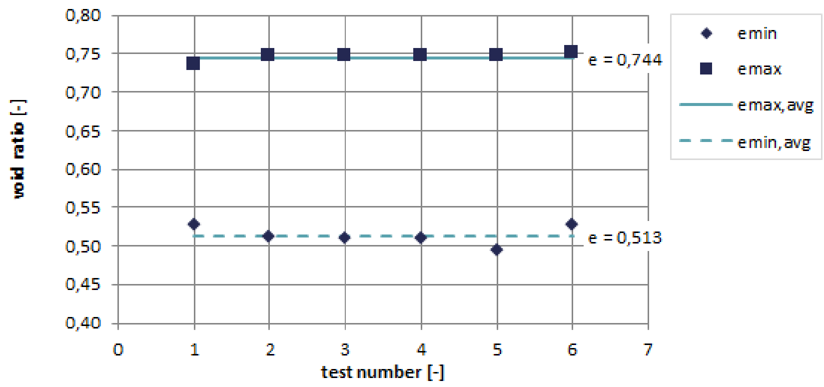

Figure G.15: e_{min} and e_{max} - Drente

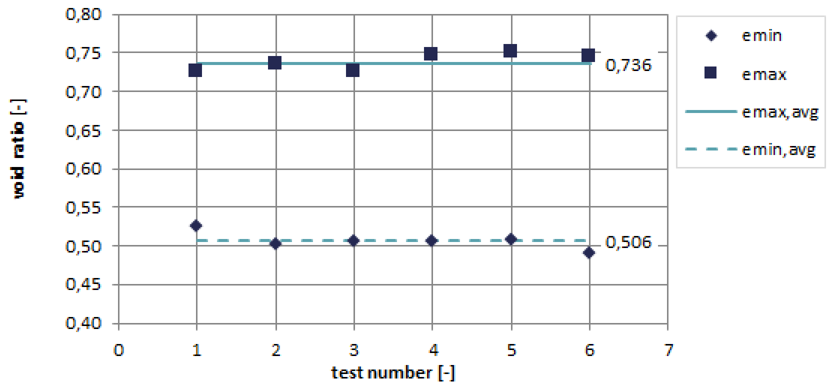

Figure G.16: e_{min} and e_{max} - Sterksel

The different void ratios are summarized in Table G.11.

	e_{d0}	e_{c0}	e_{i0}
Drente (B320-13)	0.513	0.744	0.857
Sterksel (B320-16)	0.506	0.736	0.849

Table G.11: Void ratios

G.2.3. Oedometer test

With help of the oedometer tests, h_s and n can be determined.

$$\frac{e_i}{e_{i0}} = \frac{e_c}{e_{c0}} = \frac{e_d}{e_{d0}} = exp\left(-\frac{p_s}{h_s}\right)^n \tag{G.15}$$

Equation (G.15) by [Gudehus, 1996] is used to fit h_s and n.

Test Procedure

The oedometer tests were performed at three different densities, very loose, very dense and medium dense. Before starting the tests, the oedometer set up is calibrated and the arm factor is determined. For the oedometer used, the arm factor is equal to 11.16. Using this factor the loading scheme is as follows:

Load step	Weight (kg)	Total weight (kg)	Force (kN)	Vertical effective stress (kpa)
1	0.25	0.25	24.525	8.82
2	0.5	0.75	73.575	26.45
3	1	1.75	171.675	61.72
4	5	6.75	662.175	238.06
5	10	16.75	1643.175	590.73
6	20	36.75	3605.175	1296.08
7	20	56.75	5567.175	2001.43
8	10	66.75	6548.175	2354.11
9	10	76.75	7529.175	2706.78
10	10	86.75	8510.175	3059.46
11	10	96.75	9491.175	3412.14

Table G.12: Load scheme

Figure G.17: Oedometer set-up

Figure G.18: Detail oedometer set-up

After testing, the sand was sieved again to check if crushing occurred. This was not the case, so no measures had to be taken.

Test Results

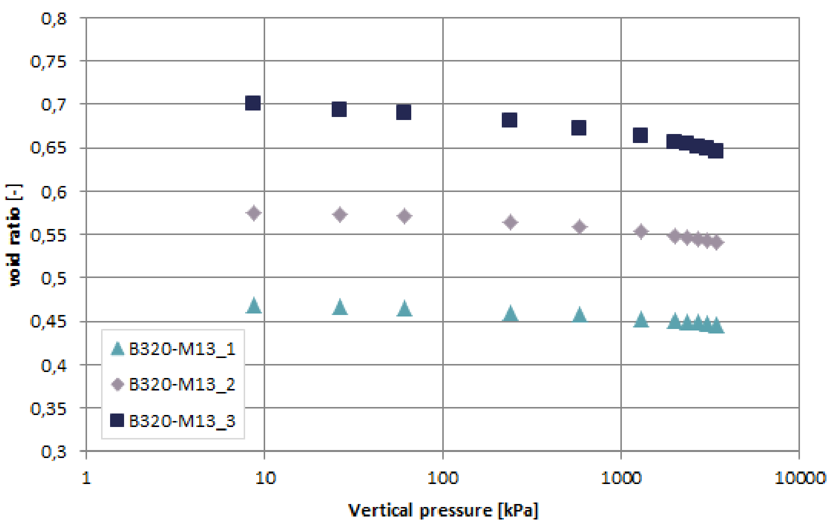

Figure G.19: Oedometer - Drente

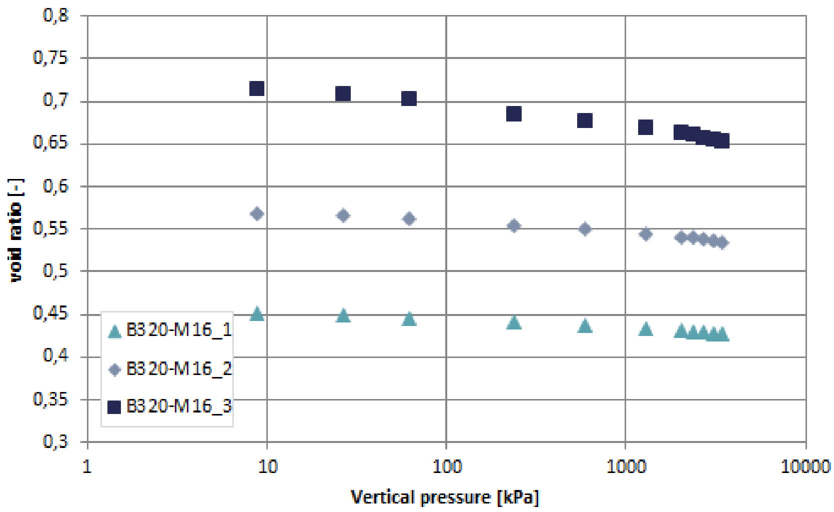

Figure G.20: Oedometer - Sterksel

Parameter Results

In the Figures G.21 and G.22, the parameters h_s and n are determined and fitted using the formula of [Gudehus, 1996] (G.15). The dotted line uses equation (G.15) directly. For the solid line, the void ratio is calculated fitting the curve on the data points varying h_s and n. Table G.13 summarizes the results of hs and n for both Drente and Sterksel.

	h_s (GPa)	n
Drente (B320-13)	11	0.40
Sterksel (B320-16)	14	0.36

Table G.13: h_s and n fitted using theory

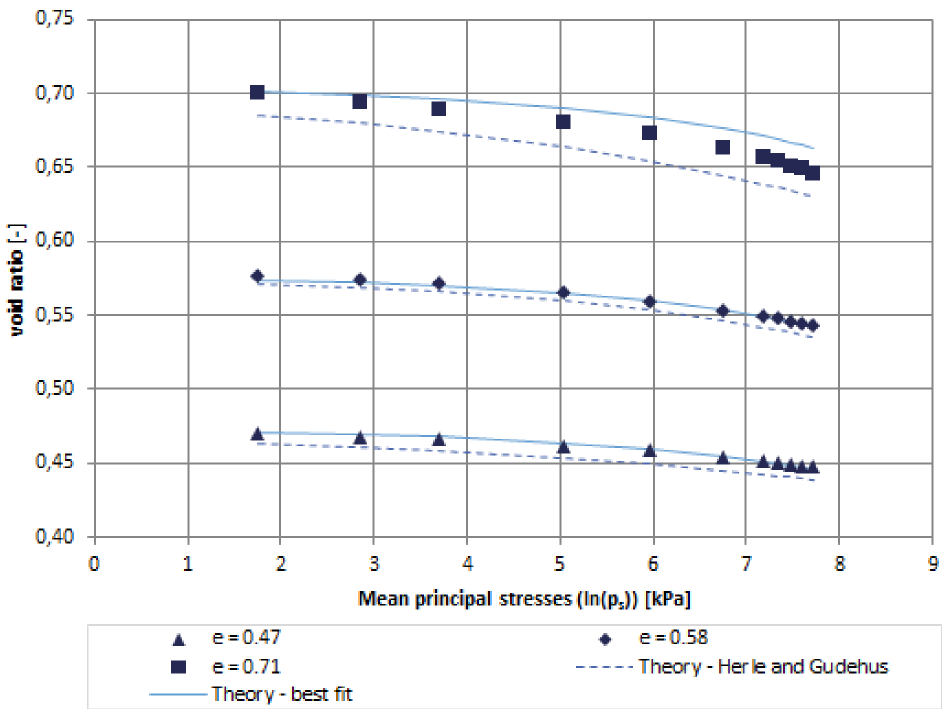

Figure G.21: Oedometer fit - Drente

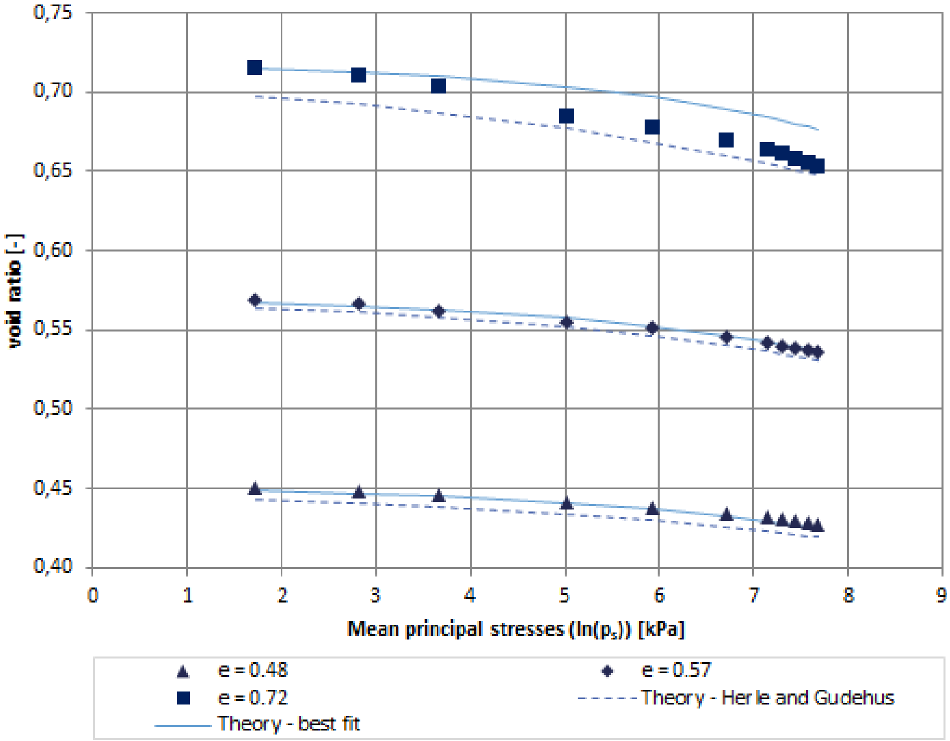

Figure G.22: Oedometer fit - Sterksel

Comparison using PLAXIS Soil Testing Facility (STF)

To check if the results of the oedometer test are modelled correctly within the hypoplastic formulation, the PLAXIS STF is used. In this feature, element tests are numerically approximated using a single soil element. The continuum formulation of the constitutive model is used as a basis for this behaviour. The results for the different void ratios are displayed below. As shown in Figures G.23 to G.28, the theoretically determined h_s and n values do not fit the test result when implemented in the hypoplastic formulation. To overcome this issue, for each void ratio the best fit is created in PLAXIS. Next, an average fit over the three different void ratios is made per soil to determine the overall best fitting h_s and n parameters.

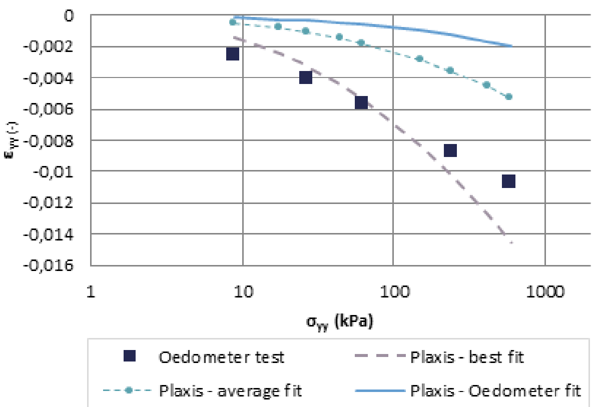

Figure G.23: $\epsilon_{yy}, \sigma_{yy}$-diagram Drente - e = 0.47

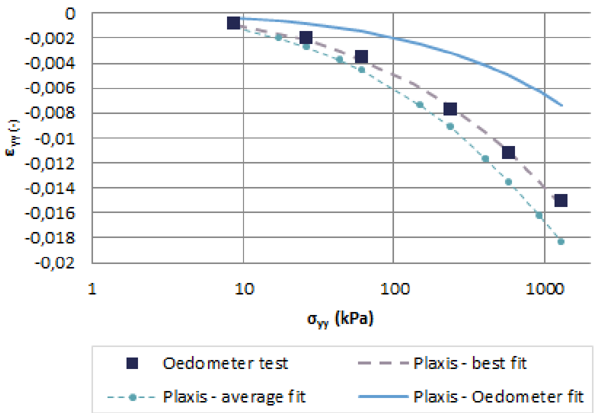

Figure G.24: $\epsilon_{yy}, \sigma_{yy}$-diagram Drente - e = 0.58

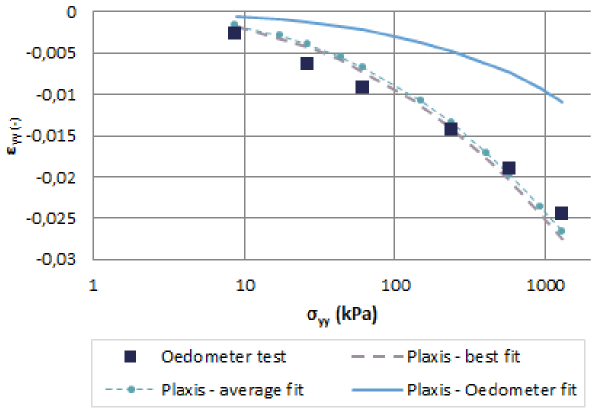

Figure G.25: $\epsilon_{yy},\sigma_{yy}$-diagram Drente - e = 0.71

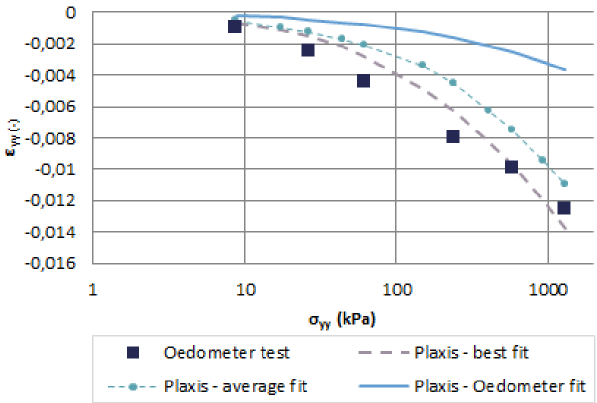

Figure G.26: $\epsilon_{yy},\sigma_{yy}$-diagram Sterksel - e = 0.48

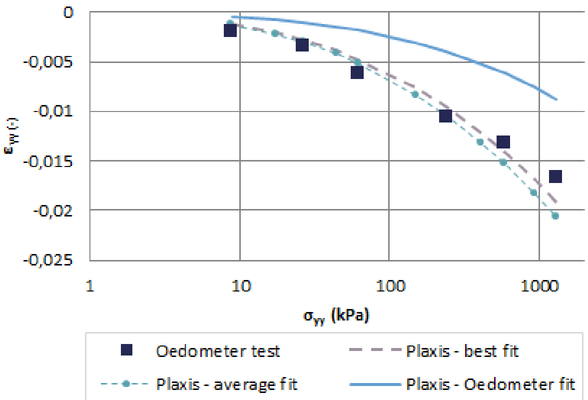

Figure G.27: $\epsilon_{yy},\sigma_{yy}$-diagram Sterksel - e = 0.57

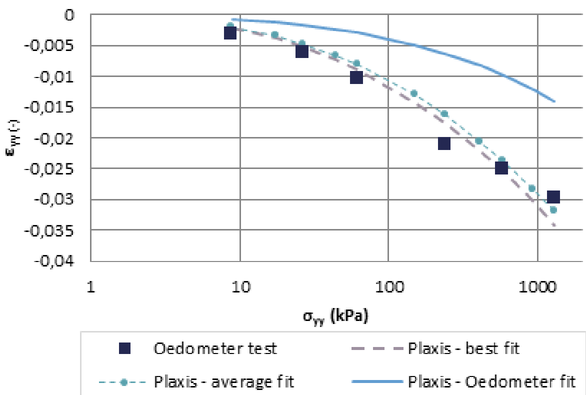

Figure G.28: $\epsilon_{yy},\sigma_{yy}$-diagram Sterksel - e = 0.72

As shown in the Figures above (G.23 - G.28), the void ratios for the densest sample have a lower e than emin which does not make sense. However, the JGS method [JGS, 1996] to determine e_{min} uses a relative light tapping stick and a heavy mould. Therefore, it was possible to get a lower void ratio in the oedometer sample. As this is theoretically speaking impossible, it is hard to make a proper fit for the densest samples of both soils. Another important thing to notice is the difference between h_s and n determined using PLAXIS. They differ significantly from the theoretical values gained from fitting equation (G.15) by [Gudehus, 1996]. Table G.14 and Table G.15 sets out this difference.

	PLAXIS - Average fit	PLAXIS - Theoretical fit
Drente (B320-13)	13	11
Sterksel (B320-16)	10	14

Table G.14: h_s (GPa)

	PLAXIS - Average fit	PLAXIS - Theoretical fit
Drente (B320-13)	0.27	0.40
Sterksel (B320-16)	0.26	0.36

Table G.15: n

As PLAXIS will be used to model the pile response, the values determined with the STF will be used in this thesis. These values are summarized in Table G.16.

	hs (GPa)	n
Drente (B320-13)	13	0.27
Sterksel (B320-16)	10	0.26

Table G.16: Summary h_s and n; fitted using PLAXIS

After concluding the above and using the h_s and n parameters from Table G.16 in the numerical model, it was noted the soil stiffness was not high enough. Therefore the stiffness parameters had to be checked again. This time the results of the STF were compared with CPT data and CPT correlations like presented in Appendix E. The main correlations used are the correlation determining the initial void ratio and E_{50}^{ref} from CPT data. Changing h_s, n and e for a triaxial compression test, E_{50}^{ref} from the STF was fitted to the E_{50}^{ref} found using CPT correlations. Figures G.29 - G.33 show the results of the STF. In these figures, the secant represents E_{50}^{ref}. As the influence of h_s and chances in h_s are minor it was not varied.

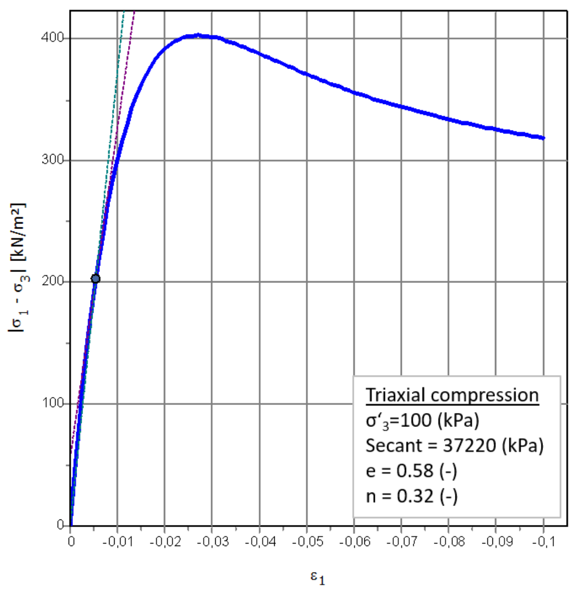

Figure G.29: STF results for the standard parameter set

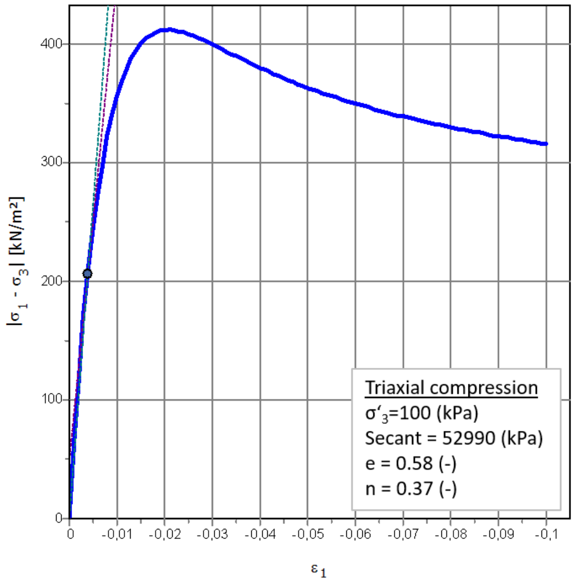

Figure G.30: STF results for n=0.37 (-)

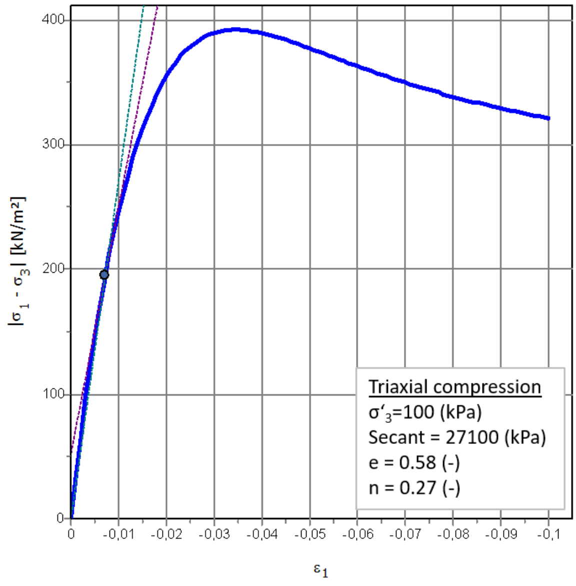

Figure G.31: STF results for n=0.27 (-)

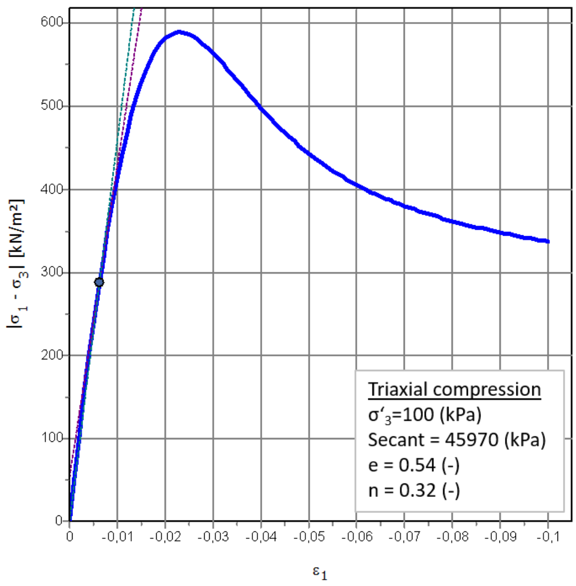

Figure G.32: STF results for e=0.54 (-)

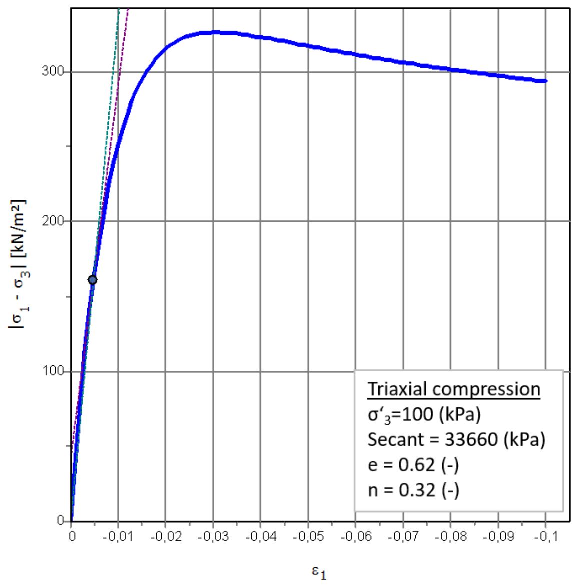

Figure G.33: STF results for e=0.62 (-)

In the end, it is concluded the n parameter needed to be adjusted to 0.32 (-) for a void ratio of 0.58 (-). Changing the void ratio, according to the CPT correlation, might introduce the need to change n as well. Therefore n and e are both taken into account in the sensitivity analysis conducted in Appendix G.4.

G.2.4. Direct shear test

The α parameter is preferably determined using a triaxial setup. However, as it was impossible to perform triaxial tests, shear box tests were done to approximate α. This parameter relates the peak friction angle (ϕ_p) to the dilatancy rate (υ_p). Both parameters can be determined from a triaxial test as well as from a shear box test.

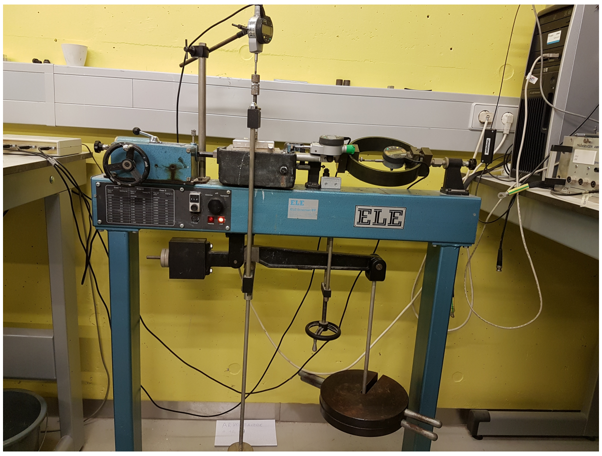

Figure G.34: Direct shear box testing equipment

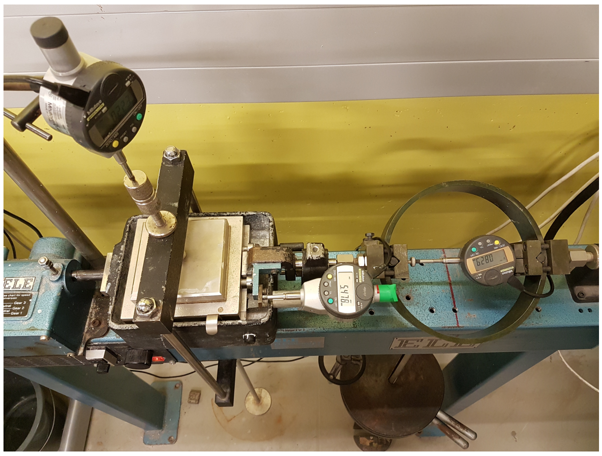

Figure G.35: Direct shear box testing equipement top view

Test Procedure

Direct shear tests are performed for two different relative densities. For determining α, dilative behaviour needs to occur, hence 80% and 90% relative density were arbitrarily chosen. For both relative densities, the direct shear tests were performed at different stress levels. This ensures deviations as a result of heterogeneity are minimized. Normal stresses were taken at 100 kPa, 200 kPa and 300 kPa, since these are realistic stress levels. Before performing the test, the arm factor is determined at 10.28. During testing, it is important to watch the top cap displacement. When it tilts, the vertical displacement becomes inaccurate. This can result in continuing vertical displacement of the top cap after full dilation (Figure G.36) and unrealistic dilation rates can occur.

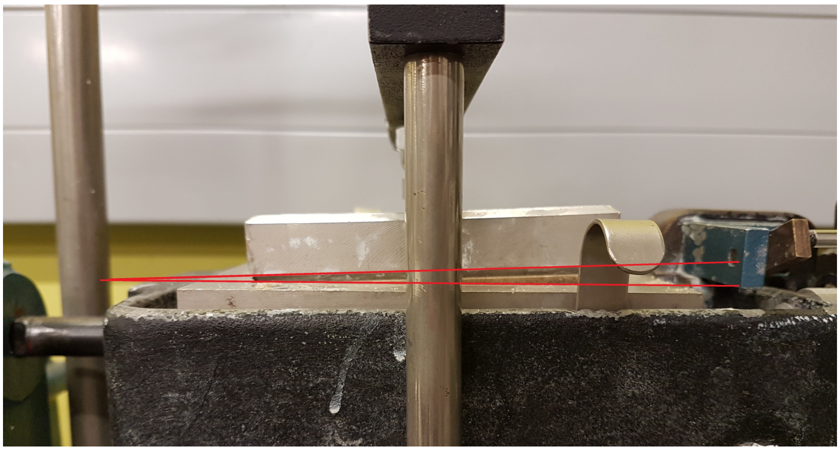

Figure G.36: Tilting of the top cap after shearing

Test Results

From the results of the shear box tests both a $\sigma'_{yy}, \epsilon_{yy}$-diagram and a $\epsilon_v, \epsilon_{yy}$-diagram are plotted. From these graphs, respectively ϕ_p and the v_p can be determined. Next, these parameters are used to calculate α using the equation (G.16).

$$\alpha = \frac{ln\left(\frac{6((2+K_p)^2+a^2K_p(K_p-1-tan\psi_p))}{a(2+K_p)(5K_p-2)\sqrt{4+2(1+tan\psi_p)}}\right)}{ln\left(\frac{e-e_d}{e_c-e_d}\right)} \tag{G.16}$$

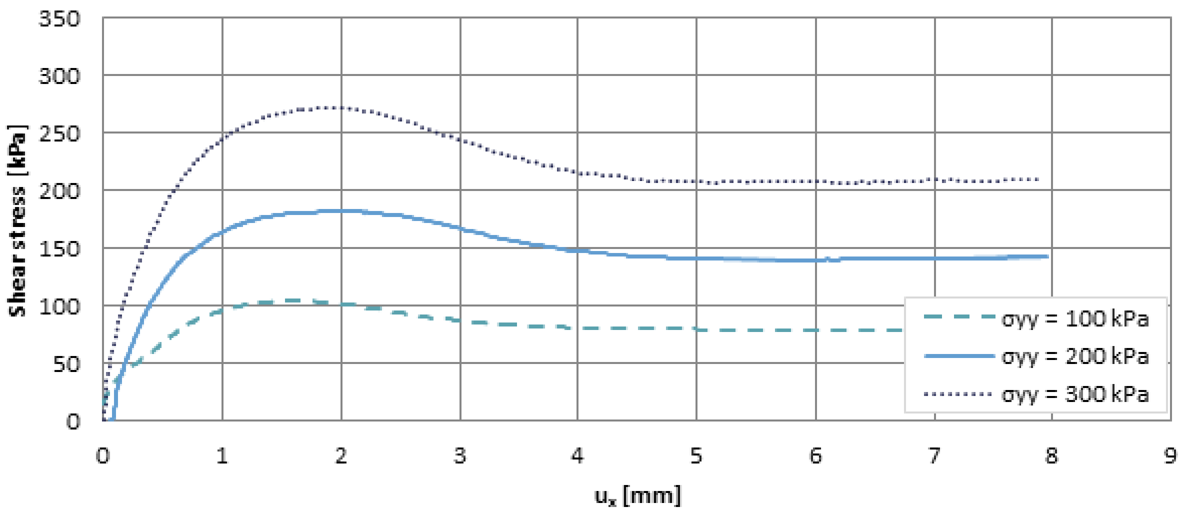

Figure G.37: τ, u_x-diagram - Drente (R.D. = 90%)

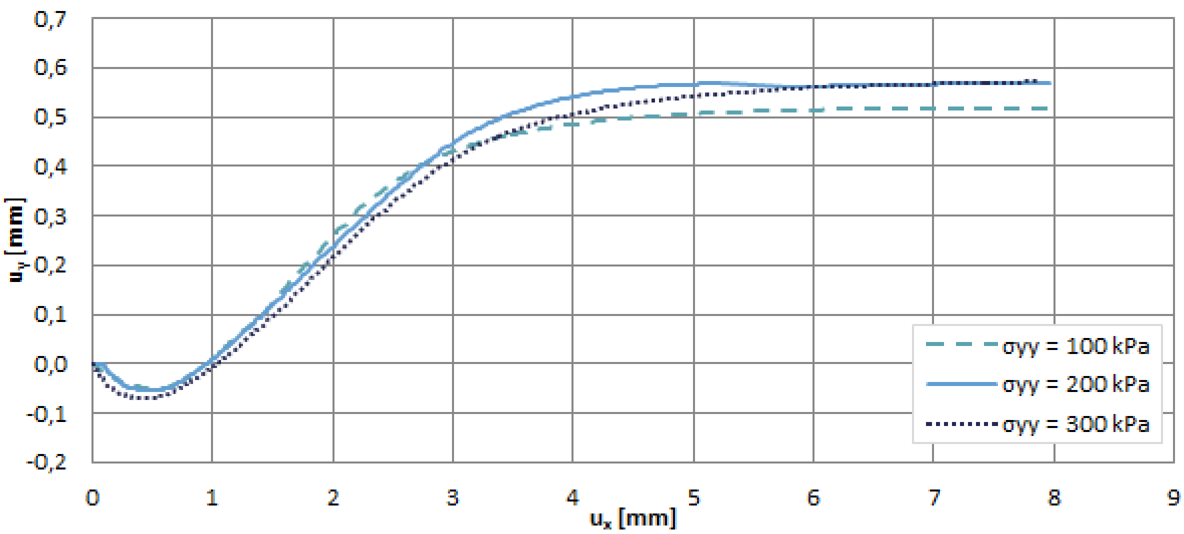

Figure G.38: u_y, u_x-diagram - Drente (R.D. = 90%)

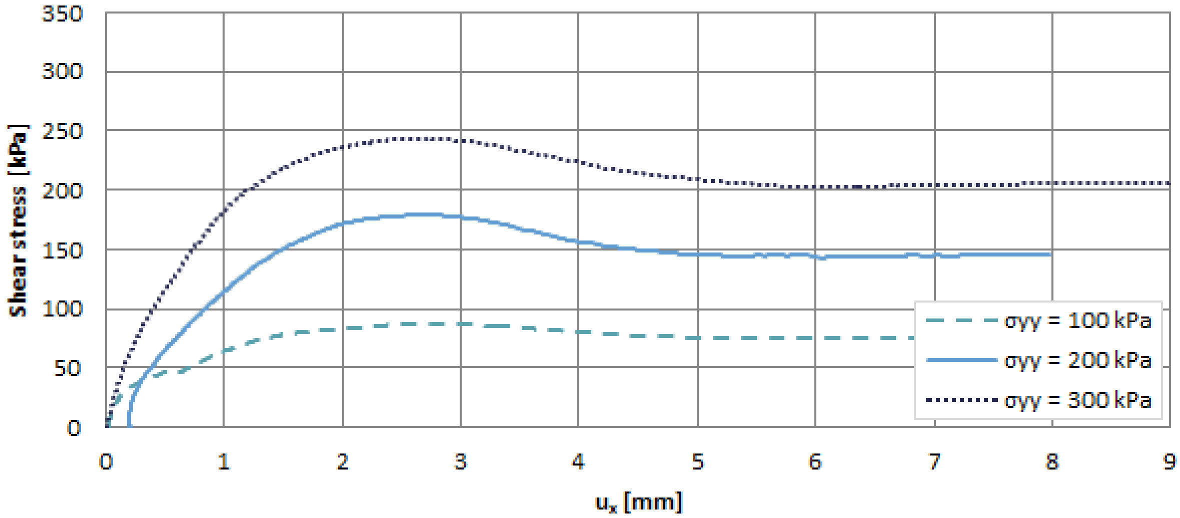

Figure G.39: τ, u_x-diagram - Drente (R.D. = 80%)

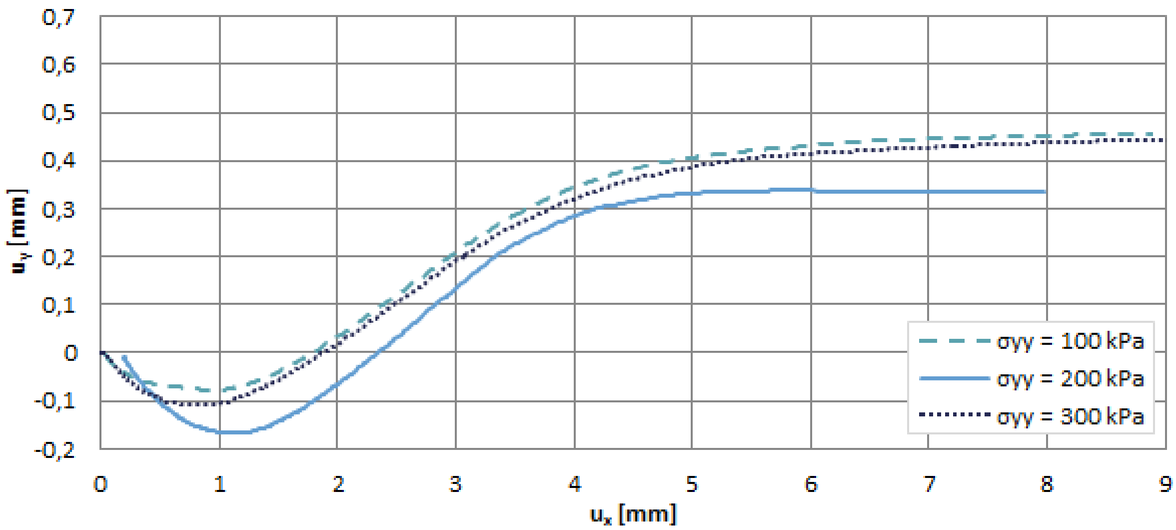

Figure G.40: u_y, u_x-diagram - Drente (R.D. = 80%)

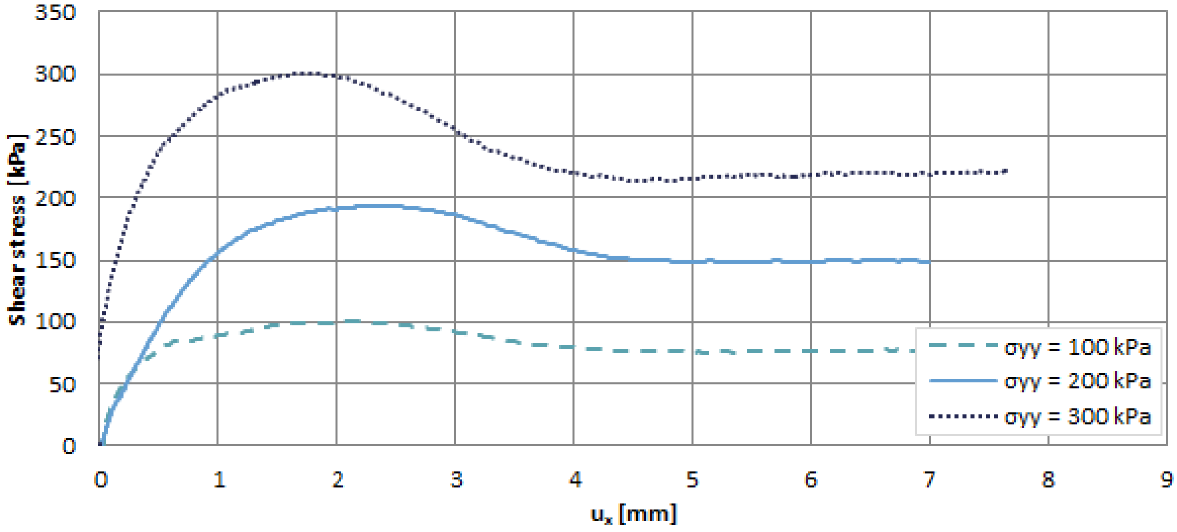

Figure G.41: τ, u_x-diagram - Sterksel (R.D. = 90%)

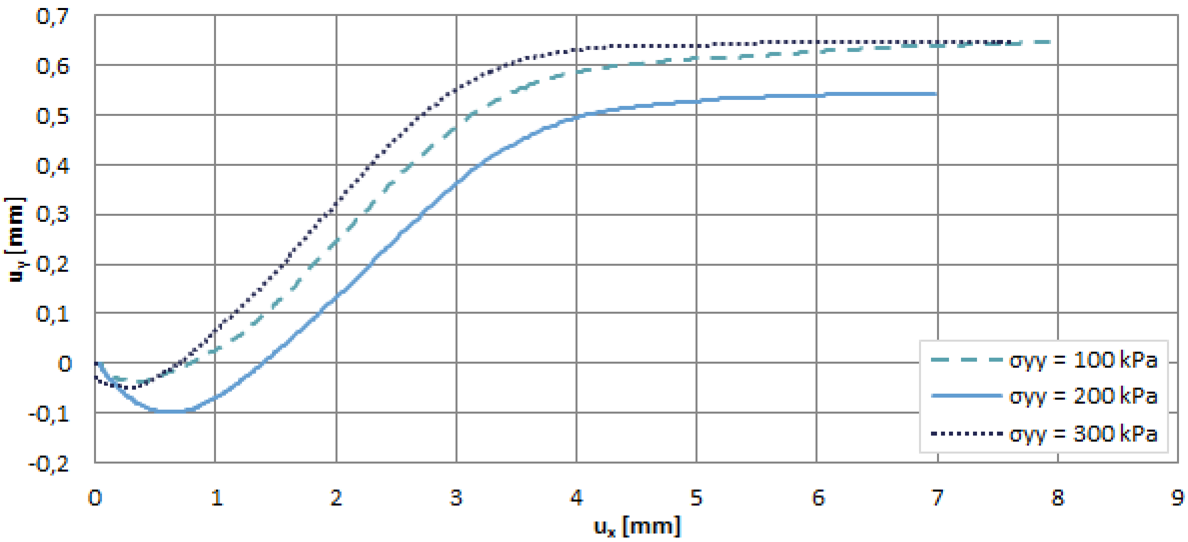

Figure G.42: u_y, u_x-diagram - Sterksel (R.D. = 90%)

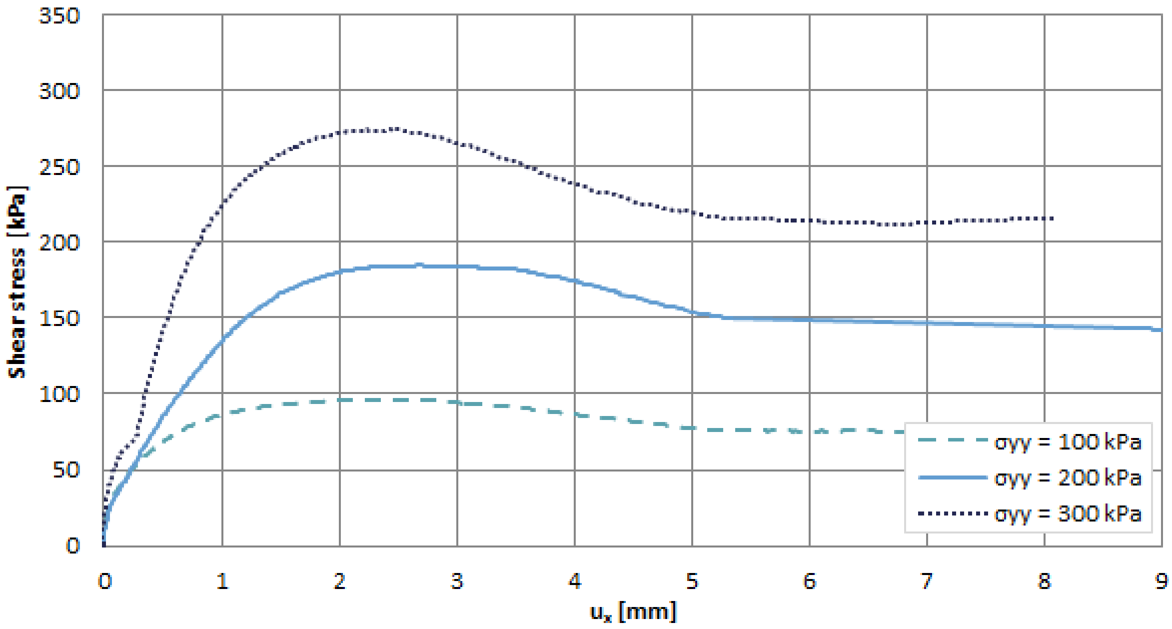

Figure G.43: τ, u_x-diagram - Sterksel (R.D. = 80%)

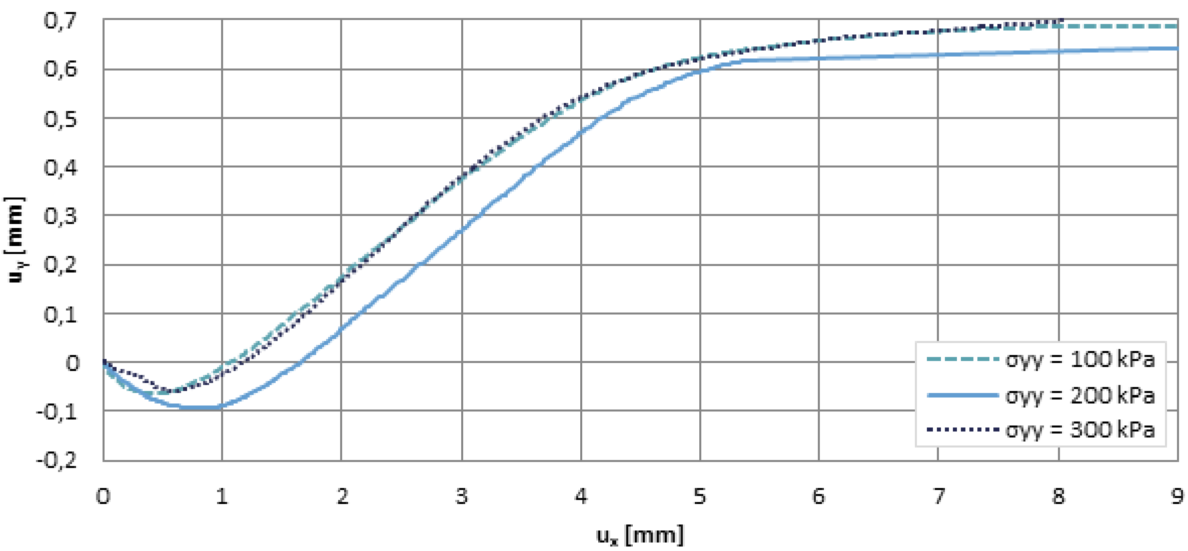

Figure G.44: u_y, u_x-diagram - Sterksel (R.D. = 80%)

Parameter Results

From the graphs in the previous subsection, the ν_p and ϕ_p are determined. Using equation (G.16) α is calculated resulting in the following values.

# Test	**1**	**2**	**3**	**4**	**5**	**6**	
Relative density (%)	80	80	80	90	90	90	
σ'_{yy} (kPa)	100	200	300	100	200	300	
$\nu_p (^o)$	42.11	38.15	38.17	30.38	34.23	30.02	
$\phi_p (^o)$	44.32	41.19	41.37	39.24	40.73	38.34	
							Average
α	0.152	0.1448	0.1469	0.1504	0.1577	0.154	**0.1510**

Table G.17: α Drente

# Test	**1**	**2**	**3**	**4**	**5**	**6**	
Relative density (%)	80	80	80	90	90	90	
σ'_{yy} (kPa)	100	200	300	100	200	300	
$\nu_p (^o)$	33.34	34.40	36.19	39.90	38.07	41.92	
$\phi_p (^o)$	42.00	41.66	41.60	43.11	42.98	44.26	
							Average
α	0.1568	0.1719	0.1895	0.1436	0.1345	0.1499	**0.1577**

Table G.18: α Sterksel

Comparison using PLAXIS Soil Testing Facility (STF)

Implementing the above-found parameters into the STF of PLAXIS. It can be checked if the α found in the previous subsection matches. It should be noted that the STF can only simulate a direct simple shear test, which shows a different mobilization of shear stresses compared to the direct shear box. In terms of the $\tau - \epsilon_1$ development, this translates into a longer mobilization from peak to residual shear stress. Since the peak and residual shear stress should have similar values, they are used to check whether α is approximately right.

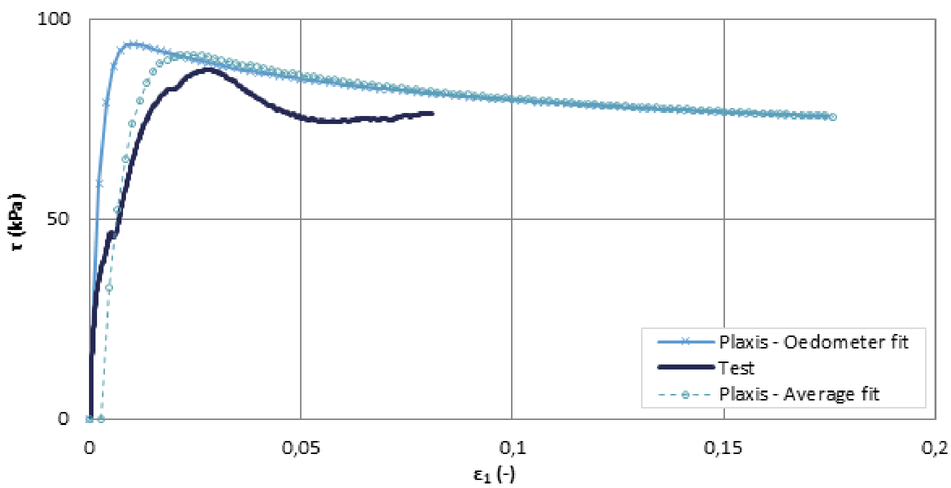

Figure G.45: τ, ϵ_1-diagram - Drente (R.D. = 80%, $\sigma'_{yy} = 100kPa$)

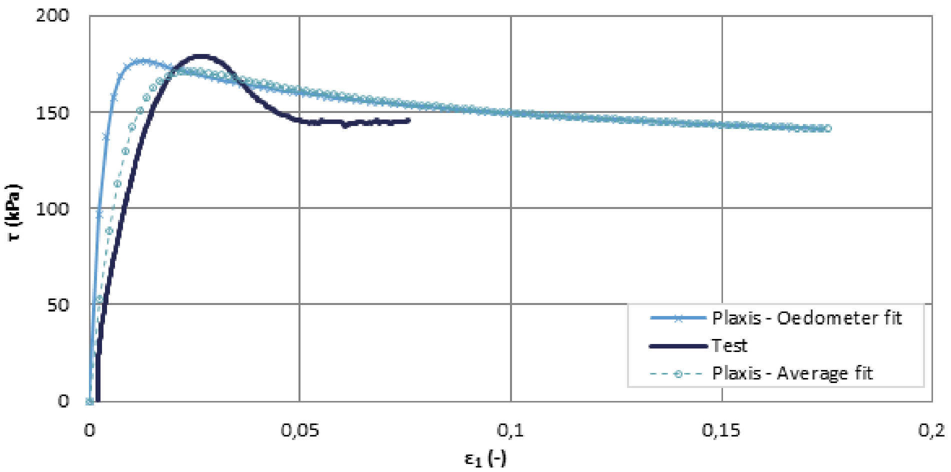

Figure G.46: τ, ϵ_1-diagram - Drente (R.D. = 80%, $\sigma'_{yy} = 200kPa$)

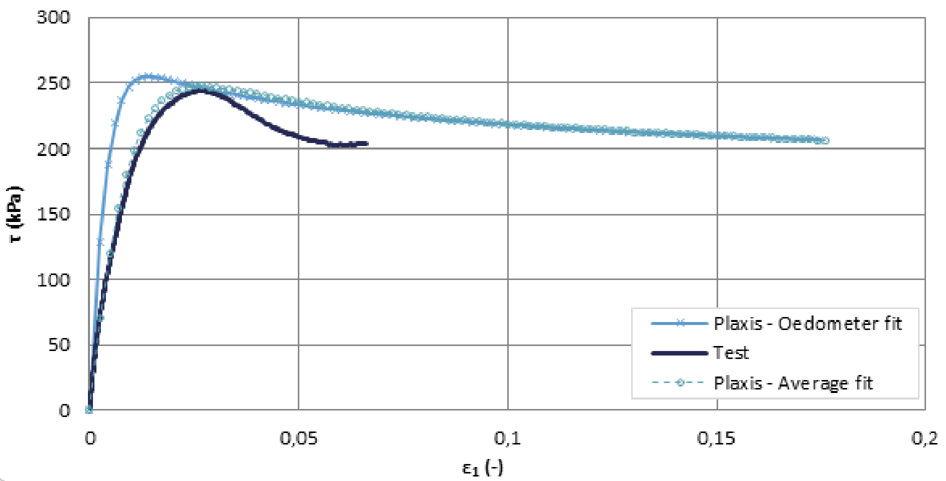

Figure G.47: τ, ϵ_1-diagram - Drente (R.D. = 80%, $\sigma'_{yy} = 300kPa$)

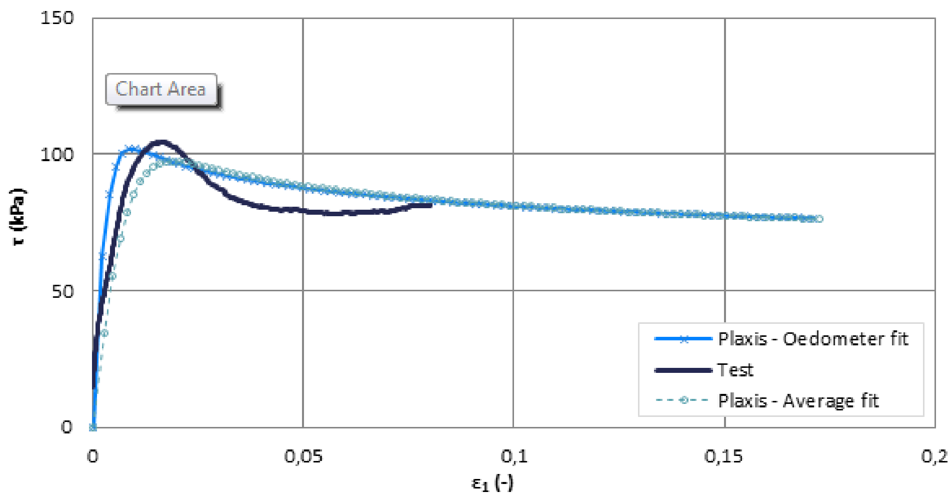

Figure G.48: τ, ϵ_1-diagram - Drente (R.D. = 90%, $\sigma'_{yy} = 100kPa$)

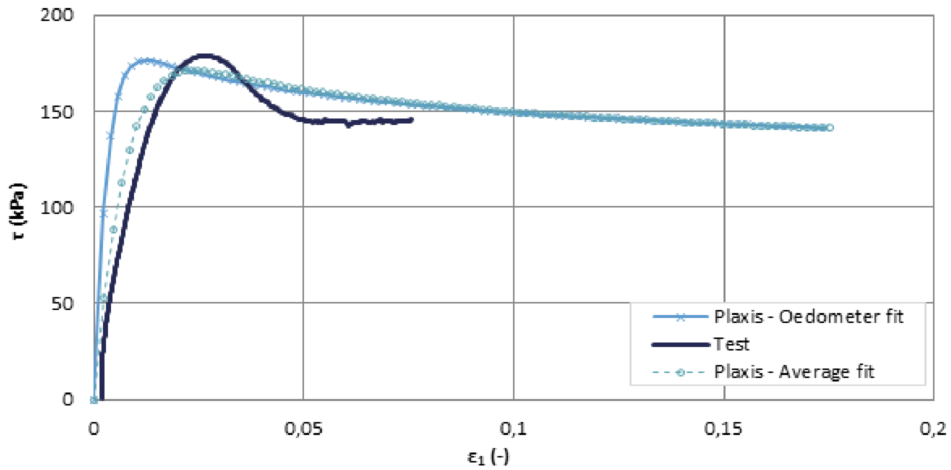

Figure G.49: τ, ϵ_1-diagram - Drente (R.D. = 90%, $\sigma'_{yy} = 200kPa$)

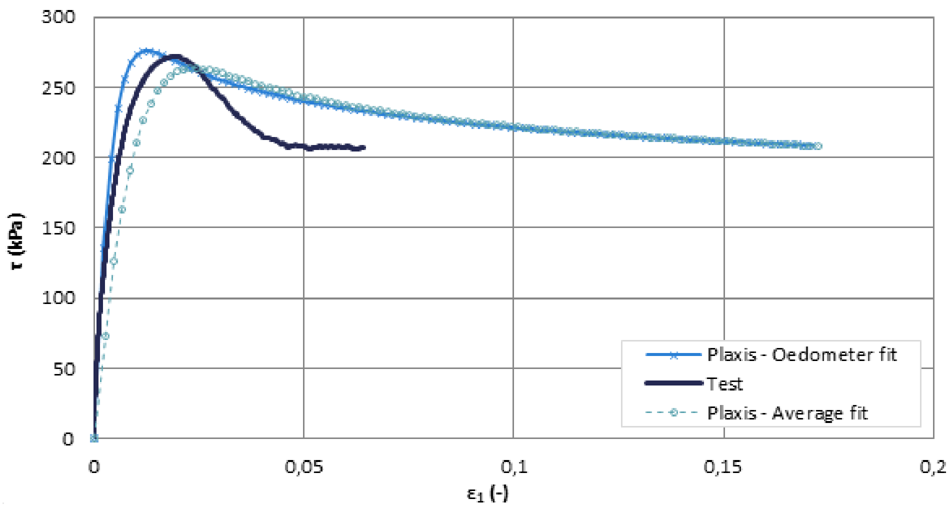

Figure G.50: τ, ϵ_1-diagram - Drente (R.D. = 90%, $\sigma'_{yy} = 300kPa$)

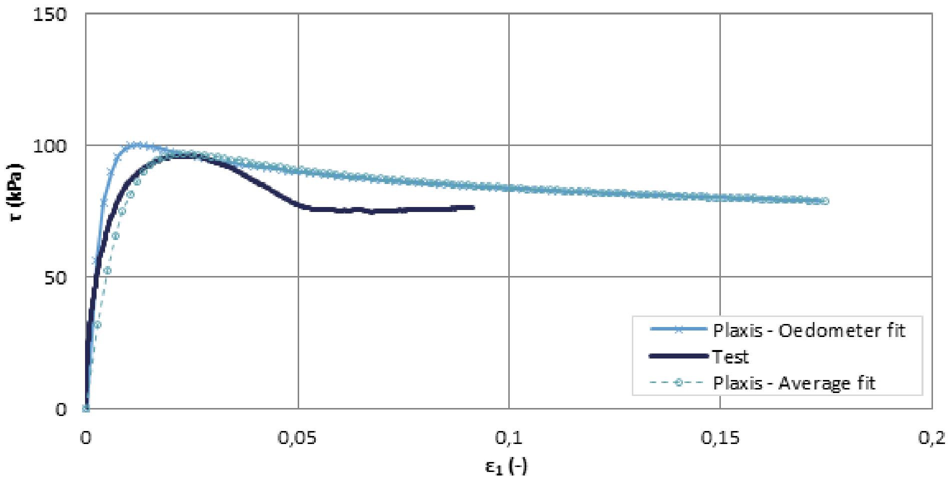

Figure G.51: τ, ϵ_1-diagram - Sterksel (R.D. = 80%, $\sigma'_{yy} = 100kPa$)

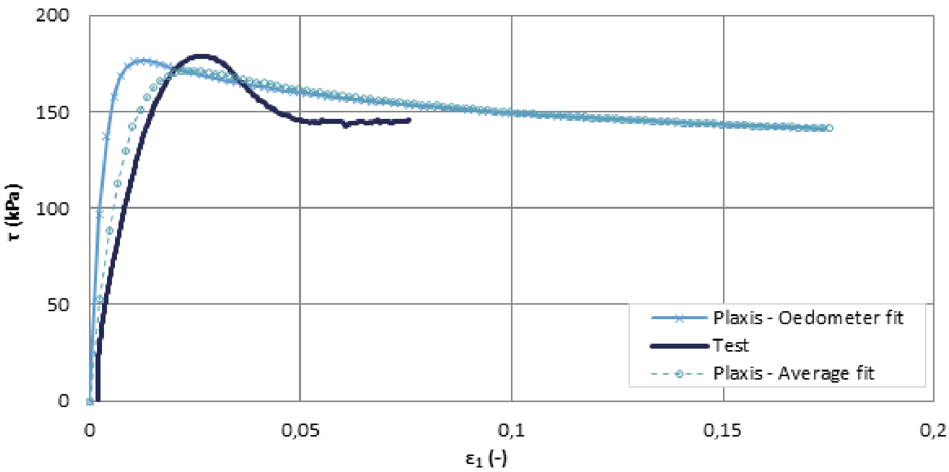

Figure G.52: τ, ϵ_1-diagram - Sterksel (R.D. = 80%, $\sigma'_{yy} = 200kPa$)

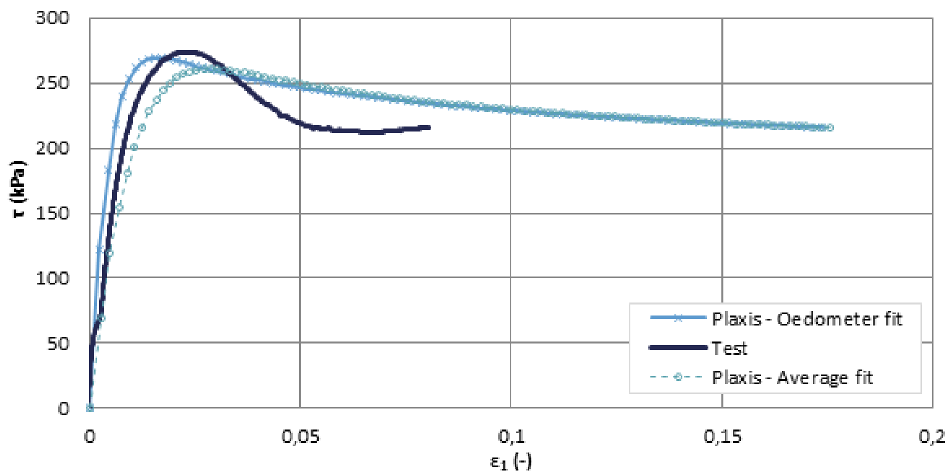

Figure G.53: τ, ϵ_1-diagram - Sterksel (R.D. = 80%, $\sigma'_{yy} = 300kPa$)

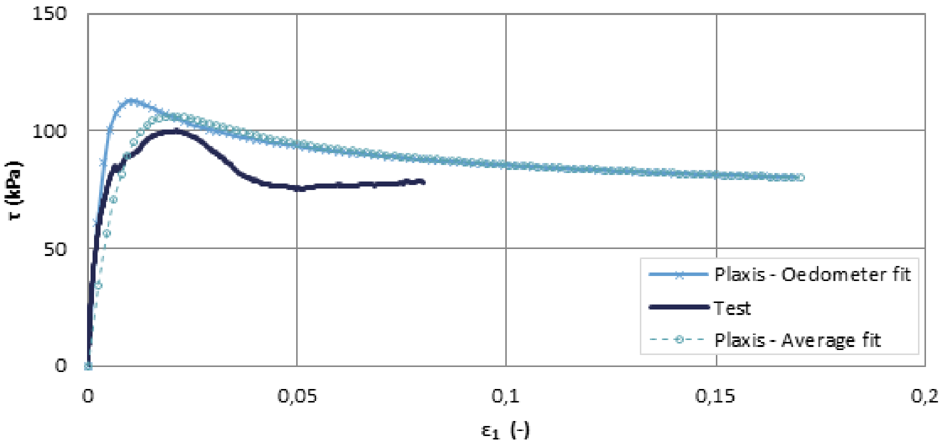

Figure G.54: τ, ϵ_1-diagram - Sterksel (R.D. = 90%, $\sigma'_{yy} = 100 kPa$)

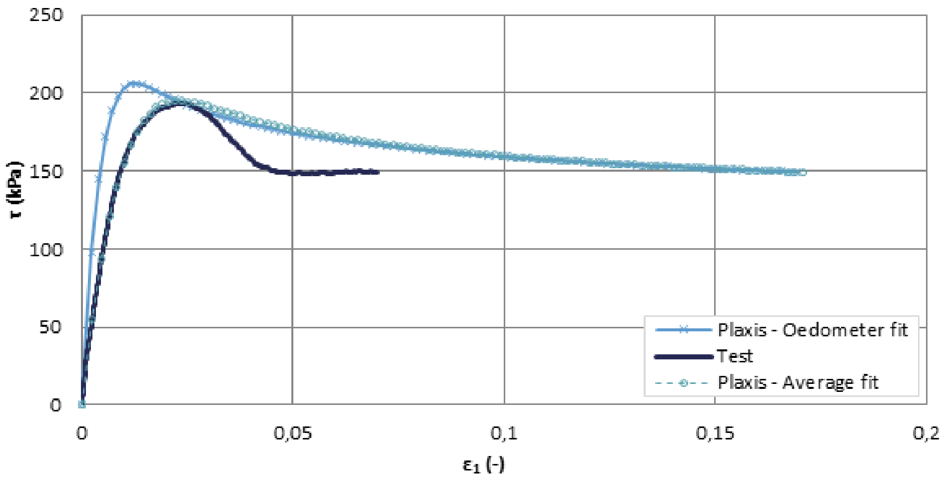

Figure G.55: τ, ϵ_1-diagram - Sterksel (R.D. = 90%, $\sigma'_{yy} = 200 kPa$)

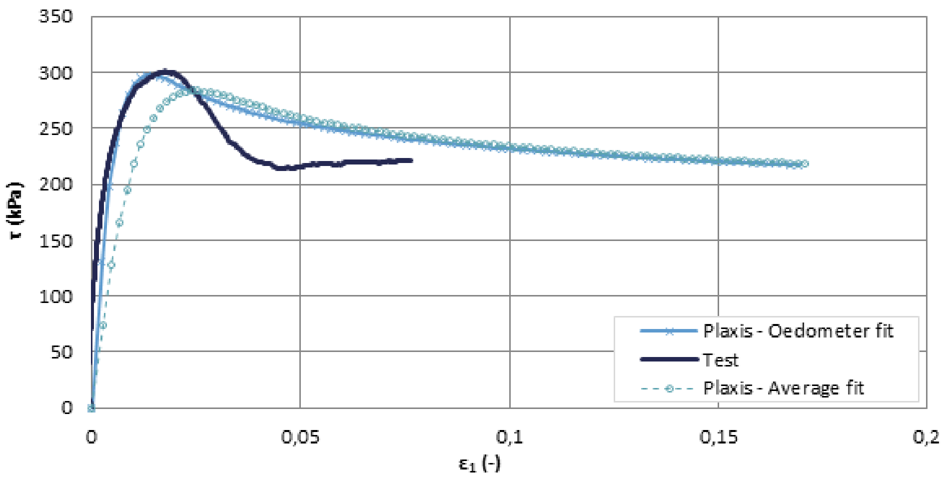

Figure G.56: τ, ϵ_1-diagram - Sterksel (R.D. = 90%, $\sigma'_{yy} = 300 kPa$)

Both the Oedometer fit and the average fit of Plaxis give results which are in the order of magnitude of the direct shear tests. Therefore, α determined in the previous subsection will be used further on.

G.2.5. Conclusion

Both soils have comparable HP parameters. This is set out in Table G.19

	$\phi_c (^o)$	h_s (GPa)	n	e_{d0}	e_{c0}	e_{i0}	α	β
Drente (B320-13)	31.06	13	0.27	0.513	0.744	0.857	0.1510	1
Sterksel (B30-16)	32.75	10	0.26	0.506	0.736	0.849	0.1577	1

Table G.19: Hypoplasticity parameters Drente and Sterksel Formation

Last, it is important to notice β is set to 1. This value can actually vary [Gudehus, 1996], but as the influence of this parameter is small it is not calculated and is simply chosen to be 1 as recommended by [Gudehus, 1996] for natural, non-cohesive soils.

G.3. Model Geometries

G.3.1. Kruithuisweg, Delft

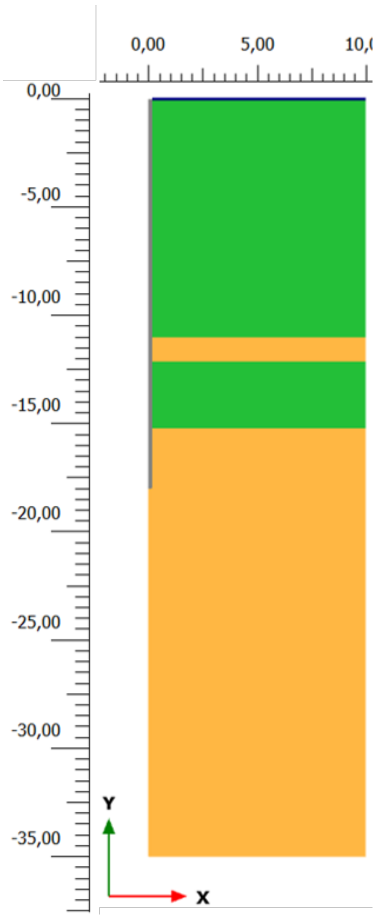

Figure G.57: Geometry KH II (scale in m)

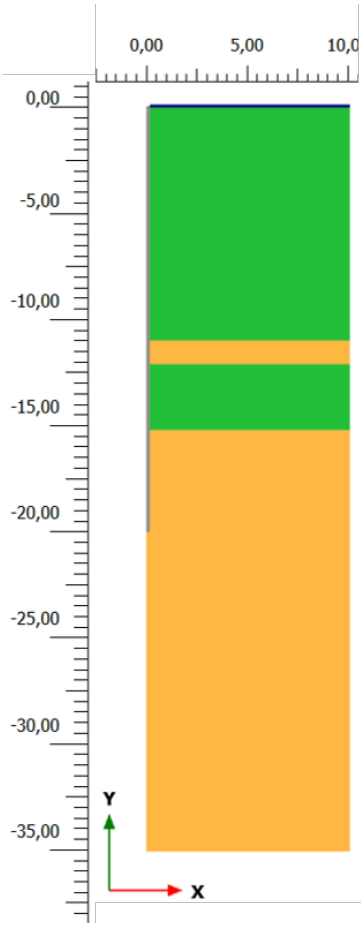

Figure G.58: Geometry KH III (scale in m)

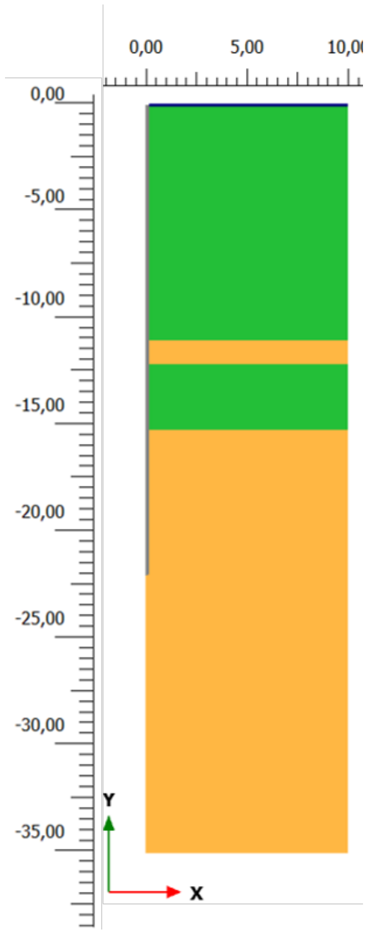

Figure G.59: Geometry KH IV (scale in m)

G.3.2. 2-layered soil model

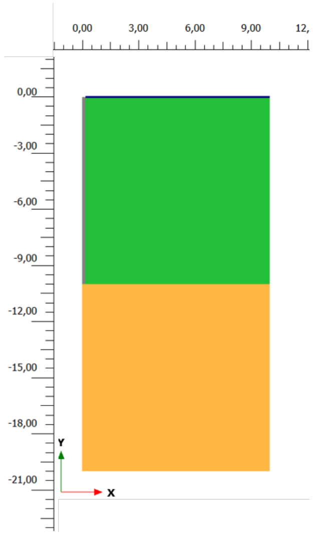

Figure G.60: Geometry pile 0D into the non-cohesive layers (scale in m)

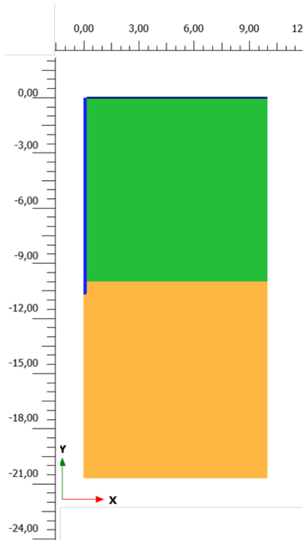

Figure G.61: Geometry pile 2D into the non-cohesive layers (scale in m)

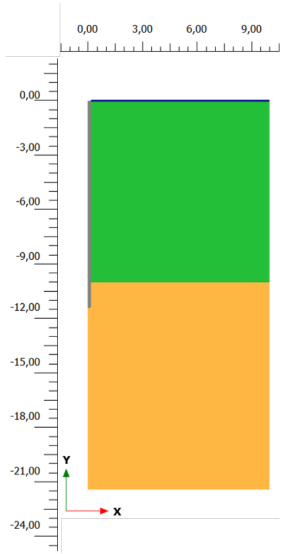

Figure G.62: Geometry pile 4D into the non-cohesive layers (scale in m)

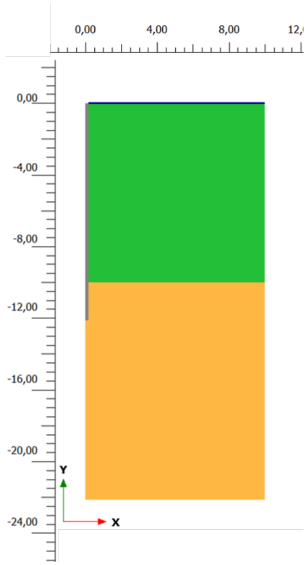

Figure G.63: Geometry pile 6D into the non-cohesive layers (scale in m)

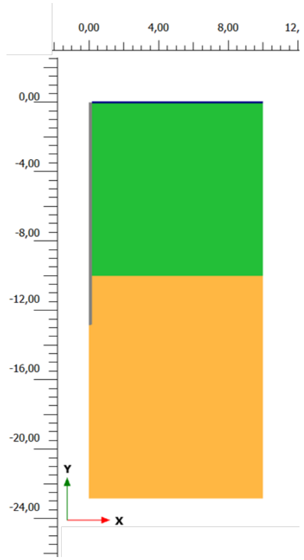

Figure G.64: Geometry pile 8D into the non-cohesive layers (scale in m)

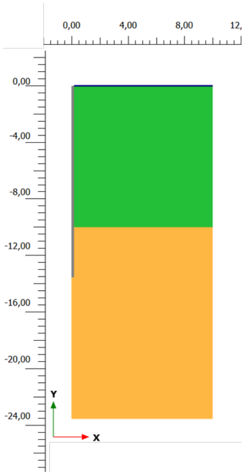

Figure G.65: Geometry pile 10D into the non-cohesive layers (scale in m)

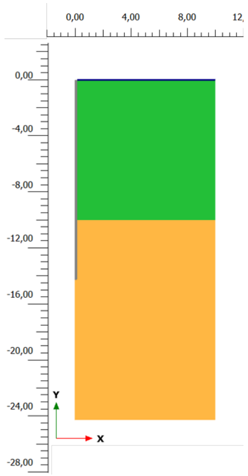

Figure G.66: Geometry pile 12D into the non-cohesive layers (scale in m)

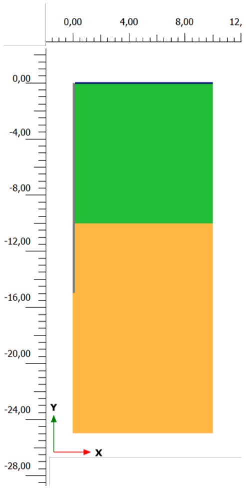

Figure G.67: Geometry pile 14D into the non-cohesive layers (scale in m)

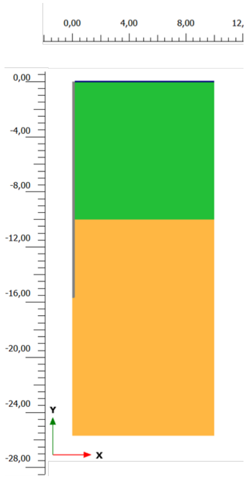

Figure G.68: Geometry pile 16D into the non-cohesive layers (scale in m)

G.3.3. Sand column

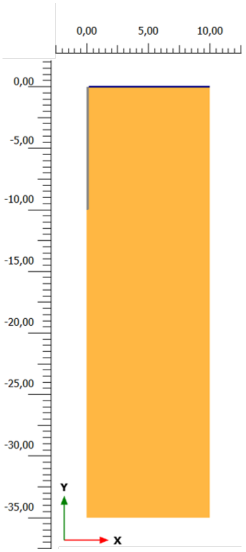

Figure G.69: Geometry of the non-cohesive soil column, pile tip level at -10m (scale in m)

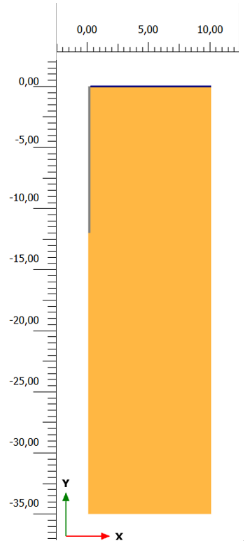

Figure G.70: Geometry of the non-cohesive soil column, pile tip level at -12m (scale in m)

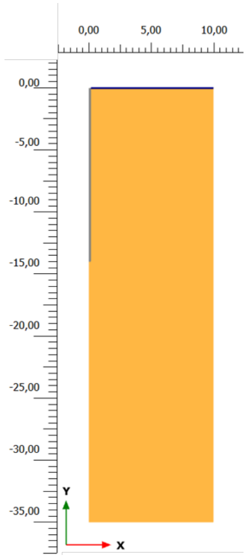

Figure G.71: Geometry of the non-cohesive soil column, pile tip level at -14m (scale in m)

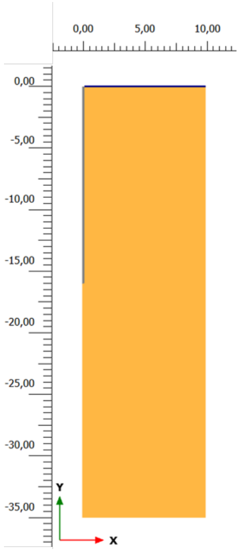

Figure G.72: Geometry of the non-cohesive soil column, pile tip level at -16m (scale in m)

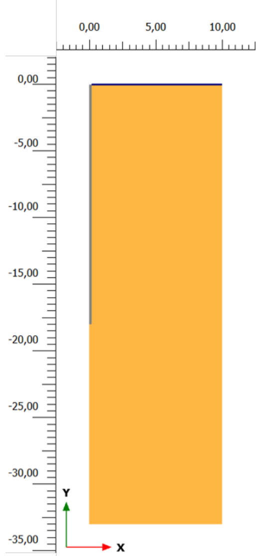

Figure G.73: Geometry of the non-cohesive soil column, pile tip level at -18m (scale in m)

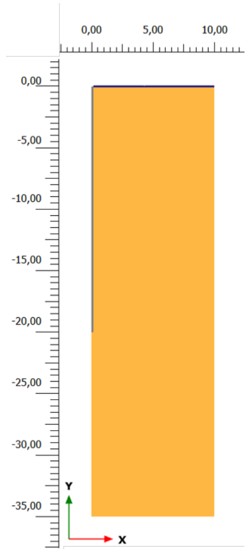

Figure G.74: Geometry of the non-cohesive soil column, pile tip level at -20m (scale in m)

G.4. Sensitivity Analyses

A sensitivity analysis was conducted to determine the influence of the different parameters of the HP model. This analysis is performed on model 1. This way it can be compared to test data and in the end, a set of parameters is validated. The three different installations depths at Kruithuisweg, Delft are assessed. The parameters considered in this sensitivity analysis are set out in Table G.20.

		Standard	Variation 1	Variation 2	Optional variation
Horizontal pre-stressing	ux (m)	0.005	0.004	0.003	0.006
Static Load inducing residual load	Qr (kN/m^2)	14000	12000	10000	8000
Initial void ratio	e (-)	0.58	0.62	0.54	
Stiffness parameter	n (-)	0.32	0.37	0.27	

Table G.20: Parameter variations

After performing the parameter variation from Table G.20, meaning keeping the standard parameter set and changing only one of the parameters, a combination of adjusting parameters was done. These combinations were compared to the test data available and fitted. Besides creating the best fit, the pile tip capacity from PLAXIS was compared to the measured pile tip capacity. This was done to check the values for u_x and Q_r.
It should be noted Q_r can be translated to F_r (a load on top of the pile) by dividing it by the area of the pile which is ≈ 0.1.
The coming subsections perform the same parameter variation for the three different piles modelled (KH II, KHIII and KH IV).

G.4.1. Parameter Variation KH II

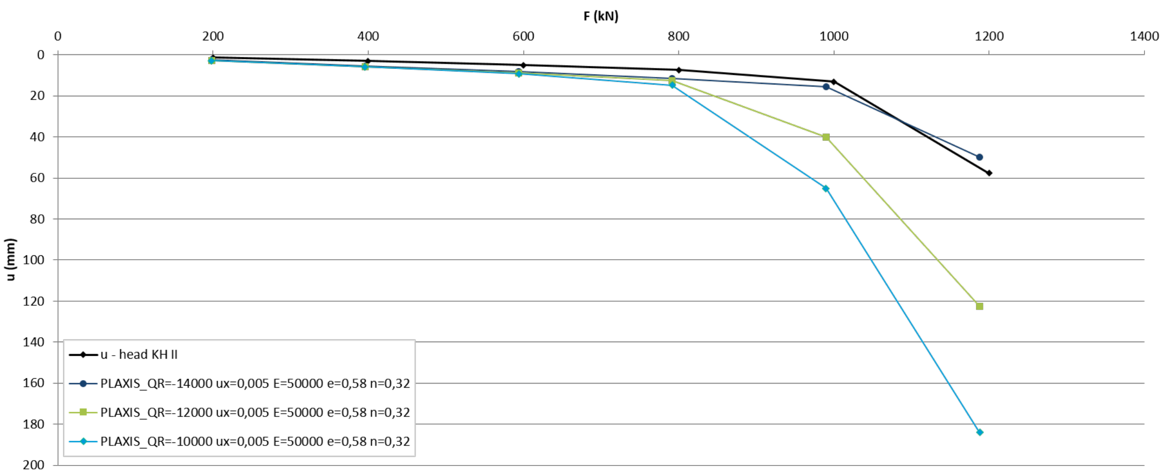

Figure G.75: F, u_y-diagram with changing the static load inducing the residual load (Q_r) for pile KH II

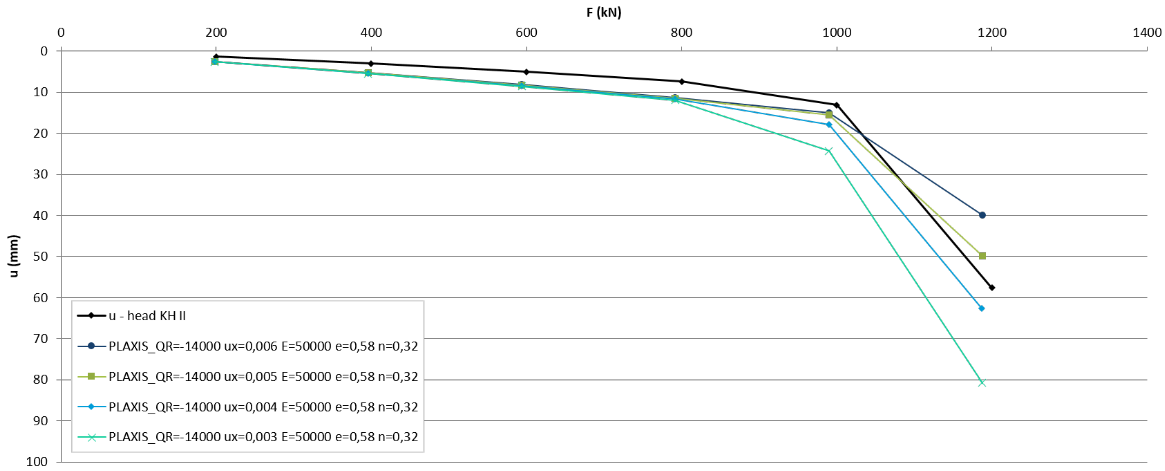

Figure G.76: F, u_y-diagram with changing horizontal pre-stress (u_x) for pile KH II

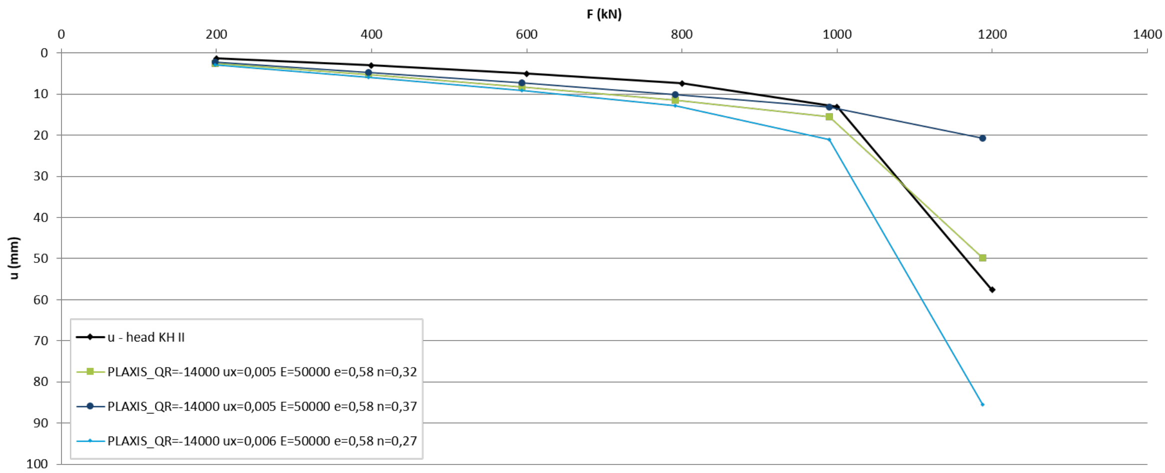

Figure G.77: F, u_y-diagram with changing stiffness (n) for pile KH II

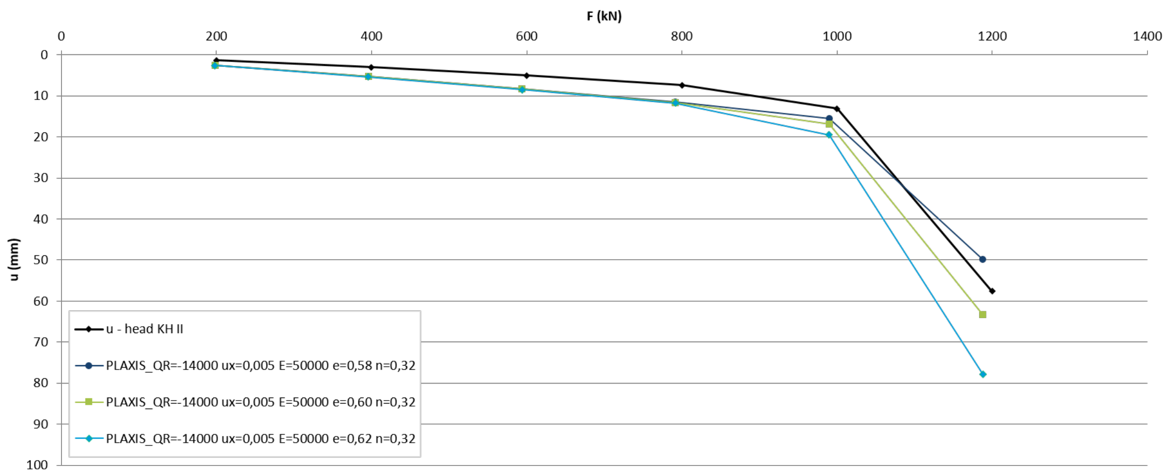

Figure G.78: F, u_y-diagram with changing initial void ratio (e) for pile KH II

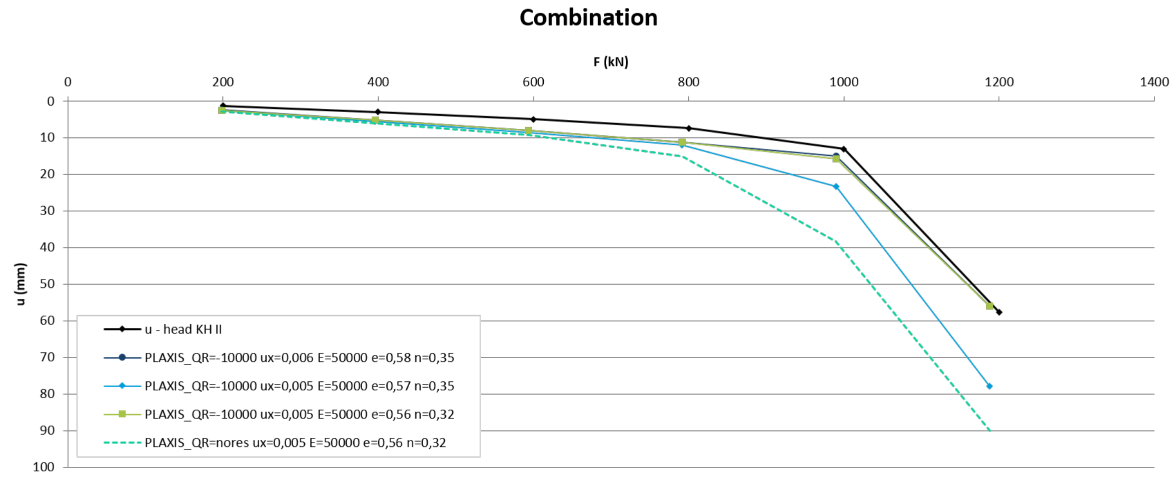

Figure G.79: F, u_y-diagram with several changing parameters for pile KH II

G.4.2. Parameter Variation KH III

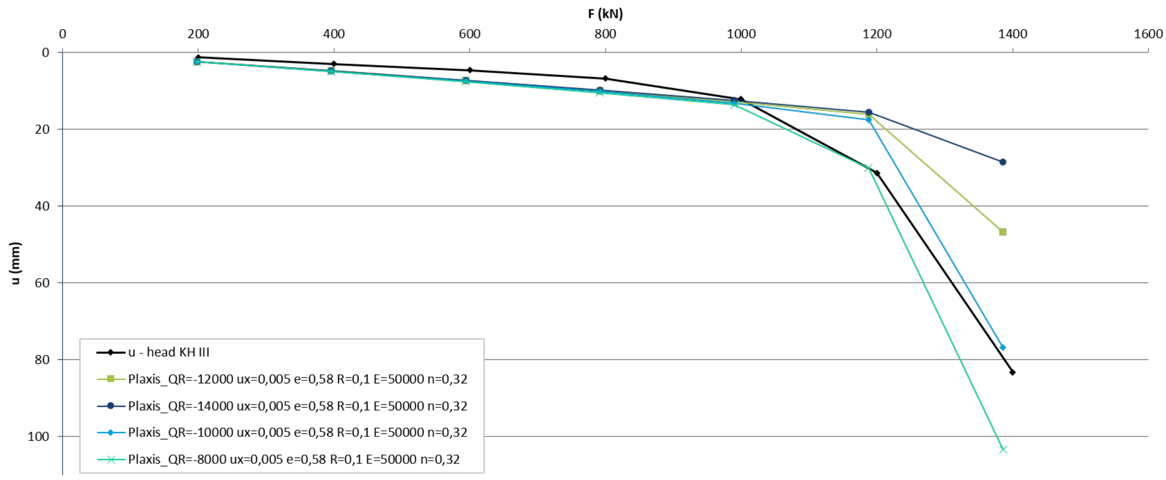

Figure G.80: F, u_y-diagram with changing the static load inducing the residual load (Q_r) for pile KH III

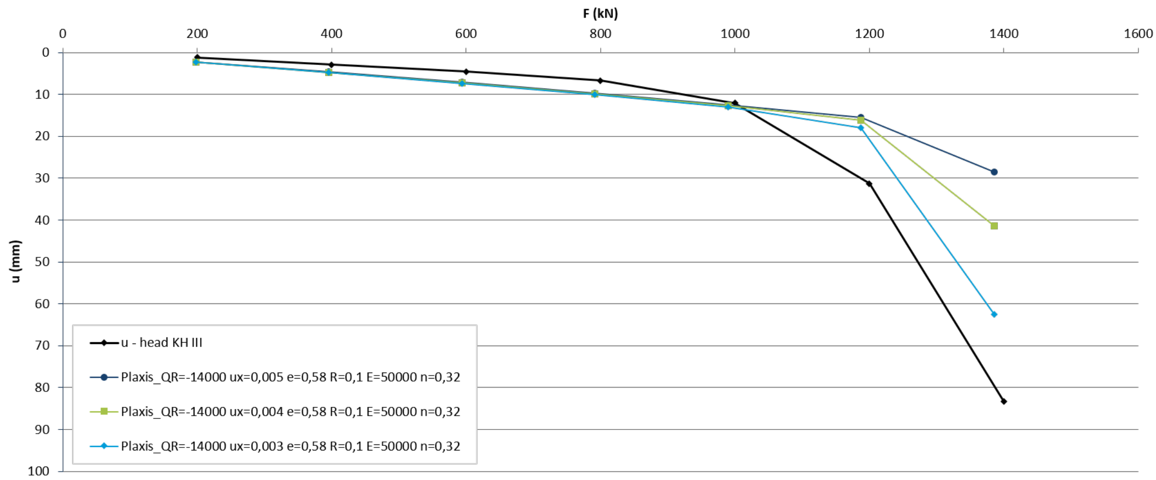

Figure G.81: F, u_y-diagram with changing horizontal pre-stress (u_x) for pile KH III

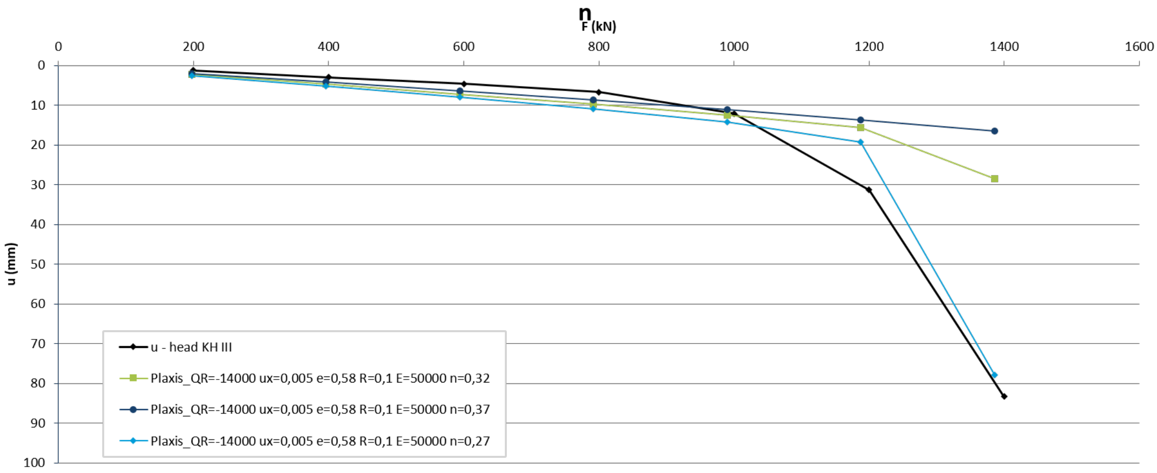

Figure G.82: F, u_y-diagram with changing stiffness (n) for pile KH III

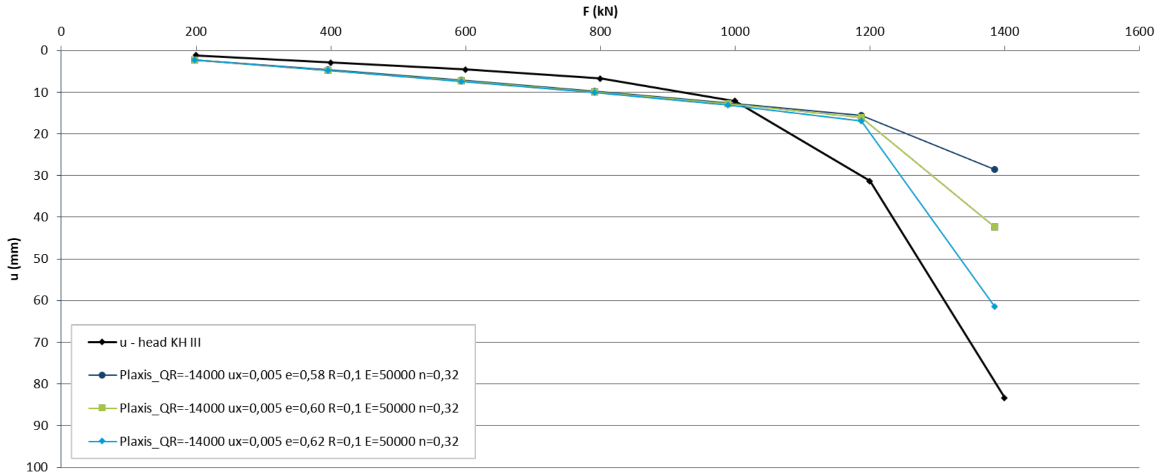

Figure G.83: F, u_y-diagram with changing initial void ratio (e) for pile KH III

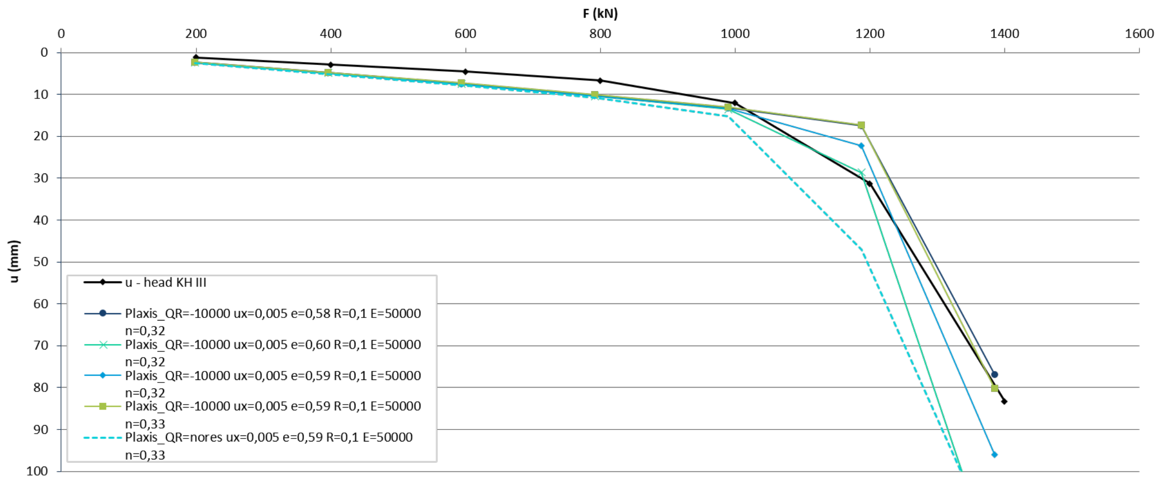

Figure G.84: F, u_y-diagram with several changing parameters for pile KH III

G.4.3. Parameter Variation KH IV

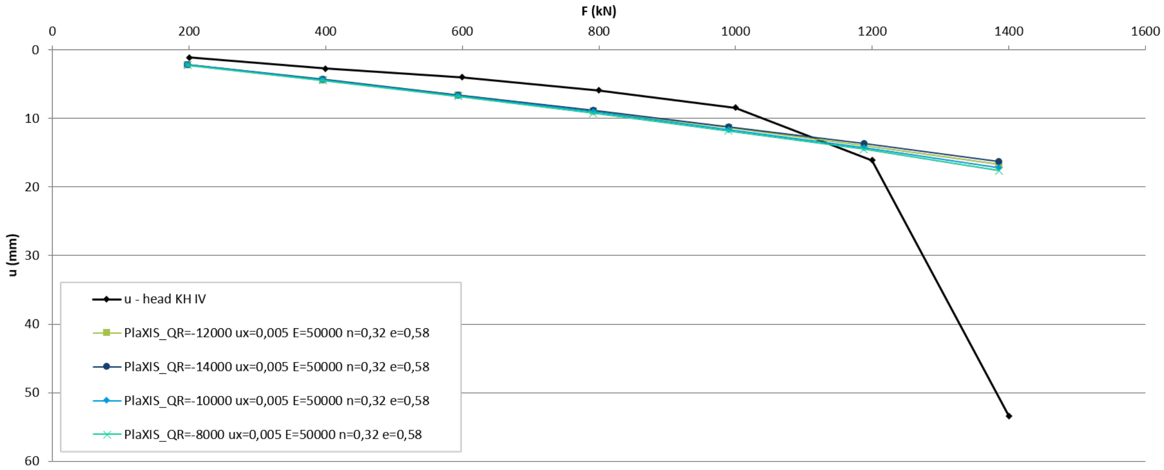

Figure G.85: F, u_y-diagram with changing the static load inducing the residual load (Q_r) for pile KH IV

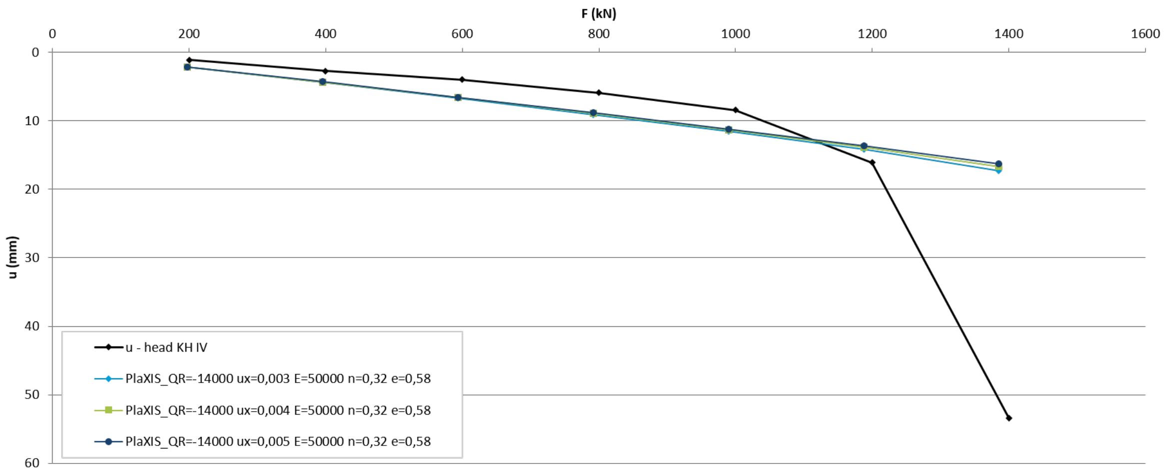

Figure G.86: F, u_y-diagram with changing horizontal pre-stress (u_x) for pile KH IV

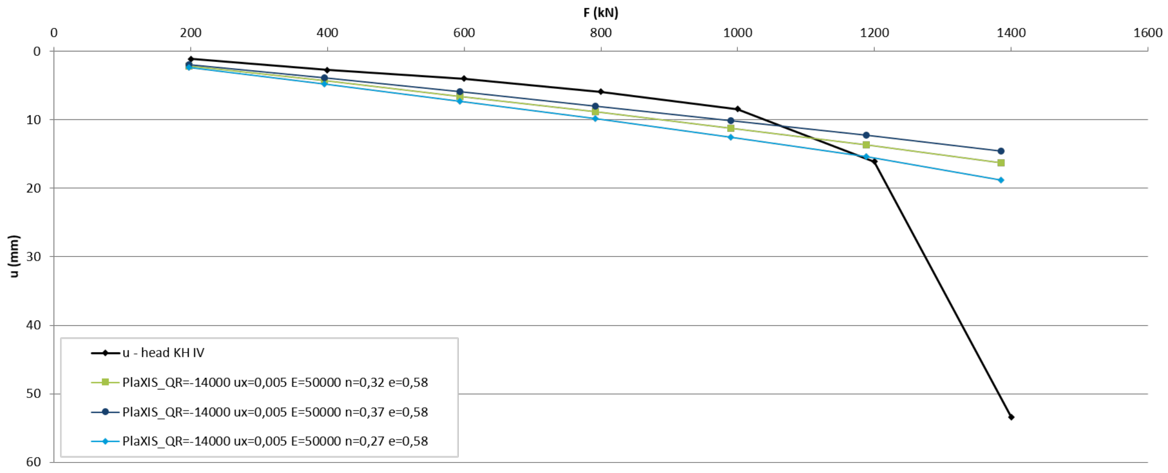

Figure G.87: F, u_y-diagram with changing stiffness (n) for pile KH IV

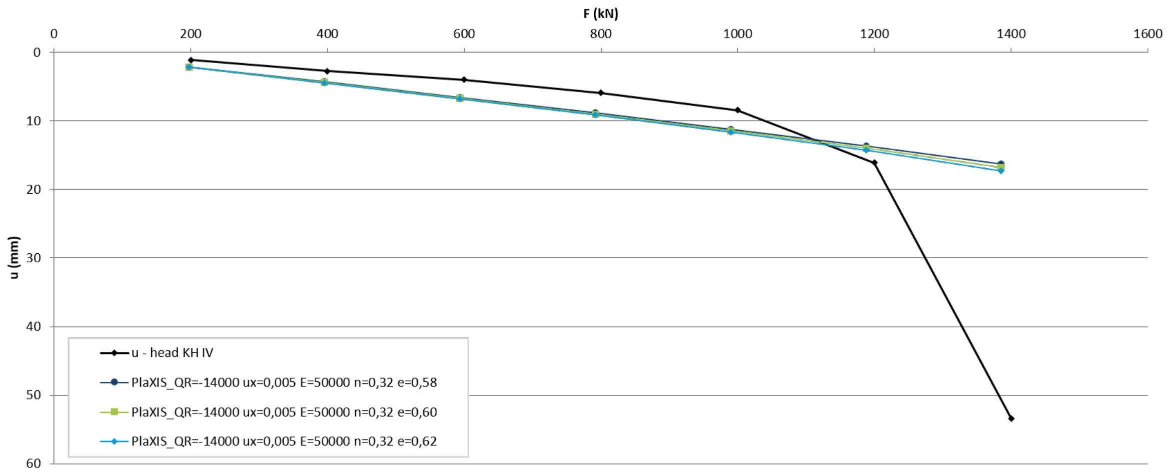

Figure G.88: F, u_y-diagram with changing initial void ratio (e) for pile KH IV

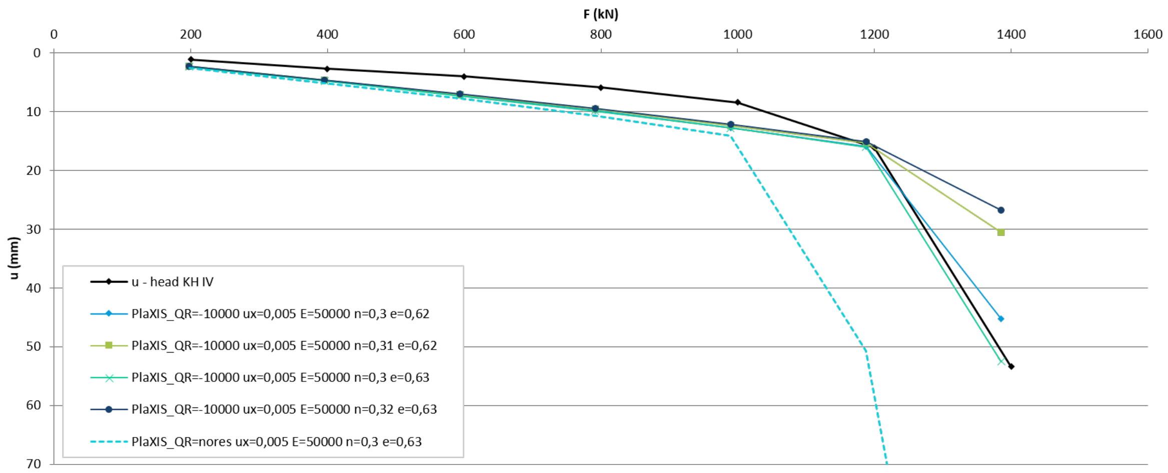

Figure G.89: F, u_y-diagram with several changing parameters for pile KH IV

G.5. Vertical stress distribution for model 2 - 16D

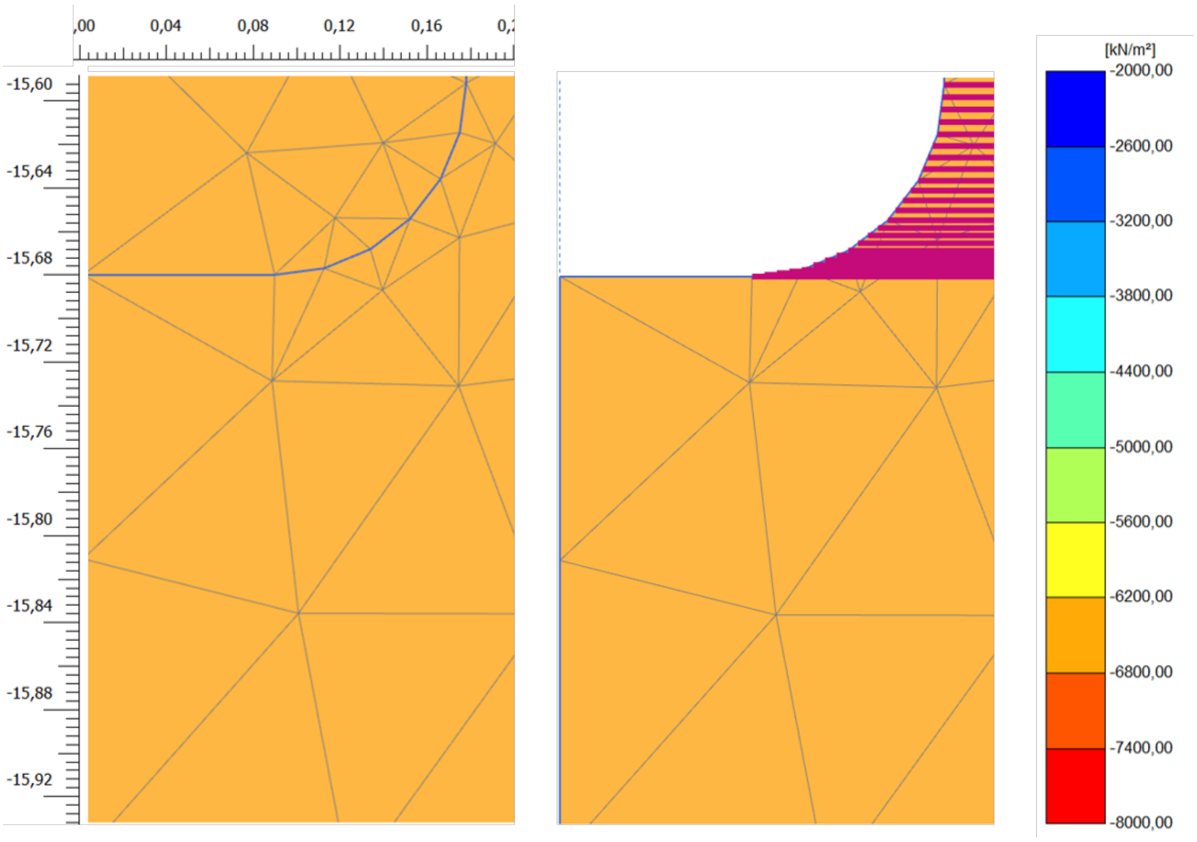

Figure G.90: Vertical stress distribution at the pile tip for, from left to right, the initial phase, horizontal pre-stressing phase, activating pile phase

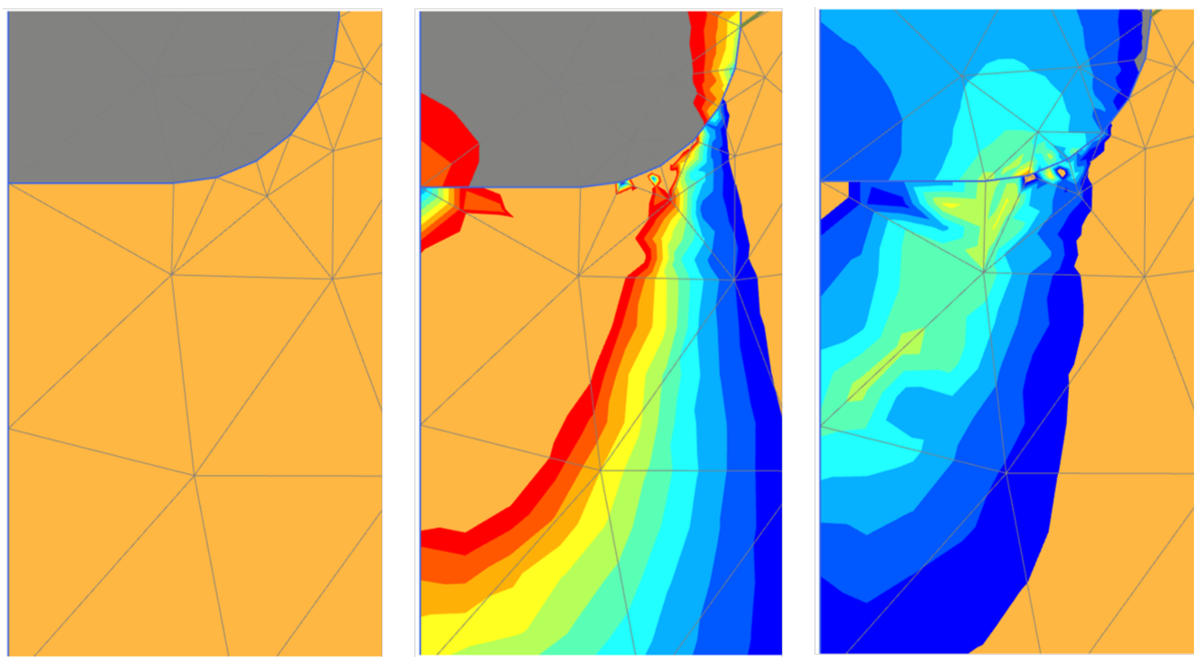

Figure G.91: Vertical stress distribution at the pile tip for, from left to right, inducing the residual load phase, unloading phase

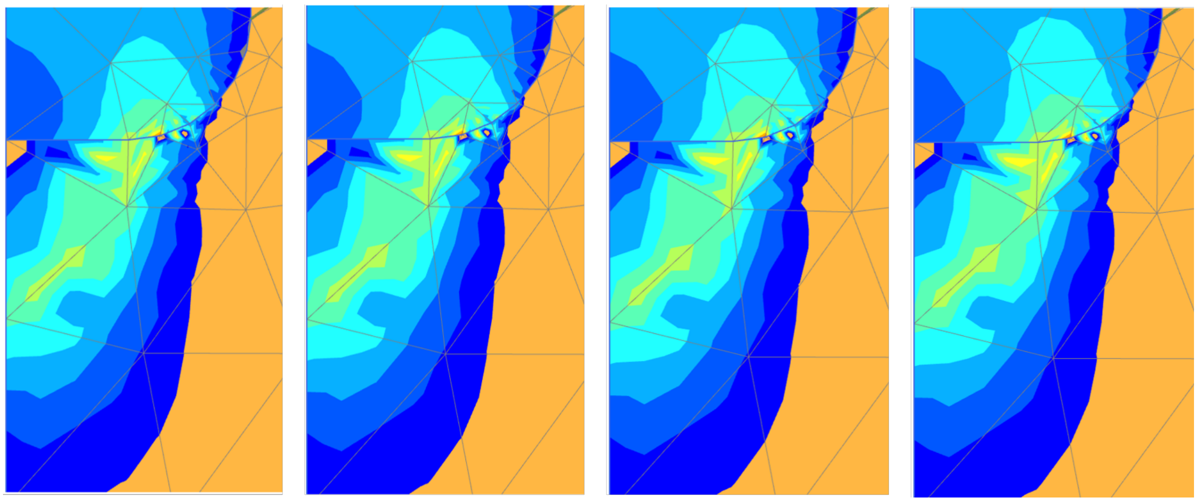

Figure G.92: Vertical stress distribution at the pile tip for, from left to right, loading phases 50, 75, 100, 125 kN

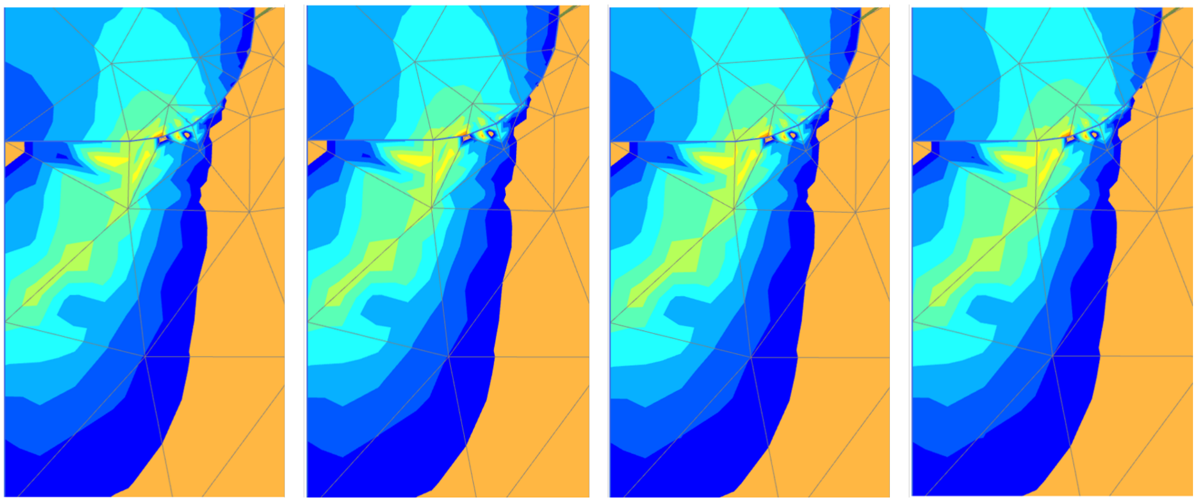

Figure G.93: Vertical stress distribution at the pile tip for, from left to right, loading phases 150, 175, 200, 225 kN

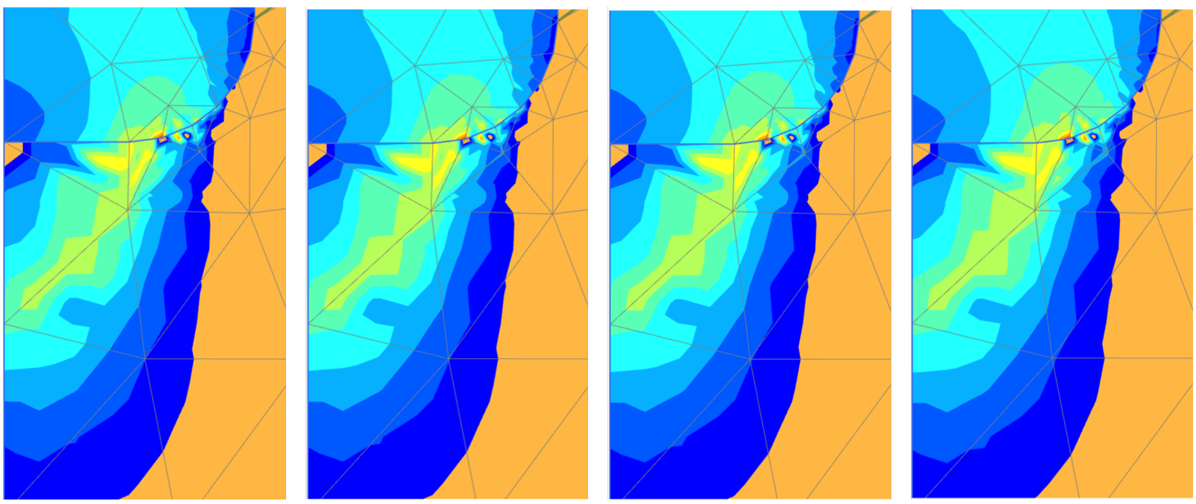

Figure G.94: Vertical stress distribution at the pile tip for, from left to right, loading phases 250, 275, 300, 350 kN

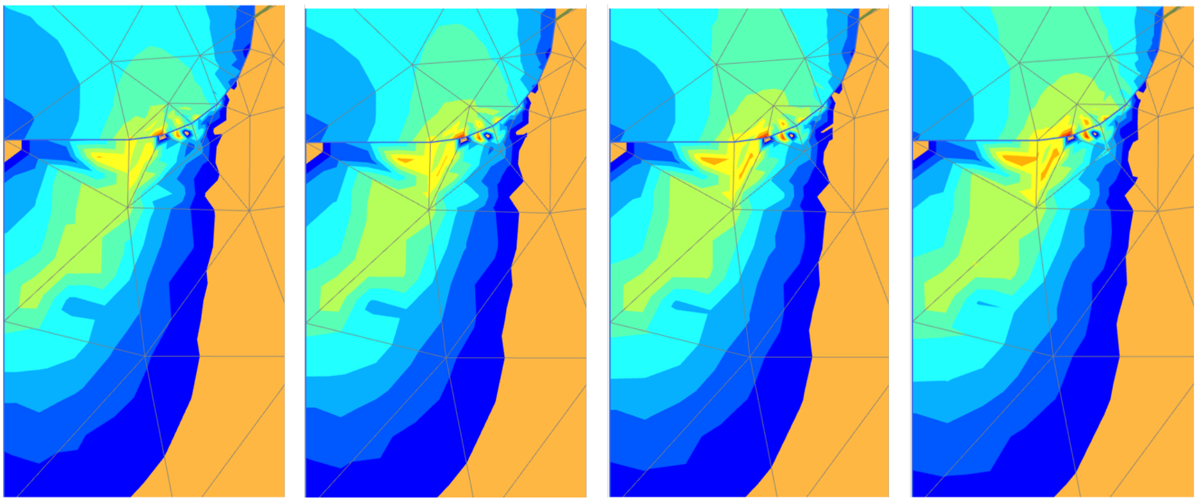

Figure G.95: Vertical stress distribution at the pile tip for, from left to right, loading phases 400, 500, 600, 700 kN

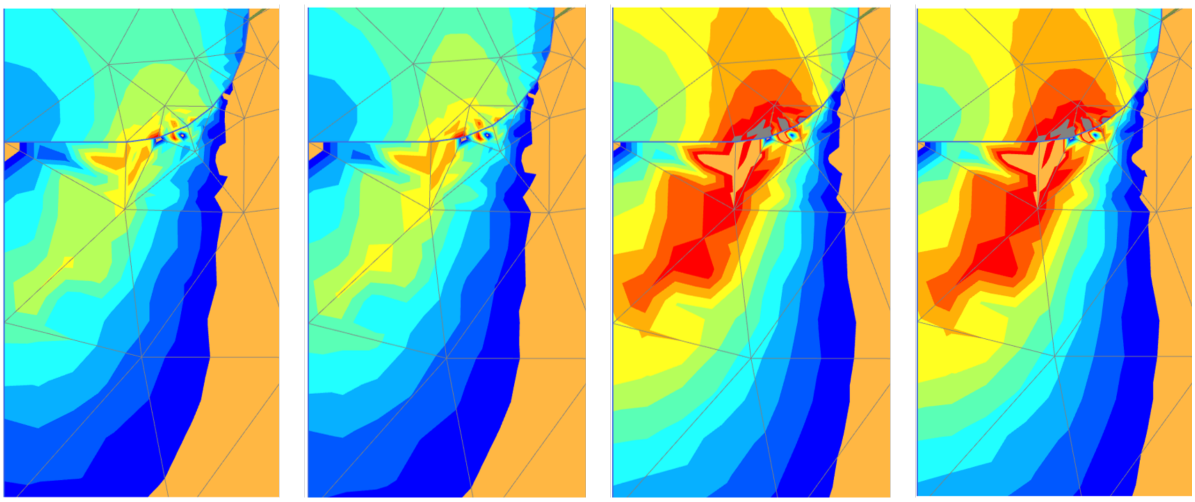

Figure G.96: Vertical stress distribution at the pile tip for, from left to right, loading phases 800, 900, 1000, fail kN

When loading phase 1000 kN starts, a clear increase in the vertical stresses at the pile tip is visible. This is due to the fact the shaft failed in this load step. This means all the stresse are now concentrated to the pile tip.

H

Test Procedure Scaled Tests

This Appendix was made in cooperation with Erik Beutick and Patrick IJnsen

The scaled pile test program at Van 'T Hek is initiated by Van 'T Hek, Volker Staal en Funderingen and BAM in cooperation with TU Delft. The tests are performed by BREM under the supervision of Allnamics.
The test program has mixed interests. First of all the piling contractors are interested in the pile tip capacity of the screwed piles. With the results, they hope to be able to assess the influence of the pile tip shape on α_p.
The other involved party, the TU Delft has two different aims. One of them is to investigate the time-dependent pile capacity. The other is the presence or contribution of residual loads to the pile tip capacity (this thesis).

To be able to answer the above aims to the best extend the test program is set out below.The test setup consists of 8 scaled instrumented piles in a sand fill enclosed by sheet piles. Four piles are closed-end displacement piles which serve as reference piles to four screwed displacement piles. Two of the screwed piles have a flat tip, the other two have a conventional tip.
To test the piles, they will be loaded in compression up to failure. During installation and loading, the strains are measured along the pile shaft and close to the pile tip for the driven piles. The strains for the screwed piles will be measured along the centre axle of the piles. The strains are measured using fibre optics.

H.1. Site Layout

Before going deeper into the test procedure, the site layout is discussed. As mentioned before, the tests will be conducted in a sand fill enclosed by sheet piles in Zuid-Oost Beemster. To be exact, at the site of the head office of Van 'T Hek. The excavation created to conduct the tests is schematized in Figure H.1. The soil at the boundaries of the excavation is supported by sheet piles with a length of approximately 13 m. The total size of the pit is 15.2 x 8.2 m.
The procedure of preparing the pit is as follows: first, the pit was excavated to a depth of 2 m. Next, the support structure was installed before fully excavating the pit to its final depth of 4 m. The bottom of the pit is 'sealed' by stiff clay (Beemster clay). Last the pit was re-filled with fine sand and the support structure was removed.

Due to the impermeable clay, the water level in the sand fill will rise when it rains. Drainage is placed at the bottom of the pit underneath the fill. Furthermore, a pump pit is placed in one of the corners of the excavation. This way, water levels can be controlled when required.The ground water table is monitored using two stand pipes

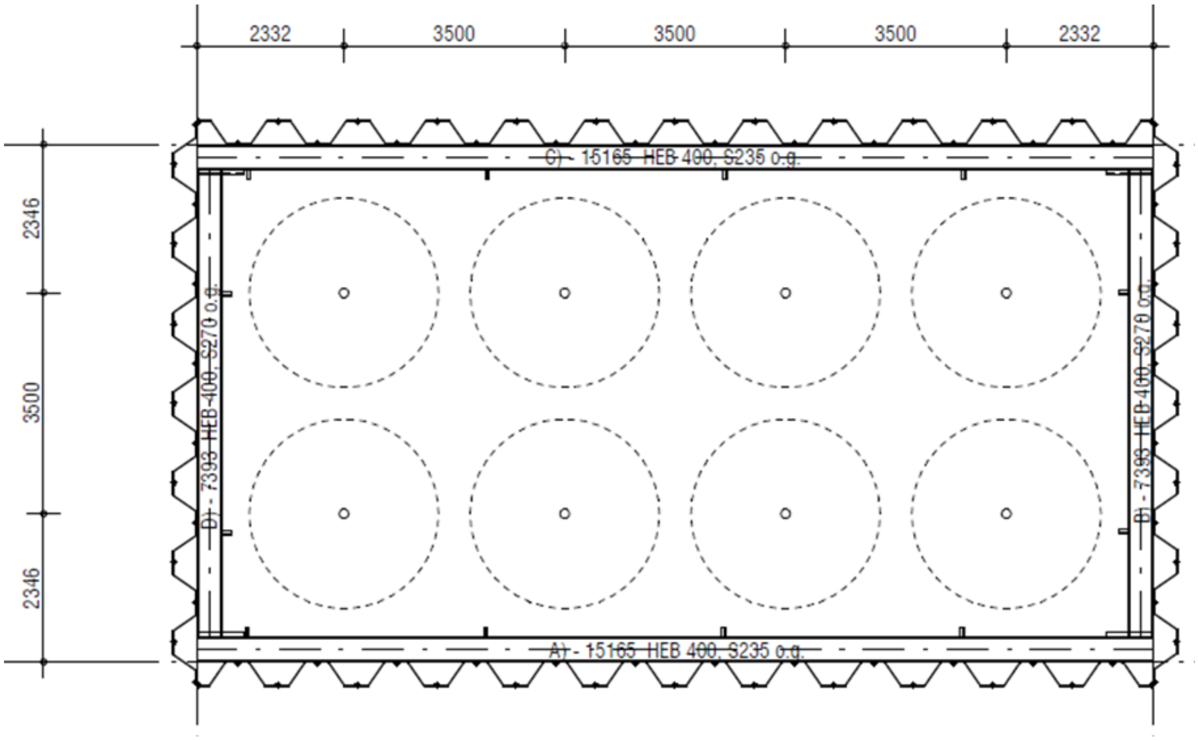

Figure H.1: Scheme of the test site

H.2. Soil Profile and Characteristics

The tests are conducted in a man-made sand fill, created according to the above-explained procedure. The sand is applied and compacted in layers of approximately 300 mm. The density is checked by a hand CPT before applying a new layer. From each layer, samples were taken.
Fine sand with specific characteristics (D50 = 0.2 -0.35 mm) was selected for the backfill. The following soil characteristics are determined:

- Sieve analyses to check D50 (Sieving according to British standard)
- Angle of internal friction (Angle of repose according to [JGS, 1996])
- Minimum and Maximum void ratio ([JGS, 1996])
- Relative density (calculated from CPT data and e_{min} and e_{max} [JGS, 1996])
- Angularity and sphericity (Microscopic photographs)

The results of the above-named test are shown in Figures H.2 - H.7. The procedure of conducting the test is the same as for the test performed to determine some of the HP parameters, see Appendix G.2.

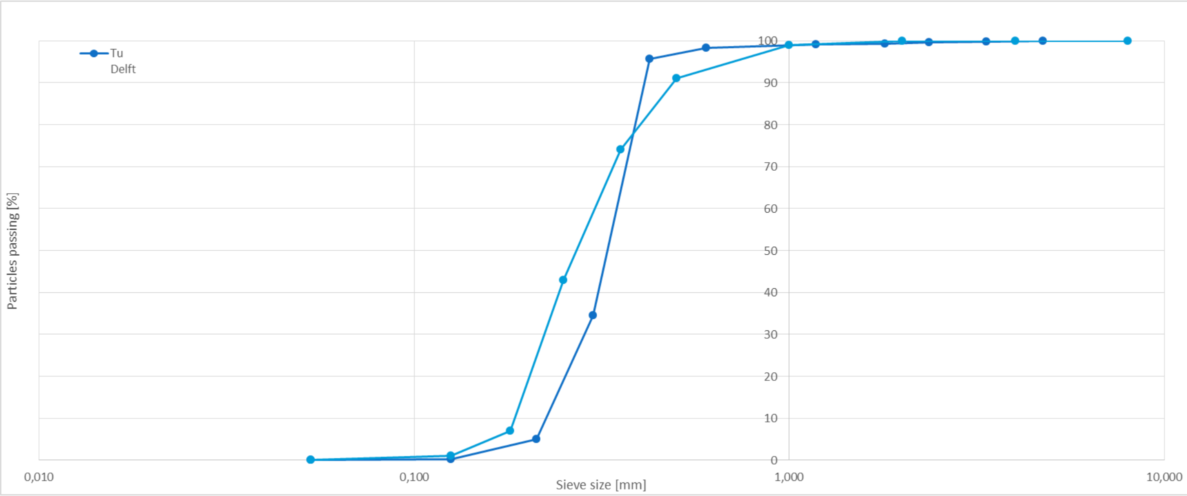

Figure H.2: Sieve curvature sand for scaled tests

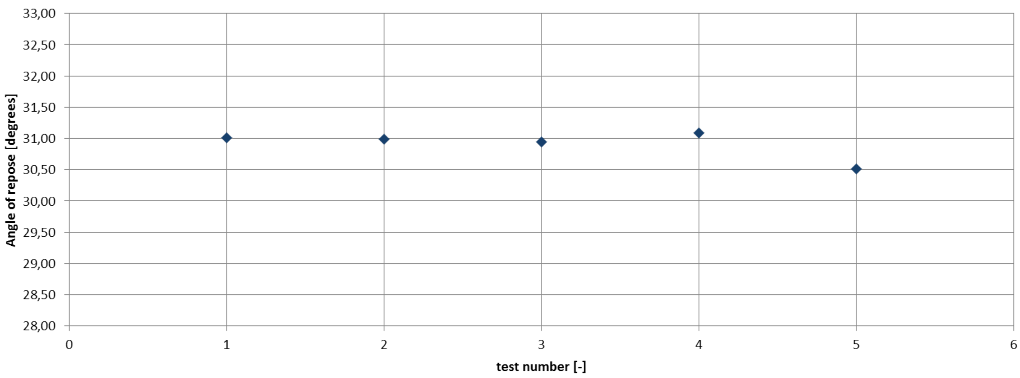

Figure H.3: Constant volume friction angle for sand for scaled tests

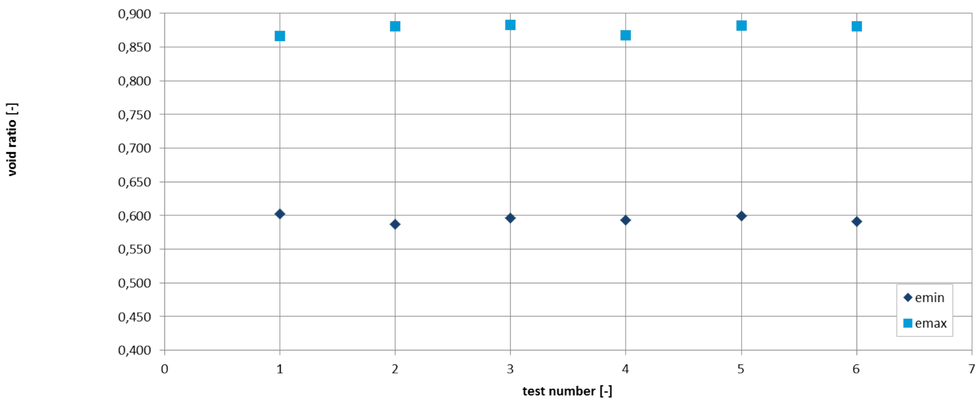

Figure H.4: Void ratios e_{min} and e_{max} for sand for scaled tests

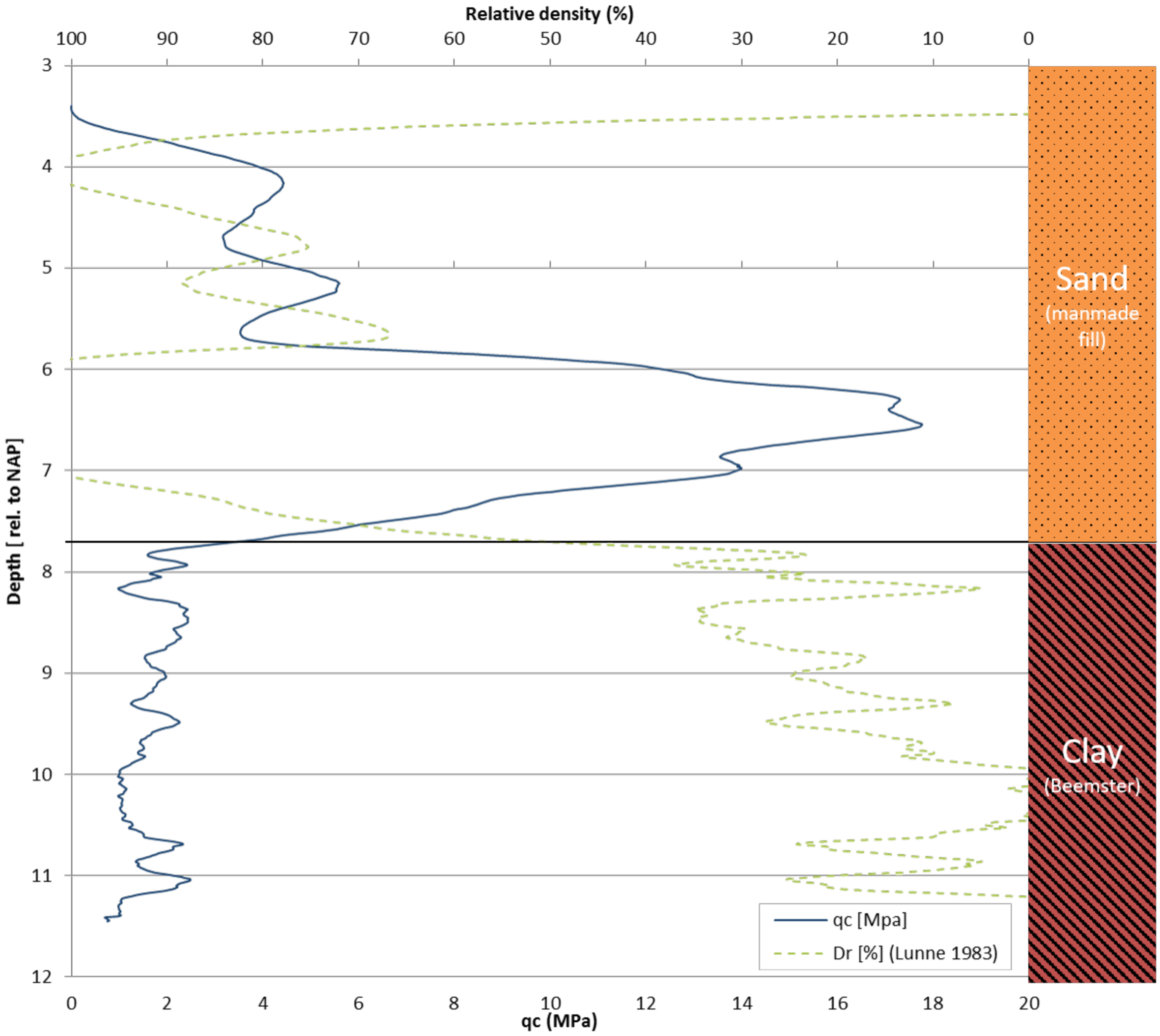

Figure H.5: Cone resistance and relative density profiles for test pit for scaled tests

Figure H.6: Microscopic photograph sand for scaled test

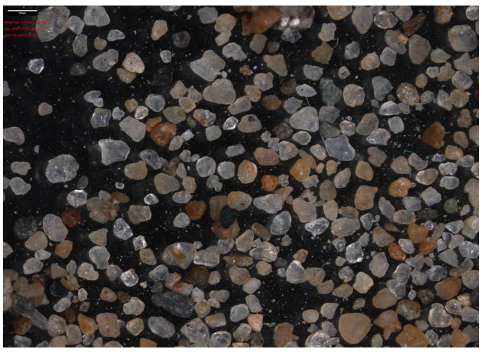

Figure H.7: Microscopic photograph sand for scaled test

Table H.1 summarizes the above data.
Fine sand was chosen as the piles are scaled (D_{pile}=150mm). Using fine sand will reduce the risk of having trouble with scale effects. By applying and densifying the fill in layers a homogeneous compaction rate is expected. The rate of compaction will also be determined by seismic measurements. The seismic measurement profiles will be made by the University of Zagreb.

ϕ_c (-)	e_{min} (-)	e_{max} (-)	D50 (mm)
30.91	0.60	0.88	0.33

Table H.1: Soil Parameters for sand for scaled tests

The aim is to find q_c-values between 10 and 15 MPa over the zone $2D_{eq}$ above and $2D_{eq}$ below the pile tip. These values are representative q_c-values at pile tip levels for Dutch soils. Figure H.5 show q_c-values in this order of magnitude between N.A.P. -6 to -7.5 m. The CPT profile in Figure H.5 is an average of all the CPT profile which have been made.
When the test pit is ready the location of the piles will be determined. At all 8 locations, a CPT will be performed. A standard 10 tons cone will be used with double inclination measurement and a cone tip surface of 10cm2.

H.3. Piles

As mentioned before, a total of eight piles will be tested. The outer diameter (D) of the pile is $\approx 150mm$ and the embedded length is 2500 mm ($> 15D$).
The slip surface below the pile tip is expected to be well above the bottom of the sand fill. It is assumed, the failure surface will have a maximum extend of 4D (600 mm) below the pile tip. The horizontal zone of influence of the piles is expected to be less than 10D for granular soils with an angle of internal friction up to 40^o.

H.3.1. Screwed Displacement Piles

The screwed displacement piles have a solid core ($D_{cone} = 70mm$) which extends itself over the full length of the pile. A small trench is created over the full length of the core to install the fibre optics. The trench continues over the bottom of this massive centre axle to the opposite side where it returns to the top. Material is welded over the full circumference and length of the centre axle for a good binding between core and grout (see Figure H.10).
During installation of the pile, when the pile tip is at its final depth, a funnel with grout is placed on top of the casing. When the casing is retrieved voids will be filled with grout. The excess grout volume in the funnel has to provide the grout pressure that exceeds the horizontal soil pressure.
After testing all piles, the screwed piles will be extracted and the exact dimensions of the grout body will be determined.

Conventional Tip The scaled conical conventional tip is built up of steel plate segments of which the centre axle is rectangular. The plates have a thickness of 5 mm and the steel quality is S235. Figure H.8 shows a drawing of the conventional tip.

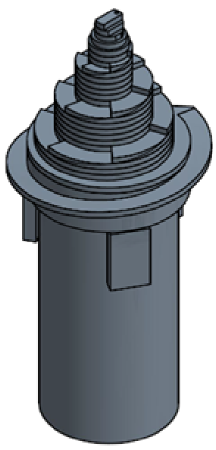

Figure H.8: Drawing of scaled conventional pile tip

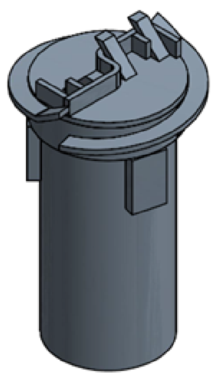

Figure H.9: Drawing of scaled flat tip

Flat Tip The scaled flat tip is a flat tip with welded cutting teeth. The teeth are built up from 5 mm S235 steel plates. Figure H.9 shows this type of pile tip.

Figure H.10: Photos of the screwed pile (tip and core)

Closed-end steel piles Four closed-end steel piles are used as a reference to the screwed piles. The piles have an outer diameter of 150 mm. The diameter is constant over the full pile length, no enlarged footing is used. The wall thickness and thickness of the base plate is 10 mm. A small trench is cut in the outer shaft to facilitate the fibre optic strings. The trenches are located on opposite sides of the pile and continue over the bottom plate.

H.3.2. Instrumentation

Instrumentation is done by Brem together with Marmota. As mentioned before, the piles will be instrumented with fibre optic strings. These fibre optic strings measure strain at an interval of 1000 mm. Each pile is instrumented with two strings so that strain is measured every 500 mm along the pile shaft or centre axle. The strain is measured as close to the pile tip as possible. Not only the interval becomes smaller by the use of two strings, the test is also more robust. When one string fails, still some results will be available.
The strings and its sensors are in the prior mentioned trenches. For protection, the sensors will be covered in silicone kit and the string will be covered with an epoxy hardener. To check the response of the sensors prior to pile installation the closed-end piles and centre axles of the screwed displacement piles will be installed in a frame construction and tested by applying a load with a hydraulic press. The loads applied during the check will be in the order of the loads applied during the test.

H.4. Installation of the Piles

The influence of adjacent piles will be minimalized by optimizing the spacing of the piles and order of installation. For this reason, the driven piles are installed before the screw displacement piles.

H.4.1. Closed-ended steel piles

Dependent on CPT-data, the installation depth of the 8 piles will be determined. The embedded length is expected to be around 2500 mm. The piles will be driven by a mini rig with a ram weight of 400 kg or less, the drop height of the ram will be 250 mm. During installation displacement, blow count and strain in the pile will be recorded. The aim is to have 15 to 30 blows per 250 mm displacement.
Prior to installing the instrumented piles, a non-instrumented closed-end steel pile will be installed to calibrate the installation equipment. This is required in order to have sufficient blow counts per unit displacement to simulate a realistic installation process. The concern is, the weight of the equipment will simply push the scaled piles into the ground. This was not the case. Therefore, no adjustments had to be made to the above-explained procedure.

H.4.2. Screwed Displacement Piles

The screwed displacement piles will be installed by a mini rig with a rotary head which applies its force on the casing, the minimum diameter of the casing is 123 mm. During installation revolutions, torque, displacement and strain will be recorded.
A funnel will be placed on top of the casing when the pile is at its designed depth. The funnel is filled with an excess of grout mortar. When retrieving the casing the grout will flow and fill all the voids. The strengthening time required for the grout prior to testing is at least 28 days. The mortar used is Cugla limited shrinkage mortar.

H.5. Load Test

The piles will be tested in compression. The load is applied by a hydraulic jack. A load cell is placed between the jack and the pile head (the screwed piles are loaded at the centre axle). To check the load cell measurement, the pressure in the hydraulic jack is measured by means of a pressure sensor and a calibrated digital manometer.
The base capacity of the piles is expected to be in the order of 170 to 270 kN for a cone resistance between 10 and 15 MPa and a 150 mm base diameter. The theoretical shaft capacity of the piles with a constant diameter and an embedded length of 2500 mm will be in the order of 60 to 120 kN. This means the total bearing capacity will be in between 230 and 390 kN.
A max load of 400 kN (40 tonnes) is expected to be sufficient to load all piles to failure. A stack of eight steel dragline mats with a weight of 50 to 60 kN each should be satisfactory. Strain will be measured by continuous measurement prior to installation, during installation and for some time after installation. Also, the strain will be measured prior to testing, during the compression test as well as during unloading. The measured strain prior to the load test might be different from the measurement after installation (e.g. temperature difference, soil stress state). The test will be conducted by BREM under Supervision of Allnamics. The response of the sensors is monitored and recorded from a site office and the complete test will be documented with a GoPro.

H.5.1. Pile Settlement

Settlement of the pile is measured at the pile head. Three digital probes will record settlement. Three reference points will be installed within 10 m from the piles. These reference points are used to measure heights and displacements during installation and testing. The settlement needs to be verified with the reference points after each load step. The error of the measurement is supposed to be less than 0.2% of the actual displacement with a max of 1mm [Normcommissie 351 006 'Geotechniek', 2017b].
The dead weight, hydraulic jack and load cell have to be repositioned after every test. The positioning of the jack and load cell is a precise job. The jack and cell have to be vertically aligned with the pile. Bending of the equipment has to be monitored.
Furthermore, influences of the surrounding need to be limited. Vibrations or weather influences like rain, wind and sun might affect the results.

H.5.2. Test Scheme

Initially, all piles are tested once. The virgin capacity is determined. The piles are tested at different moments after installation in order to assess the time-dependent capacity. Table H.2 shows the time schedule of for testing the piles.

Pile	Test moment
First closed-ended steel pile	+/- 1 day after installation
Second closed-ended steel pile	+/- 14 days after installation
Third closed-ended steel pile	+/- 30 days after installation
First screwed pile flat tip	+/- 30 days after installation
First screwed pile conventional tip	+/- 30 days after installation
Second screwed pile flat tip	+/- 30 days after installation
Second screwed pile conventional tip	+/- 30 days after installation
Fourth closed-ended steel pile	+/- 60 days after installation

Table H.2: Pile testing schedule

H.5.3. Failure Criteria

The piles will be loaded till a constant displacement is found. This is most likely with a larger displacement than 10%D. With the 10%D failure criterion [Normcommissie 351 006 'Geotechniek', 2017a], only a small displacement is required due to the small pile diameter. The error in measuring this displacement will be relatively large, therefore this failure criteria is not met. The exact load scheme can be found in Table H.3. Figure H.11 shows an example of a load scheme and Table H.4 gives a more detailed discription of the load schem and when to move to the next load step.

Load step	**Applied force (kN)**
0-force	10
F1	52.5
F2	95
F3	137.5
F4	180
F5	222.5
F6	265
F7	307.5
F8	350
F9	392.5
F10	435

Table H.3: Load scheme

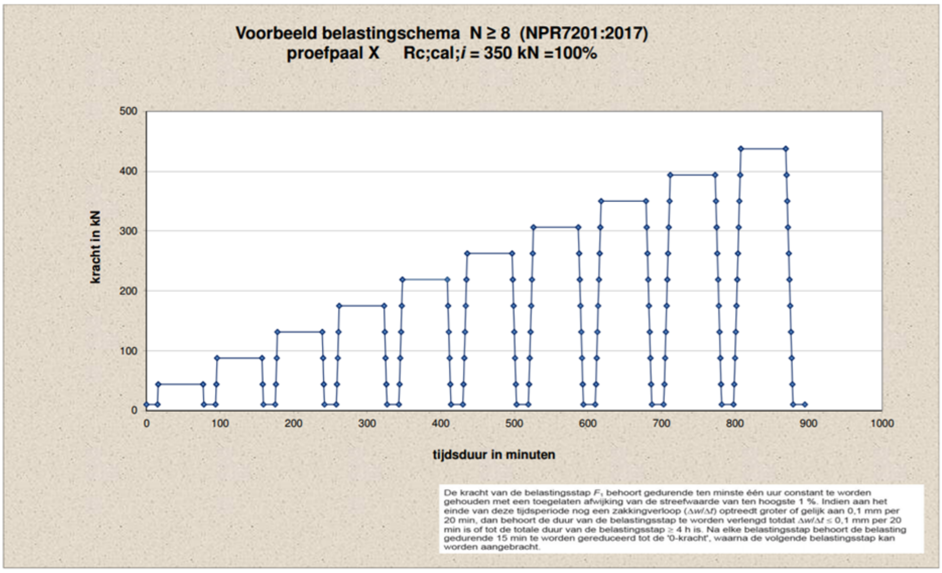

Figure H.11: Example load scheme

Criteria for when to move to a next load step are set out in Table H.4.

Step	Description	Remarks
1	Apply 0-force to the pile head	max 0-force is 10 kN
2	Increase the load to the first load step F1	Increasing the load is supposed to take at least 5 minutes
3	Maintain constant load step F1 for at least 1 hour	Max deviation is 1% of designed load F1
4	If, after 1 hour $\delta w/\delta t > 0.1$ mm in 20 minutes the duration of load step F1 has to be increased till $\delta w/\delta t < 0.1$ mm in 20 minutes or till the total duration of the load step is > 4 hours	w = settlement
5	Unload the pile to the 0-force for 15 minutes	
6	Repeat steps 2 to 5 but this time apply load steps F2 to F8.	
7	Pile failure is reached when a continuing displacement is found for a constant load	

Table H.4: Criteria to move to next load step [Normcommissie 351 006 'Geotechniek', 2017b]

List of Figures

List of Tables